UNIVERSIDAD COMPLUTENSE DE MADRID
FACULTAD DE CIENCIAS QUÍMICAS
Departamento de Química Orgánica I

NUEVAS APLICACIONES DEL (60)FULLERENO EN NANOCIENCIA
(NEW APPLICATIONS OF (60)FULLERENE FOR NANOSCIENCE)

MEMORIA PARA OPTAR AL GRADO DE DOCTOR
PRESENTADA POR

Andrea La Rosa

Bajo la dirección de los doctores

Nazario Martín León,
Salvatore Filippone

Madrid, 2013

©Andrea La Rosa, 2013

UNIVERSIDAD COMPLUTENSE DE MADRID
FACULTAD DE CIENCIAS QUÍMICAS
Departamento de Química Orgánica

NUEVAS APLICACIONES DEL [60]FULLERENO EN NANOCIENCIA
(NEW APPLICATIONS OF [60]FULLERENE FOR NANOSCIENCE)

Ph.D. Thesis

Andrea La Rosa
Madrid, 2013

NUEVAS APLICACIONES DEL [60]FULLERENO EN NANOCIENCIA

(NEW APPLICATIONS OF [60]FULLERENE FOR NANOSCIENCE)

Supervisors:

Prof. Nazario Martín León

Dr. Salvatore Filippone

Ph.D. candidate:

Andrea La Rosa

MADRID

Septiembre, 2013

Some of the results discussed within this Memory have been published in the following papers:

Germà Garcia-Belmonte, Pablo P. Boix, Juan Bisquert, Martijn Lenes, Henk J. Bolink, Andrea La Rosa, Salvatore Filippone and Nazario Martín, "Influence of the Intermediate Density-of-States Occupancy on Open-Circuit Voltage of Bulk Heterojunction Solar Cells with Different Fullerene Acceptors", *J. Phys. Chem. Lett.* **2010**, *1*, 2566.

H. J. Bolink, E. Coronado, A. Forment-Aliaga, M. Lenes, A. La Rosa, S. Filippone and N. Martín, "Polymer solar cells based on diphenylmethanofullerenes with reduced sidechain length", *J. Mater. Chem.*, **2011**, *21*, 1382.

Katalin Gillemot, Charalambos Evangeli, Edmund Leary, Andrea La Rosa, M. Teresa González, Salvatore Filippone, Iain Grace, Gabino Rubio-Bollinger, Jaime Ferrer, Nazario Martín, Colin J. Lambert, and Nicolás Agraït, "A Detailed Experimental and Theoretical Study into the Properties of C_{60} Dumbbell Junctions", *Small* **2013**, DOI: 10.1002/smll.201300310.

During the PhD thesis, I spent some weeks for secondment periods in Switzerland for the physical characterizations and conductance studies of some of the molecules reported in this Memory. The visited laboratories are:

-Electrochemical Nanoscience Laboratories in University of Bern under the supervision of Prof. Thomas Wandlowski from the 30th of april 2012 to 16th of may 2012.

-Nanoscale Electronics Group at IBM Research Laboratories under the supervision of Dr.a Heike Riel from the 30th of july to the 10th of agust 2012.

As concern the scientific activities beyond the research, I want to mention the scientific congresses and schools in which I took part during my PhD study, starting from the most recent.

Congress Name: "Closing Funmols Network"
Contribution: Oral Presentation
Titles: "Synthesis of dumbbell molecules at UCM"
Site: Madrid (Spain)
Date: from 16/02/2013 to 17/02/2013

Congress Name: "Funmols Network"
Contribution: Oral Presentation and Poster
Titles: "Chemistry, Properties and Applications of C_{60}-dumbbells type molecular wires" and "Molecular wires hanging C_{60} as anchor group for STM and MCBJ studies"
Site: Durham (England)
Date: from 10/09/2012 to 13/09/2012

Congress Name: "Funmols Network"
Contribution: Oral Presentation.
Title: "C_{60}-dumbbells type molecular wires"
Site: Adelsdorf (Germany)
Date: from 17/05/2012 to 20/05/2012

Congress Name: "Funmols Network"
Contribution: Oral Presentation.
Title: "Synthesis of fluorene-fullerene dumbbell-type molecular wires"
Site: Zurich (Switzerland)
Date: from 16/01/2012 to 18/01/2012

Congress Name: "Funmols Network and ECME 2011"- *European Conference on Molecular Electronics*
Contribution: Oral Presentation and poster session.
Title: "C_{60}-fluorene dumbbells for molecular wires"
Site: Barcelona (Spain)
Date: from 05/09/2011 to 10/09/2011

Congress Name: "The First Symposium on Carbon Nanoform"
Contribution: Flash Oral Presentation.
Title: "C_{60}-fluorene dumbbells for molecular wires"
Site: Toledo (Spain)
Date: 2-3/06/2011

Congress Name: "Funmols Network"
Contribution: Oral Presentation.
Title: "Molecular wires with different linkage to C_{60}. Progress at UCM"
Site: Bern (Switzerland)
Date: from 10/02/2011 to 11/02/2011

Congress Name: "Summer School on Molecular Electronics"
Contribution: Attending at lesson presentations.
Title: "Summer School"
Site: Billund (Denmark)
Date: from 21/06/2010 to 26/06/2010

Congress Name: "Funmols Workshop"
Contribution: Oral presentation.
Title: "C_{60}-Dumbell type molecular wires"
Site: Muggendorf (Germany)
Date: from 15/04/2010 to 18/04/2010

Congress Name: "ICME 2010" – *International Conference on Molecular Electronics*
Contribution: Oral presentation in FunMols Meeting and Poster Session during the ICME
Title: "Dumbbell type molecular wires"
Site: Emmetten (Switzerland)
Date: from 04/01/2010 to 09/01/2010

Congress Name: "ECME 2009" – *European Conference on Molecular Electronics*
Contribution: Oral presentation in FunMols Workshop
Title: "Molecular Wire at UCM"
Site: Copenhagen (Denmark)
Date: from 07/09/2009 to 12/09/2009

Congress Name: “Material School”
Contribution: only participation
Title:
Site: Elche (Spain)
Date: from 08/02/2009 to 13/02/2009

Ai miei genitori, Alfredo e Maria Pia e, a mio fratello
Stefano che sempre ho avuto vicino, pur vivendo lontani,
durante questi anni di lavoro e formazione.

Sempre ho pensato a voi e sempre vi penserò,
ovunque il futuro mi porterà.

"Have the courage to follow your heart and intuition. They somehow already know what you truly want to become" cited by Steve Jobs

El presente trabajo ha sido realizado en el Departamento de Química Orgánica de la Universidad Complutense de Madrid bajo la dirección del Prof. Nazario Martín y del Dr. Salvatore Filippone, a quienes agradezco sinceramente su inestimable apoyo y ayuda en llevar a cabo el trabajo sea experimental que teórico. En particular os agradezco para haberme dado confianza en lo que ha sido mi recorrido científico dentro de un proyecto europeo (FunMols). Gracias a este último tuve la posibilidad de conocer científicos de todo el mundo y de fama importante y, de poder participar a distintos congresos de importancia europea y internacional. Este aspecto me ha hecho crecer desde un punto de vista profesional.

En la realización de este trabajo han participado otros grupos de investigación: en alguno de ellos tuve el placer de estar para mis dos estancias durante el periodo del doctorado. Agradezco mucho su contribución en lo que han sido y que serán los trabajos finales. Entre ellos voy a nombrar:

El grupo del Prof. Nicolas Agräit de la Universidad Autonoma de Madrid por su colaboración en entender como ocurre el transporte de electrones en molécula tipo dumbbell mediante un enfoque completamente nuevo basado en la medida de STM en una sola molécula en condiciónes estandard.

El grupo de la investigadora Heike Riel (IBM Reseach, Zurich, Suiza) por su disponibilidad y realización de estudios de movimientos moléculares sobre superficie de oro (estancia de dos semanas).

El grupo del Prof. Thomas Wandlowski de la Universidad de Berna (Suiza) por su colaboración sobre el estudio del transporte de electrónes es sístemas tipo dumbbell usando STM y MCBJ y, también, de su manera de organización sobre superficie de oro (estancia de tres semanas)

El Prof. Silvio Decurtins de la Universidad de Berna (Suiza) y su estudiante Hui Li por su visita en el laboratorio de Nazario Martín León donde se llevaron a cabo la síntesis y caracterización de dumbbells basados en BDF como entidad central.

El grupo del Prof. Colin Lambert de la Universidad de Lancaster (Inglaterra) para los estudios de transmissión electrónica a través de DFT.

El grupo del Prof. Dirk M. Guldi de la Universidad de Erlangen, por la realización de los estudios fotofísicos.

Quiero agradecer, en manera particular, al personal del C.A.I de Resonancía Magnetica Nuclear de la Facultad de Ciencias Químicas,en las personas de Lola, Helena, Margarita y Ángel, como lo de Masas en las personas de Nour, Cristina y Amparo. De la misma manera agradezco el SIdI de la Universidad Autónoma de Madrid. Su apoyo a la investigación ha sido relevante en la caracterización de las moléculas finales y de los intermedios.

Después de los agradecimientos a los miembros de las colaboraciónes cientifícas, pasaré a agradecer las personsas, Profesores, post doctorandos y doctorandos que hicieron y siguen haciendo parte activa de este estupendo grupo de trabajo.

Entre los "mayores" un particular agradecimiento a Juan Luis "Murcia" llamado GianGigi como el gran portero de la selección de Italia. Tuve la posibilibad, en los primeros seis meses de mi tesis, de trabajar con el y su capacidad de explicarte las cosas y la manera de hacerlas, reflejan mi idea de colaboración cientifíca. Además de ser un muy bueno investigador es también una persona estupenda, dentro y fuera del trabajo...bueno, para mi ya un "amigo" sobre quien poder contar. Muchas gracias GianGigi por todo.

Maria Ángeles, Betti, Carmencita, Luís Sanchez, Margarita Suarez, Juan Luis Toledo, Andreas, Ángel, David cierran el circulo de los mayores de este grupo. Sin ellos ni uno de nosotros hubiese podido llegar a ser bien formado como ahora y por eso, agradezco todos ellos para su esfuerzos. Gracias.

Y ahora toca a los "CABROOONES" del laboratorio. Esperando que no me olvide de nadie, estoy obligado a empezar con mi superamigo "Antonino". Desde el primer dia que puse mis pies en el laboratorio he notado que este chico era y, sigue siendo, un compañero de trabajo muy majete y eso ha permitido que nuestros cáracteres muy similares se juntasen para generar una amistad fuerte que espero se mantenga en le futuro. No tanto excelente ha sido tu ayuda en hacerme aprender un idioma tan parecido al italiano....cuantas situaciónes, emociones, momentos de vida hemos pasado juntos y compartido y, cuantos recuerdos tengo de ti y de nuestras amistad que me voy a llevar

conmigo en el sitio donde iré. Eres una persona estupenda, nada más. GRACIAS.

El listado de la gente ahora puede tomar forma y empezaré desde lo que me han conocido en los primeros años.

Agustín (Agu para mi punto de vista o también José Luís Podevilla) un gran amigo fuera y dentro del trabajo, Martita (primera chica que conocí en Madrid), rubia de pelo largo, cabronceta y super maja, una amiga a 360 grados, Helenita ("Nequik o ColaCao?") un concetrado de energía, Raul ("El Robocop"), Pierre Antoine ("El Francés") un amigo especial "transalpino", Jose ("Giuseppe"), Alberto Insuasty ("Muchachito") para las viejas y nuevas generaciónes que pisaran este laboratorio, Javi ("El Nuevo") más que un amigo y también compañero de mesa a mi mano derecha, Juan ("El Madridista") nada que decir sobre su gana de bromear, un amigo y compañero de mesa a mi mano izquierda, Daniel ("El Sueco") muy simpatico y muy buen colega de trabajo, Edu ("El Madrileño por el Mundo") amigo y compañero de viajes, Silvia ("La Spagnola") no la para nadie, Laura ("La Asturiana") ¡es la leche!, Noelia (la ritardataria) mejor decirle una hora antes si hay que quedar con ella, Sarita ("La Nueva Marta") stupenda ragazza, Alberto DJ ("El fry") el perezoso, Sonia ("La Manchega") imprescindible su armonia, Carmen ("La del Imdea") la loca de Fito, Luis ("El de Strasburgo") para todos Luismo desde siempre, Vanesa ("La Catalizadora") lista para catalizar y la del "Sabes", Valentina ("La Schizzata") un poco "grugnona" e innamorata pazza di Andrea Pirlo, Fulvio ("El Barese") ormai californiano, Carlos ("El Maquina") dejo libre interpretación..., Gustavo ("La Pizza"), Enrique ("Enrique VIII") lo del HPLC, Jaime ("El Heavy más Light") lo llamavan el niño de Talavera, Macarena ("La Andaluza") y la "s" donde "ettá", Fatima ("Fatimuchi") una amiga y persona sincera, Rosa, Marina, André ("El Brasileño"), Maria ("La Alemana") ¿un hombre más en laboratorio?, Emilio, Virginia ("La Secreteria") una mujer espléndida y siempre sonriente, Alberto ("El Kepa") siempre en movimiento, Paula ("La Calavera") la que agguanta el Kepa.

A mis amigos del proyecto FunMols: Charalambos ("El Turco") amigo de trabajo, cenas y fiestas, Murat ("El verdadero Turco"), Hui ("La Cina") un concetrado de simpatia, Marta ("La Danesa") para mi siempre mi "rolling

girl" favorida, Christina ("La Bavarese") ¡que chica!, Giorgio ("El Siciliano"), Kata y Ian ("Los Teóricos Ungaros"), mi querido fratello Pavel ("El Mexicano") persona excepcional y encantadora y muy amante de los idiomas. A todos vosotros digo que ha sido un placer conoceros y pasar momentos indimenticables a lo largo de cuatro años. Como olvidarse de los momentos pasados juntos en toda europa durante y después de los congresos. Gracias.

A la gente del CSIC: Anto, Richard, Constanza y Almu. Gracias por compartir unos momentos bonitos de mi vida madrileña. Os llevaré siempre conmigo.

A todos mis amigos "madrileños" que por necesidad nos hemos encontrado en esta ciudad encantadora, os digo Gracias y que pueda seguir esta nuestra amistad.

A todos los químicos de la tercera planta más cercanos a mi y que no son del grupo de materiales moléculares, Gracias por haber agguantado otro Italiano más de esta ciudad.

A Salvatore ("U Cumpaesanu") un agradecimiento particular después de aquel formal. En primer lugar has estado una persona a mi cercana y, luego, un colaborador científico. Gracias por todo lo que hiciste desde el primer dia que veniste a recogerme a Barajas.

Per ultimi ma non nei miei pensieri, ai miei genitori e a mio fratello che, seppur lontani, mi hanno sempre sostenuto nelle scelte prese finora e che mi sono sempre vicino in tutti i momenti della mia vita. A loro è diretto il mio più grande ***GRAZIE*** *per tutto l'affetto che mi hanno dato come figlio e come fratello e, per l'educazione ricevuta e il senso di rispetto verso gli altri. Non vi cambierei per niente al Mondo. Vi voglio bene.*

ABBREVIATIONS AND ACRONYMS

In this memory, we have used the abbreviations and acronyms according to the: "Guidelines for authors", *JOC* updated January 2013. Moreover, the following abbreviations and acronyms have been employed in the text:

ACN	Acetonitrile
AFM	Atom Force Microscopy
AM0	Air Mass 0
AM1.5	Air Mass 1.5
β	Attenuation Factor
BDA	Benzendiamine
BDC60	1,4-bis(fullero[*c*]pyrrolidin-1-yl)benzene
BDF	Benzodifuran
BDT	Benzendithiols
BHJ	Bulk HeteroJunction
CE	Counter Electrode
CP-AFM	Current Probe Atomic Force Microscopy
CR	Charge Recombination
CS	Charge Separation
CS_2	Carbon Disulphide
CT	Charge Transfer
CV	Cyclic Voltammetry
DBA	Donor-Bridge-Acceptor
DCM	Dichloromethane
DEPT	Distortionless Enhancement by Polarization Transfer
DHBT	Dihydrobenzothiophene
DMF	N,N-dimethylformamide
DPM	Diphenylmethanofullerene
DSSCs	Dye Synthesized Solar Cells
ED	Electron Donor
E_F	Fermi Energy
eq	Equivalentes
EQE	External Quantum Efficiency
E_{ox}	Oxidation Potential
E_{red}	Reduction Potential
ESI	Electrospray
ET	Electron Transfer
Et_2O	Diethyl Ether
EWG	Electron Withdrawing Group
eV	Electronvolt
exTTF	Extended Tetrathiafulvalene
fA	Femto Ampere
Fc	Ferrocene

fcc	Face centered cubic
FF	Fill Factor
G_0	G zero or G note
GCE	Glassic Carbon Electrode
η	Conversion Efficiency
HC	High Conductance
hcp	Hexagonal close packing
HMBC	Heteronuclear Multi Bond Correlation
HOMO	Highest Occupied Molecular Orbital
HPLC	High Performace (Pressure) Liquid Chromatography
HSQC	Heteronuclear Single Quantum Coherence Spectrospcopy
Hz	Hertz
I	Current
I_h	Icosahedral symmetry
IPR	Isolated Pentagon Rule
IQE	Internal Quantum Efficiency
ISC	Inter-system crossing
ITMS	Ionic Trap Mass Spectrometry
ITO	Indium Tin Oxide
J_{SC}	Short Circuit Current
L	Stretching Distance
LC	Low Conductance
LDOS	Local Density of States
LUMO	Lower Unoccupied Molecular Orbital
MALDI-TOF	Matrix Assisted Laser Desorption Ionization - Time of Flight
MCBJ	Mechanically Controllable Break Junction
MDMO-PPV	poly[2-methoxy-5-(3′,7′-dimethyloctyloxy)-1,4-phenylenevinylene
MHz	MegaHertz
μA	Micro Ampere
μ_d	Electrochemical Potential of the source
μ_s	Electrochemical Potential of the drain
MJ	Molecular Junction
MWs	Molecular Wires
Nano	10^{-9} m
Nanotech	Nanotechnology
NaOH	Sodium Hydroxide
NBS	N-Bromosuccinimide
NCS	N-Chlorosuccinimide
NP	Nanoparticle

***o*DCB**	1,2-dichlorobenzene
OFETs	Organic Field Effect Transistors
OFls	Oligofluorenes
OLEDs	Organic Field-Emitting Diodes
OPE	Oligophenylenethynilene
OPV	Oligophenylenvinilene
OPTs	Oligothiofenes
P3HT	Poly-(3-hexylthiophene)
PCBM	Phenyl-C_{61}-butyric acid-methyl ester
PDI	Perylene-3,4:9,10-bis(dicarboximide)
PET	Photoinduced Electron Transfer
PHJ	Planar HeteroJunction
PID	Proportional Integral Derivative
ppm	Part per milion
PPV	Poly-*p*-phenylenvinylene
PTSA	Para-Toluensulfonic Acid
PTZ	Phenothiazine
RE	Reference Electrode
ROE	Rotating-Frame Overhauser Enhancement
SAM	Self Assembly Monolayer
STM	Scanning Tunnelling Microscopy
STM-BJ	Scanning Tunnelling Microscopy Break Junction
STS	Scanning Tunnelling Spectroscopy
SWNT	Single Wall Carbon Nanotube
T(E)	Trasmission probability
TBAF	Tetrabutylammonium Fluoride
TCB	Trichlorobenzene
TCNQ	Tetracyano-*p*-quinodimethane
TEA	Triethylamine
$\mathbf{t_{off}}$	Natural Lifetime
TTF	tetrathiafulvalene
UPS	Ultraviolet Photoemission Spectroscopy
UHV	Ultra-High Vacuum
$\mathbf{V_{OC}}$	Open Circuit Voltage
WE	Working Electrode

INDEX

INTRODUCTION

1. INTRODUCTION

1.1 Nanoscience and Nanotechnology

Usually, we think about the progress as an actual argue but also as a word that changed the style and the quality of human life since the 50s to the end of the 20^{th} century. What will be, therefore, the new way of thinking about progress in this new century? And, what will scientific, technological and social innovations add to the society? It is possible to find at least one answer to these questions in the real meaning of two keywords: *Nanoscience* and *Nanotechnology*.

Nowadays, it is relevant to think about a feasible way to understand how *Nanoscience and Nanotechnolgy* are going to take part into our life. These two words are frequently used both in scientific literature and in common language.[1] It is curious how everybody seems to know what *Nanotechnology* (called in spoken and advertising language "*nanotech*") is, but even within the scientific community its meaning is not so clear. *Nanoscience* has exactly the same destiny. It is, thus, essential to give the correct meaning. To be artless, we can think about *Nanoscience* and *Nanotechnology* as a new branched science related to *nano* (10^{-9} m) objects. To be more professionals, we have to imagine *Nanoscience* like the study of the performance of ultra-small structures, materials and devices, usually around 1-100 nm and, much more important, it includes the manipulation of materials on an atomic or molecular size.

Nanotechnology could be basically considered as the engineering of functional systems at molecular scale. Furthermore, we can observe a direct application of *Nanoscience*. In its original sense, nanotechnology refers to the ability to build up items with newest tools.

Another interesting meaning could be given by the word dissociation: *Nano*, *Science* and *Technology*.[2] Everybody has his own idea of these three words but everybody agrees that all of them belong to the "*progress*".

"*Nano*" is essentially referred to something really little, invisible to the normal human eye. It is a prefix for something which measure 10^{-9} m, one billionth meter or "*nanometer*". The term "nano" is, therefore, used to usher the other

[1] M. Reisch, *Chem. Eng. News* **2004**, *82*, 8.
[2] V. Balzani, *Small* **2005**, *3*, 278.

two words: thus, *Nanoscience* and *Nanotechnology* are science and technology for objects of nanometer dimensions. We can also think these words are used to circumscribe the newest branches of science and technology related to the atomic and molecular structures.

"Science" did always exist and it will survive until there will be something to discover, to study, to develop. *Science* is correlated to the discoveries and innovations that changed our life from many centuries ago until now. It is a huge field which includes the macroscopic and microscopic world: astronomy, medicine, biology, physics, chemistry and what else could be related to the knowledge of the world surrounding us and the improvement of our life as well. In such specific case, science is moving towards technology.

About "*Technology*", we use to think to all the devices we touch and manage daily: mobiles, computers, TV, home tools, cars, etc…A beautiful meaning of technology is given by Balzani;[2] according to him, technology is defined as "*the ability of taking advantage of the progress of the science to create novel opportunities for practical application to get better our life*." Thus, technology is the driving force for the progress and the improvement of our life quality.

There is a side effect of this word. If we think about technology as progress, it is easy to recognize how it has also been used for negative purposes such as wars, violence, terrorism. The beautiful concept of "great asymmetry" of the word technology is thus reported by S. J. Gould:[3]

"The essential human tragedy, and the true source of science's potential misuse for destruction, lies in a great asymmetry in our universe of natural laws. We can only reach our pinnacles by laborious steps, but destruction can occur in a minute fraction of the building time, and can often be truly catastrophic. A day of fire destroyed a millennium of knowledge in the library of Alexandria, and the shot of one assassin can launch a preventable war. We have no choice, for humans must wonder, ask and seek—and science must break through the strictures of custom—to become either our greatest glory, and our most potent engine of benevolent change, or an accelerator of destruction on the wrong side of the great asymmetry".

[3] S. J. Gould *Science* **1998**, *279*, 812.

Today, *Nanotechnology* is inside the common tools we use for our works (*e.g.* computers, electronics devices for imaging and reading, etc.), in photovoltaic panels for renewable energy, in agriculture,[4] in medicine and health care,[5] in cosmetic,[6] in food industry.[7]

The first person, who coined the term *Nanotechnology* in 1974, was Norio Taniguchi which affirms that *Nanotechnology* is related to materials smaller than 1 micron. K. Eric Drexler was who promoted this word in the 80s. He contemplated *Nanotechnology* as an original idea to build up machines in molecular scale until nanometer ranges.

Another visionary of the miniaturization process was *Richard Feymann*, who said during his speech in an annual meeting of the American Physical Society at California Institute of Technology (Caltech) in 1959, the following words:[8]

"I would like to describe a field, in which little has been done, but in which an enormous amount can be done in principle. This field is not quite the same as the others in that it will not tell us much of fundamental physics (in the sense of, "What are the strange particles?") but it is more like solid-state physics in the sense that it might tell us much of great interest about the strange phenomena that occur in complex situations. Furthermore, a point that is most important is that it would have an enormous number of technical applications. What I want to talk about is the problem of manipulating and controlling things on a small scale.

As soon as I mention this, people tell me about miniaturization, and how far it has progressed today. They tell me about electric motors that are the size of the nail on your small finger. And there is a device on the market, they tell me, by which you can write the Lord's Prayer on the head of a pin. But that's nothing; that's the most primitive, halting step in the direction I intend to discuss. It is a staggeringly small world that is below. In the year 2000, when they look back at this age, they will wonder why it was not until the year 1960 that anybody began seriously to move in this direction".

All these new concepts result in such way in an improvement of cultural and social life-style. Therefore, *Nanotechnology* is the candidate to become so important in the future.

---

[4] A. Ditta, From *Advances in Natural Sciences: Nanoscience and Nanotechnology* **2012**, *3*, 033002/1.
[5] S. Hatziantoniou, C. Demetzos, *Pharmakeutike* **2006**, *19*, 86.
[6] P. Singh, A. Nanda, From *Toxicological & Environmental Chemistry*, Ahead of Print.
[7] L. Rashidi, K. Khosravi-Darani, From *Critical Reviews in Food Science and Nutrition* **2011**, *51*, 723.
[8] R. P. Feymann, *Caltech Engineering and Science*, **1960**, *23*, 22.

Anyway, science and technology will keep on walking together even passing from the micro-world to the nano-world. Several scientists suppose that the future stays in *Nanoscience* and *Nanotechnology*.

It is recognized that in the last decades, the scientific branches were getting closer and closer once we were moving towards the *nano*-world (Figure 1).

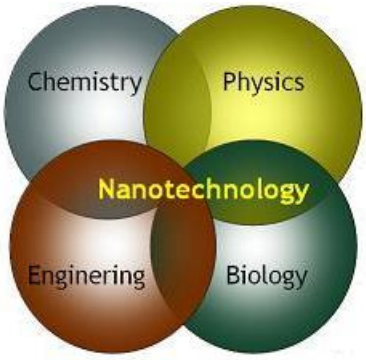

Figure 1. Nanotechnology as an interdisciplinary science.

The actual technological development, in particular in the field of *Nanoscience*, needs innovative materials with optical, magnetic, electronic and optoelectronic properties. Specially, thanks to organic synthesis, it has been possible to think and, afterwards, create new organic molecular materials with their own functions and applications in different devices. In particular, such materials are based on four different principles: structure, processing, performance and properties (Figure 2).

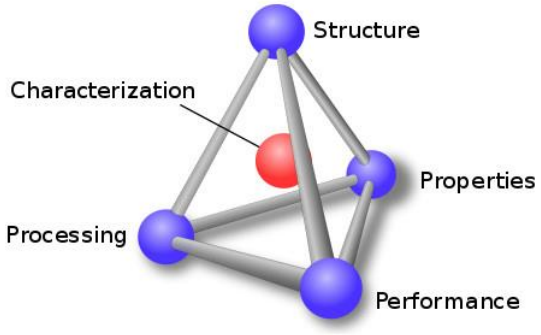

Figure 2. The four principles at the base of organic molecular materials.

It is interesting to note how molecular organic materials show several advantages compared with inorganic ones. First of all, the huge range of organic reactions let the chemists to introduce chemical modifications onto basic structures in order to have changes on their chemical and physical properties.

In such a way it is possible to tune the properties of the desired material depending upon the functions we are looking for. Furthermore, these materials have to be easy to handle in order to create devices.[9]

Among the typical disadvantages of organic materials for industrial applications, we can mention the lack of chemical, thermal, photochemical or electromagnetic stability, and the quite low reproducibility of their properties. This means the loss of their physical properties after a well-defined turnover number.

Another crucial point to be analysed in *Nanoscience* and *Nanotechnology* development is the "social impact" that they will produce. This aspect represents an enigma to be discovered. But it has always been a factor to consider because the scientific and technological innovations could have to be corresponded to the real time forever.

1.2 Miniaturizations: "top-down" and "bottom-up" approaches

The miniaturization process of components for the build-up of useful devices is, nowadays, obtained by top-down approach (it will be discussed below). *Gordon Moore*, the co-founder of Intel® Company, presented in 1965 the theory of the electronic evolution, well known as *Moore's Law*[10]. In his opinion, the price and the size of the integrated transistors of circuits based onto silicon materials is going to be divided into a factor of two roughly every 18 months. Currently, the transistors size reaches the nanometric scale.

[9] a) J. S. Miller, *Adv. Mater.* **1990**, *2*, 98; b) A. Kraft, A. C. Grimsdale, A. B. Holmes, *Angew. Chem. Int. Ed. Engl.* **1998**, *37*, 402.

[10] G. E. Moore, *Electronics*, **1965**, 38.

It appears the unique physical limitation to the above mentioned law, since some quantum phenomena could affect the circuit optimization.

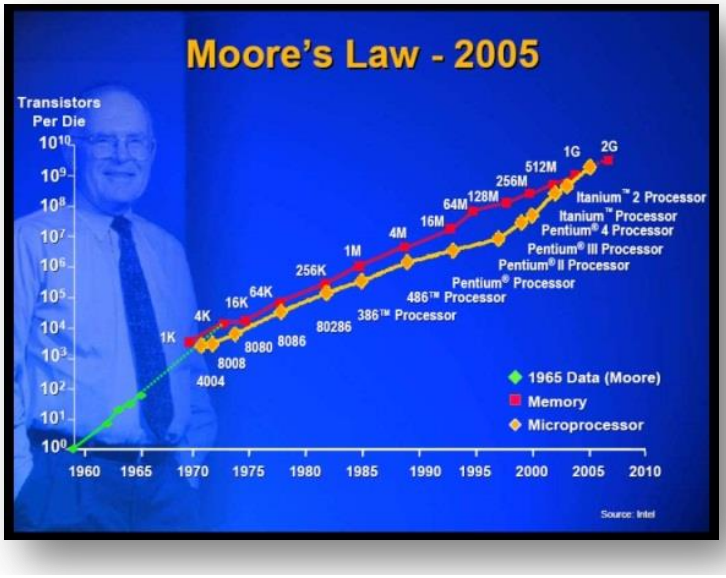

Figure 3. Graphic representation of the silicon integrated transistors number in function of the time (in years).

Moore's Law explains how the improvements in electronics devices such as computers, memory capacities, sensors and pixels in usual cameras are related to this exponential technological growth. In agreement with the theory, the technological growth had a big exponential behaviour up to 2010 (Figure 3). From 2010 to 2013, the exponential growth has a rest until the next years in which transistors counts and density are to double each three years. Anyway, Moore's Law describes a driving force of technological and social change in the late 20th and the early 21st centuries. The new scientific network provides for the development of new devices made, for instance, by organic materials. Thus, we can confer to the material the properly chemical modification in order to have different physical properties.Doing that, for instance, we can measure the electron transfer along the molecules in their fundamental state.[11]

[11] a) M. R. Wasielewski, *Chem. Rev.* **1992**, *92*, 435; b) R. T. Hayes, M. R. Wasielewski, D. Gosztola, *J. Am. Chem. Soc.* **2000**, *122*, 5563; c) H. Duerr, S. Bossmann, *Acc. Chem. Res.* **2001**, *34*, 905; d) J. M. Endtner, F. Effenberger, A. Hartschuh, H. Port, *J. Am. Chem. Soc.* **2000**, *122*, 3037; e) *Acc. Chem. Res.* **1999**, *32*, 191. Special Number dedicated to *Molecular Materials in Electronics and Optoelectronic Devices.*

The first theoretical and experimental efforts in this field began in the 70s with a work (inspired by nature) published by Aviram and Ratner,[12] in which was predicted theoretically that a DBA system (Donor-Bridge-Acceptor) could be connected, as a part of an electric circuit, to two metal electrodes and acts as molecular junction (MJ). In particular D is a donor, *e.g.* tetrathiafulvalene (TTF) and A is an acceptor, *e.g.* tetracyano-*p*-quinodimethane (TCNQ). It should act as a molecular rectifier because it enables the electronic transfer in only one direction. The proposed rectification is due to the electron transfer (ET) in the following direction: cathode - acceptor – donor – anode (Figure 4).

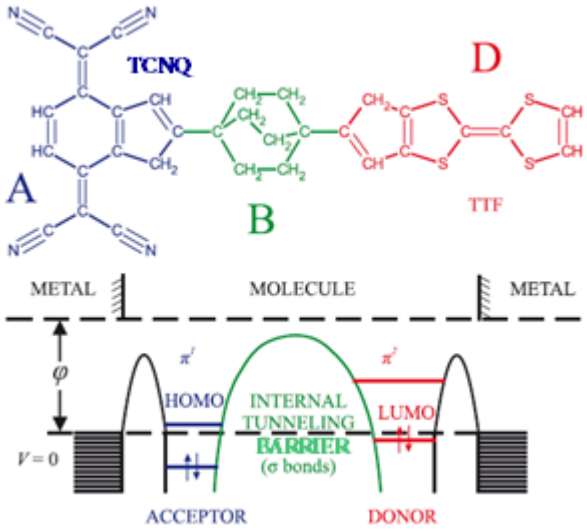

Figure 4. First proposal of molecular organic rectifier.

The top-down approach leads physicists and engineers to manipulate smaller pieces of matter by lithographic techniques and related ones. Unfortunately, the top-down approach has a limitation for dimensions smaller than 100 nm,[13] due to the lower limit of light wavelength employed in lithographic processes. Furthermore, there are many concerns about the semiconducting behaviour of silicon below such limits.

[12] A. Aviram, M. A. Ratner, *Chem. Phys. Lett.* **1974**, *29*, 277.

[13] R. F. Service, *Science* **2001**, *293*, 785.

The alternative to this limitation is the *bottom-up* approach, which let us to build up nanostructures from nano or subnanoscale objects (atoms and molecules). Such approach is the way because chemists, being able to manipulate atoms and molecules, are in perfect position to contribute to the development of *Nanoscience* and *Nanotechnology*. Also for such a reason, chemists are going to change their point of view about the traditional chemistry: the molecules or atoms change their chemical behaviour when in a nanoscale environment. One of the most remarkable example is graphene[14] (it conferred the Nobel award in Physics in 2010 to André Geim and Kostantin Novoselov). This novel material has the properties of no conductor in the microscopic world as graphite (multi-layered graphene material), but it becomes conductor in the nanoscale world as graphene (bidimensional material). In the same way, the chemical reactivity of some metals could be envisaged or changed passing by micro to nano world. Using the bottom-up approach, chemists can play with the atoms or molecules giving them particular properties and perform specific functions or obtaining beautiful nano-objects without any kind of function. To see them, physics help chemistry using newest tools such as STM (scanning tunnelling microscopy) and AFM (atomic force microscopy). STM will be explored in more details within this memory.

Nanoscience and *Nanotechnology* are still in their infancy period. At the present, new exciting results and sometimes disappointments alternate on the scene, as always happens in new fields. Hopefully, they will contribute to solve the four big problems that face the large part of earth's population: food, health, energy and pollution. Doing that, scientists don't have to forget the aforementioned "great asymmetry" principle.

[14] a) J. C. Meyer, A. K. Geim, M. I. Katsnelson, K. S. Novoselov, T. J. Booth, S. Roth, *Nature* **2007**, *446*, 60; b) K. S. Novoselov, A. K. Geim, S. V. Morozov, D. Jiang, Y. Zhang, S. V. Dubonos, I. V. Grigorieva, A. A. Firsov, *Science* **2004**, *306*, 666.

BACKGROUND

2. BACKGROUND

2.1 Introduction to [60]fullerene

2.1.1 C_{60} structure and general reactivity

Fullerenes are a family of molecules constituted exclusively by carbon atoms. In sharp contrast with the other carbon allotropes, diamond and graphite, they present a precise number of carbon atoms, spatially disposed in high symmetric closed cages with defined shape and geometry. Similarly to fullerenes and nanoonions, carbon nanotubes, single wall (SWNT) or multi wall (MWNT) and nanohorns feature curved surface of trigonal hybridized carbon atom but forming an indefinite net (see Figure 5). Finally, graphene, where carbon atoms are arranged in a hexagonal plane pattern, could be described as a sheet of graphite.[15]

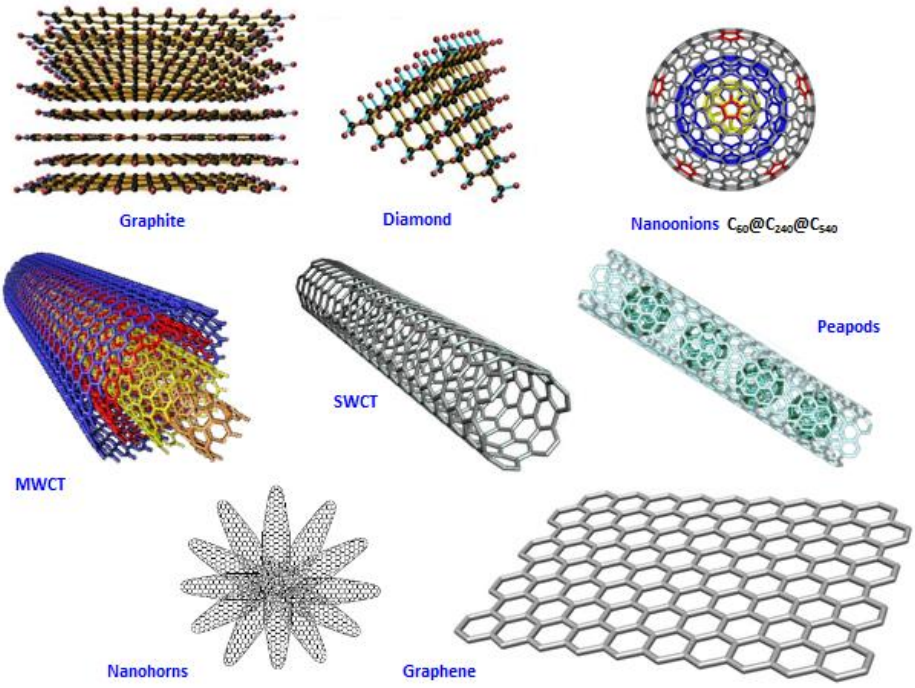

Figure 5. Some of the known carbon nanoforms.

[15] E. H. L. Falcao, F. Wudl, *J. Chem. Techn. & Biotechn.* **2007**, *82*, 524.

As a consequence of its molecular nature, fullerenes represent the first class of molecules made by only carbon atoms able to be dissolved in common organic solvents.[16] In particular, the smallest stable fullerene and the most studied is C_{60}. It has an icosahedral symmetry (I_h) made by 12 pentagonal rings and 20 hexagonal rings kept together by two different bonds (Figure 6): the shorter are [6,6] double bonds (1.37 Å) and the longer are [5,6] single bonds (1.45 Å).

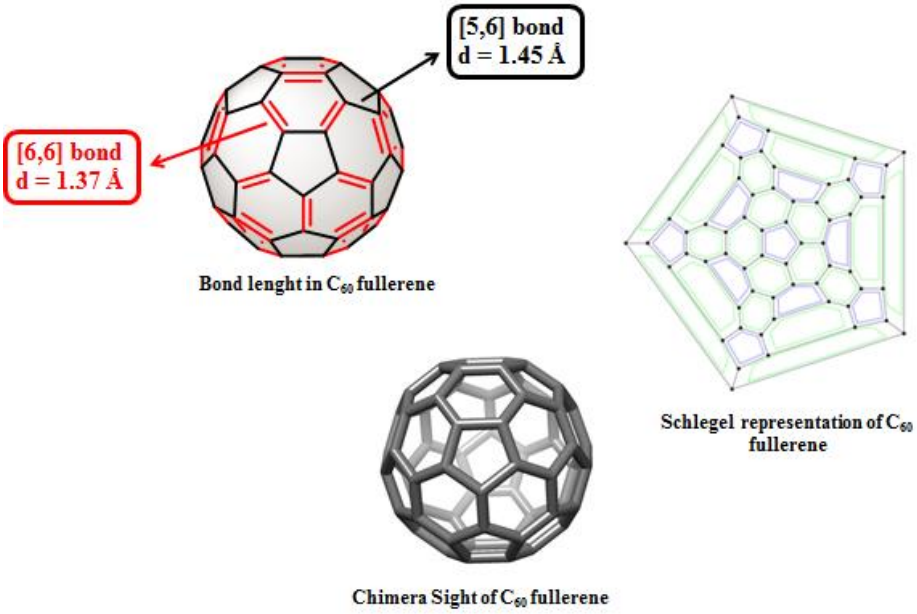

Figure 6. Different representations of C_{60} molecule with bond lengths.

The bond length alternation in the C_{60} molecule shows that the double bonds are located at the junctions of the hexagons and there are no double bonds inside the pentagonal ring. Each hexagon exhibits a cyclohexatriene character and each pentagon a [5]radialene character.

Owing to the convex shape of fullerene generated by the presence of pentagons that tilts the organization of hexagon rings into a constrained cage-shape, each

[16] See some fullerene books as: a) D. M. Guldi, N. Martín Eds., *Fullerenes: From Synthesis to Optoelectronic Properties*, Kluver Academic Publishers, Dordrecht, the Netherlands, **2002**; b) F. Langa, J.-F. Nierengarten Eds., *Fullerenes. Principles and Applications*, RSC, Cambridge, United Kingdom, **2007**; c) N. Martín, F. Giacalone, Eds., *Fullerene Polymers. Synthesis, Properties and Applications*, Wiley-VCH, **2009**; d) A. Hirsch, Michael Brettreich, *Fullerenes-Chemistry and Reactions*, Wiley-VCH, **2005**.

carbon atom shows a peculiar $sp^{2,3}$ hybridization.[17] The driving force of the reactivity of fullerene is due to the release of strain energy that comes out from the saturation of one or more double bonds. As a consequence to this principle, the most reactive site will be situated between two adjacent hexagonal rings.

The stability of C_{60} has been demonstrated through the *isolated pentagon rule* (IPR), developed by H. Kroto in 1987. It says that the local tension enhances with the number of shared bonds between two pentagon rings (pentalene), leading to less stable molecules. Owing to this rule, the easier fullerenes to be formed will be those in which two pentagons must be separated by hexagonal rings.[18]

The presence of pentagons not only produces a major tension of the bond angle of the molecule, but, also, a destabilization of the π-electron cloud.[19] In this regard, a spherical shape distributes the strain as evenly as possible and minimize the anisotropic contribution to the strain energy.

As aforementioned, C_{60} fullerene, differently from the other allotropic carbon forms, can be functionalised to obtain new compounds more soluble in common organic solvents. Because fullerene's family does not have any kind of functionalization, its reactivity becomes peculiar and restricted to the transformation of sp^2 into sp^3 carbon atoms. The fullerene chemical behaviour is comparable with an electron poor poly-olefin. Therefore, it gives rise to addition reactions onto double bonds, which are more reactive than a normal olefin. This better reactivity resides on its strain generated by the curvature of the fullerene shape. This aspect is pronounced in C_{70} molecule where the equatorial region has different reactivity compared with the more reactive polar regions. Among all known organic reactions, the nucleophilic addition and the cycloaddition reactions have been widely employed to modify fullerenes for their practical applications.

[17] R. C. Haddon, *Acc. Chem. Res.* **1992**, *25*, 127.
[18] H. W. Kroto, *Nature* **1987**, *329*, 529.
[19] T. G. Schmalz, W. A. Seitz, D. J. Klein, G. E. Hite, *Chem. Phys. Lett.* **1986**, *130*, 203.

2.1.2 C_{60} optoelectronic properties

The discovery of C_{60} with its remarkable properties has prompt a great interest in the search of potential applications. C_{60} shows unique optical[20], electronic[21] and photophysical[22] properties which make C_{60} buckyball prominent in the field of organic electronics and in applications in some devices.

Fullerenes present remarkable electron acceptor properties. The small reorganization energy[23] (the energy cost due to the structural modification to go from a neutral species to a negatively charged species) make them extremely useful as acceptor component in ET processes. Indeed, the electrochemical behaviour of C_{60} species was analysed by cyclic voltammetry (CV).[24] As result of this work, it has been possible to define the exact value of threefold degenerated *lower unoccupied molecular orbital* (LUMO, t_{1u}) of C_{60} and its derivatives as well. LUMO orbitals resides at 1.5-2.0 eV above the fivefold degenerated *higher occupied molecular orbital* (HOMO, h_u). The six electron acceptor reversible capability of fullerene came out in experiments at -10° C in a solution of toluene:ACN,[25] and recently, in systems in which C_{60} has been immobilized onto electrodes.[26] Thanks to this property, either C_{60} or its derivatives may be employed as *n*-type conducting materials in photovoltaic devices as well as in organic electronics. Other feasible applications concern its use as superconducting and ferromagnetic materials,[27] in the fabrication of photoelectric and molecular electronic devices,[28] in artificial photosynthetic systems,[29] or in systems with non-linear optical properties.[30]

[20] L. W. Tutt, A. Kost, *Nature*, **1992**, *356*, 225.
[21] L. Echegoyen, *Acc. Chem. Res.* **1998**, *31*, 593.
[22] D. M. Guldi, M. Prato, *Acc. Chem. Res.* **2000**, *33*, 695.
[23] D. M. Guldi, *Chem. Commun.* **2000**, 321.
[24] R. E. Haufler, J. Conceicao, L. P. F. Chibante, Y. Chai, N. E. Byrne, S. Flanagan, M. M. Haley, S. C. O'Brien, C. Pan, *J. Phys. Chem.* **1990**, *94*, 8634.
[25] Q. Xie, E. Pérez-Cordero, L. Echegoyen, *J. Am. Chem. Soc.* **1992**, *114*, 3978.
[26] N. M. Alpatova, N. F. Goldshleger, E. V. Ovsyannikova, *Russian J. Electrochem.* **2008**, *44*, 79.
[27] A. F. Hebard, M. J. Rosseinsky, R. C Haddon, D. W. Murphy, S. H. M. Glarum, T. T. M. Palstra, A. P. Ramirez, A. R. Kortan, *Nature* **1991**, *350*, 600.
[28] a) D. M. Guldi, B. M. Illescas, C. M. Atienza, M. Wielopolski, N. Martín, *Chem. Soc. Rev.* **2009**, *38*, 1587; b) L. Ouali, V. Krasnikov, G. Hadziioannon, *J. Am.Chem. Soc.* **2000**, *122*, 7467.
[29] E. Peeters, P. A. van Hal, J. Knol, C. J. Brabec, N. S. Sariciftci, J. C. Hummelen, R. A. J. Janssen, *J. Phys. Chem. B* **2000**, *104*, 10174.
[30] N. J. Long, *Angew. Chem., Int. Ed.* **1995**, *34*, 21.

The photophysical properties of C_{60} show an absorption spectra where the strong absorptions for C_{60} lie at 213, 257 and 329 nm (with ε_{max} = 135000, 175000, 51000 respectively) and also a typical sharp absorption peak at 408-410 nm. An extensive series of weak and broad bands is observed between 420 and 620 nm which may be referred to the first order forbidden singlet-singlet transitions between HOMO (h_u) and LUMO (t_{1u}).[31] From the singlet excited state, C_{60} passes rapidly to the most stable triple excited state through a inter-system crossing (ISC) process. Such excited specie survives for 133 μs (lifetime) in degased solvent and it is deactivated by non-radiative process to the ground state. When the oxygen is present, the triplet excited state of C_{60} promotes the formation of singlet molecular oxygen acting, therefore, as sensitizer.

Moreover, fluorescence emission of singlet excited state (S_1) can be seen at 703 nm ($\Phi_f = 1 \times 10^{-4}$) but phosphorescence is too weak to be observed.

[31] K. Kordatos, T. Da Ros, M. Prato, R. V. Bensasson, S. Leach, *Chem. Phys.* **2003**, *293*, 263.

2.2 Molecular wires (MWs)

A "*molecular wire*" may be considered as the simplest component within an electronic circuit. In its broadest definition, a molecular wire has been defined as a molecule connected between two reservoirs of electrons such as two metal electrodes.[32] Often its behaviour is referred to a molecule that conducts electrical current between two electrodes;[33] or even more narrowly as a device that conducts in a regime wherein the distance-dependence of electron transfer may be very "weak".[34]

Two different strategies have been employed to study the behaviour of a single molecule as a molecular wire: i) "*photoinduced electron transfer*" (PET) process, measuring the kinetics of electron transfer process by photophysical study of the decay of the relevant transient species in systems like donor-bridge-acceptor;[28a] ii) studying the molecular behaviour by "*scanning tunnelling microscopy*" and by "*mechanically controllable break junction*" (MCBJ) at the nanometer scale. The influence of the so called "*anchor group*" plays an important role in this kind of studies.[35] Properties of molecular wires such as stiffness of organic material, chemical, thermal, photochemical, electromagnetic stability and, good capability to transport electrons in a directional path at nanometric distance are of paramount importance.

[32] E. G. Emberly, G. Kirczenow, *Phys. Rev. B* **1998**, *58*, 10911.
[33] A. Nitzan, M. A. Ratner, *Science* **2003**, *300*, 1384.
[34] W. B. Davis, W. A. Svec, M. A. Ratner M. R. Wasielewski, *Nature* **1998**, *396*, 60.
[35] M. Mayor, H. B. Weber, *Angew. Chem. Int. Ed.* **2004**, *43*, 2882.

2.2.1 Photoinduced Electron Transfer: "Macroscopic Approach"

PET processes are studied on organic molecules of type DBA and consist in an irradiation of the molecule by an external impulse; the molecule, so excited, distributes the charge over its π surface until the formation of the radical cation onto the donor moiety or the bridge and, the radical anion onto the acceptor unit thus giving rise to a charge separated state. In general, the donor moiety is irradiated but in some cases also the bridge or the acceptor may be irradiated as well (Figure 7).

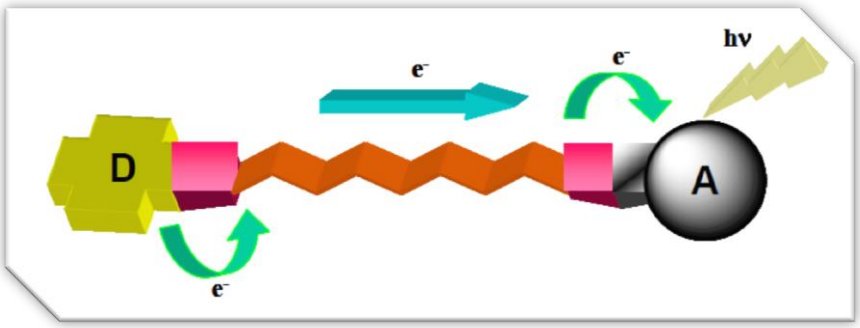

Figure 7. Model DBA system and its electron transfer from the donor to the acceptor unit.

Many examples of DBA systems have been reported in literature until now.[36] Chemistry plays an important role in the design and synthesis of such molecules and a wide variety of donor moieties and acceptor units (in our case fullerene) have been reported so far. Concerning the bridge, the general and more common is to have a π-conjugated system in order to make the electron transfer feasible along the wire. Better performances are obtained if this conjugation is extended to the donor and/or acceptor moiety. In such systems, the electron transfer rate is a factor that depends essentially of the nature of the donor and acceptor fragments, the reorganization energy λ and, the electronic coupling (V) induced by the bridge with the donor and acceptor, respectively. The energy difference between the donor and acceptor gives rise to a redox potential gradient responsible of the electron transfer as a cascade process. The

[36] O. S. Wenger, *Chem. Soc. Rev.* **2011**, *40*, 3538.

large distance charge transfer (CT) is an intrinsically non adiabatic process,[37] which can be understood in terms of a nonradiative decay process between the vibronic levels of DA and excited species D^+A^-, respectively. The rate of such phenomena is distance dependent; if the bridge's length is large, the hopping mechanism is favourable, whilst if the bridge's length is small, the tunnelling effect or "super-exchange electron transfer" is preferred. It is now important to clarify these two effects.

During the tunnelling effect (denominated for the first time by Kramers[38] and then by Anderson[39]), the electron transfer occurs from the donor to the acceptor through a tunnel in the energy barrier (Figure 8). During the electron transfer, the orbitals of the bridge are only used as a mean of coupling with no nuclear movement along the bridge (no charge resides on the bridge). This mechanism is no temperature dependent and occurs when the bridge orbitals (above all the LUMO) are not energetically accessible or, in other words, when the electronic coupling is not considerable.

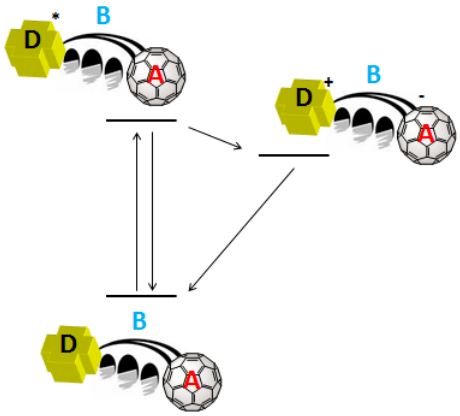

Figure 8. Super-exchange electron transfer or tunnelling effect over DBA system.

[37] a) R. A. Marcus, N. Sutin, *Biochem. Biophys. Acta, Rev. Bioenerg.* **1985**, *811*, 265; b) E. Emberly, G. Kirczenow, *Nanotechnology* **1999**, *10*, 285; c) J. Jortner, *J. Chem. Phys.* **1976**, *64*, 4860.
[38] H. A. Kramers, *Physica* **1934**, *1*, 182.
[39] P. W. Anderson, *Phys. Rev.* **1950**, *79*, 350; b) P. W. Anderson, *Phys. Rev.* **1959**, *115*, 2.

In case that hopping mechanism is prevailing, the bridge orbitals take directly part of intermediate energetically affordable states which dispose changes in the molecular geometry due to the formation of a charged intermediate excited state which evolves to the more stabilised species where positive charge resides on the donor and negative charge on the acceptor (Figure 9). The bridge is thus acting as a pathway for the electron transport; the electronic coupling between bridge and terminal moieties is now considerable and the orbitals of the bridge (especially LUMO) are energetically accessible to promote an electron transfer along the bridge itself. This phenomenon is temperature dependent.

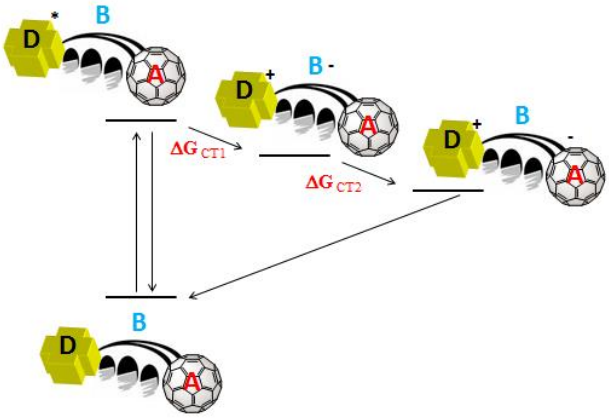

Figure 9. General hopping effect over DBA system.

To resume and in agreement with Jortner *et al.*,[40] the hopping mechanism happens when: i) there is a near-resonant charge injection (E_G) where the energy levels of the donor and the bridge units are similar or when the energy level of the donor is not so much higher than that of the bridge; ii) there is a vibrational overlap of the states referred to the ionic formed couple, iii) does exist a vibrational overlap of the states referred to the ionic formed couple in which the charge is localized in the linker between the donor and the acceptor unit. Therefore, this mechanism is extremely dependent of the nature of the bridge, the charge diffusion from the donor to the acceptor and temperature. Figure 9 shows that in the initial state, donor, bridge and acceptor are neutral. In the excited state, the donor is oxidized and the bridge is reduced. At this moment, if the difference in energy of both states is huge, a super-exchange ET

[40] J. Jortner, M. Bixon, T. Langenbacher, M. E. Michel-Beyerle, *Proc. Natl. Acad. Sci. U.S.A.* **1998**, *95*, 12759.

occurs; otherwise super-exchange or hopping mechanism can compete if this energy gap is comparable to the reorganization energy or electronic coupling.

Anyway, the quality of a molecular wire can be obtained by the Equation 1, where the kinetic constant of the electron transfer process is given by:

$$k_{ET} = k_0 \exp(-\beta R_{DA})$$

Equation 1. Equation for the kinetic constant of ET processes.

where k_0 is the temperature-dependent prefactor typical for the deactivation of charge transfer processes and it depends on the donor-acceptor, r_{D-A} distance. β is the so called "attenuation factor" used for the quality of the wire and it is independent of the distance. As smaller the β value, the better chance that the charge does not suffer any penalization during the transfer processes. In other terms, the lower is the beta value, the weaker is the distance-dependence of the wire. The β value is a parameter for the whole DBA system where donor and acceptor are molecular units or metallic contacts and, it is strictly not referred to the bridge itself. Thus, for a fixed bridge, the β value is dependent on the energetic level difference of the subunits forming the bridge,[41] which can be understood in terms of electronic coupling between the components of the systems under study.

Upon light irradiation on the organic molecules, charge separation is observed in DBA system. The subsequent charge recombination process depends on the nature of the molecule. In general, *charge recombination* (CR) processes are some orders of magnitude slower than *charge separation* processes (CS). The kinetic study of CS and CR for a molecular series with different wire-length allows to achieve the lifetime of the charge separated state, using time resolved absorption spectroscopic techniques.

[41] M. P. Eng, B. Albinsson, *Angew. Chem. Int. Ed.* **2006**, *45*, 5626.

Finally, from the logarithmic representation of both constants k_{CT} or k_{CR} *versus* $r_{D\text{-}A}$, the β value is obtained (slope of the lines) in a comparable way, as shown for the triad C_{60}-*o*PPE-exTTF synthesized in our group (Figure 10).[42]

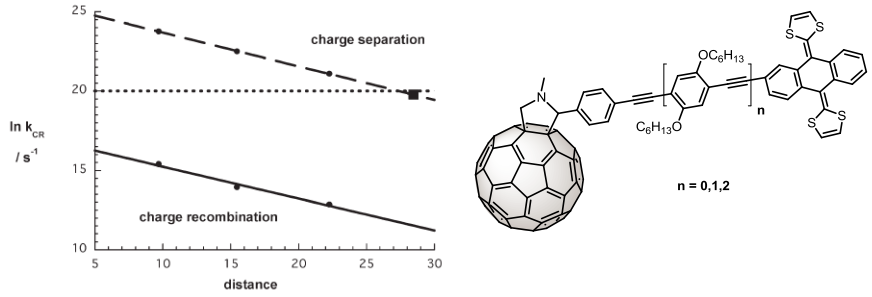

Figure 10. CT and CR of C_{60}-*o*PPE-exTTF triads. The dotted line represents the singlet lifetime of fullerene.

DBA molecules behave upon light irradiation as artificial photosynthetic systems which have allowed the study in a simple way of rather natural complex processes. Furthermore, they are also of interest for photovoltaic applications where electron transfer processes upon light irradiation play a fundamental role.[43]

[42] M. Wielopolski, C. Atienza, T. Clark, D. M. Guldi, N. Martín, *Chem. Eur. J.* **2008**, *14*, 6379.
[43] a) N. Martín, L. Sánchez, M. A. Herranz, B. Illescas, D. M. Guldi, *Acc. Chem. Res.* **2007**, *40*, 1015; b) special number on "*Organic Photovoltaics*" (Eds.: J. L Brédas, J. R Durrant), *Acc. Chem. Res*. **2009**, *42*, 1689.

2.2.2 Fluorene bridge in wire-like molecules

Oligofluorenes (OFls) have also been linked to donor and acceptor molecules in DBA systems in order to study the effect of the length bridge in the charge separation and recombination phenomena by photoinduced electron transfer experiments. In the work of Wasielewski and coworkers,[44] oligofluorenes act as bridge between a phenothiazine (PTZ) donor moiety and a perylene-3,4:9,10-bis(dicarboximide) (PDI) acceptor unit. Semiempirical AM1 method clearly shows that OFls have a torsional angle of 85°, 59° and 37° relative to PTZ, PDI and adjacent fluorene units in the ground state, respectively. Our attention is focused on the value of torsional angle between the two fluorene units that are far from the planarity due to a single bond connection. This aspect has to be taken into account during the conductive measurements where the most planar is the molecular system, the larger will be the overlapping of the π orbitals and, subsequently, a better electronic communication is achieved. It has been calculated that the torsional angle value between the fluorene units decreases passing from two fluorene units to three or four units. Interestingly, theoretical calculations reveal that the HOMO of the excited species *o*FL$^{\bullet+}$ is completely localized onto the bridge (Figure 11). In Fl-Fl bridge, it is spread over all the surface of bifluorene while, enhancing the number of monomers, it is situated at the terminal fluorenes providing excellent electronic coupling between the donor and the bridge as well as between the bridge and the acceptor.

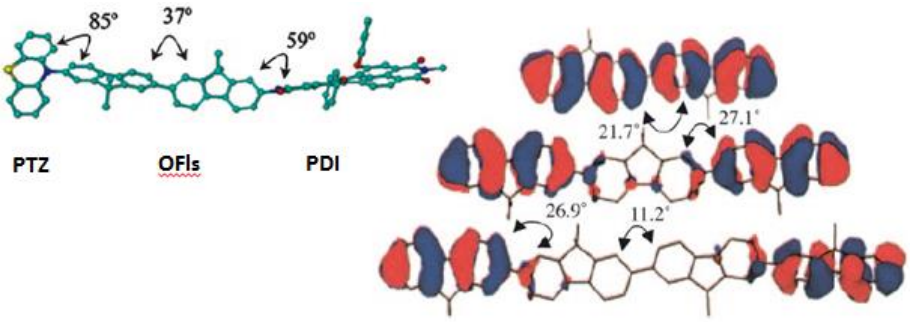

Figure 11. Molecular modelling of PTZ-$(OFl)_2$-PDI with the torsional angle between each subunit (left) and, HOMO orbitals representation for the OFLs$^{\cdot+}$ bridges (right).

[44] R. H. Goldsmith, L. E. Sinks, R. F. Kelley, L. J. Betzen, W. Liu, Emily A. Weiss, M. A. Ratner, M. R. Wasielewski, *Proc. Natl. Acad. Sci. U.S.A.*, **2005**, *102*, 3540.

As consequence, the charge separation and the charge recombination phenomena are only weakly distance dependent; even elongating the bridge, the conductance value does not change significantly. Therefore, the β value does not depend on the length of the wire and, an attenuation factor of 0.093Å^{-1} has been found. In particular, the charge recombination process through oligofluorenes is dominated by incoherent hopping at long distance and occurs on the nanosecond scale for these systems.

Olygofluorene-based DBA systems involving C_{60} and extended tetrathiafulvalene (exTTF) have been prepared in our group[45] to study the wire-like behaviour of the fluorene bridge (Figure 12). The β value found for our system was 0.09 Å^{-1} exactly the same that found by Wasielewski *and col.* which reveals the excellent intrinsic properties of the oligofluorene as a bridge for charge transport.

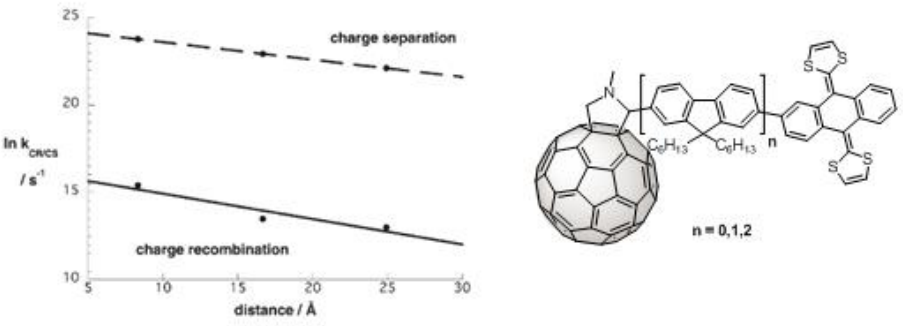

Figure 12. Variation of the kinetic constant versus distance for a series of OFls with its charge separation and charge recombination process. The slope of both mechanism represents the attenuation factor for these systems.

[45] C. Atienza-Castellanos, M. Wielopolski, D. M. Guldi, C. van der Pol, M. R. Bryce, S. Filippone, N. Martín, *Chem. Commun.* **2007**, 5164.

2.2.3 Molecular junctions: a "Nanoscopic Approach" studied by STM and MCBJ techniques

Charge transport on a single molecule has caught the attention of many scientists in the last ten years. The understanding of all the processes that are involved into electron transport are the basement of future nano-circuits. In this regard, *Nanoscience* as an interdisciplinary field helps us to figure out the principles, mechanisms and, aspects of this nano-phenomena.

Nowadays, the modern techniques may help us to understand what are the physical and chemical mechanisms that underlie behind electron transfer through a single molecule. There are some techniques[46] to fabricate the devices and, among them we have to mention: i) scanning tunnelling microscopy, ii) current probe atomic force microscopy (CP-AFM), iii) scanning tunnelling spectroscopy (STS) or STM-break junction (STM-BJ), iv) crossed-wire geometry, v) nanoparticle junctions, vi) mechanically controlled break junctions, vii) electromigration setups, nanopores, and viii) liquid metal junctions employing mercury or eutectic alloys of gallium and indium.

The experiments are characterized by a strong coupling (low-resistance contacts) between the molecule and the metal leads. To achieve the strong coupling, we have to consider two parameters: i) clean metal surface, easy to be achieved by ultra-high vacuum (UHV) and ii) the contact area should not come in contact with liquid or gaseous solvents.

In any case, theoretical studies of the electronic conductance of one molecular wire bring together different methods from chemistry and physics. Quantum chemistry is used to model the energy of the molecule. It is also incorporated into the study of the coupling between the molecule and the metallic reservoirs. Once these issues have been addressed, it is possible to proceed to the electron transport problem. Currently, Landauer theory[47,32] is used and it relates the conductance to the electron transmission probability. According to this theory, physical processes are getting easier if the transport of electrons is consider as one electron elastic scattering problem. An electron incident from the source lead with an energy *E*, has a transmission probability *T(E)* to scatter through the molecule into the drain lead. By determining the transmission probability for a range of energies around the Fermi energy (E_F) of the source lead, the finite temperature, finite voltage and Landauer formula can be used to calculate

[46] J. Loos, *Adv. Mater.* **2005**, *17*, 1821.
[47] R. Landauer, *Phys. Lett. A* **1981**, *85*, 91.

the transmitted current I as a function of the bias voltage, V , applied between the source (left lead) and drain (right lead).

$$I(V) = \frac{2e}{h}\int_{-\infty}^{\infty} \mathrm{d}E T(E)\left(\frac{1}{\exp[(E-\mu_s)/kT]+1} - \frac{1}{\exp[(E-\mu_d)/kT]+1}\right)$$

Equation 2. Landauer Formula.

where μ_s and μ_d are the electrochemical potentials referred to the source and drain, respectively. They are defined to be μ_s = E_F + eV/2 and μ_d = E_F - eV/2. T(E) has been found by solving the Schrödinger equation for one electron where its wavefunction is a sum of three wavefunctions of the propagating electron in the source lead, within the molecule (for the electron tunnelling and not scattering to the source) and in the drain lead.

The conductance of a single molecular junction is substantially depending on the local density of state (LDOS) of the contact metal atoms at the Fermi level, energy difference between the molecular and the metal orbitals (E_i - E_F) and the extent of the hybridization of the orbitals. Large value of LDOS, small E_i - E_F and effective orbital hybridization are essential to have a high conductivity in the molecular junction. Furthermore, as we will discuss afterwards, the stability of the molecular wire within the junction is of paramount importance for the conductance value which will depend not only on this aspect. Chemistry point of view cannot be set aside for the study of the molecular junction stability.

Herein, we will discuss in detail the scanning tunnelling microscopy together with mechanically controllable break junction techniques and, therefore, it is advisable to analyse them separately into two new sections.

2.2.3.1 Scanning tunnelling microscopy (STM)

Scanning tunnelling microscopy was introduced 25 years ago, for the first time by Gerd Binnig and Heinrich Rohrer[48] in the IBM research laboratories in Zurich (Figure 13b). Because of this invention, they were awarded the Nobel Prize in Physics in 1986. In this way, they revolutionised the manner to think about new electronic circuits made by only one molecule,[49] which acts as molecular junction between two electrodes. At the beginning, it was an excellent tool to see the nanoscale structures under ultra-high vacuum conditions such as atoms and molecules onto the surface. However, modern applications of STM go beyond the simple visualizations.

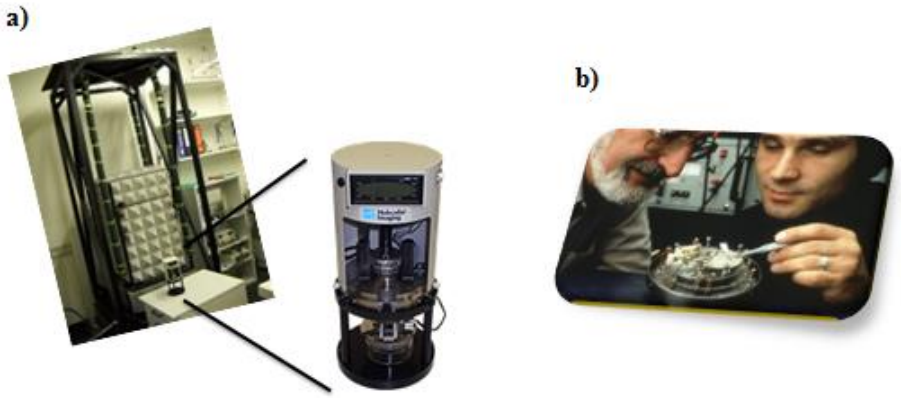

Figure 13. a) Typical STM setup on an anti-vibrational box; b) Gerd Binnig and Heinrich Rohrer working over STM at IBM Research Laboratories.

The STM is based onto the electron tunnelling effect, well known in quantum mechanics. In sharp contrast with classical mechanic, a particle with small dimension, such as the electron, can cross an energetic barrier higher than its own kinetic energy.

[48] G. Binnig, H. Rohrer, C. Gerber, E. Weibel, *Phys. Rev. Lett.* **1982**, *49*, 57.

[49] a) K. S. Kwok, J. C. Ellenbogen, *Materials Today* **2002**, *5*, 28; b) K. S. Kwok, *Materials Today* **2003**, *6*, 20.

Figure 14 shows a representation of such phenomena during STM analysis.

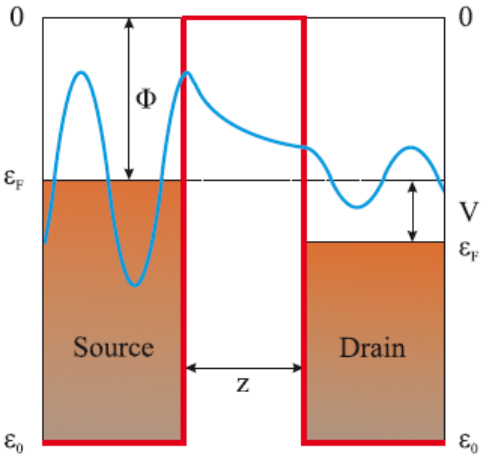

Figure 14. Tunnelling effect and tunnelling in one dimensional source-gap-drain junction. The potential barrier is red line, the electron wavefunction is blue.

The probability for an electron with mass peer to m_e to cross an energetic barrier Φ and a width z, is given by the following equation, where the electron current will strictly depend on this probability.

$$P(z) = \exp\left(-\frac{4\pi}{h}\sqrt{2m_e\Phi}\cdot z\right)$$

$$I \propto P(z)$$

Indeed, if the probability is zero, no current can be generated.

The probability tunnel *P(z)* through the barrier exponentially decreases with barrier width *z*. Such decrease is proportional to square root of the barrier height Φ. The probability *P(z)* is exactly the same already seen in the Landauer formula expressed as T(E) in the Equation 2. At first glance, the Φ and *z* parameters are related to the nature of the molecule bridging the junction which may be seen as a "*resistor*" in the nanodevice. In particular, the energetic barrier Φ is associated to the molecular orbital energy levels, above all in the LUMO orbital. Depending by its nature and its accessibility, the electron transfer process can occur with a superexchange or with hopping mechanism. For instance, it is noteworthy that alkanes modified properly to create the junction use their σ orbitals. The higher energy value of σ* orbital, which corresponds to a big Φ in the figure above, allows the electron transfer only in a superexchange manner (tunnelling, the electron transfer through the LUMO is forbidden). On the other hand, if the molecule is formed by a π orbital system the electron transfer can occur via tunnelling or hopping mechanism in function of the length *z*. This is possible because the molecular orbitals π and π* are more accessible in terms of energy with respect to the σ ones.

In a STM instrument, a sharp metal tip, or probe, is put in contact with a conductive metal surface as shown in Figure 15.

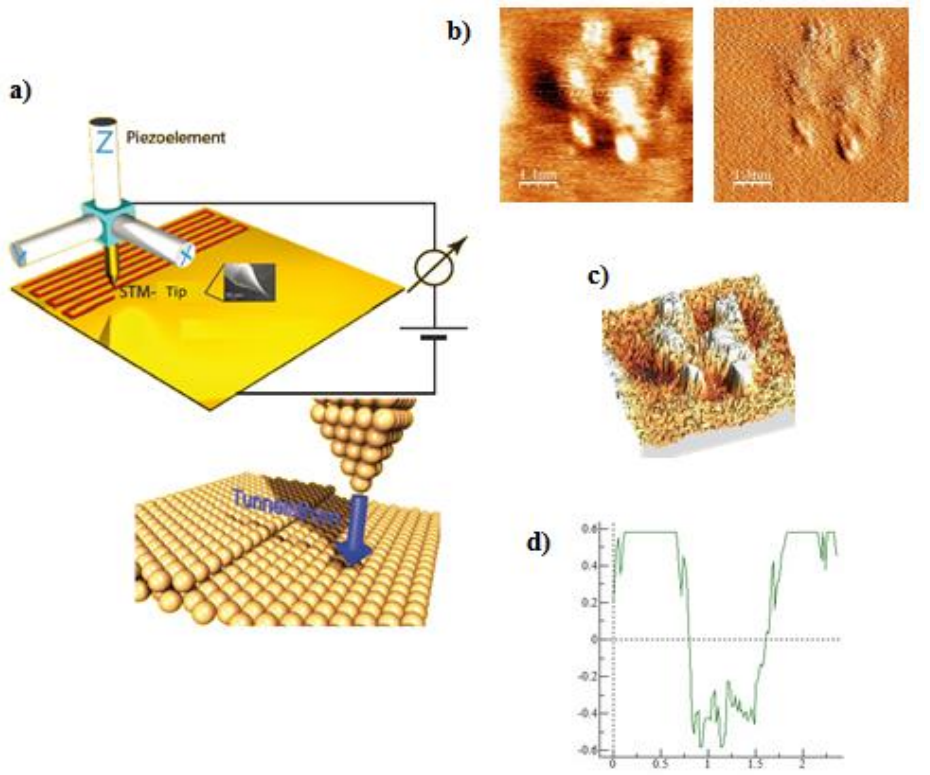

Figure 15. a) STM analysing gold surface; b) current and topography data shown with STM; c) 3D view of the same area of b); d) height profile.

The voltage difference or "bias", applied between tip and sample causes the ET by tunnelling via the gap. The tunnelling current applied (I_T), is measured by the preamplifier with a high sensitivity in the range values of 1 pA to 100 nA. The surface scan process of the tip is controlled by the aid of a piezo element, moving it in lateral directions, while the tip-sample separation *z* is controlled by another piezo element.

STM can work in two operational modes. In the first, "constant current mode", the current is kept constant via a feedback circuit by adjusting the *z* position of the probe. The value of the current is selected according to the application, typical values are between 0.01−10 nA. The final information is recorded as an array of (x, y, z) data either in three-dimensional (3D) or two-dimensional (2D) images (see Figure 15b and c). In the latter, the vertical scale is represented by the gradient of the colour which stands for topography. In particular, the brighter colour typically designates an higher surface. By tracing it, a surface height profile can be obtained, as shown in Figure 15d.

The second STM operational mode is the "constant height mode" where the vertical position of the tip is kept constant during the lateral scanning while the value of the tunnelling current is recorded as a function of the tip position. Similarly to the previous case, the array of (x, y, I_T) data provides information on surface topography.

Despite its versatility and its wide application, STM has at least two limitations we want to stress herein. The STM technique in constant-current mode is not providing direct information about the surface topography but it only measures the constant tunnelling current. We can thus assume that the constant tunnelling current profiles and the surface topography coincide. However, the local variation of tunnelling barrier as well as other processes, such as the tunnelling mediated by adsorbed species, may lead to characteristics in STM images that are not related to the topography. The important limitation is that STM *per se* is not providing "chemical" information about the composition of the surface.

2.2.3.2 Mechanically Controllable Break Junction (MCBJ)

In a very simple manner, the concept of "break junction" may be attributed to an electronic device which consists of two metal wires separated by a nanogap. It was first introduced in 1985 by Moreland and Ekin using a Nb-Sn filament. Since then, the method has been modified and developed further by Muller *et al.* and Van Ruitenbeek[50] *et al.* for the study of electronic transport processes in atomic-size metallic point contacts and wires.

Reed *et al.*,[51] Kergueris *et al.*,[52] Reichert *et al.*[53] and Smit *et al.*[54] pioneered the MCBJ technique to measure charge transport through single molecules.

To achieve the nanoscale objects, it is necessary to build up a new set-up which overcomes the size limitation of the different lithography techniques such as e-beam lithography (20 nm as most and not so reproducible), electro-migration and electro-deposition lithography. Another limitation is the no-flexible support in which two electrodes are situated.

MCBJ allows the control of electrode separation with high reproducibility, stability and precision,[55] due to the short distance between the two free standing electrode tip ends and the support. In consequence, the formation, the strengthens and the stretching of molecular junction can be controlled in time of seconds, even at room temperature and in solution. The fabrication of an ideal set-up requires the consideration of the following key factors: i) the conductance of different molecular wires, ii) the tunnelling decay in subnanometer scale which requires a precise current value ranging from microampers (μA) to femtoampers (fA), iii) the mechanical vibrations due to the pushing rod (it bends the MCBJ support) should be minimized as much as possible, iv) single molecule studies are influenced by the environment and further precautions should be demanded (protection from oxygen, light, etc...).

[50] J. M. van Ruitenbeek, A. Alvarez, I. Pineyro, C. Grahmann, P. Joyez, M. H. Devoret, D. Esteve, C. Urbina, *Rev. Sci. Instrum.* **1996**, *67*, 108.
[51] M. A. Reed, C. Zhou, C. J. Muller, T. P. Burgin, J. M. Tour, *Science* **1997**, *278*, 252.
[52] C. Kergueris, J. P. Bourgoin, S. Palacin, *Phys. Rev. B* **1999**, *59*, 12505.
[53] J. Reichert, R. Ochs, D. Beckmann, H. B. Weber, M. Mayor, H. von Löhneysen, *Phys. Rev. Lett.* **2002**, *88*, 176804.
[54] R. H. M. Smit, Y. Noat, C. Untiedt, N. D. Lang, M. C. van Hemert, J. M. van Ruitenbeek, *Nature* **2002**, *419*, 906.
[55] N. Agraït, A. L. Yeyati, J. M. van Ruitenbeek, *Phys. Rep.* **2003**, *377*, 81.

An example of a MCBJ setup [56] to which corresponds all these features is the following one (Figure 16):

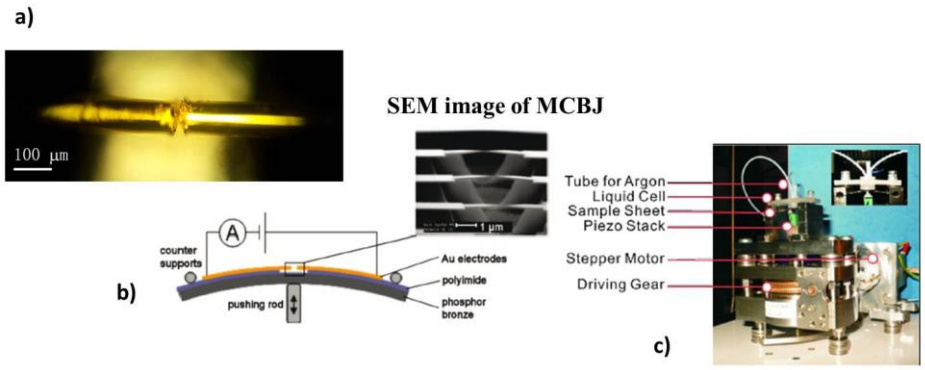

Figure 16. a) Gold filament showing the section of about 10 nm to be used in the experiment; b) MCBJ scheme with SEM image of the section; c) typical MCBJ setup with an overview of its components.

The MCBJ controller is based on a laboratory-built bipotentiostat. Two custom-designed bipolar and tuneable logarithmic *I–V* converters were implemented for measuring the current of the two gold leads labelled as working electrodes (WE1 and WE2). The reference electrode (RE) and the counter electrode (CE) serve to control the potential. The driving signal of the piezo stack is supplied by an additional A/D-converter output of the controlling unit. The controller unit provides three analogical control signals. The first one controls the potential of WE1, which is particularly important for advanced electrochemical experiments with the MCBJ setup. The second one controls the voltage difference between the two working electrodes WE1 and WE2 (bias voltage), which drives the current through the two gold electrodes for the conductance measurements. The third channel controls the voltage output for the piezo stack in the range of 0 to 50 V allowing the displacement of the piezo stack down to 10 µm. The stable and precise operation of the logarithmic *I–V* converter over a wide dynamic current range requires strict temperature control. In order to avoid any interferences with the temperature-control unit, an analogue proportional-integral-derivative (PID) controller with diodes as

[56] W. Hong, H. Valkenier, G. Mészáros, D. Zsolt Manrique, A. Mishchenko, A. Putz, P. Moreno García, C. J. Lambert, J. C. Hummelen, T. Wandlowski, *Beilstein J. Nanotechnol.* **2011,** *2*, 699.

heating elements has been installed. It keeps the temperature of the current-sensing diodes of the logarithmic *I–V* converter within ±0.05 K.
The above brief description about the set-up is of great importance for the knowledge of the typical MCBJ measurements.
Essentially, a metal platform, easily to be blended, is used as support for the gold electrodes. The gold wire is stuck with an organic polymeric glue (epoxy resin) to the support. The gold wire in between is cut manually under optical microscope to reduce the thickness of the metal wire from 100 μm to about 10 μm. This thickness will be further controlled by the piezo movement of the set-up. Over it, few μLs of compound solution is used for the electron transport properties of that material in a liquid cell or in solid state (the solvent is usually removed before making the electrical contacts).
MCBJ can be used in the *conductance-distance* setting measurements or in the *current-voltage* (*I-V*) setting measurements curves. During the conductance-distance measurements, only the opening traces of the electronic circuit are recorded (when the gold-gold junction is broken).

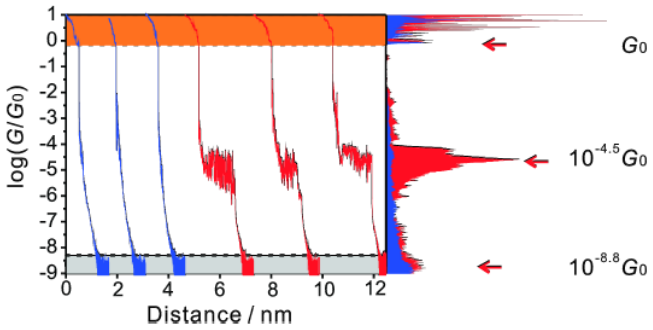

Figure 17. Conductance - Distance curves for a typical MCBJ analysis.

The typical conductance-distance graphic could be separated into three conductance value regions: from 1 to 0 (orange in Figure 17) in which the junction is formed by gold-gold atoms which progressively break (the last value is seen at 1 G_0 (*G zero* or *G note* value, $G_0=2e^2/h=1/12.9k\Omega$). The conductance varies stepwise when a metallic nanobridge is elongated. The step height is of the order of G_0 and the average step length corresponds roughly to the lattice constant, *i.e*. the size of an atom in the solid. For certain metals, *e.g.* Au, Pt and Ir, the tendency to form longer (last) steps has been shown to be an

indication of the formation of one or few atoms wide chains.[57] At a certain point of the elongation the conductance starts to evolve exponentially with the distance - a clear indication of vacuum tunnelling and, hence, the fact that the bridge has been broken. Since for every experiment the constriction atoms arrange differently, the opening traces vary from run to run when cycling the distance. From 0 to -8.5 log(G/G_0), the **metal/junction/metal** is formed with a characteristic plateau. From -8.5 the current noise effects are evident, due to the thermal vibration of molecular junction at room temperature. The blue line is referred to the measurements without the molecular wire but only with the neat solvent. The most reliable conductance of molecular wire is obtained by statistical approach after thousands and thousands experiments done in few minutes and shown in typical histogram (right panel of Figure 18). By other end, the *I-V* curves are recorded only during the stretching process within a single open-closure cycle. For the *I-V* curve it is possible to control the opening and closure process thanks to the high stability of MCBJ setup.

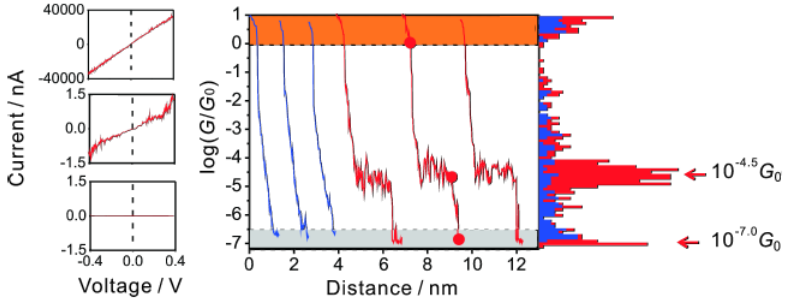

Figure 18. I/V curves for typical MCBJ analysis.

Owing to the open-closure circuit creating during the measurements, it is again easy to distinguish three zones in the above graphic (marked by a red dot), as in the case of before. *I–V* traces of the gold–gold contacts are linear, and represent ohmic characteristics, whereas *I–V* curves of the molecular junctions are nonlinear assuming a symmetric *S*-shape. They provide an important test platform to estimate the relative positions of molecular levels and the Fermi levels of the leads, based on a comparison with *ab-initio* transport calculations and the corresponding transmission curves.[58] Figure 19 shows a typical

[57] a) A. I. Yanson, G. R. Bollinger, H. E. van den Brom, N. Agraït, J. M. van Ruitenbeek, *Nature* **1998**, *395*, 783; b) H. Ohnishi, Y. Kondo, K. Takayanagi, *Nature*,**1998**, *395*, 780; c) P. Velez, S. A. Dassie, E. P. M. Leiva, *Chem. Phys. Lett.* **2008**, *460*, 261.
[58] E. Lörtscher, H. B. Weber, H. Riel, *Phys. Rev. Lett.* **2007**, *98*, 176807.

example of measurement done by MCBJ; the conductance-distance measurements graphic has been divided into sectorial regions in order to attribute the plausible phenomena of molecules within the gold-gold junction.

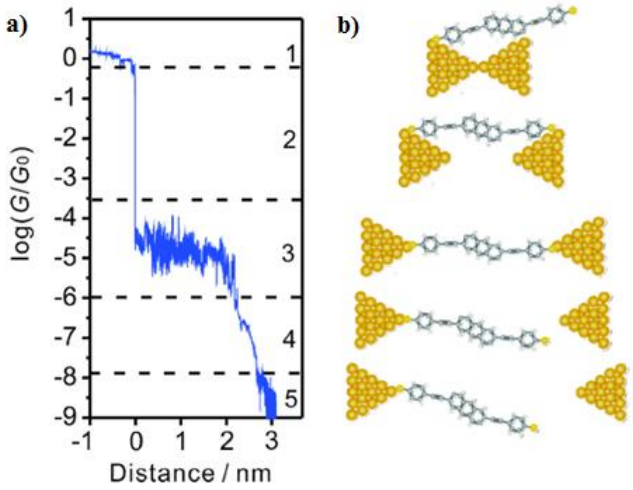

Figure 19. Sectorial model of the breaking process of the MCBJ. a) A typical trace with labels indicating various stages of the process. b) Model of the formation and breaking of single molecular junction (MJ).

The sectorial region **1** shows the direct metal-metal contact followed by a tunnelling decay where the molecule is not attached yet (sectorial region **2**) with the metal junction broken. The sectorial region **3** shows the molecular junction plateau whose stability depends by anchor groups nature. Sectorial region **4** and **5** represent respectively a tunnel decay due to the loss of one molecular contact point (molecular junction is broken) and the region of noise. The advantages of such technique are related to the work conditions: i) room temperature experiments; ii) possibility to work with relatively more concentrated solution (order of 10^{-3} M); iii) very fast results after few minutes. Despite these features, we have also to mention the disadvantages (above all compared with STM technique): i) impossibility to know how many molecules are in the leads gap; ii) the electrode geometry is not so clear as in the STM studies. The comparison between both techniques makes possible to distinguish what kind of studies have already been done for the transport mechanism. The design of new molecules and the fabrication of nano-devices play an important role in the *know-how* of such processes.

2.2.4 Anchoring groups

Along with the chemical structure and electronic properties of the molecular bridge, the anchor groups and their ability to wire the molecule between two metal leads play also an important role in the electron transport. Several simple molecules have been sandwiched between two metal leads hanging different anchor groups with the aim to understand either their stability and function in the junction or how they may influence the electron transport through their contact with the metal surface.

One of the most critical issues in molecular electronics is to find the appropriate anchor groups which has to provide both stability and high contact transparency. For this perspective, it is important to find guidelines in order to choose the best anchor group for the electronic measurements. Each of them have a physical parameter related with their bond strength with the metals. This is called "metal-molecule" contact (electric coupling between metal and anchor group) and it is represented as Γ_L for the left lead and Γ_R for the right lead (Figure 20). This is an energetic coefficient which could be seen as an energetic barrier that electrons must overcome, when transported by the source metal surface to the drain metal surface passing within the molecule or not. For instance, thiols have minor electric coupling than cyano groups, which make them better anchor groups.

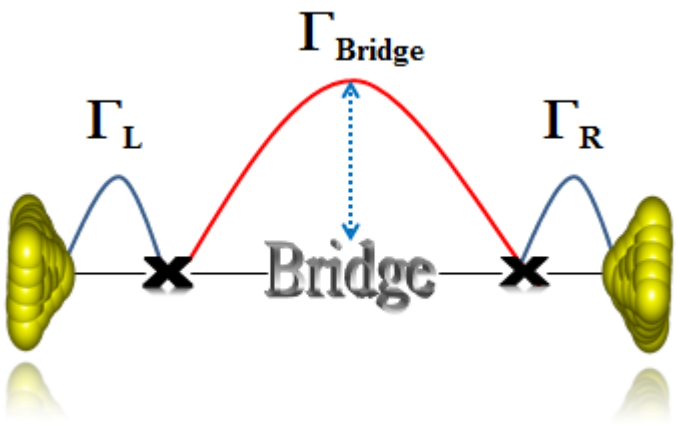

Figure 20. Schematic representation of energetic barriers of molecular junction. The energetic barrier of the bridge can change in dependence of the bridge chemical nature.

The stability of the junction has been studied through STM experiments in many cases where different anchor groups have been used. Herein, we want to briefly discuss the stability of the covalent interaction formed between an alkanedithiol and the gold surface (Au-S contact, see Figure 21). STM creates and breaks down the molecular junction repeatedly thus it becomes convenient for the study of metal-contact stability of anchor groups.

More specifically, all the interactions have an own lifetime during the experiments which depends on the nature of the anchor groups and of the surface.

It has been demonstrated that the "*natural lifetime*" of a metal-molecule contact is the average time of the metal-molecule contact from the thermal fluctuations up to the breakdown.[59]

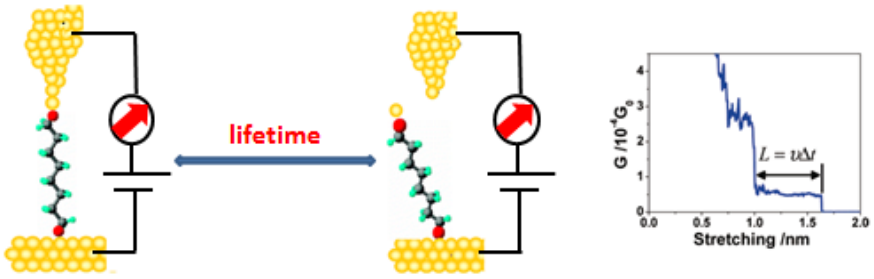

Figure 21. Left picture shows the breakdown; right diagram represents conductance trace against stretching until the breakdown of MJ.

The results shown in Figure 21 suggested that the breakdown of the molecular junction occurs in the Au-Au bond closer to the Au-S (one Au atom remains attached to the sulphur atom of the molecule already free). The breakdown process is thermoactivated; parameters like average lifetime and binding strength are liable to thermoactivation.

In addition to the electron transport characteristics, the conductance measurements obtained during the analysis also provide information concerning the stability of the molecular junctions.[60] Moreover, the conductance values may be affected by the microscopic bond breakdown and by the rearrangement of metal atoms near the metal-molecule contact. The typical observed plateau signify formation of single-molecule junctions where the step width represents two features: i) the approximate length of the

[59] Z. Huang, F. Chen, P. A. Bennett, N. J. Tao, *J. Am. Chem. Soc.* **2007**, *129*, 13225.
[60] M. Tsutsui, K. Shoji, K. Morimoto, M. Taniguchi, T. Kawai, *Appl. Phys. Lett.* **2008**, *92*, 223110.

molecule and ii) the time duration (Δt) from the formation to the breakdown of the junction (the lifetime of the MJ) which can be extrapolated by classical physical laws, as shown in Figure 21. The stretching distance (L) provides information about the nature of the metal-molecule contact and the breakdown process. The time duration, when extrapolated to zero stretching rate, furnishes us a measure of the natural lifetime of molecular junction. As already mentioned, the natural lifetime is a thermodynamic parameter and the whole breakdown process of one molecule can be described by a thermodynamic theory. According to it, the breakdown of a molecular junction can also occur without any kind of external inputs but just because of mechanical fluctuations present in the system. In such case, the natural lifetime (t_{off}) is given by the following "*Arrenhius-type formula*":

$$t_{off} = t_D exp\left(\frac{E_b}{k_B T}\right)$$

Equation 3. Arrenhius type equation for the metal-molecule stability.

where t_D is the diffusion relaxation time, E_b is the dissociation energy barrier or binding energy as well, k_B is Boltzmann's constant and T is the temperature in Kelvin. The product of Boltzmann's constant and T gives the average thermal energy parameter at that specified T. This reflects the nature of the molecular junction that undergoes a thermoactivated spontaneous breakdown. During the experiments, the forces applied to stretch the bond make more unstable the metal-molecule contact due to a decrease of the E_b term in the Equation 3.

For a better understanding about the nature of anchor groups, it is reasonable to analyse them by their chemical nature. For this reason, we may divide them into:

1. Monodentate anchor groups: thiol,[61] amine,[62] cyano (isocyanate),[63] isothiocyanate,[64] selenium compounds,[65] pyridine,[66] phosphine,[67] diazonium compounds.[68]
2. Bidentate anchor groups as nitro compounds,[69] carboxylic acids[70] and dithiocarboxilic acid.[71]
3. "Multidentate" anchor group as fullerene C_{60}.

In the next section, the influence of the nature of the first two families is investigated, whilst C_{60} molecule deserves a single section afterwards.

[61] A. Ulman, *Chem. Re*v. **1996**, *96*, 1533.
[62] L. Venkataraman, J. E. Klare, I. W. Tam, C. Nuckolls, M. S. Hybertsen, M. L. Steigerwald, *Nano Lett.* **2006**, *6*, 458.
[63] B. Kim, J. M. Beebe, Y. Jun, X. Y. Zhu, C. D. Frisbie, *J. Am. Chem. Soc.* **2006**, *128*, 4970.
[64] C.-H. Ko, M.-J. Huang, M.-D. Fu, C. H. Chen, *J. Am. Chem. Soc.* **2009**, *132*, 756.
[65] S. Yasuda, S. Yoshida, J. Sasaki, Y. Okutsu, T. Nakamura, A. Taninaka, O. Takeuchi, H. Shigekawa, *J. Am. Chem. Soc.* **2006**, *128*, 7746.
[66] a) B. Q. Xu, X. Y. Xiao, N. J Tao, *J. Am. Chem. Soc.* **2003**, *125*, 16164; b) M. Kamenetska, S. Y. Quek, A. C. Whalley, M. L. Steigerwald, H. J. Choi, S. G. Louie, C. Nuckolls, M. S. Hybertsen, J. B. Neaton, L. Venkataraman, *J. Am. Chem. Soc.* **2010**, *132*, 6817.
[67] Y. S. Park, A. C. Whalley, M. Kamenetska, M. L. Steigerwald, M. S. Hybertsen, C. Nuckolls, L. Venkataraman, *J. Am. Chem. Soc.* **2007**, *129*, 15768.
[68] a) D. M. Shewchuk, M.T. McDermott, *Langmuir* **2009**, *25*,4556; b) L. Laurentius, S. R. Stoyanov, S. Gusarov, A. Kovalenko, R. Du, G. P. Lopinski, M. T. McDermott, *ACS Nano* **2011**, *5*, 4219.
[69] L. A. Zotti, T. Kirchner, J. C. Cuevas, F. Pauly, T. Huhn, E. Scheer, A. Erbe, *Small* **2010**, *6*, 1529.
[70] F. Chen, X. L. Li, J. Hihath, Z. F. Huang, N. J. Tao, *J. Am. Chem. Soc.* **2006**, *128*, 15874.
[71] Y. Xing, T.-H. Park, R. Venkatramani, S. Keinan, D. N. Beratan, M. J. Therien, E. Borguet, *J. Am. Chem. Soc.* **2010**, *132*, 7946.

2.2.5 Monodentate anchoring groups

2.2.5.1 Thiol anchor group

Thiol is considered a good anchor group thanks to the covalent bond with gold surface forming a strong and irreversible (from a chemical point of view) interaction. Now, it results interesting to understand how the covalent bond is formed between the sulphur atom and gold. To do that, it is mandatory to render explicit the electronic configuration of both atoms. The sulphur atom has the outer sphere $3s^2$ and $3p^4$ while gold atom has $6s^1$, $6p^0$ and $5d^{10}$. These orbitals are (on charged) to create the interaction. The 5d(Au) orbitals interact weakly with the valence orbitals of the S atom and do not contribute significantly to the S-surface bond.[72] On the other hand, the interactions between the 3s(S) or 3p(S) orbitals and the 6s(Au) or 6p(Au) orbitals are relatively large, and in particular, the 3s(S)-6p_z(Au) and 3p(S)-6s(Au) interactions play a dominant role. As a consequence, the sulphur atom can interact with gold in agreement with these configurations (Figure 22):

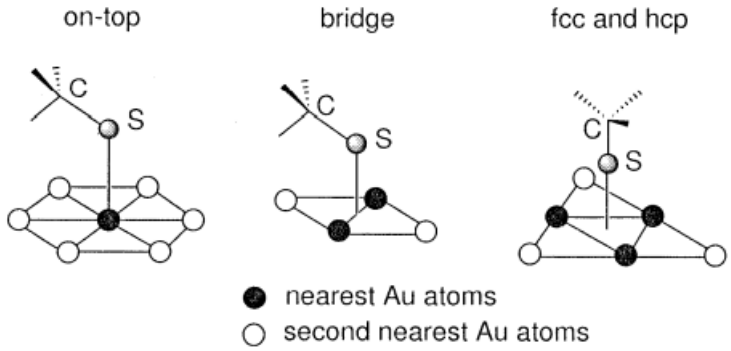

Figure 22. S-Au interaction for a methanothiolate molecule.

In the on-top configuration (also called "atop"), the σ-type 3p_z(S)-6s(Au) interactions dominate because the π-type interactions, formed by 3p_x(S)-6s(Au) and 3p_x(S)-6p_z(Au), are not so relevant. By the other end, the bridge configuration is still dominated by σ-type interaction for 24% but the two π-type interactions become predominant with a 38% of contribution in the final configuration. Thus, the π-type S-Au(111) interactions play an important role and they result more stable than the on-top configuration. Where there is the mayor contribution of π-type interaction is in the hollow models (face centred

[72] M. Tachibana, K. Yoshizawa, A. Ogawa, H. Fujimoto, R. Hoffmann, *J. Phys. Chem. B* **2002**, *106*, 12727.

cubic *fcc* and hexagonal close packing *hcp*) which results in the strongest interaction. Anyway, it seems that there is a cooperative effect of the gold atoms passing from the on-top to the hollow configuration following the order *fcc* and *hcp* > bridge > on-top.
Owing to the different anchoring geometry which produces changes in the configuration of the junction and to the cooperative effect of the gold atom, the conductance value of a molecular junction can vary up to a factor of three, passing from an atop configuration to a hollow configuration (Figure 23).[73]

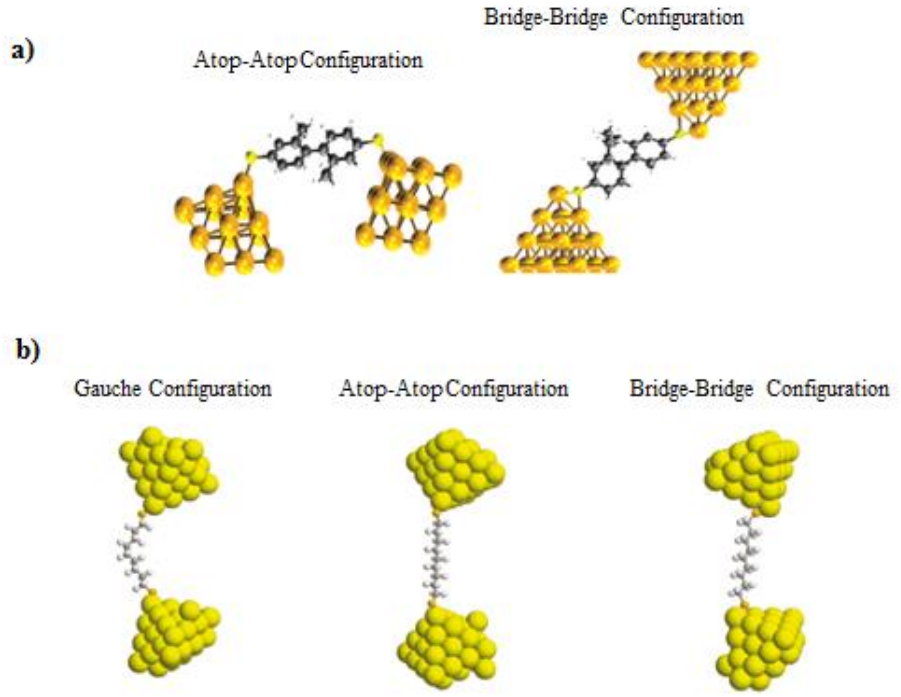

Figure 23. a) Configurations for a biphenyl dithiol molecule; b) Configurations for an alkanedithiol.

As already mentioned, the stability of the junction created by the anchor group is one of the most important factors in these measurements. The sulphur atom can be inserted in the junction as pure thiol (-SH),[74] protected by methylated or

[73] H. Basch, R. Cohen, M. A. Ratner, *Nano Lett.* **2005**, *5*, 1668.
[74] C. Li, I. Pobelov, T. Wandlowski, A. Bagrets, A. Arnold, F. Evers, *J. Am. Chem. Soc.* **2008**, *130*, 318.

acylated groups (-SCH_3 or –$SCOCH_3$).[75] These protected groups are easily removed under chemical conditions. In case of acetylated thiols, the use of organic or inorganic base has been investigated with the discovery of different molecular junction formations depending on the type of base and also the concentration employed. The β values found by using different techniques for alkanedithiols with different length, are almost independent of bias in the low bias range,[76] and have values of 0.83 ± 0.04 $Å^{-1}$ and 0.94 ± 0.06 $Å^{-1}$.[77]

Moreover, thanks to its stability, it is possible to do reactions onto a surface in which a molecular scaffold bringing a sulphur atom has been previously hanged in a chemically irreversible manner.[78]

In the same way, the well-known *tetrathiafulvalene* has been sandwiched within two gold leads even as pristine molecule[79] or as bridge of the molecular wire as reported by our group.[80]

Another interesting anchor group based on sulphur atom is the dihydrobenzothiophene (DHBT). It has been previously investigated by Venkataraman *et al.*[81] and, recently, by Bryce *et al.*[82]

The latter, inspired by the work of Venkataraman, decided to build up oligoynes which brings the aforementioned ending groups. Such constrained anchor groups stabilize the position of the sulphur lone pair in comparison with an analogue flexible dithioether thus increasing the chance of single molecule junction formation and enhancing the single molecule conductance. Previous results demonstrates that STM and MCBJ of such compounds are in agreement and show two conductance values from 10^{-2} G_0 to 10^{-4} G_0 which are due to the configuration changes of the molecule during the whole process: formation of

[75] R. Huber, M. T. González, S. Wu, M. Langer, S. Grunder, V. Horhoiu, M. Mayor, M. R. Bryce, C. Wang, R. Jitchati, C. Schönenberger, M. Calame, *J. Am. Chem. Soc.***2007**, *130*, 1080.
[76] W. Wang, T. Lee, M. A. Reed, *Phys. Rev. B* **2003**, *68*, 035416.
[77] a) B. Xu, N. J. Tao, *Science* **2003**, *301*, 1221; b) T. Lee, W. Wang, J. F. Klemic, J. J. Zhang, J. Su, M. A. Reed, *J. Phys. Chem. B* **2004**, *108*, 8742; c) D. J. Wold, R. Haag, M. A. Rampi, C. D. Frisbie, *J. Phys. Chem. B* **2002**, *106*, 2813.
[78] a) M. Taniguchi, Y. Nojima, K. Yokota, J. Terao, K. Sato, N. Kambe, T. Kawai, *J. Am. Chem. Soc.* **2006**, *128*, 15062; b) Seong Ho Choi, BongSoo Kim, C. Daniel Frisbie, *Science* **2008**, *320*, 1482; c) M. Mayor, *Angew. Chem. Int. Ed.*, **2009**, *48*, 5583.
[79] M. Taniguchi, M. Tsutsui, K. Shoji, H. Fujiwara, T. Kawai, *J. Am. Chem. Soc.* **2009**, *131*, 14146.
[80] F. Giacalone, M. A. Herranz, L. Grueter, M. T. Gonzalez, M. Calame, C. Shönenberger, C. R. Arroyo, G. Rubio-Bollinger, M. Velez, N. Agraït, N. Martín, *Chem. Commun.* **2007**, 4854.
[81] J. S. Meisner, M. Kamenetska, M. Krikorian, M. L. Steigerwald, L. Venkataraman, C. Nuckolls, *Nano Lett.* **2011**, *11*, 1575.
[82] PhD thesis of Murat Gulcur: "The Synthesis and Transport Properties of Conjugated Molecular Wires", University of Durham (England), **2012**.

the junction, stretching with conformational rearrangements, breakage of the junction.

2.2.5.2 N-terminated anchor groups

Amine, pyridine and cyano belong to this class of simple but interesting anchor groups. A comparison of them have been done to understand if the nitrogen atom with its lone pair can reduce the energy barrier of the metal-contact area despite its intrinsic chemical electron nature as electron-donating (ED) or electron-withdrawing (EWG).

- Amine anchor group, either as alkyl[62] or aryl,[83] tethered with the gold atom through a donor-acceptor adduct made by the lone pair of nitrogen and the gold atom as acceptor unit, acting as an acid-base couple. The bonding site between gold and amine is a simple delocalization of two electrons of the N lone pair to the smooth surface of gold atoms, which gives rise to only one possible manner to form the Au-amine junction. The gold-amine bond will not be strongly directional and, the molecular junction formation is relatively unconstrained by the link structure and can form easily in only one mode. To further investigate the binding site, DFT calculations[62] indicated that in flat Au(111) surface, 1,4-butanediamine does not bind near the atop site in an upright configuration but, it does bind to an Au adatom (vicinal gold atom showed in Figure 24) with an estimated binding energy of 0.5 eV as a result of good electronic coupling between Au and the lone pair of nitrogen. The flexibility of this binding in amine end alkanes has been studied through theoretical calculations. As shown in the figure below, the energy cost to flex the Au-N-C angle by ± 15 degrees is about 0.2 eV (counting contributions from both contacts). Interestingly, the Au-Au-N angle has a much softer degree of freedom, especially to the wide-angle side. Alkyl and arylamines bind preferentially to the undercoordinated gold atom in the junction.

[83] S. Y. Quek, L. Venkataraman, H. J. Choi, S. G. Louie, M. S. Hybertsen, J. B. Neaton, *Nano Lett.* **2007**, *7*, 3477.

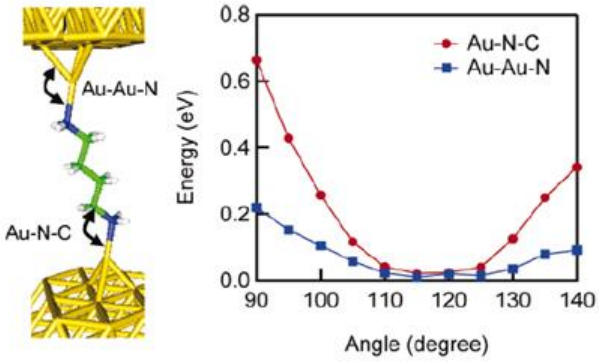

Figure 24. Junction configuration of alkane diamine with the N atom binding to an undercoordinated Au adatom and its energy values in function of two types of angles.

In general, aliphatic amines are more stable at high voltage values (they can resist up to 900 mV of bias) compared with arylamines such as aniline.[84] Therefore, while we gain stability with the alkyldiamine in the junction, we record a low value of conductance compared with aryldiamines which have less stability in the contact (up to 450 mV). These studies have been performed using a STM setup in current-voltage mode, experiments which put in evidence the stability of the molecular junction at different voltage values. Comparing also the conductance peak width, we can make some conclusions about the stability of different molecules: in particular, the narrow widths represents good stability of the junction (less value of conductance in the counts *vs* conductance trace).

As well as the alkyldiamines, 1,4-benzenediamine exhibits a good interaction with gold surface.[83] It shows good stability compared with analogue systems, like 1,4-benzenedithiol and 1,4-benzenediisonitrile where the whole system is destabilized by, in the first case, the variety of attachment point of sulphur and, in the second case, the easy oligomerization[85] and variation in binding site of the isonitrile group.[86]

Anyway, the electron transport along these molecules (alkyl or aryl) occurs via a superexchange mechanism through the HOMO level which has a similar

[84] J. R. Widawsky, M. Kamenetska, J. Klare, C. Nuckolls, M. L. Steigerwald, M. S. Hybertsen, L. Venkataraman, *Nanotechnology* **2009**, *20*, 434009.
[85] S. Lin, R. L. McCarley, *Langmuir* **1999**, *15*, 151.
[86] J. I. Henderson, S. Feng, T. Bein, C. P. Kubiak, *Langmuir* **2000**, *16*, 6183.

energy value to that of the gold Fermi energy level. This aspect has been demonstrated for aryldiamines via:

- DFT calculations[83] considering the molecule within the Au(111) junction at time "zero", before the application of a defined bias. The HOMO level is closer to the gold E_F level while the LUMO is situated at about 2.5 eV of energy far from the gold E_F.
- Empirical data using ultraviolet photoemission spectroscopy (UPS) and X-ray analysis in monolayer structures formed by different benzenediamines.[87]

Both results fit well with the experimental data obtained by STM break junctions over 1,4-diaminobenzene properly substituted with either ED or EWG groups, destabilizing or stabilizing the HOMO level value, with the consequent better conductance traces for ED group with respect to the EWG group (Figure 25).[88]

As conclusion, the narrow distribution seen during the experiments is in agreement with the fact that amine anchor groups can sustain an high bias voltage because the nitrogen atom attaches the surface in well-defined motif (the differences in the nanocontact structure have low influence in the conductance values), making it an anchor group highly selective but flexible. Maintaining constant the conductance while the junction is elongated, the molecule remains linked to the undercoordinated gold atom. All these features have been equally found in 1,4-benzenediamine molecules which, according to Neaton *et al.*,[83] give arise to a conductance value lower than 1 G_0, referred to the formation of unimolecular junctions. Furthermore, in this study, they analysed the fluctuations of conductance values in agreement with feasible conformations of the molecular junction.

[87] M. Dell'Angela, G. Kladnik, A. Cossaro, A. Verdini, M. Kamenetska, I. Tamblyn, S. Y. Quek, J. B. Neaton, D. F. Cvetko, A. Morgante, L. Venkataraman, *Nano Lett.* **2010**, *10*, 2470.
[88] L. Venkataraman, Y. S. Park, A. C. Whalley, C. Nuckolls, M. S. Hybertsen, M. L. Steigerwald, *Nano Lett.* **2007**, *7*, 502.

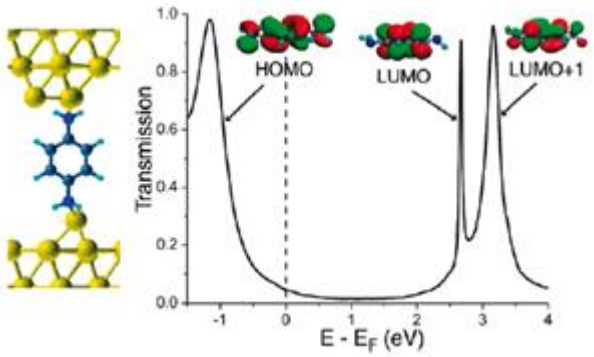

Figure 25. One of 15 possible configurations for 1,4-diaminobenzene within the junction and orbitals representation as a function of the energy for this configuration.

Among the fifteen reliable molecular structure configurations, differing from tilt angle, bonding configuration (*cis*/*trans*), binding site and, Au contact structures, the above drawn configuration (Figure 25) seems to be the most easy to be studied also in terms of energy-dependent transmission. The latter property gives us an idea of the relative energies of HOMO, LUMO and LUMO+1 levels of the molecule within the junction. From the experimental and theoretical results over the 1,4-benzenediamine, the Au-N linkage does not significantly change with the variation of junction geometries. Owing to the isotropy of the Au 6s orbital, little configuration variations have small impact on the electronic coupling at low value of bias. In typical STM break junction experiments, where the molecular junction is repeatedly formed and broken, the N atom moves from adatom to the atop position (vertex) with a sliding process over the gold pyramid surface. Since the conductance for these configuration is similar, this process would appear as one single plateau in the conductance versus length in the bidimensional graphic.

- The nitrogen atom of pyridine belongs to the aromatic ring. Its lone pair is perpendicular to the aromatic system and it could encourage the linkage with gold atom in a directional way. It could also represent an interruption point (bottleneck) to the electron transmission because this lone pair orbital is not aligned with the pyridine π orbitals as in the case of aniline.

It has been demonstrated that the pyridine anchor group of different molecules showed two conducting configurations:[89] molecular junctions start in a high-conductance configuration that can be elongated over a distance that depends on the molecular length and generally terminate with a low-conductance plateau. The electrode separation in the low-conducting state is consistent with a vertical geometry where the molecule is probably bound to apex atoms on each electrode; it depends on the angle α between the s orbital of the Au atom and the lone pair of N in the pyridine ring (Figure 26).

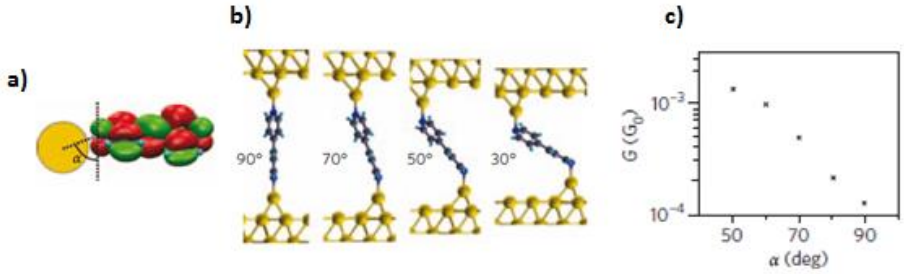

Figure 26. a) angle α between the s orbital of Au and the lone pair of N in 4,4'-bipyridine; b) angle tilted molecule within the gold junction; c) dependence of conductance values from the tilted angle in the junction.

Decreasing such angle, the value of conductance increases thanks to the most prominent contribution of π orbitals belonging to the pyridine ring.
The high conducting state corresponds to junctions with an electrode separation that is smaller than the length of the whole molecule. These findings have been corroborated by scattering-state density functional theory (DFT)-based conductance calculations, which show that the low-conducting state is associated with a vertical geometry in which the N-Au bonds are aligned with the molecular backbone (and are therefore perpendicular to the π system), while the high-conducting state is associated with a geometry in which the molecule is tilted, resulting in an increased coupling between the gold atoms of the electrode and the molecular π system (Figure 27).

[89] S. Y. Quek, M. Kamenetska, M. L. Steigerwald, H. J. Choi, S. G. Louie, M. S. Hybertsen, J. B. Neaton, L. Venkataraman, *Nat. Nanotechnol.* **2009**, *4*, 230.

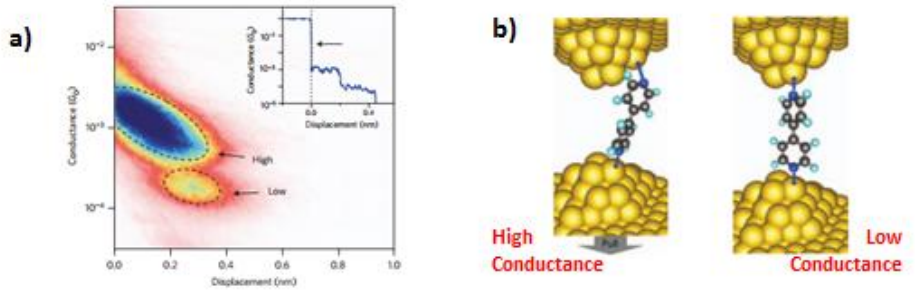

Figure 27. a) High and low conductance values in bidimensional graphics with a typical bypiridine conductance trace (inset) and; b) possible changes in the junction configuration to explain the high and low conductance.

To overcome this trend of pyridine molecules, many groups have investigated the nature of tripodal pyridine basement which, at least according to the theory, may contribute not only to maintain the robustness of surface point attachment but also to control the molecular orientation.[90] Unfortunately, there are no conductance measurements over these systems until now.

A stability comparison of amine and pyridine anchor groups has been observed through the study of the rupture force of single molecular junctions. The concept to measure the rupture force of single molecular junctions along with the measurements of conductance is completely new.[91] The rupture force can be determined by analysing the cantilever deflection in the point in which the metal-metal contact (case of gold) or metal-molecule contact breaks.

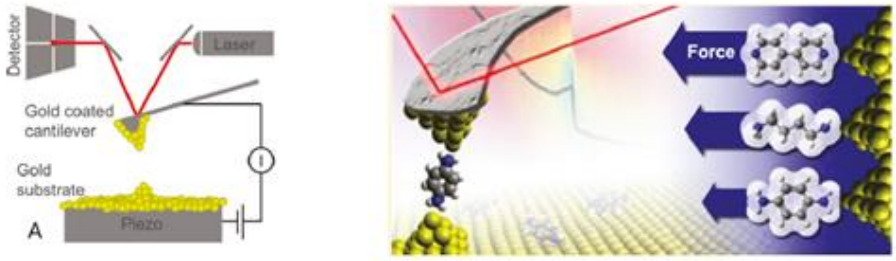

Figure 28. Modified AFM (left) and rupture force for the study of N-terminated molecules.

[90] Y. Ie, T. Hirose, H. Nakamura, M. Kiguchi, N. Takagi, M. Kawai, Y. Aso, *J. Am. Chem. Soc.* **2011**, *133*, 3014.
[91] a) M. Frei, S. V. Aradhya, M. Koentopp, M. S. Hybertsen, L. Venkataraman, *Nano Lett.* **2011**, *11*, 1518; b) M. Frei, S. V. Aradhya, M. S. Hybertsen, L. Venkataraman, *J. Am. Chem. Soc.* **2012**, *134*, 4003.

Using a properly modified AFM setup, Venkataraman *et al.* showed for the first time that the force required to break a gold-gold contact is 1.4 nN (nano Newton, Figure 28). In the same manner, they analysed 4,4'-bipyridine, alkanediamine and 1,4-diaminobenzene. In such a way, the stability of each single molecule junction has been envisaged; furthermore, a comparison between the different anchor groups used, even belonging to the same family, becomes important to understand what anchor group may be the most promising. The rupture forces found, are 0.8 ± 0.08 nN, 0.69 ± 0.06 nN and 0.5 ± 0.09 nN for 4,4'-bipyridine, 1,4-diaminoalkane and 1,4-diaminobenzene, respectively. This clearly demonstrates that 4,4'-bipyridine is more stable than diaminoalkane and diaminobenzene as molecular junction and it is in agreement with all the considerations done about these three anchor groups.

- To finish this section, the cyano group has also demonstrated good affinity with a gold surface.[92] It is interesting that, in this case, the electron-withdrawing nature of cyano as substituent in the molecule can affect the electron transport. Indeed, its nature stabilizes the HOMO and LUMO energy levels, making the last one closer to the Fermi energy level of the metal leads. It has been demonstrated that for cyano molecules, the electron transport takes place through the LUMO orbital (the most energetically accessible). STM experiments demonstrated that it is possible to form molecular junctions with this functional group as end part of the molecule, commercially available or synthetically fabricated. DFT calculations over biphenylcyano molecules showed that they anchor to the metal lead according to the most stable interaction in an atop configuration, either with only one gold atom (linear configuration) or with gold atoms in the "terrace-type" motif, as shown in Figure 29. These two atop configurations result to be the most stable thanks to the coordination of the N lone pair with the gold atom in a directional mode.

[92] A. Mishchenko, L. A. Zotti, D. Vonlanthen, M. Burkle, F. Pauly, J. C. Cuevas, M. Mayor, T. Wandlowski, *J. Am. Chem. Soc.* **2011**, *133*, 184.

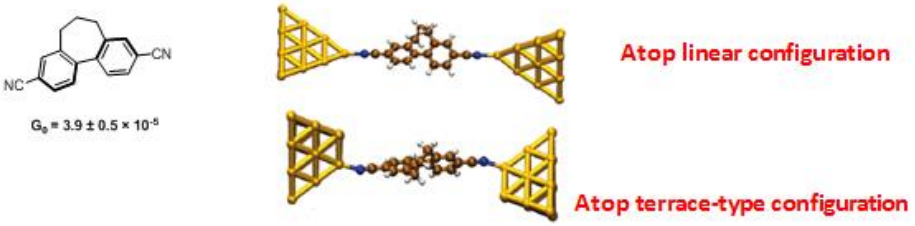

Figure 29. Molecular junction formation made by cyano groups in two typical atop configurations for the biphenyl represented. The G_0 value is referred to the STM experiments.

This was the first time in which a molecular junction has been formed using these molecules. (Either Kiguchi[93] *et al.* or Zotti *et al.*[69] did not report any conductance values for these systems using MCBJ).

2.2.5.3 Other monodentate anchor groups

Particular relevance in the formation of molecular junctions has to be given to phosphines as a new anchor group even with bulky substituents like aryls or with simple methyls as substituents. There have some features which could be taken into consideration *e.g.* the nucleophilic character of phosphine, their ease to be synthesized, as the possible directional attachment to the gold surface through the lone pair of phosphorus. Also, the well-known chemistry of phosphine as ligand for metal complexes (above all with Au) in asymmetric catalysis could help us to imagine it as a new anchor group. It has been reported that the binding energy of diphenyl phosphines (1.2 eV) to the gold surface is the double of that of methyl sulphide or amines (0.6 eV).[67] However, a problem of stability of such compounds has to be considered even in the synthesis or in the formation of the junction. The chemical and physical stability of alkane dimethyl phosphines have been carefully analysed in order to compare them with amines and methyl sulphide analogue molecules in STM break junction experiments. The results, shown in Figure 30, demonstrate that the junction formed with dimethyl phosphines as anchor groups has a better value of conductance with respect to methyl sulphides and amines.

[93] M. Kiguchi, S. Miura, K. Hara, M. Sawamura, K. Murakoshi, *Appl. Phys. Lett.* **2006**, *89*, 213104.

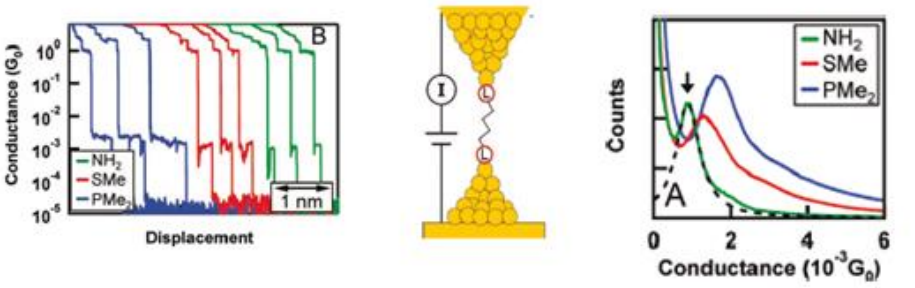

Figure 30. Comparison in conductance traces for amines, methyl sulphides and dimethyl phosphines alkanes.

Furthermore, the clear plateau observed for the dimethyl phosphine groups do not leave any doubt on the fact that such group gives rise to a stable connection where the binding site is well-defined and electronically selective. With a further analysis, the σ donation from the lone pair of the atom to the gold is strongest for phosphines, followed by amines and, scarce for the sulphides. On the other hand, the π back-donation from gold atom to the linker atom is more relevant in phosphines than in sulphides and amines.

As well as for dimethyl phosphines, also for diphenyl phosphines the stability of the contact along with conductance measurements have been carried out. [94] The experiments and calculations suggest very strongly that the Ph_2P-Au bond is well-coupled to the alkane backbone. In particular, the measurements have been performed with different alkyl chains as bridge and, all of them, showed the same behaviour within the metal contacts with a length-dependence in the conductance values.

[94] R. Parameswaran, J. R. Widawsky, H. Vazquez, Y. S. Park, B. M. Boardman, C. Nuckolls, M. L. Steigerwald, M. S. Hybertsen, L. Venkataraman, *J. Phys. Chem. Lett.* **2010**, *1*, 2114.

2.2.5.4 Au-C direct anchor group

An interesting manner to overcome the energy barrier in the metal contact binding site could be the direct addition of a carbon atom to the gold surface into a directional, stable and reproducible mode. Some studies have been carried out using diazonium salts, organotin compounds as precursors and, more recently, trimethylsilyl terminated molecules.[95] This new concept to create Au-C direct σ bond paves the way towards the studies of new molecular junction formations which can provide a promising platform in nanoscale assembly.

- Diazonium salts are species widely used in organic chemistry and easy to be prepared by several synthetic or commercial amines. The electrophilic reactivity of these compounds and their stability allow us to handle them and use them as really versatile organic scaffolds for organic synthesis. An example of reactivity is given by Suzuki coupling and azocoupling reactions. Thus, Tour *et al.*, have investigated the formation of direct C-C bond onto single wall carbon nanotube (SWNT) using diazonium salts.[96]

These compounds are electrochemical species which may be spontaneously reduced by i) the metal surface, ii) chemical reactions, iii) ultrasonication, iv) heating or v) mechanical scratching to form an aryl radical which anchors onto the gold surface even in nanoparticles[68] or in organized surfaces, for instance Au(111). The Au-C bond is covalent. Recently, Pinson *et al.* have developed a photochemical procedure to graft the diazonium salts onto surfaces.[97] The photografting, particularly in the visible range, is an interesting alternative deposition procedure thanks to its simplicity and to the possibility of patterning surfaces by the use of masks or stamps (for an exact surface geometry) or by the strategies developed in standard photolithographic procedures. This strategy has been applied over many types of substrates like indium tin oxide (ITO), copper, iron, or gold.

[95] W. Hong, H. Li, S.-X. Liu, Y. Fu, J. Li, V. Kaliginedi, S. Decurtins, T. Wandlowski, *J. Am. Chem. Soc.* **2012**, *134*, 19425.
[96] B. K. Price, J. M. Tour, *J. Am. Chem. Soc.* **2006**, *128*, 12899.
[97] M. Busson, A. Berisha, C. Combellas, F. Kanoufi, J. Pinson, *Chem. Commun.* **2011**, *47*, 12631.

The contact binding site of diazonium salts is much more stable and directional compared with that of thiols resulting in a tightly binding site. In the same way, a comparison with -NH_2 anchor groups is mandatory to stress the importance to have a direct link where the metal-molecule contact barrier is minimized or eliminated; while -NH_2 groups create selective but flexible molecular junctions, diazonium salts form with gold a strong, robust and directional interaction which constrains the molecule to be stiff. Thus, they afford less fluctuations in the conductance experiments than that produced by amine groups as a result of more stable molecular junction formation.

Recently, Tao *et al.*[98] have designed a dimethoxy biphenyl diazonium salt which has been synthesized and used in a mixed setup where a bi-potentiostat has been connected to STM break junction. Doing that, it has been possible to control electrochemically the formation of molecular junctions through diazonium radical reactions. The Au-C contact has been observed after electrochemically reduction of aryl diazonium salts at about -650 mV versus Ag/AgCl. The cyclic voltammetry experiment displays two scan cycles (see Figure 31).

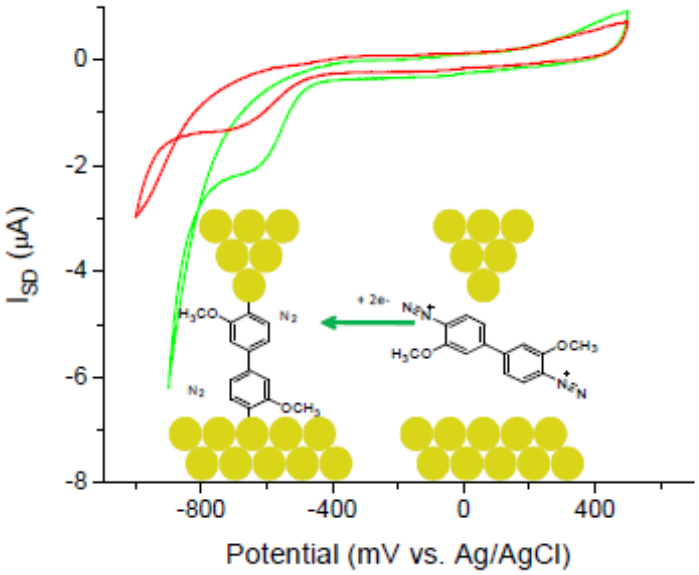

Figure 31. Electrochemical reduction of biphenyl diazonium salts with the formation of molecular junctions in a STM break junction setup.

[98] T. Hines, I. Díez-Pérez, H. Nakamura, T. Shimazaki, Y. Asai, N. J. Tao, *J. Am. Chem. Soc.* **2013**, *135*, 3319.

Dividing the experiment in two regions, there is no evidence of oxidation waves for these systems at positive potential values, while a clear irreversible wave is observed in the reduction region related to the diazonium salt reduction. Applying only one potential scan to the solution, no further phenomena (absorption onto the working electrode, side radical reactions to form new species, etc..) have been stressed. The surface passivation has been observed by the peak intensity current decrease at -650 mV, formed after the second scan cycle; it demonstrates therefore the irreversibility of the radical reaction (once created the molecular junction, it remains well anchored to the surface).

During the STM experiments, when the tip is retracting in the absence of the molecule, an exponential decay of the conductance is observed; in the presence of molecule, a conductance plateau has been recorded referred to the formation of unimolecular junction.

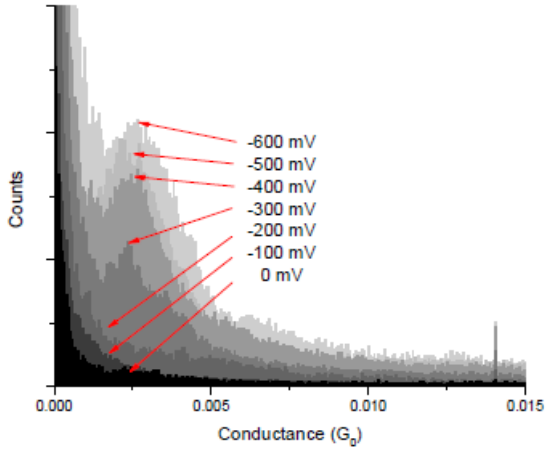

Figure 32. Conductance histograms at different values of bias for diazonium salts.

The conductance histograms in linear scale shows how at values between 0 and -200 mV the conductance peak is not so evident (low yield of molecular junctions have been formed at this reduction potential values) whilst at value from -300 mV to -600 mV, the conductance histogram shows a defined peak at 2.3×10^{-3} G_0 which increases linearly with the increasing of the voltage in the cyclic voltammetry circuit (Figure 32).

This value differs from Venkataraman *et al.* work data[99] (they found 0.1 G_0) which generates the same junction using trimethyltin instead of diazonium salt as reported in the lines beneath.

- Similarly to diazonium salts, organotin compounds showed the same chemical behaviour to form Au-C binding site. In particular -$SnMe_3$ (trimethyl organotin) has been used for this purpose. The removal of the organotin group occurs during the measurements with STM break junction, leading to the formation of covalent Au-C bonds (Figure 33). The direct bonding to gold surface by trimethyl tin terminated molecules is stronger than that of other anchor groups like thiols and amines because of the directional mode to be attached onto the surface. Indeed, the conductance values for such systems are significantly higher. In particular, for the C4 alkyl chain, the found value (~0.09 G_0) is around 100 times larger than that achieved for 1,4-diaminobutane.[62]

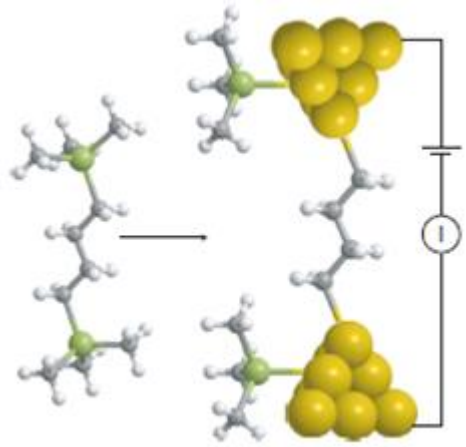

Figure 33. Molecular junction generated by alkane tin compounds with different -CH_2 units.

[99] W. Chen, J. R. Widawsky, H. Vázquez, S. T. Schneebeli, M. S. Hybertsen, R. Breslow, L. Venkataraman, *J. Am. Chem. Soc.* **2011**, *133*, 17160.

Further conclusions related to the better anchor group have been carried out by STM experiments concerning not only the decay constant β but also the stability and flexibility of the molecular junction formation. Figure 34 makes a comparison between diamine terminated alkyl chains and trimethyl tin analogue alkyl chains.[100]

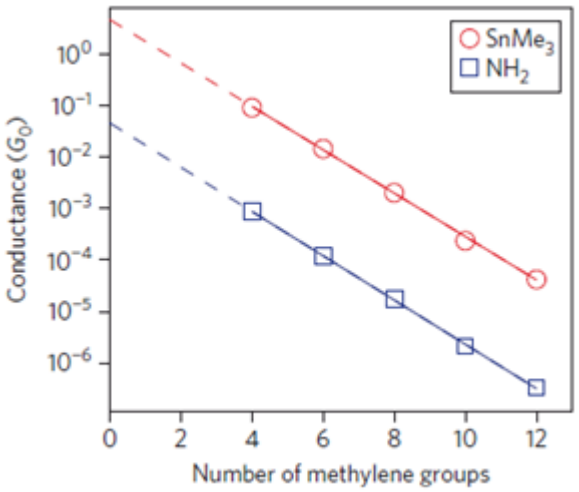

Figure 34. Conductance in logarithmic scale versus number of methylenes either in $SnMe_3$-terminated alkane or in diamine end alkanes.

The expected better electronic communication in Au-C direct link compared with Au-N in amine anchor groups has been underlined for the alkyl molecules with a significant enhancement of conductance of about one order of magnitude, passing from amines to trimethyl tin anchor groups.

The experimental β value, obtained for these systems, is 0.97 ± 0.02 Å and it is comparable with that of alkanedithiols and alkanediamines indicating that the electron transfer occurs in non-resonant tunnelling (super-exchange) mode across the saturated methylene bridge (the slope of red line and blue line in Figure 34 is similar).

More deeply, the DFT calculations demonstrated that the contact formation, in terms of energy required for the rupture of C-$SnMe_3$ bond (~ 0.3 eV), is lower

[100] Z. L. Cheng, R. Skouta, H. Vazquez, J. R. Widawsky, S. Schneebeli, W. Chen, M. S. Hybertsen, R. Breslow, L. Venkataraman, *Nat. Nanotechnol.* **2011**, *6*, 353.

than that found for the rupture of Sn-CH_3 bond. This encourages the direct binding of C to the gold instead of the Sn-Au binding as shown in Figure 35.

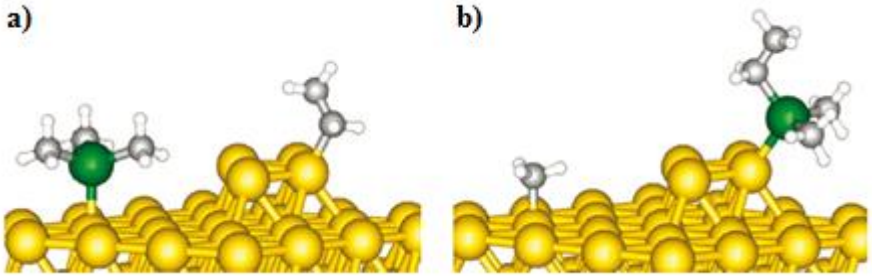

Figure 35. a) C-$SnMe_3$ *in situ* rupture against b) Sn-Me bond rupture.

It has been observed by DFT calculations that $SnMe_3$ motif could attach to different positions over the surface while the ethylene bridge binds selectively to an undercoordinated gold atom of the tip or in an atop configuration on the gold surface as shown in the Figure 35.

At the same time of alkane tin compounds, benzene di-tin compounds have been used to study the formation of Au-C bonds. It is noteworthy that conductance of ditin benzene derivatives is not very high (C4 conducts better than benzene[101]), in contrast to what has been found with other linkers.[62] The explanation for this finding, is that the gold atoms are not well coupled with the benzene π cloud. To improve this electronic coupling, dibenzyl trimethyl stannane has been synthesised and used to create the junction *in situ*, forming a *p*-xylylene molecular wire. It is highly conducting due to a better coupling with the π orbitals of the benzene; this does not occur when Au is directly linked to the benzene core.[99] Figure 36, a comparison between direct metal molecule coupling and -NH_2 coupling with the analogue molecules reflects an improvement of conductance values around two orders of magnitude in favour of the direct linkage with gold surface. It shows the length dependence effect over the conductance value; the decay constant has been extrapolated by the graph and it is peer to 1.9 per phenyl unit.[99]

[101] M. Guohui, S. Xin, L. Sun, R. Zhang, P. Wei, S. Sanvito, S. Hou, *Nanotechnology* **2010**, *21*, 495202.

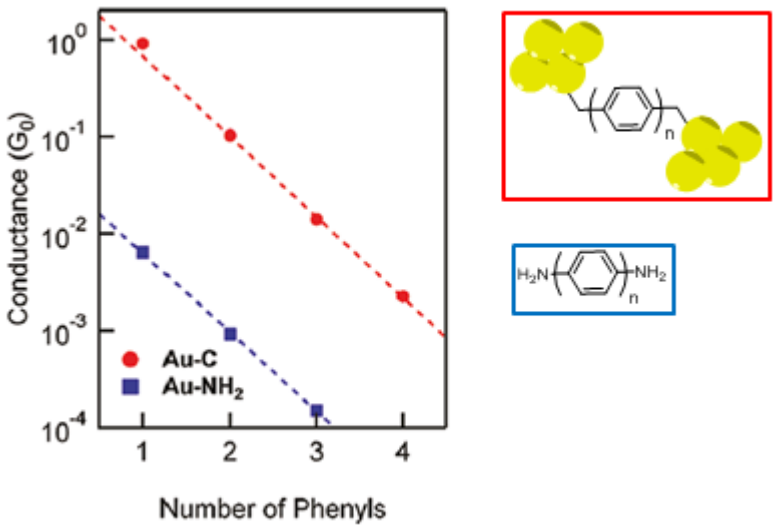

Figure 36. Conductance versus number of phenylene rings and comparison with polyphenyl diamine series.

During the radical formation of the junction, it is possible to obtain the dimer of the phenyl stannane according to the reaction scheme shows below (Scheme 1):

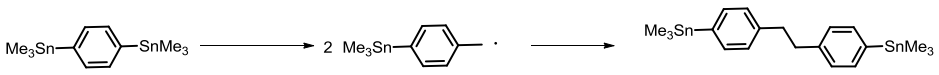

Scheme 1. Radical dimerization of phenyl tin compounds.

This has been experimentally observed for phenyl di-trimethyl stannanes (as shown in Scheme 1) but also for the biphenyl core. Its evidence formation is in the lower conductance plateau observed due to the formation of ethylene bridge between the two phenyl units. Thus, for this system there is a better electronic coupling with the metal leads but scarce conjugation.

The disadvantage in using organotin compounds is their toxicity during the synthesis of the final product, above all in industrial scale. There are two most used strategies to prepare them. One foresees the treatment of bromine compounds with Mg to form the Grignard reagent which undergoes a substitution reaction with R_3SnCl. The second considers direct treatment of bromine compounds with a lithium salt of stannanes. The typical radicalic

procedure for hydrostannanes initiated by AIBN with halogen derivatives is not recommended because it is quite difficult to control the radical reactions: the rate constant is 10^{-9} - 10^{-10} M^{-1} s^{-1} in non-viscous solvent with an energy barrier of the order of 1-2 Kcal mol^{-1}.

- Trimethylsilyl (TMS) terminated molecules based onto OPE cores have been designed, synthesized and analysed by MCBJ technique with the support of STM images[95] and gap-mode Raman spectroscopy in Au(111)/molecule/Au Nanoparticle (NP).[102]

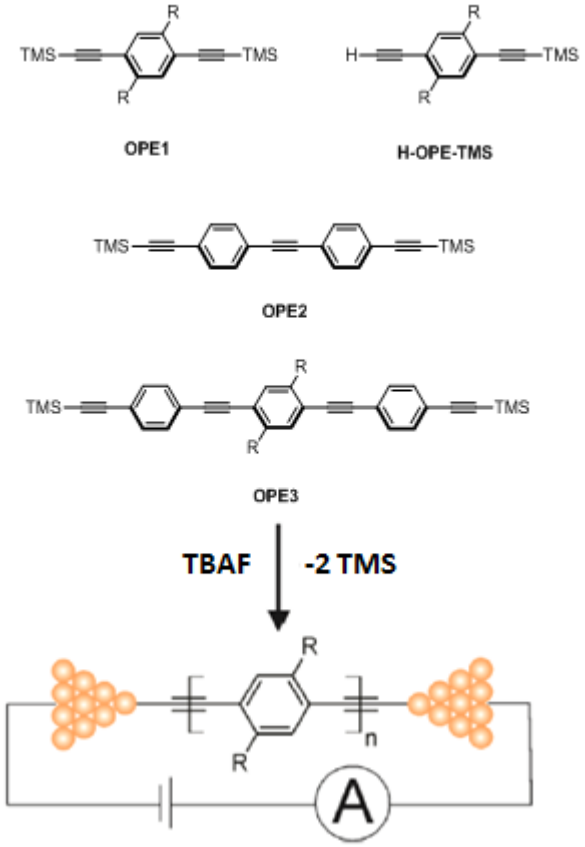

Figure 37. MCBJ picture of different OPE systems.

[102] L. Cui, B. Liu, D. Vonlanthen, M. Mayor, Y. Fu, J.-F. Li, T. Wandlowski, *J. Am. Chem. Soc.* **2011**, *133*, 7332.

The Au-C σ bond linkage with the surface is formed after heterolytic rupture of the C-Si bond in the presence of tetrabutylammonium fluoride base (TBAF). This is the most important difference between trimethylsilyl precursors and diazonium salts or trimethylstannane molecules where the junction is formed after homolytic bond rupture. In an attempt to clarify the formation of the Au-C σ bond, gap-mode Raman spectroscopy shows a red shift of about 200 cm^{-1} in the single stretching mode of C-C triple bond (normally at 2150 cm^{-1}). The shift provides an experimental data which indicates that the molecule is attached onto the gold surface. Indeed, the presence of gold directly attached to the carbon of the terminal triple bond provokes the reduction of C-C triple bond character, due to the donation and back-donation phenomena, with a consequent red shift towards lower frequencies (cm^{-1}), considering it as a partial double bond.

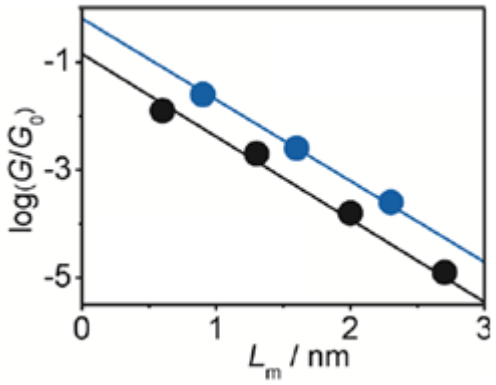

Figure 38. Logarithmic scale of conductance values for Au-C OPE systems (blue dots) and their comparison with dithiols analogue molecules (black dots).

Once more, the decay constant β of such series (3.3 ± 0.1 $Å^{-1}$) has been found to be comparable with that of dithiols terminated OPEs systems (3.4 ± 0.1 $Å^{-1}$) measured under the same conditions (Figure 38). [103]

Thanks to these results, it is reasonable thinking that the deprotection of TMS terminated OPEs molecules generates a molecular junction; across it, the electron transfer proceeds through superexchange electron transfer mechanism. Furthermore, a comparison with the Au-S generated by dithiol OPE systems, shows a better conductance value of more or less one order of magnitude

[103] V. Kaliginedi, P. Moreno-García, H. Valkenier, W. Hong, V. M. García-Suárez, P. Buiter, J. L. H. Otten, J. C. Hummelen, C. J. Lambert, T. Wandlowski, *J. Am. Chem. Soc.* **2012**, *134*, 5262.

which depends on the best coupling in the Au-C metal contact. In this way, it has been proved that the trimethylsilyl group could be an interesting alternative to the -$SnMe_3$, studied by Venkataraman *et al*.,[99] which can avoid the problems related to the use of stannanes.

Because the Au-C, born from a 2sp carbon hybrid orbital with the gold 5d orbitals, is stronger than the Au-Au bond, the stretching of the molecule is accompanied by the breaking of the junction with the removal of one gold atom remaining attached to the carbon atom. This feature has been suggested by Wandlowski *et al.* in the study of trimethylsilyl OPE systems.[102]

2.2.6 Bidentate anchoring groups

2.2.6.1 Nitro anchor group

Nitro-compounds have been taken into consideration as bidentate anchor groups because of their resonant structure. Nowadays, the anchoring mechanism is not clear at all even though an interaction between the negative delocalized charge over oxygen (and nitrogen) atoms with gold surface could be envisaged. The latter, perhaps, intervenes with a back-donation to positive charged nitrogen (Figure 39).

Figure 39. Possible interaction between a nitro anchor group and the gold atom.

There are no many examples in literature of direct binding of nitro moiety with the metal lead. One is referred to nitrotolane molecules in which this anchor group has been compared with the previously synthesized thiols and nitrile tolanes,[104] using MCBJ experiments in solution. The *I-V* curve of the nitrotolane molecule shows for the 30% of all the formed junctions the symmetric and asymmetric behaviour and about 30% of jumps (too difficult to be analysed because of the instability of the junction). To have a reliable data in the *I-V* curve, its shape has to be the most similar to an "*S*" (Figure 40). This means that either starting from negative potential or from positive, the conductance remains the same in absolute value. Positive and negative potential experimental methods are related to the possibility of applying the bias voltage from the tip to the surface and viceversa.

[104] T. Kirchner, B. Briechle, E. Scheer, *Acta Physica Polonica A*, **2012**, *121*, 410.

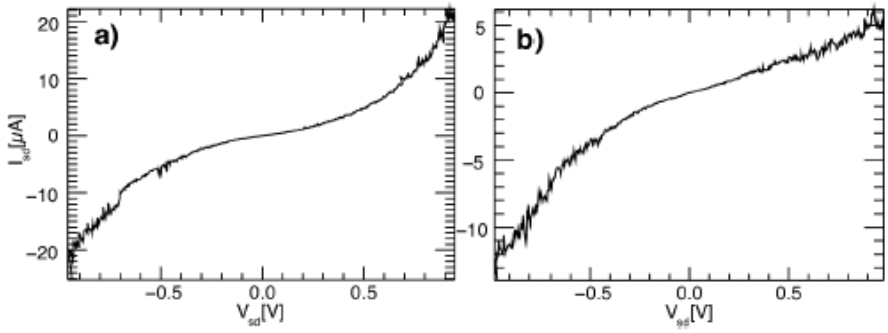

Figure 40. a) Symmetric I-V curve measured for nitrotolane and b) asymmetric "*S*" shape of I-V curve.

For the nitro group, the situation is slightly complicated: its function as anchor group is not as good as that of thiols because the mechanical coupling with the metal is not so reliable. For instance, in the presence of protected thiols in a molecule containing nitro groups, the nitro moiety demonstrates a certain interaction with gold surface which does not exist at the time of thiol deprotection (thiols have much more affinity with the gold surface than the nitro groups).[105]

[105] X. Zeng, C. Wang, A.S. Batsanov, M.R. Bryce, J. Gigon, B. Urasinska-Wojcik, G.J. Ashwell, *J. Org. Chem.* **2010**, *75*, 130.

2.2.6.2 Carboxylic acid anchor group

The binding nature of -COOH is not yet completely understood. Ionic and coordination interactions are, perhaps, the responsible for the binding to gold surface.[70] The experiments have been performed using STM setup with a solution of 1 mM of target material in H_2O. The tip has been approached to the surface with a constant small rate to guarantee its gently approach to the surface. This stands for a good procedure which is employed in most of the cases. During the contacting process, some molecules may remain hanged to the tip thanks to the anchor groups which create the contact. When the tip is pulled away, the current slopes down to zero (open-close circuit). Such process has been repeated for a large number of experiments and the results, generally, show ~30% of well-defined conductance peaks related to unimolecular junction formation, ~50% of smooth decay curves typic of direct tunnelling between tip and surface gold, ~20% of noisy curves. The most prominent peak is at 2.7×10^{-4} G_0 which is referred to the unimolecular junction formation, called also high conductance value (HC) due to the presence of another peak at 0.27×10^{-4} G_0. It has been stressed that both values have repeated peaks at multiple of 2.7 or 0.27 respectively. Tao *et al.* found the same behaviour in

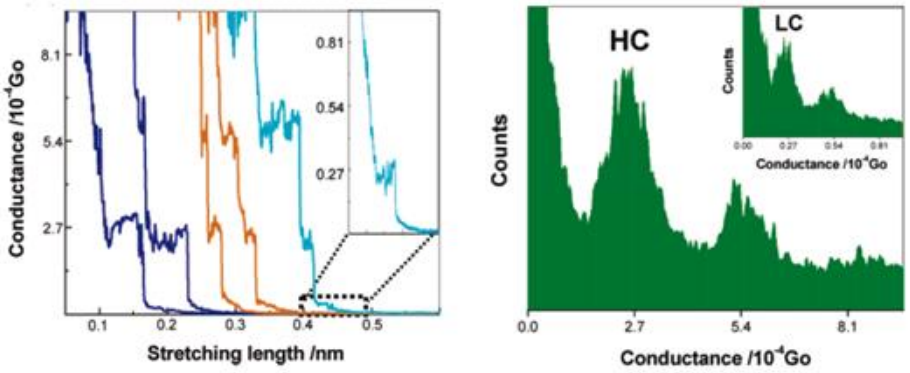

Figure 41. Conductance traces and histogram for dicarboxylic butane. Molecular junctionc conductance value is shown with an high value (HC) and low value (LC).

alkanedithiols too.[106] The histogram graphic shows the Gaussian curves related to the high and low conductance traces (Figure 41). The width of these curves gives us a parameter of stability of the molecule within the junction because at

[106] X. L. Li, J. He, J. Hihath, B. Q. Xu, S. M. Lindsay, N. J. Tao, *J. Am. Chem. Soc.* **2006**, *128*, 2135.

each value of conductance below this Gaussian curve belongs to a particular geometry configuration of the molecule. Therefore, the conductance value assigned, is only the most probable value which has been found in thousands and thousands of measurements.

Some experiments at different values of pH can display a better metal coupling of the carboxylic acid: the deprotonated species (carboxylic anion) has better coupling with gold surface (electrostatic interaction). The better coupling with gold may be obtained at basic pH, where the acid moiety is deprotonated. This experiment could be also performed for amines, if they can be easily dissolved in water. Butane dicarboxylic acid has the following values of acidic dissociation constant, pK_1 = 4.42 and pK_2 = 5.41. At pH = 1 the acid can only interact with gold through the lone pair of the oxygen atom of carboxy part, even though O is more electronegative than Au. At this value of pH, the conductance value reported by the authors is 1.5×10^{-4} G_0 (green area in Figure 42).

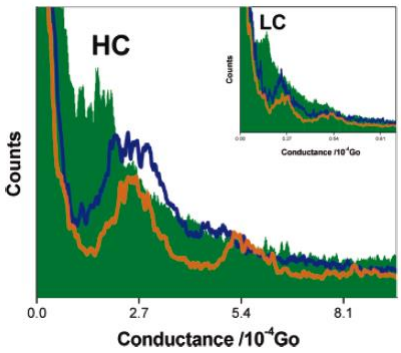

Figure 42. pH dependence in the conductance values for butane dicarboxylic acid.

At basic values of pH, *i.e.* 13, the acid moiety is totally deprotonated and it forms a bidentate anchor group due to the delocalization of negative charge in the carboxylic functional group, with an enhancement of binding ability to attach to gold surface. This situation gives rise to the value of 2.7×10^{-4} G_0 shown in Figure 42 as a blue curve. This is also the anchoring mechanism for typical dye sensitized solar cells (DSSCs) or Grätzel solar cells,[107] where acid moiety interacts with titanium oxide as surface electrode. If the pH condition are in between of the two p*K*s values for dicarboxylic acids, either the protonated species or the deprotonated ones are present in the solution. In this case the peak at 2.7×10^{-4} G_0 is smaller (orange line in Figure 42).

[107] a) S. Kim, J. K. Lee, S. O. Kang, J. Ko, J. H. Yum, S. Fantacci, F. De Angelis, D. Di Censo, M. K. Nazeeruddin, M. Grätzel, *J. Am. Chem. Soc.* **2006**, *128*, 16701; b) M. Grätzel, *Inorg. Chem.* **2005**, *44*, 6841; c) A. Hagfeldt, M. Grätzel, *Acc. Chem. Res.* **2000**, *33*, 269.

Despite these aspects, the -COOH remains a no suitable anchor group if compared with thiols and amine.

2.2.6.3 Dithiocarboxylic acid anchor group

Dithiocarboxylic acids linkers, also called carbodithioates, have been studied on systems like OPEs, focusing the attention over this anchor group compared with the pure thiols.[71] Important conclusions have been carried out by STM experiments. First of all, the carbodithioate end molecules provide a better coupling with the gold surface reducing the energy barrier in the interface between gold and the molecule. For such reason, they show larger conductance values than thiol terminated analogue molecules due to the sulphur hybridization in these systems. Thus, it is reasonable to talk about a cooperative effect of sulphur atoms at the moment of the contact with gold atoms. The molecular junction thus formed, is capable to generate a "mixed electron transport mechanism", basically formed by super-exchange and hopping mechanisms via the HOMO level that is the most aligned molecular orbital with the E_F of gold. The appealing carbodithioate anchor group has been firstly investigated by Tivanski *et al.* in a biphenyl system[108] but, no more studies have been carried out so far.

[108] A. V. Tivanski, Y. F. He, E. Borguet, H. Y. Liu, G. C. Walker, D. H. Waldeck, *J. Phys. Chem. B* **2005**, *109*, 5398.

2.2.7 Influence of wire-length on G_0 value

In this section, we want to stress the effect of wire-length onto G_0 value regardless of the anchoring of terminal groups onto the surface, already widely discussed in the previous sections. Nevertheless, some comparisons between the different anchor groups are important for a better understanding, using the wire-length as fixed and unambiguous parameter. Another nice treatment over the length effect onto G_0 value will be done for the molecular wires based on alkane from that based on aryl units.

In an interesting paper, already reported,[62] alkanediamines have been used to study this phenomena.

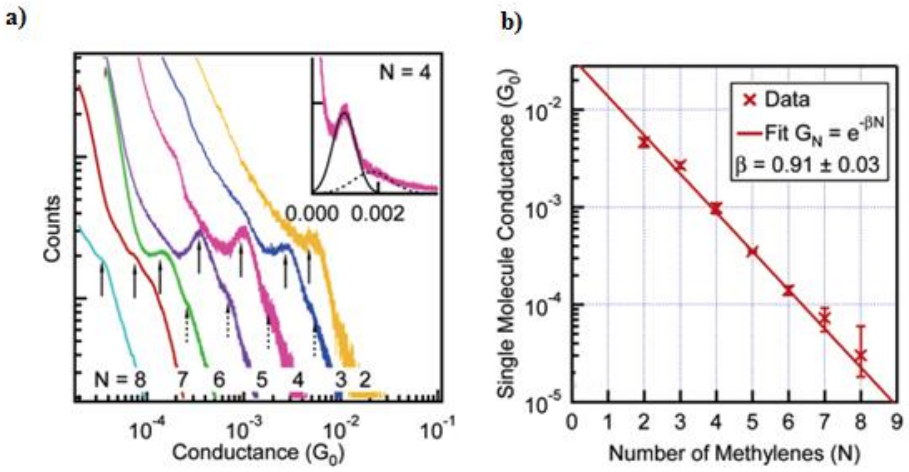

Figure 43. a) Conductance traces of alkanediamines from 2 to 8 methylene units as bridge; b) conductance histogram plotted against the number of methylenes.

Figure 43a shows the conductance histograms obtained, after several opening-closing circuit in the STM setup, for the series of alkanediamines up to 8 number (N) of methylenes. Solid arrows indicate the unimolecular conductance trace while the dashed arrows show the formation of at least two molecules within the junction. Figure 43b shows the calculated β value of such series using the conductance values versus the number of methylene units. The tunnelling decay constant (β), analogue to the attenuation factor in studies of bulk solution for PET analysis, is 0.91 ± 0.03 per methylene unit or 0.77 ± 0.03 $Å^{-1}$ for this series and it is comparable to that of alkanedithiols determined by different methods.[77]

Several studies have also been performed with arylamines. The conductance value reported for DBA is 6.4×10^{-3} G_0. The effect of different substituents (ED or EWG) over DBA molecule conductance has been investigated and discussed in terms of molecular orbitals involved in the electron transfer process.[87] We direct this discussion to the section 2.2.9 on the"influence of molecular geometry in G_0" where a deep analysis has been done onto these systems.

Regarding the Au-C bond, formed by alkane-$SnMe_3$ precursors, the G_0 value decreases with a factor of one order of magnitude for every two carbons added to the molecule (Figure 44).

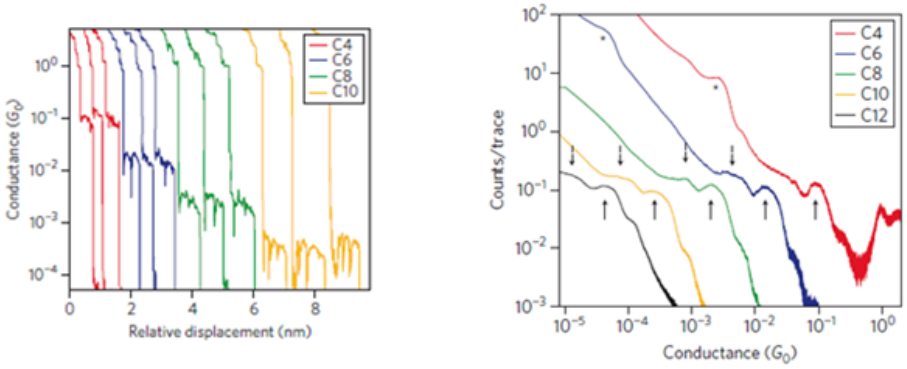

Figure 44. Conductance traces recorded by STM break junction of direct Au-C bonds generated by trimethylstannanes of alkanes.

The experimental data in Figure 44 show three interesting features of such systems:

1. The upward arrows are referred to the main conductance peak of each system and corresponds to the plateau observed in conductance versus length displacement after the formation of molecular junction as shown in Figure 44
2. The asterisks for C4 and C6 conductance traces correspond to the main conductance peak of C8 and C12, respectively. It may be explained by the statistical formation *in situ* of alkyl chain with double methylene number. The *in situ* dimerization is the evidence proof of cleavage of the -$SnMe_3$ group during the experiments. The mechanism is not well-defined and it may occur through: i) first absorption of one side of the

target molecule, which dimerizes before bridging the gold atoms of the drain metal contact, ii) via a reductive elimination mechanism.[109] To avoid such dimerization, some experiments have been carried out with low concentrated solution of the target molecule.

3. The downward dashed arrows indicates a shoulder at conductance value below the main peak: it is referred to structural rearrangements of the molecular junction during the open-close circuit (sharp dips in the left Figure 44 for each trace). The lack of such dips for C4 could indicate that, because of the shortest length of ethylene bridge, no rearrangements occur within the junction, making it the most stable molecular junction in this series.

The same approach used for alkane chains has been studied for the 2-4 poly-*p*-phenyls molecular wire with trimethylstannane end groups. They have been designed and synthesized for the application in STM break junction setup. The results are shown in the Figure 45.

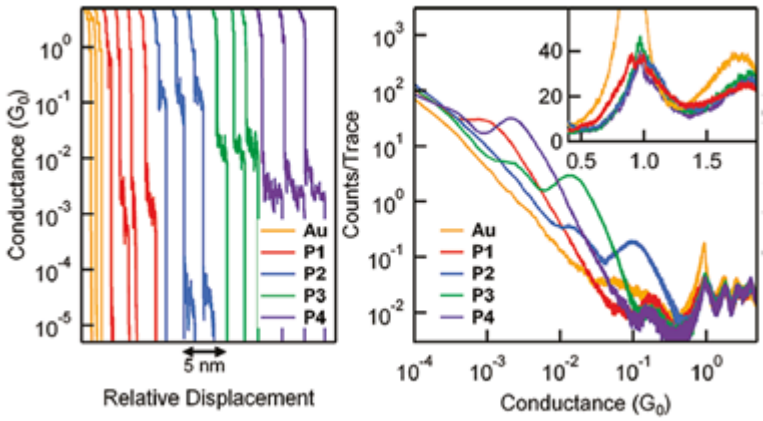

Figure 45. Individual conductance traces (left) and conductance histograms of over 10000 traces (right) for polyphenyl molecules up to 4 units.

The individual conductance traces show a clear plateau for the molecule with 2, 3 and 4 phenyl units (P2-P4) but for the P1 molecular junction is tricky to distinguish its value from that of the gold-gold contact (0.9 G_0 experimental value versus theoretical value of 1 G_0). The found values are 0.1 G_0, 1.4×10^{-2} G_0 and 2.2×10^{-3} G_0, respectively. Another plateau at lower conductance value

[109] M. A. Bennett, S. K. Bhargava, D. C. R. Hockless, L. L. Welling, A. C. Willis, *J. Am. Chem. Soc.* **1996**, *118*, 10469.

(1×10^{-3} G_0 and 3×10^{-3} G_0 for P1 and P2, respectively) was attributed, as well as in the alkyl trimethyl stannanes, to the *in situ* radical dimerization of benzylic radicals, generated by the homolytic cleavage of the C-$SnMe_3$ bond, to form an ethylene bridge between two benzene moieties. The ethylene moiety represents the bottleneck for the electron transport across the molecule itself (see Scheme 1). To verify the lower conductance value for P1, the *p*-xylylene dimer has been synthesized and measured under the same conditions reported above. It shows a clear peak at 1×10^{-3} G_0 which unmistakable demonstrated the *in situ* dimerization of P1. To also validate the experimental value of 0.1 G_0 for P2 molecule (biaryl core), the trimethyltin terminated analogue fluorene has been synthesized and its value has been found to be 0.17 G_0. The lower conductance value for the byaril system reflects a strict dependence from the torsional angle which is approximately zero in the fluorene molecule (this aspect will be argued in the following section).

The clear plateau observed in MCBJ experiments of trimethylsilyl OPE molecules, showed in Figure 46, also demonstrated how it is possible forming molecular junction simply by the use of a so common protected group in organic chemistry. Such plateau is related to the unimolecular conductance traces for each system: in Figure 46, the blue line trace is referred to the OPE1, the red to the OPE2, the green to OPE3, the black to the H-OPE-TMS. The alkynylide, formed *in situ* via TBAF deprotection, reacts very fast with the surface to create the direct, robust molecular junction. MCBJ experiments have been performed in a solution containing 0.5 mM of target molecules, 1.0 mM of TBAF dissolved in tetrahydrofuran (THF) and protected by the ambient with decane (this operation prevents the absorption of environmental absorbates).

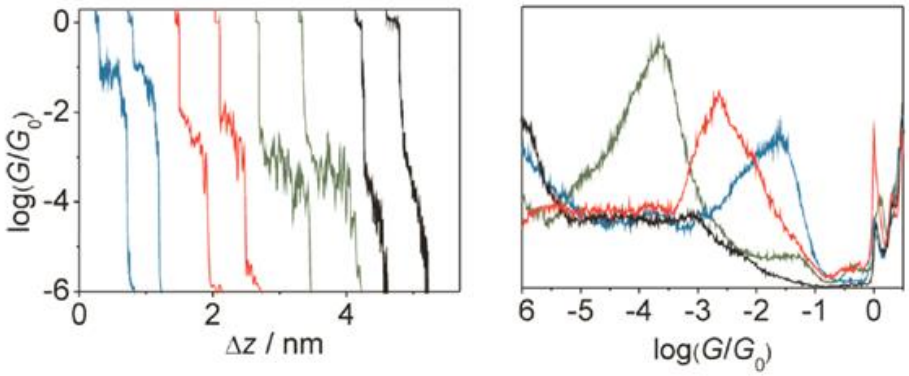

Figure 46. Conductance traces for the TMS-OPE systems studied with the MCBJ setup.

It is noteworthy to mark the case of H-OPE-TMS molecule: it does not provide one clear plateau due to the impossibility to form molecular junction for monosubstituted alkyne. Indeed, neither the presence of TBAF is sufficient to deprotonate the terminal alkyne, due to its high bond dissociation energy[110] and to the pKa value peer to ~ 30. Thanks to the one dimensional logarithmic scale graphic, the following conductance values, $10^{-1.8}$ G_0, $10^{-2.7}$ G_0, $10^{-3.5}$ G_0, have been attributed to OPE1, OPE2, OPE3 species.

In these experiments, lower values of conductance have been also registered and they have been attributed to the dimerization process which may be favoured, as first suggestion, by gold catalysed oxidative coupling for terminal alkynes.[111] This process has also been demonstrated using gap-mode Raman spectroscopy, under an exposure time higher, which provides a clear enhancement of one peak referred to the C-C triple bond between two aryl rings at around 2200 cm^{-1}. Further Raman analysis of chemically synthesized dimers OPE2 and OPE3 confirm the presence of this peak. The dimerization process does not occur when the solution is left under the same conditions (even for 24 hours) without the presence of gold atoms (NMR and Raman spectroscopy have been used to support this conclusion), or when applying a negative charge to the gold leads (the dimerization process is quenched but the junction formation is saved).

[110] a) H. Shiromaru, Y. Achiba, K. Kimura, Y. T. Lee, *J. Phys. Chem.* **1987**, *91*, 17; b) J. Segall, R. Lavi, Y. Wen, C. J. Wittig, *Phys. Chem.* **1989**, *93*, 7287.

[111] a) K. Kamata, S. Yamaguchi, M. Kotani, K. Yamaguchi, N. Mizuno, *Angew. Chem., Int. Ed.* **2008**, *47*, 2407; b) S. Adimurthy, C. C. Malakar, U. Beifuss, *J. Org. Chem.* **2009**, *74*, 5648; c) W. Yin, C. He, M. Chen, H. Zhang, A. Lei, *Org. Lett.* **2009**, *11*, 709; d) Z. Chen, H. Jiang, A. Wang, S. Yang, *J. Org. Chem.* **2010**, *75*, 6700; e) M. Zhu, M. Ning, W. Fu, C. Xu, G. Zou, *Bull. Korean Chem. Soc.* **2012**, *33*, 1325.

2.2.8 Influence of molecular conjugation and the substituent on G_0 value

It is well-known that conjugation is an important feature for molecular electronics. The π orbitals overlap of aryl compounds stands for an highway for the electrons. The main aspect of conjugation is related to the functionalization of one molecule. For instance, it is well-known that functionalization at *para* positions in an aryl moiety leads to a better conductance value than that at *meta* positions.[112] An example is reported by Venkataraman *et al.* over dimethylthio stilbene molecules.[113] They synthesized these molecules and used them to study the conductance properties along with the force of the molecular junction just formed. The setup used for such purpose is an AFM (atomic force microscope) where the junction is formed between an Au-coated cantilever and the Au-on mica substrate represented in Figure 47:

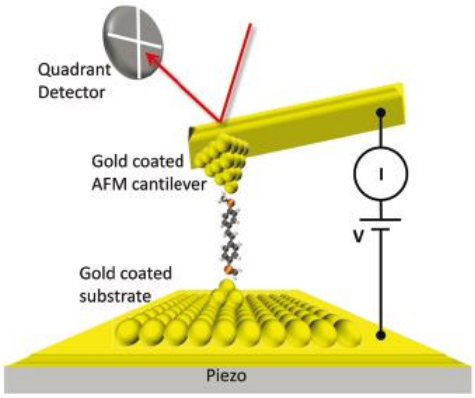

Figure 47. Schematic AFM used for the measurements of bonding force and conductance in dimethylthio stilbene.

For the first time, they were able to demonstrate that *meta* substituted stilbenes form mechanically stable contacts with gold but do not show a measurable conductance value due to the quantum mechanical interference within the junction. The cantilever allows them to continuously measure the deflections which give an idea about the force bonding-rupture of the molecular junction. Figure 48 shows this behaviour.

[112] M. Mayor, H. B. Weber, J. Reichert, M. Elbing, C. von Hänisch, D. Beckmann, M. Fischer, *Angew. Chem. Int. Ed.* **2003**, *42*, 5834.
[113] S. V. Aradhya, J. S. Meisner, M. Krikorian, S. Ahn, R. Parameswaran, M. L. Steigerwald, C. Nuckolls, L. Venkataraman, *Nano Lett.* **2012**, *12*, 1643.

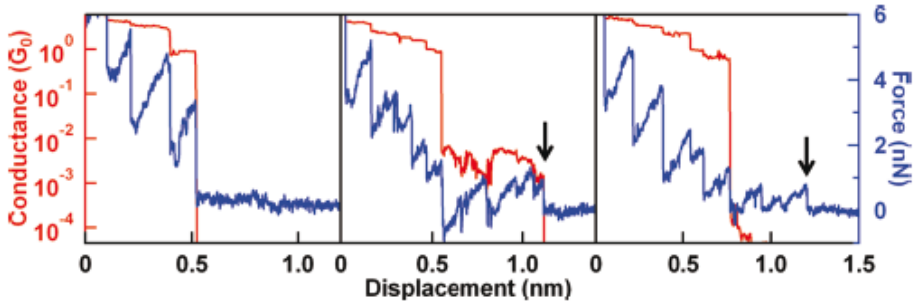

Figure 48. Traces showing simultaneously conductance (red, left axis) and force bonding rupture (blue, right axis) for Au-Au contact, Au/*para*-stilbene/Au and Au/*meta*-stilbene/Au junctions.

Starting from the left, the gold-gold junction is formed without any molecules in the experiment. The middle graphic represents the junction formation with *para* stilbenes while the right graphic shows as no evidence of measuring conductance value has been recorder when *meta* stilbenes were used to form the junction. Blue lines give us an idea about the formation of the junction and the slope of each force ramp indicates the stiffness of metal-molecule-metal junction, if formed.[114] When the contact is formed the force starts to be higher until the rupture of the junction. At this process, which is repetitive, a stepwise decrease of conductance has been observed (red line) until the rupture of the junction, indicated with a solid bold arrow in the graphics. Sometimes the abrupt step is also attributed to the conformational rearrangement of the molecule within the metal-metal contact. This is the case of *para* stilbene where an abrupt dip is observed at around 0.75 nm while the molecular junction is still hanged. Furthermore for the first two graphics (starting from the left) no more conductance or force features have been seen once the molecular junction is broken. In contrast, *meta* stilbenes show multiple force features after the rupture of the Au-contact with no evidence of molecular plateau, as already argued. The conductance value recorded by this experiments is 1.3×10^{-3} G_0.

In an attempt to understand the real influence of the π character of one molecule over the conductance traces, three patterns of conjugation are depicted in Figure: i) linear enhancement of molecular wire with ethynylene spacer between the aryl units, ii) diagonal increment length and iii) vertical

[114] S. V. Aradhya, M. Frei, M. S. Hybertsen, L. Venkataraman, *Nature Mater.* **2012**, *11*, 872.

increment of aryl units. For instance, in the work by Wandlowski *et al.*, an important comparison of molecule behaviour in the junction has been done focusing the attention onto the effect of vertical conjugation, π-conjugation up to the so called "cross-conjugation" in antraquinone molecules, and linear conjugation in olygophenylenethynilene bridges (OPE).[103]

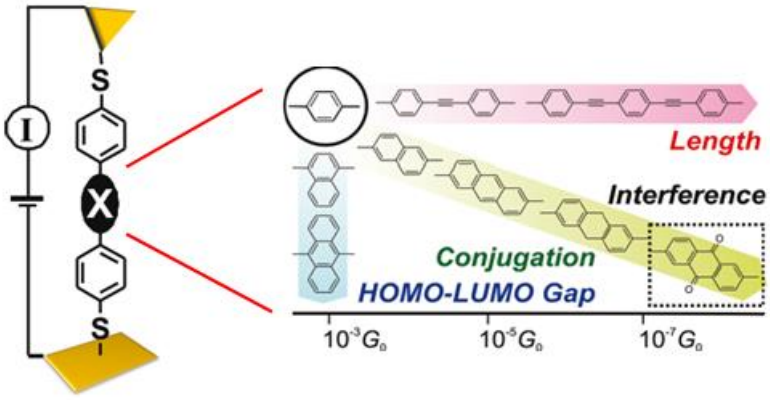

Figure 49. Extension of conjugation and its chemical and physical behaviour related with conductance value.

They synthesized dithiols terminated molecules where the **X** core is correctly substituted for their purpose with the aryl systems shown in Figure 49. They have measured either via STM-BJ and MCBJ how the enhancement of the length in **X** core demonstrates an aggravation of the conductance values (see the OPE systems). Even in the case of diagonal conjugation, the conductance values slope down with the increase of aryl subunit (aryl > naphthalene > anthracene) until the complete break of conjugation in the dihydroanthracene and in the peculiar case of the anthraquinone core. In the latter molecule, the carbonyl groups delocalize the conjugation towards them, thus interrupting the aryl conjugation. This phenomenon is called "cross-conjugation".
When the number of subunits (in this case aryl moieties) vertically increases to the electron transport preferred pathway (in general the linear one), the HOMO-LUMO gap becomes smaller in terms of energy value, creating therefore an organic material with semiconducting properties. If the HOMO-LUMO gap decreases, the conductance value increases. Therefore, the increase of the molecular length along with the increase of HOMO-LUMO gap in vertical conjugation get worse the conductance measurements.

2.2.9 Influence of molecular geometry on G_0 value

The conformation of molecules within the junction can affect, in some way, the tunnelling current.[115] The influence of torsion angle φ in flexible systems such as free biphenyls ($\varphi_{phenyls}$ = 34°) has been stressed and studied during the last years (Figure 50). The authors found that the conductance follows a $\cos^2\varphi$ correlation.[116]

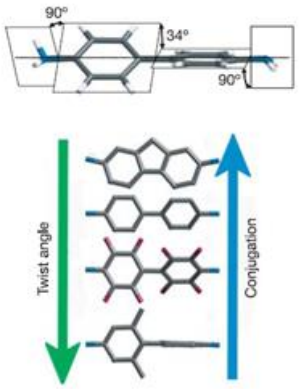

Figure 50. Effect of torsional angle in diamine aryl systems.

The conductance molecular property is expected to change with the torsional angle value of the molecule, always keeping fixed the distance between the two anchor groups (i.e., for the biphenyl dithiols terminated molecules, this value is around 1.06 nm which reflects the molecular length). Obviously, the planar molecule should be the best one in terms of conductance. Fluorene, one of the characters of this Memory, is the best central core, within this family of organic compounds, to be connected into the junction because we can consider it as a constrained biphenyl with an experimental value of φ peer to 1.1° degree (x-ray structure) compared with the DFT calculations where this value has been calculated to be 2.4° degree. Thus, enhancing the number of $-CH_2$ units in the bridge between biphenyls, the torsion angle increases with the consequent decrease of conductance. For freely rotating biphenyls and for those not so much constrained, only the HOMO states of each ring can be involved in electron transfer processes, since the LUMOs are further away in energy by several eV. This will be reflect in higher energy barrier in the molecule which led us to consider the electron transfer for such systems as an overlapping of independent phenyl matrices. Indeed, we can consider the electron transfer process as the sum of the contributions of one aryl with the other, as a first approximation, above all in systems with high value of φ.

[115] V. Mujica, A. Nitzan, Y. Mao, W. S. D. M. Kemp, A. Roitberg, M. A. Ratner *Adv. Chem. Phys.* **1999**, *107*, 403.
[116] a) L. Venkataraman, J. E. Klare, C. Nuckolls, M. S. Hybertsen, M. L. Steigerwald, *Nature* **2006**, *442*, 904; b) A. Mishchenko, D. Vonlanthen, V. Meded, M. Burkle, C. Li, I. V. Pobelov, A. Bagrets, J. K. Viljas, F. Pauly, F. Evers, M. Mayor, T. Wandlowski, *Nano Lett.* **2010**, *10*, 156.

2.3 Buckminsterfullerene: an "ideal" anchoring group

As already described, several anchor groups with different chemical nature and behaviour have been analysed theoretically and experimentally in STM or MCBJ. In this regard, C_{60} molecule could really be a promising anchor group. The reasons why C_{60} could be so interesting as anchor group stay on its features: i) the high symmetry, ii) the wide contact surface made by several weak interactions between the π orbitals of fullerene and gold atoms (C_{60} can resides better on the step-edge site of the surface with respect to the terrace region),[117] iii) the *n*-type property as the medium for the electron transport, iv) molecular orientation, atomic relaxation of the molecule, good affinity with different surface layer thanks to the strong orbital hybridization between 5*d* and 6*sp* orbitals of gold with π and π* of fullerene. Such hybridization leads to a shift in the electronic density from fullerene to the gold surface (it can be seen as a back-donation if considering the movement of the electron from gold to the C_{60} molecule), when a fullerene monolayer has been organised onto the surface. It is an important feature at the moment of measuring the conductance in tunnelling regime along with the energy difference between the molecular and the metal orbitals and, with the local density of state (LDOS) of the contact metal atoms at energy Fermi level. In general, to achieve high conductivity, we need large hybridization and large local density of states of the contact metal atoms with small energy difference between the molecular and the metal orbitals.

The C_{60} spherical icosahedral geometry with the π orbital cloud represents one feature to take into account because, thanks to this and to the size of fullerene, it is possible to see directly the molecule onto the surface like a "beacon" for the measurements either on pristine fullerene or over "dumbbell-type" molecular wires.

[117] C. Rogero, J. I. Pascual, J. Gómez-Herrero, A. M. Baró, *J. Chem. Phys*. **2002**, *116*, 832.

2.3.1 C_{60} stability over surface

C_{60} fullerene has recently demonstrated good affinity with some surfaces like Ag,[118] Cu[119] and Pt[120]. Scanning Tunnelling Spectroscopy (STS) analysis has been used to snap C_{60} molecules onto an Ag surface at low temperature (7 K) and to study the effect of interaction of the molecule onto the surface. Most of individual C_{60} are located on the step-edge surface of the silver platform. Concerning Cu(111) substrate, it has been demonstrated that C_{60} forms at room temperature large two dimensional islands at the step-edge,[121] while at low temperature (77 K) the size of the islands is reduced to ten fullerene units. The motion of the molecule onto a copper surface has been investigated through a lateral manipulation technique in STM using pulling, pushing or gliding mode to move the molecule either at room temperature or at low temperature where the natural motion of the molecule is reduced or completely frozen. To understand the interaction with Pt, MCBJ experiments in ultra-high vacuum have been performed with the C_{60} molecule and the conductance values clearly demonstrated the formation of the junction which is different from that in which the fullerene is not present (Figure 51).

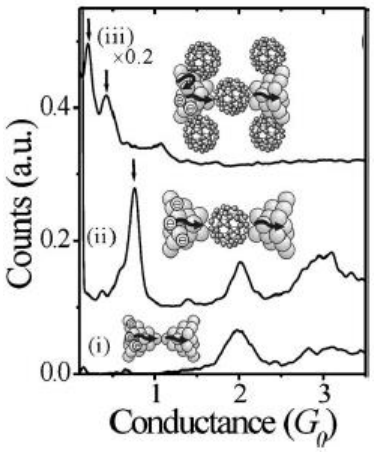

Figure 51. C_{60} junction in MCBJ setup with Pt as electrodes.

[118] X. Lu, M. Grobis, K. H. Khoo, S. G. Louie, M. F. Crommie, *Phys. Rev. Lett.* **2003**, *90*, 096802.
[119] A. Strózecka, J. Myslivecek, B. Voigtlander, *App. Phys. A* **2007**, *87*, 475.
[120] M. Kiguchi, *App. Phys. Lett.* **2009**, *95*, 073301.
[121] a) T. Hashizume, K. Motai, X.D. Wang, H. Shinohara, Y. Saito, Y. Maruyama, K. Ohno, Y. Kawazoe, Y. Nishina, H.W. Pickering, Y. Kuk, T. Sakurai, *Phys. Rev. Lett.* **1993**, *71*, 2959; b) C. Silien, N.A. Pradhan, W. Ho, P.A. Thiry, *Phys. Rev. B* **2004**, *69*, 115434.

The Pt-Pt junction has a conductance value of 2 G_0 which is still maintained when fullerene is bridging the metal junction. Furthermore, the peak related to the electron transmission along C_{60} is clearly emphasized by the presence of a peak at 0.7 G_0. In the case in which the fullerene solution is highly concentrated, the electrodes are saturated of molecules absorbed on them; consequently, the signal at 2 G_0 disappears and a new peak at a lower value of conductance appears (~0.5 G_0). It is lower compared with unimolecular junctions because of the possible electron transmission pathways along the molecules in between (Figure 52).

Thanks to these studies, the attention of the scientists moved towards the analysis of fullerene stability on gold surface.

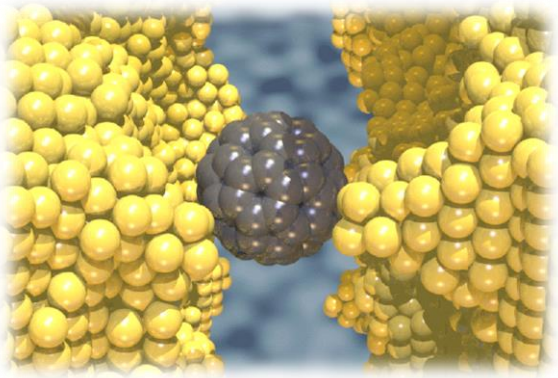

Figure 52. Fullerene molecule within gold leads.

C_{60} maintains a fairly unperturbed electronic configuration upon absorption which let us to study its stability. Pascual *et al.*[122] have frozen C_{60} molecule in a terrace of gold crystal using a high-resolution STM instrument at low temperature and under UHV. They snapped fullerene molecule immobilized over gold with different orientations where the lobs are referred to the accumulation of LDOS (density of states) (Figure 53).

[122] I. F. Torrente, K. J. Franke, J. I. Pascual, *J. Phys. Condens. Matter* **2008**, *20*, 184001.

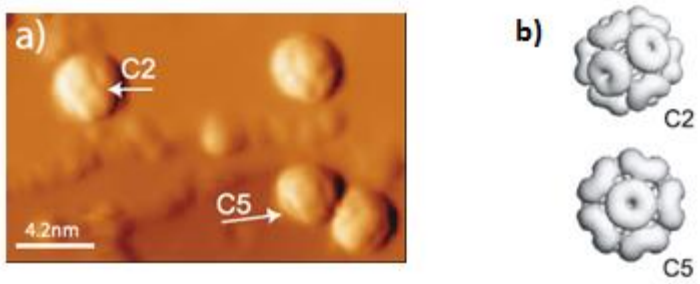

Figure 53. a) Image at 80 K of C_{60} orientation molecule over Au (111) surface; b) Isosurface of constant density of states for free fullerene showing C2 and C5 symmetry axis.

Cooling down the temperature up to 7 K and combining STM with STS techniques, it is also possible to see with more resolution the LDOS along the bond of fullerene molecule (Figure 54).

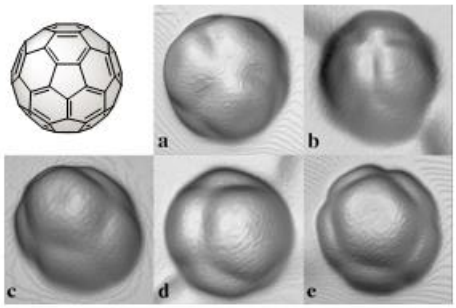

Figure 54. C_{60} surfaces with different orientation over gold crystal at 7 K.

In particular it is distinguishable a) a hexagon ring, b) [6,6] bond, c) [5,6] bond, d) an apex atom, e) an hexagonal ring by another point of view.[123]

Although binding between C_{60} and gold is weaker than that of C_{60} and other metals, it is far from negligible; the absorption energy is estimated to be 40-60 Kcal mol^{-1}. The conductance values of C_{60}/Au, C_{60}/Ag, C_{60}/Pt are respectively $0.3 \pm 0.1\ G_0$, $0.5 \pm 0.1\ G_0$ and $0.7 \pm 0.1\ G_0$ whilst in the contact created with Cu the found conductance value is $0.25\ G_0$.[124]

Moreover, Lu *et al.*, demonstrated that there are differences when C_{60} is layered over Au(111) respect to Ag(100): first, the LUMO and LUMO+1 are

[123] X. Lu, M. Grobis, K. H. Khoo, S. G. Louie, M. F. Crommie, *Phys. Rev. B* **2004**, *70*, 115418.
[124] N. Néel, J. Kroger, L. Limot, T. Frederiksen, M. Brandbyge, R. Berndt, *Phys. Rev. Lett.* **2007**, *98*, 065502.

shifted up in energy of 0.6 eV with respect to energy Fermi level of silver; second, there is no splitting of the threefold degenerated LUMO; third, the HOMO-LUMO gap is significantly larger than that measured in Ag(100) electrode experiments. By this study, it is remarkable the importance of the interaction with the surface in the measuring of LUMO, HOMO and HOMO-LUMO gap values for the C_{60} molecule. So that, it cannot be assumed a unique value for all of them, but it has been reported that its value should be around 2.3-2.9 eV over gold. This range of values differs in theoretical studies because it depends by the number of gold atoms taken into consideration and the basis set used during the calculation.

Among many types of molecules, C_{60} is suitable as anchor group for molecular bridge since its LUMO is situated at relative lower energies compared to other organic materials.

The differences between the HOMO and LUMO orbitals do not interfere with our idea to use C_{60} as anchor group. We know that the electron transfer can occur with the same probability even using the LUMO orbital as HOMO level. It becomes extremely important to consider fullerene with its intrinsic properties before analysing the effect of size and geometry of the electrode contact in the conductance experiments.

2.3.2 C_{60} electronic properties

It is well known that C_{60} is a reasonable well acceptor molecule with the possibility to accept up to six electrons as shown also in cyclic voltammetry experiments at low temperature in solution.[25] This characteristic together with the quantum loop internal current,[125] predicted using the Green's function method, make C_{60} a prominent molecule to be used in the molecular electronics field. The quantum loop internal current is a parameter which strictly depends by the degeneracy of the energy levels of C_{60} molecule and also by the symmetry of the molecule. Because C_{60} is highly symmetric, this feature is remarkable. When the current generated through source and drain finds a symmetric molecule in the middle (molecular junction), the internal current of the molecule (C_{60} for us) generates a large loop of current. A large loop current is induced in C_{60} molecule when connecting it into two electrode leads; it amounts to 24 times the source-drain current. The induced loop current distributes widely over the C_{60} molecule since it results from the interaction

[125] S. Nakanishi, M. Tsukada, *Phys. Rev. Lett.* **2001**, *87*, 126801.

among degenerate states at the LUMO. The presence of such internal loop current is an enhanced manifestation of the quantum electron transmission for C_{60} fullerene.

2.3.3 Theoretical approach over the formation of metal/C_{60}/metal junction

To study, therefore, the binding contact area of fullerene to the gold surface, we have to appeal to the theoretical calculations. The coordination of gold with the C_{60} surface is a complex phenomenon. On the basis of the infrared spectra (IR), Lyon and Andrews have suggested the possibility of gold to bind with the pentagonal ring of the C_{60} cage.[126] From a theoretical point of view, the binding site of gold atom/s can occur in different positions and with many options namely: i) single carbon atom η^1, ii) above the centre of fused six-member ring η^2, iii) the centre of fused five and six member ring, iv) above the centre of pentagonal ring η^5, v) above the centre of hexagonal ring η^6 where the η^2 is the most favourable.[127]

Even though various effects have been explored in the formation of the junction using STM technique, the "size effect of the electrode" phenomenon in the atomic scale is not so explored. For these reasons, several theoretical groups are now investigating such phenomenon using C_{60} but, unfortunately, the theoreticians are not in good agreement with themselves as widely discussed in the lines below.

Two different models are generally used to understand the atomic scale contact between the metal and the molecule (Figure 55): nanowire electrodes and bulk electrodes. The study of Zheng *et al.*[128] shows that these two kinds of electrodes can lead to big differences in the transport properties of molecular devices.

[126] J. T. Lyon, L. Andrews, *Chem. Phys. Chem.* **2005**, *6*, 229.
[127] M. K. Shukla, M. Dubey, J. Leszczynski, *ACS Nano*, **2008**, *2*, 227.
[128] X. Zheng, Z. Dai, Z. Zeng, *J. Phys. Condens. Matter* **2009**, *21*, 145502.

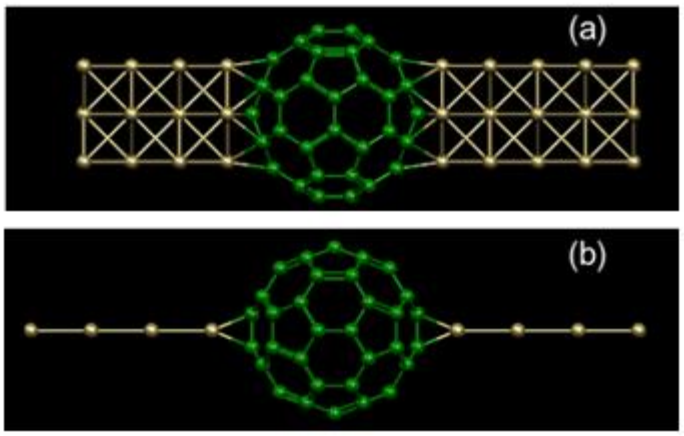

Figure 55. a) Nanowire configuration for a C_{60} junction; b) atomic chain configuration for the C_{60} molecule.

The size effect of electrodes in a C_{60} junction formation reveals with an *ab initio* study that there are differences in electron transport along the molecule itself. The transmission function in the nanowire/C_{60}/nanowire case shows wide peaks and platforms around the Fermi level and the equilibrium conductance is as large as 2.18 G_0, while in the atomic-chain/C_{60}/atomic-chain case, the transmission displays resonant peaks and the Fermi level lies between two peaks, resulting in a very small conductance of 0.027 G_0. There are more than two order of magnitude of difference.

According to Pérez Jiménez *et al.*, when the C_{60} molecule interacts with one gold atom - interaction that is supposed to be weaker - the conductance value is higher with a sharp form of the conductance band. In the case in which C_{60} interacts with two gold atoms, the interaction is stronger with a decrease of conductance value reflecting also in a broadening of their relative bands in a typical *I/V* curve.[129] The adsorption energy is smaller when the molecule sits on top of a gold atom (16 kcal mol^{-1}) than when the fullerene binds to a bridge site (35 kcal mol^{-1}, a bit higher than the double value of one gold atom), which explains the narrower and higher form of the conductance maximum corresponding to the on-top geometry with respect to the bridge site (the larger the interaction, the shorter the average time an electron resides in the corresponding molecular state which, according to Heisenberg's principle, broadens the peak). To show clearly these differences, STM has been used and

[129] A. J. Pérez-Jiménez, J. J. Palacios, E. Louis, E. SanFábian, J. A.Vergés, *Chem. Phys. Chem.* **2003**, *4*, 388.

two conductance values have been reported, one higher, already experimentally reported,[130] and one lower which has been seen for the first time.

2.3.4 Experimental evidences of metal/C_{60}/metal junction formation

For C_{60}, the possibility that gold atoms can interact with one or more than one carbon atoms due to the large curvature of C_{60}, is noteworthy. The multiple interactions are strictly depending on the rotation of the buckyball onto the surface and its location relative to gold surface atoms.[131]

Using the STM technique, C_{60} has been compressed in the pushing-pulling movement of the tip against the gold surface, revealing different conductance values.[132] In this work, an STM setup furnished by a tungsten tip was used to study the conductance of C_{60} at room temperature over an Au(110) surface. The found conductance value was 2.3×10^{-4} G_0, significantly lower in this "*heterojunction*" than in the case in which either the crystal and the tip are of the same metal "*homojunction*".

The molecular point contacts assume an important role in the drastic increase or decrease of conductance. It is described that when the value of bias is zero (metal orbital energy levels are aligned), the fullerene molecule stays close to a protuberance of the gold surface where it has much more points of contact. When a bias is applied, fullerene jumps onto the protuberance vertex because of the effect of external electric field.[133] The fullerene is so attracted. This phenomenon is in agreement with the physical phenomenon of electric charges that resides more in a tip shape objects than in the flat ones.

Several groups created the metal/molecule/metal junction using several techniques of deposition. The conductance values for C_{60} cover a huge range of G_0 from 0.1 in low temperature break junction experiments (10 K) to 5×10^{-4} G_0 at room temperature. Palacios *et al.*, also reported that C_{60} in the gold metal junction exhibits a metallic behaviour with a conductance in between 1 and 3 G_0.[134] The conductance of single molecule C_{60}, measured under different experimental setups and conditions, should be compared carefully.

[130] Y. Guo, M. Kiguchi, J. Zhao, K. Murakoshi, *Chem. Phys. Lett.* **2009**, *477*, 189.
[131] L. Wang, H. Cheng, *Phys. Rev. B* **2004,** *69*, 165417.
[132] C. Joachim, J. K. Gimzewski, R. R. Schlittler, C. Chavy, *Phys. Rev. Lett.* **1995**, *74*, 2102.
[133] R. Stadler, S. Kubatkin, T. Bjørnholm, *Nanotechnology* **2007**, *18*, 165501.
[134] J. J. Palacios, A. J. Pérez-Jimenez, E. Louis, J. A. Vergés, *Phys. Rev. B* **2001**, *64*, 115411.

It has also been measured that C_{60} between gold electrodes would form ionic contacts, giving rise to high conductance.[135]

Using MCBJ setup at 10 K in UHV, Böhler *et al.*[136] evaporated the molecule *in situ*. With this method, they obtained clean and low-resistance contacts to preserve the formation of strong coupling between the metal and the molecule. By comparing the conductance histograms and the conductance traces, they deduced that the conductance value of single C_{60} in the junction is close to 0.1 G_0. The formed junction did not show Coulomb blockade behaviour at low bias approaching to zero value, data which is remarkable to affirm that fullerene makes a strong interaction with gold, at least in UHV compared with the junction formed in solution. The Coulomb blockade may be seen as the increase of mean resistance (in our case the molecule) around zero value of bias; the molecule in between is thus considered as an insulating in which the electron transport is impeded. Using an improved UHV-STM setup, 0.2 ± 0.1 G_0 has been obtained.

Park *et al.*, proposed that the interaction between gold and fullerene is pretty physics and they reported a value of conductance peer to 2×10^{-4} G_0.[137]

Owing to the big differences of C_{60} conductance values, another effort has to be done over the study of the analysis environment.

When C_{60} is treated in solution, we have to consider some nanophenomena which may occur in the junction. We have to think that depending on the solvent of solution, C_{60} can be more or less absorbed into the gold surface. This can occur in organic solution with mesitylene where C_{60} has good solubility (1.5 mg/mL).[138] When a drop of other solvent, in which fullerene is less soluble such as *n*-decane, has put on the top of the absorbed layer to prevent either the mobility of the system or the absorption of other agents, the C_{60} molecule results already attached over gold, as a consequence of strong interaction. In an interesting work made by Guo *et al.*, the C_{60} molecule has been treated either in organic solution or in aqueous solution as well as in air to investigate its behaviour within the metal junction.[130] To do these experiments, the authors divided the work into three parts: i) measurement in air; ii) the conductance measurements were performed in mesitylene solution containing 1.0 mM C_{60}; iii) in $HClO_4$ aqueous solution.

---

[135] a) E. I. Altman R. J. Colton, *Phys. Rev. B* **1993**, *48*, 18244; b) A. J. Maxwell, P. A. Bruhwiler, D. Arvanitis, J. Hasselstrom, M. K. J. Johansson, N. Martensson, *Phys. Rev. B* **1998**, *57*, 7312.
[136] T. Böhler, A. Edtbauer E. Scheer, *Phys. Rev. B* **2007**, *76*, 125432.
[137] H. Park, J. Park, A. Lim, E. Anderson, A. Alivisatos, P. Mceuen, *Nature* **2000**, *407*, 57.
[138] R. S. Ruoff, D. S. Tse, R. Malbrota, D. C. Lorents, *J. Phys. Chem.* **1993**, *97*, 3379.

In air measurements, no trace of any molecular junction has been observed. It occurs because some environmental molecule could be absorbed onto the surface occupying the sites and altering the measurements. The alteration grade from ambient molecular absorption, such as nanoparticles and O_2, varies with the chemical species adsorbed and the percentage coverage of metal leads,[139] with the consequent occupancy of the molecular junction sites by part of absorbates. On the contrary, as shown in Figure 56, two conductance values for the experiment in 1.0 mM solution of mesitylene (red line) are referred to one C_{60} molecule in the junction and two molecules in the junction. The found values are 0.01 G_0 and 0.02 G_0, respectively.

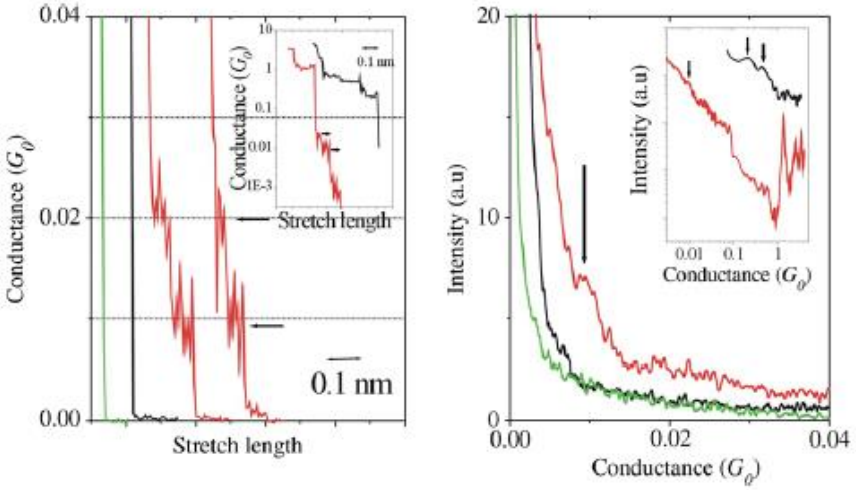

Figure 56. Experiments in solution of mesitylene for the C_{60} molecule.

Black lines are referred to the gold-gold contact, the green line to the experiment in solution of mesitylene without fullerene (neat solvent).
It has been demonstrated that the length of the last plateau of the conductance trace is directly correlated to the bond strength of the molecular junction.[140] More properly, it indicates the distance over which fullerene can be stretched before the rupture with gold metal lead. The average lengths of the last plateau, after several individual traces recorded, were 0.01 and 0.07 nm for single C_{60} molecular junctions and gold monoatomic contacts, respectively. The length for the C_{60} molecular junction was smaller than that for the gold atomic

[139] F. D. Novaes, *Rev. Lett.* **2003**, *90*, 036101.
[140] M. Kiguchi, S. Miura, K. Hara, M. Sawamura, K. Murakoshi, *App. Phys. Lett.* **2007**, *91*, 53110.

contact. This result suggests that the interaction between Au and C_{60} may exist to form the junction, but it is rather weaker than the Au–Au interaction.
The conductance measurements of the C_{60} molecular junction have also been performed in 0.1 M $HClO_4$ as shown in Figure 57. Similarly, the two steps at about 0.01 and 0.02 G_0 have been observed in the conductance trace and the 0.01 ± 0.003 G_0 peak appeared in the histogram. The conductance of the single C_{60} molecular junctions in 0.1 M $HClO_4$ was determined to be 0.01 G_0, which is consistent with the conductance value obtained in mesitylene.

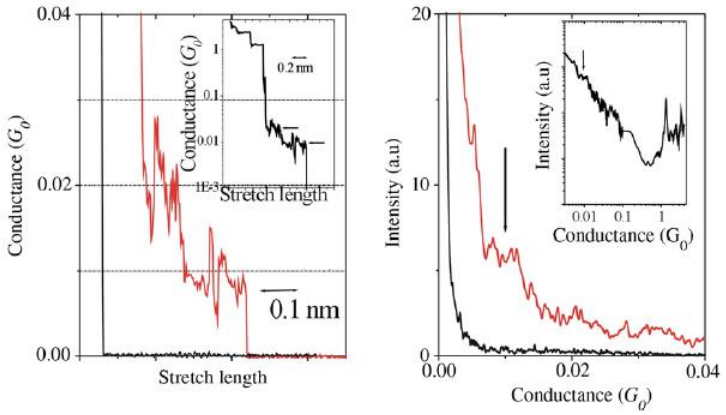

Figure 57. Experiments in aqueous solution for the C_{60} molecule.

However, the formation of the C_{60} junction in solution proceeds through a different mechanism. This can be justified by the conductance value and length of the last conductance plateau. Since the gold wire stretching was performed in solution, the metal leads were always covered by a layer of solvent molecules. The absorbed C_{60} molecules are likely to be supported by the solvent layer. Its thickness is expected to be in the order of one monolayer. During the wire stretching, C_{60} molecule would diffuse on the surface until bridging the nano-gap between the gold electrodes (to clarify it, see Figure 58). The junction is actually composed by solvent layers and the C_{60} molecule, and the reduced conductance values have been accounted for by the presence of such layer.

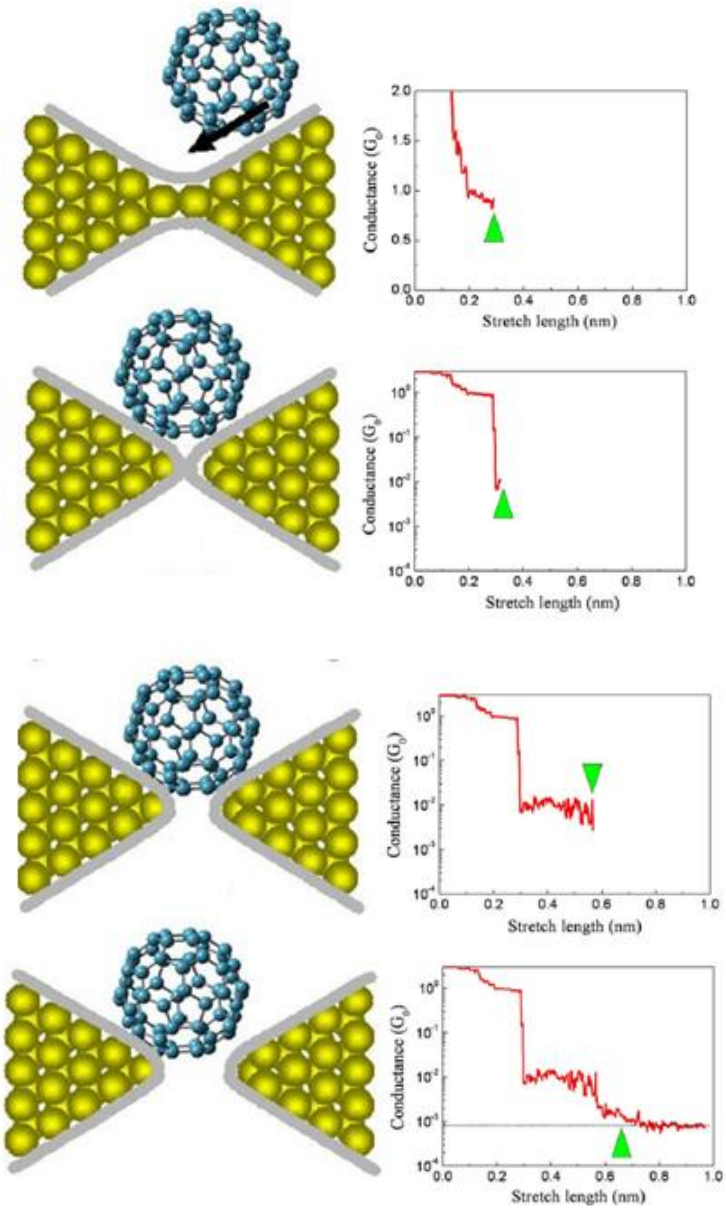

Figure 58. Sliding model of C_{60} over a completely covered gold surface by solvent monolayer. The conductance traces clearly demonstrated the molecular junction formation until the rupture.

In addition, because the interaction between C_{60} and gold would be mediated by the solvent layer, a decrease in the stretching length of the C_{60} molecular

junction appears in contrast with the UHV experiments where the solvent layer does not exist.

To summarise, the huge range of conductance values may be read as a really suitable advantage for fullerene to be used as anchor group. The main role of an anchor group is that it has to provide the correct chemical linkage to the electrodes without tuning the essential properties of the molecular backbone. In this sense, it remains to be clarified whether or not C_{60} is too invasive to be used as an anchor group.

2.4 Dumbbell-type molecular wires

Dumbbell-type molecular wires based onto fullerene may be promising molecules for STM and MCBJ studies, essentially because in this way, we can observe the effect of the wire itself, its chemical nature, its configuration between the junction, its physical parameters and, furthermore, we may compare it with the other simple molecules already used for such purposes.

We proposed the design of dumbbell-type molecular wires, in particular, with some properties that are typical for the study of molecular wires in a nanoscale approach. Among them, we can mention the stiffness, symmetry and linearity of the molecules, its intrinsic chemical and physical stability, the π conjugation between fullerene and the bridge, the visibility onto gold surface thanks to the presence of fullerene which acts as "beacon" in order to see exactly where the molecule is located before and after the measurements.

2.4.1 Historical background of dumbbell-type molecules

The synthesis of fullerene dimers, nowadays known as dumbbells owing to their shape, has been widely investigated. Essentially, there are two possible strategies to connect two C_{60} stoppers at the end of the molecules: i) the dimerization of C_{60} itself or its derivatives, ii) reaction over terminal bifunctionalised molecules.[141] The electronic interactions between the C_{60} units themselves as well as between the C_{60} units in fullerene dimers and the electroactive spacer have been the subject of different studies, especially regarding their electrochemical and photophysical properties for application in photovoltaic devices and, recently, for the conductance experiments performed in STM and MCBJ setups. Concerning the electrochemical processes in solution via cyclic voltammetry, C_{60} moieties in dumbbell-type molecular wires generally behave independently, giving rise to unique reduction waves that demonstrate the simultaneously reduction of both fullerenes.
Some dumbbell molecules have been synthesized using dimerization processes which sometimes do not reflect the typical conditions of chemical reactions. Indeed, strong conditions are mandatory to obtain this class of compounds. C_{120} separated by cyclobutane or by an heteroatom havee been obtained and their stability study together with their electrochemical properties in the past years.

[141] J. L. Segura, N. Martín, *Chem. Soc. Rev.* **2000**, *29*, 13.

Another strategy to form dumbbell fullerene molecules is represented by the alkyl radical addition of R· over C_{60}. It occurs very fast and without any kind of control over the fullerene double bonds; thus, it is quite tricky to control the formation of the species RC_{60}·. The stability of this species, which may be easily detected by electron paramagnetic resonance (EPR), hinges on the nature of the substituent R. As general rule, the steric groups give rise to rather persistent radicals RC_{60}·. There is an equilibrium between the free functionalized fullerene radical and its dimer which is dependent on the temperature. The dimerization of RC_{60}· occurs via a 1,4 addition over another C_{60} cage which is well distinguishable via UV spectra from the 1,2 adduct. The resulting dimer presents a C-C single bond between the two spheres providing a good molecular example for internal rotation and for the so called "*rotational isomerism*".[142]

Several groups have also investigated the formation of a dumbbell with a polyyne core using cyclopropane as linker with C_{60}. For instance, Diederich *et al.*, synthesized the cyclopropane fullerene derivative functionalised with a free alkyne and a protected one. Using the unprotected alkyne, they obtained in reasonable yield the dumbbell molecule through general Hay homocoupling conditions (Scheme 2).[143]

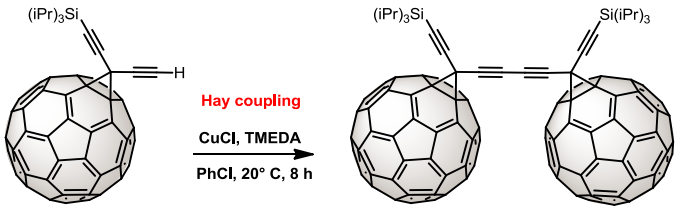

Scheme 2. Hay coupling reaction over C_{60} derivative.

Another possibility to form dimers is given by the formation of carbene species over a cyclopropane functionalization obtained by heating the precursors at high temperature (~450-550° C).[144] Once formed the carbene under these strong conditions, it can react with a double bond of a new C_{60} cage generating a spirocompound C_{121} or, it can undergo a dimerization process to form a dumbbell with a double bond between the two cyclopropane moieties.

[142] S. Lu, T. Jin, M. Bao, Y. Yamamoto, *J. Am. Chem. Soc.* **2011**, *133*, 12842.
[143] H. L. Anderson, R. Faust, Y. Rubin, F. Diederich, *Angew. Chem., Int. Ed.*, **1994**, *33*, 1366.
[144] N. Dragoe, S. Tanibayashi, K. Nakahara, S. Nakao, H. Shimotani, L. Xiao, K. Kitazawa, Y. Achiba, K. Kikuchi, K. Nojima, *Chem. Commun.* **1999**, 85.

Concerning the second strategy, the typical cycloaddition reaction, already discussed in this section, has been used as a final step for the synthesis of several compounds. In this way, a great deal of molecular bridges have been inserted between two C_{60} stoppers and among them, we can mention electroactive bridges like porphyrins,[145] bipyridines also complexed with Ru,[146] tetrathiafulvalene,[147] extended TTF unit,[148] etc. All of them have been used in further photophysical experiments. Oligophenylenvinilene (OPV) and polythiophene bridges have been trapped by fullerenes for photovoltaic devices[149] with high efficiency thanks to their timescale of charge separation *versus* charge recombination (ps *vs* μs) processes in photoinduced electron transfer studies.

Recently, also transition metals have been used to catalyse the nucleophilic addition of aryl specie over fullerene.[150]

[145] a) J. P. Bourgeois, F. Diederich, L. Echegoyen, J. F. Nierengarten, *Helv. Chim. Acta*, **1998**, *81*, 1835; b) S. Higashida, H. Imahori, T. Kaneda, Y. Sakata, *Chem. Lett.* **1998**, 605.
[146] D. Armspach, E. C. Constable, F. Diederich, C. E. Housecroft, J. F. Nierengarten, *Chem. Eur. J.* **1998**, *4*, 723.
[147] S. Ravaine, P. Delhaès, P. Leriche, M. Sallé, *Synth. Met.* **1997**, *87*, 93.
[148] S. González, N. Martín, D. M. Guldi, *J. Org. Chem.* **2003**, *68*, 779.
[149] a) J. L. Segura, N. Martín, *Tetrahedron Lett.* 1999, **40**, 3239; b) R. A. J. Janssen, P. A. van Hal, J. Knol, K. Hummelen, *European Conference on Organic Solar Cells (ECOS* 1998).
[150] a) S. Mori, M. Nambo, L.C. Chi, J. Bouffard, K. Itami, *Org. Lett.* **2008**, *10*, 4609; b) M. Nambo, Y. Segawa, A. Wakamiya, K. Itami, *Chem. Asian J.* **2011**, *6*, 590.

2.4.2 Dumbbell-type molecules in our group

In 1996, our group implemented the Prato reaction over a bridge molecule containing piperidine separating two units of benzopyrrolidino[60]fullerene (Figure 59).[151]

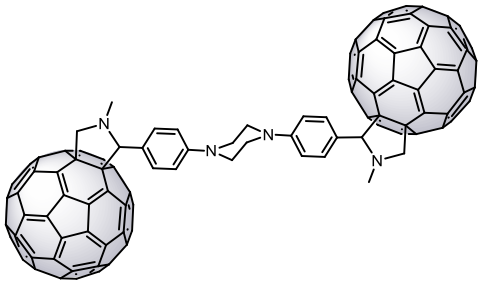

Figure 59. C_{60} dumbbell with piperidine as spacer.

A step forward has been realized in 2002 when an enantiopure C_{60} dumbbell was synthesized using an optically pure 1,1'-binapthyl core properly functionalized (Figure 60).[152] This core has been attached to fullerene cage using Bamford-Stevens protocol to obtain a cyclopropane. Both enantiomers have been isolated and characterized by conventional spectroscopic techniques and electrochemically too. The structure of both chiral dimers was determined by using theoretical calculations at the semiempirical PM3 level. In agreement with previous references, torsion angles of about 75° were determined between both naphthalene units, thus preventing conjugation between them. Due to the absorption in the visible region, the optical rotation of the chiral C_{60} dimers prepared was difficult to be determined in an accurate mode. However, we were able to measure the circular dichroism (CD) spectra of enantiomerically pure compounds.

[151] A. I. De Lucas, N. Martín, L. Sánchez, C. Seone, *Tetrahedron Lett.*, **1996**, *52*, 9391.
[152] F. Giacalone, J. L. Segura, N. Martín, *J. Org. Chem.* **2002**, *67*, 3529.

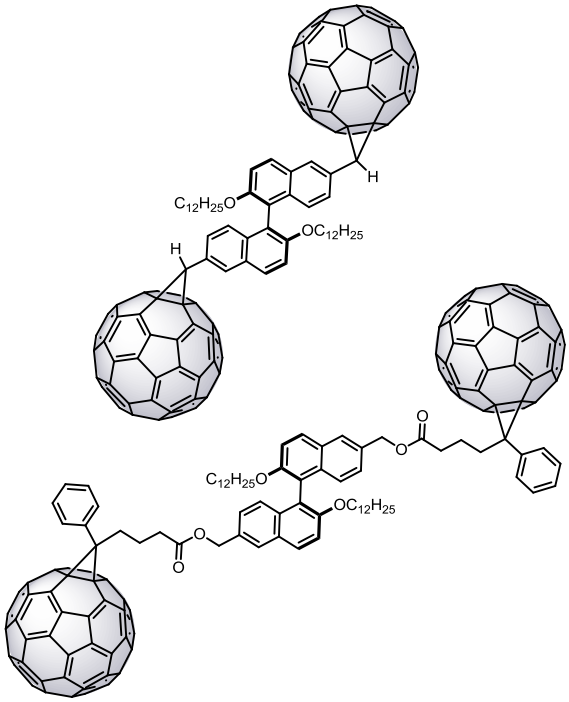

Figure 60. C_{60} enantiomerically pure dumbbells.

As already mentioned, some π-conjugated oligomers have been employed in DBA systems but also in triads like C_{60}-olygomer-C_{60}. Among them, we can mention OPV, OPE, oligothiophenes (OPTs)[153] and OFls. C_{60}-olygomer-C_{60} dumbbells based on naphtalene, benzene and thiophene spaced by vinyl moieties have also been synthetized in our group. All of these electroactive bridges have been covalently linked to C_{60} through Prato reactions.[154] The synthesis of C_{60}–OPE–C_{60} is based on the preparation of π-conjugated oligo-phenyleneethynylenes (OPEs) that must have two common features: i) the presence of solubilizing long alkyl chains, due to the well-known poor solubility of these rigid rod-like structures, and ii) the presence of functional groups at the terminal positions for further chemical reactions with C_{60}.

[153] a) P. A. van Hal, J. Knol, B. M. W. Langeveld-Voss, S. C. J. Meskers, J. C. Hummelen, Renè A. J. Janssen, *J. Phys. Chem. A* **2000**, *104*, 5974; b) E. H. A. Beckers, P. A. van Hal, A. Dhanabalan, S. C. J. Meskers, J. Knol, J. C. Hummelen, R. A. J. Janssen, *J. Phys. Chem. A* **2003**, *107*, 6218.
[154] L. Sánchez, M. A. Herranz, N. Martín, *J. Mater. Chem.* **2005**, *15*, 1409.

OPE oligomers has been attached to ethynyl groups[155] bearing additional aldehyde terminal functionalities to carry out a Prato reaction to obtain fullerene dimers (Figure 61):[156]

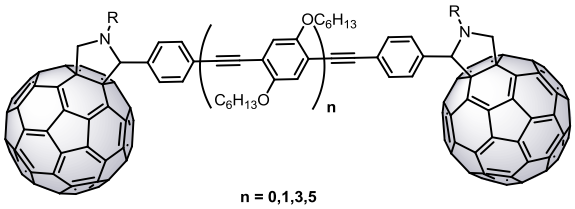

Figure 61. C_{60}-OPE-dumbbells.

OFls have also been trapped with two C_{60} stoppers in a recent paper published by our group.[157] In this work, the dimer, trimer and pentamer of fluorene units directly linked have been synthesized and attached to C_{60} through pyrrolidine rings as the result of Prato reaction (Figure 62). Such series have been characterized via electrochemical methods and photophysical studies. Electrochemical data showed an amphoteric behaviour with three reversible reduction waves for the C_{60} and irreversible oxidations for OFls without any kind of electronic interaction between the electronic partners (donor represented by the bridge and acceptor represented by the C_{60}) in the ground state.

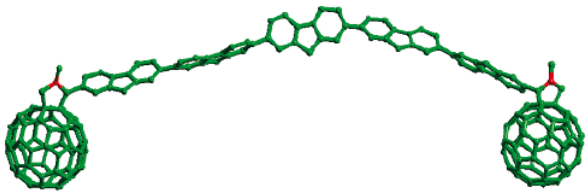

Figure 62. OFls dumbbell-type molecular wire with pyrrolidine linker; for clarity the alkyl chains in position 9 of each fluorene have been omitted.

[155] a) K. Komatsu, Y. Murata, N. Takimoto, S. Mori, N. Sugita, S. M. Wan, *J. Org. Chem.* **1994**, *59*, 6101; b) J. F. Eckert, J. F. Nicoud, J. F. Nierengarten, S. G. Liu, L. Echegoyen, N. Armaroli, F. Barigelletti, L. Ouali, V. Krasnikov, G. Hadziioannou, *J. Am. Chem. Soc.* **2000**, *122*, 7467; c) S. Fukuzumi, H. Imahori, H. Yamada, M. E. El-Khouly, M. Fujitsuka, O. Ito, D. M. Guldi, *J. Am. Chem. Soc.* **2001**, *123*, 2571; d) Y. Shirai, Y. Zhao, L. Cheng, J. M. Tour, *Org. Lett.* **2004**, *6*, 2129.

[156] C. Atienza, B. Insuasty, C. Seoane, N. Martin, J. Ramey, G. M. A. Rahman, D. M. Guldi, *J. Mater. Chem.* **2005**, *15*, 124.

[157] C. van der Pol, M. R. Bryce, M. Wielopolski, C. Atienza-Castellanos, D. M. Guldi, S. Filippone, N. Martín, *J. Org. Chem.* **2007**, *72*, 6662.

2.4.3 MCBJ of dumbbell-type molecules

In 2008, a novelty has been investigated in the application of dumbbells in the field of molecular electronics concerning the study of conductance measurements through MCBJ as molecular wires.[158] In principle, such types of molecules were allocated to the study of charge separation and charge recombination for possible application in photovoltaic devices. Unfortunately, this application did not give the desired results. Therefore and, thanks to the surface property of fullerene, they begin to be explored as good molecular objects in which the electrons can move from one electrode to the other, acting as a molecular junction. As already remarked, the 3D shape of fullerene lets to have a big area of contact with gold and, the easy to hybridize strongly with it, paves the way towards new fantastic but almost real application. Martin *et al.* compared two simple commercially available molecules with a synthetic dumbbell molecule containing the same core and connected to the fullerene through the nitrogen of pyrrolidine rings (Figure 63).[158]

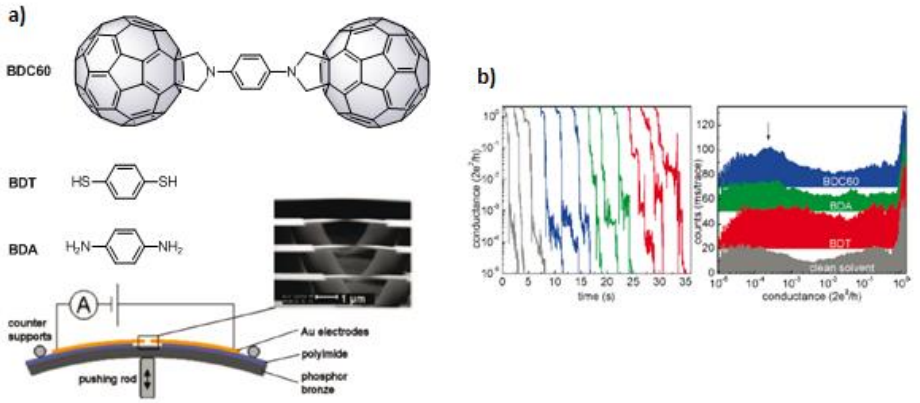

Figure 63. a) MCBJ setup and molecules investigated; b) conductance *vs* time and histogram of the experiments for the three molecules.

It has been demonstrated that C_{60} can act as good anchor group in MCBJ setup which gives rise to reproducible measurements as it is possible to note in Figure 64 where a broad peak (~ 3×10^{-4} G_0), marked by an arrow, is more evident in the case of 1,4-bis(fullero[*c*]pyrrolidin-1-yl)benzene (BDC60) with

[158] C. A. Martin, D. Ding, J. K. Sorensen, T. Bjornholm, J. M. van Ruitenbeek, H. S. J. van der Zant, *J. Am. Chem. Soc.* **2008**, *130*, 13198.

respect to the other two molecules, benzene dithiols (BDT) and benzene diamine (BDA). The analysis of the molecular junction stability made by the C_{60} has been carried out by the deep investigation of conductance in function of the time. It results more stable than BDT and BDA molecular junctions (Figure 64).

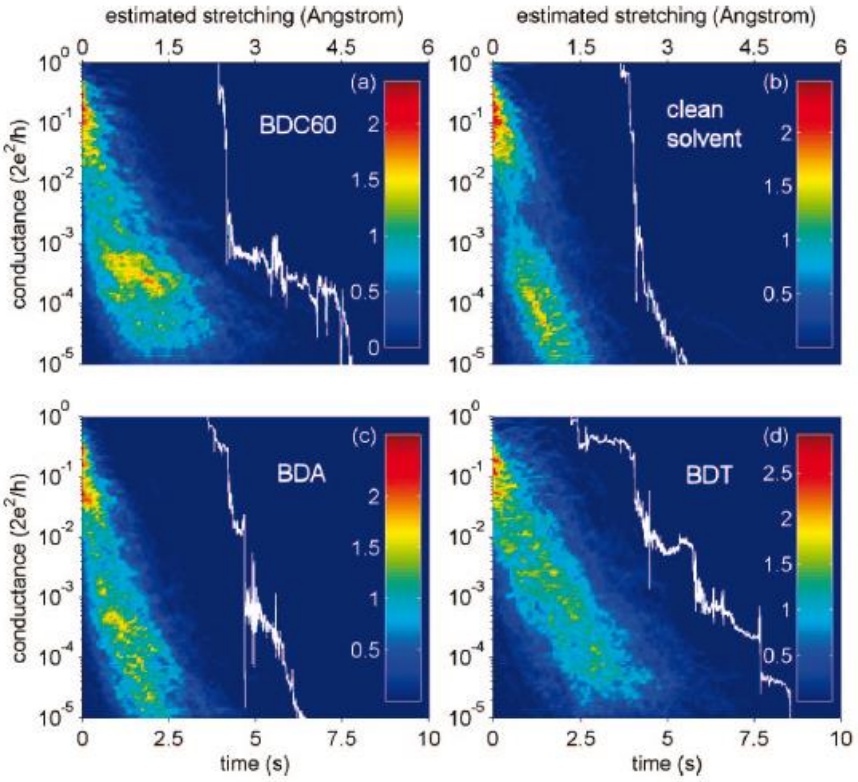

Figure 64. In each histogram, one single trace is marked in white for the dumbbell molecule (a), clean solvent (b), BDA (c), BDT (d). The experimental counts have been normalized and are colour-encoded in the right side of each histogram. The estimated stretching (Angstrom) in the upper part of the histogram gives an idea of the stability of the junction.

The *ab initio* DFT calculations in combination with non-equilibrium Green functions have been used to study the electron transport along this dumbbell type molecule.[159] Considering the properties of C_{60} in the contact with surface, it is reasonable to think the C_{60} as en extended electrode. In this work, the authors give a widely explanation about the relation between the C_{60} absorption site and the found conductance value: when C_{60} absorbs with an hexagonal ring the conductance value is higher ($\sim 4 \times 10^{-4}$ G_0) of one order of magnitude than when C_{60} absorbs with 6:6 bond. Furthermore, they theoretically demonstrated that the conductance values of this dumbbell molecules is independent of molecule geometry within the junction. It is also found that the conductance is mainly determined by six unoccupied state LUMOs situated over both fullerene backbones.

2.4.4 STM of dumbbell-type molecules

More recently, in 2011, a challenging approach to unambiguously measure the conductance of only one molecule under ambient conditions has been performed by Leary *et al.* using a home-built STM modified setup.[160] This technique could be seen as a better mean compared with MCBJ to understand the behaviour of the molecule within the gold leads. In the studies until now done with STM, when the tip is fishing in the molecule layer made onto the surface, the values of conductance can be referred to *n* molecules which are attached to the tip and the exact number of molecules cannot be extracted by the measurements. Other systems propose the use of gold nanoparticles with the correct diameter to be hanged to the tip in order to define better the contact surface for the measurements.[161] A common factor among all the possible methods of conductance measurements is that they attempt to define the conductance of a single molecule by carrying out a statistical analysis of many individual junctions. Problematically, there is no consensus on the best type of statistical approach to adopt. This can lead to data being interpreted differently by different groups, making difficult the comparison of results for the same compound. To overcome the mismatches between several groups, it should be

[159] T. Tada, K. Yoshizawa, *Chem. Phys. Chem.* **2002**, *3*, 1035.
[160] E. Leary, M. T. González, C. van der Pol, M. R. Bryce, S. Filippone, N. Martín, G. Rubio-Bollinger, N. Agraït, *Nano Lett.* **2011**, *11*, 2236.
[161] X. D. Cui, A. Primak, X. Zarate, J. Tomfohr, O. F. Sankey, A. L. Moore, T. A. Moore, D. Gust, G. Harris, S. M. Lindsay, *Science* **2001**, *294*, 571.

useful to find a straightforward approach to do these studies, *i.e.* wiring only one molecule. For the better understanding of conductance in dumbbell molecules, the STM experiments at low temperature (5.2 K) either with Au (111) or Cu(111) have recently been done over two C_{60} stacked molecules. In this way, we can understand if the electron transfer in dumbbell molecules with short length may occur through two fullerenes instead of the whole molecule including the effect of the electro-active bridge. Although the C_{60} contact with Cu is better[162] than with Au, the gold surface is easier to be manipulated and it gives us reproducible experiments. Only with Au surface, there is a strict dependence between the conductance value and the absorption orientation of C_{60}. Furthermore and really recently, Evangeli and coworkers measure the conductance and the thermopower of one C_{60} and two C_{60}s within the gold junction of an home-built STM.[163] The different "reactivity" of both surfaces may represent an explanation of such phenomena. Figure 65 shows three situations of conductance traces using Cu as substrates.

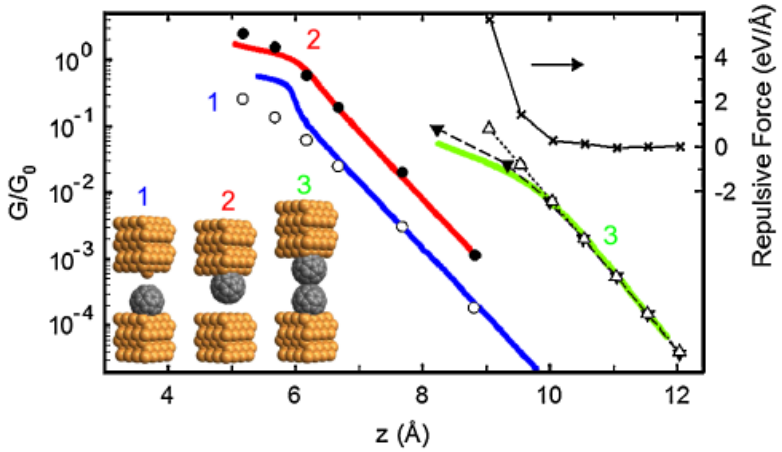

Figure 65. STM experiments on Cu(111) surface in three possible cases. Experiments (solid lines) *vs* calculations (symbols).

Curve 1 was obtained with a sharp metallic tip approaching to one C_{60} molecule. The right part of the trace corresponds to the tunnelling trace. Contact is indicated by an inflection of the trace at 0.3 G_0 in agreement with previous measurements on similar systems. Curve 2 represents a measurement with a C_{60} tip approaching the copper surface. Surprisingly, the contact

[162] G. Schull, N. Néel, M. Becker, J. Kröger, R. Berndt, *New J. Phys.* **2008**, *10*, 065012.
[163] C. Evangeli, K. Gillemot, E. Leary, M. T. González, G. Rubio-Bollinger, C. J. Lambert, N. Agraït, *Nano Lett.* **2013**, *13*, 2141.

conductance of 1.0 G_0 is substantially higher than with C_{60} on the surface (see the inflection of red line). Finally, the C_{60} tip was also approached to a C_{60} molecule on the substrate where the absorbed C_{60} is modelled to lay on a hexagon while the C_{60} on the tip side is adsorbed on a [5,6] bond. The displacement axis now shows the C_{60} to C_{60} centre distance which produces an offset of about 3.6 Å. The contact conductance of 0.01 G_0 is an order of magnitude smaller than expected, by theoretical point of view, for a C_{60} dimer.
In contrast to the experimental observation of a plateau, such model predicts an exponential dependence of the conductance on the C_{60}-C_{60} separation (open triangles in Figure 65) and no significant influence of the C_{60}-surface distance (filled triangles in Figure 65). This difference is due to an intermolecular repulsion at small distances that deforms the contact (crosses in Figure 65).
Experiments like these require low temperature in order to prevent diffusion of the molecules across the surface and UHV to reduce the molecular motions and, sometimes, to prevent redox processes of molecules not so stable under ambient conditions. It is thus, not easy to wire one molecule within two gold leads at ambient conditions. Despite this, Leary *et al.*[160] have designed an STM experiment which allow us to target only one molecule onto the surface, before and after the measurements. To successfully achieve this level of junction control, they used a difluorene C_{60} end-capped molecule (dumbbell) where fullerenes serve as effective anchor groups and beacons of the whole molecule (Figure 66). Using a diluted solution of the dumbbell molecule (ranging from 10^{-7} to 10^{-10} M), they have imaged and, afterwards, measured the conductance of such dumbbell with a gold tip. The images of the molecules onto the surface shows clearly the possibility to isolate only one molecule from the rest with diluted experimental conditions. The dumbbell appears as two big hills on the gold surface with a distance of 2.2 ± 0.3 nm, similar to that predicted, and they seem to be more stable and fixed than pristine C_{60} capable to move onto gold surface.

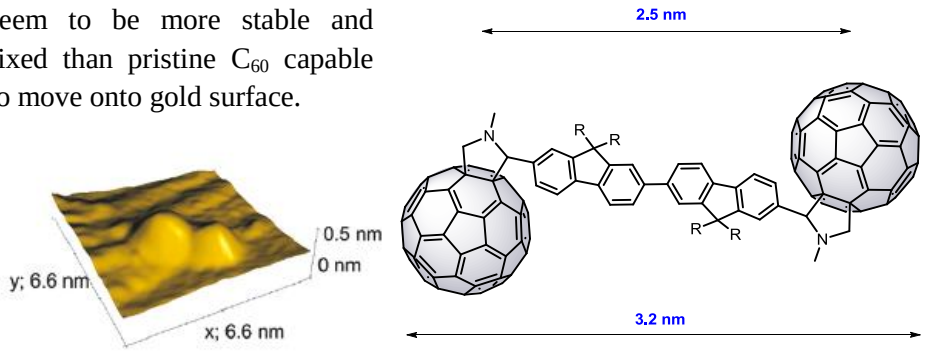

Figure 66. Surface visualization of a difluorene dumbbell molecule.

After its visualization, the conductance experiments have been carried out as follow: the tip was placed directly over the molecule and approached slightly to arrive a fixed value of G_{set} with an estimated separation of 1.8 nm from the tip to the surface in order to have the tip at 1 nm above one fullerene. Something to be underlined is that with the tip distance can be adjusted, varying the G_{set} value: increasing it, the distance will be reduced and viceversa.
The conductance *vs* distance traces have been recorded doing cycles of ON-OFF every two seconds. The revealed jump up of the conductance value could be attributed to the formation of molecular junction within the leads (Figure 67).

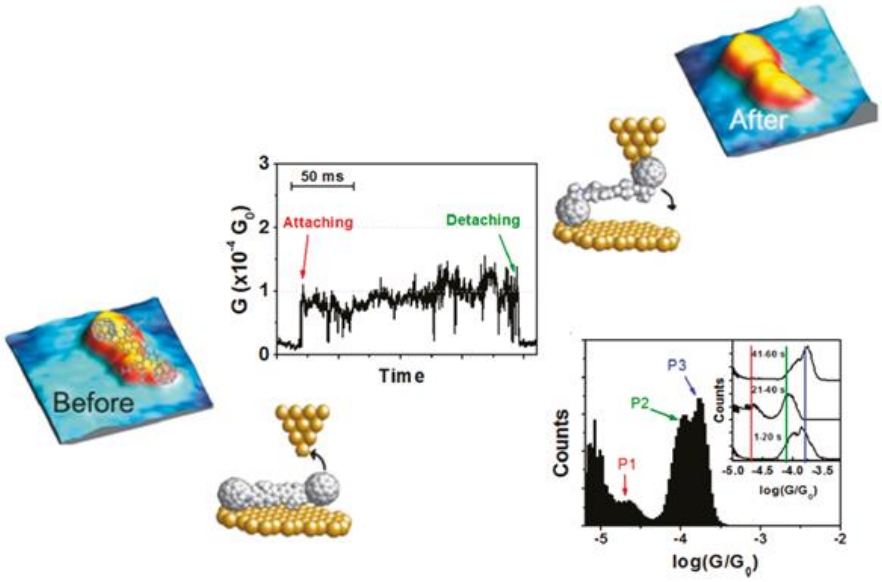

Figure 67. Evidence of molecular junction formation and its conductance values in the histogram.

To be sure that the junction is formed, they tried to pull away the tip from the molecule decreasing the G_{set} value and no evidence of molecular junction has been seen (the molecule stay onto the surface). In the histogram above, three peaks have been found during the experiments and they can be surely assigned to different molecular conformations and different point of contacts of the C_{60} with the surface. For sure, they cannot be attributed to the presence of more than one molecule in the junction. An interesting comparison of the conductance peak with the junction time formation clearly shows (the inset in

Figure 67) the predominant geometry configuration of the molecule bridging the metal gap. For these configurations, the conductance values can vary from 10^{-4} G_0 to 10^{-5} G_0.

Moreover, while the dumbbell is wired, stability junction controls have been achieved by carrying out stretching experiments where the conductance trace has been recorded slowly following the tip movement (Figure 68). The observed conductance plateau showed the stability of the molecule over a distance of several Å. After stretching, it has been possible to achieve the distance from the tip to the surface of about 2.3 nm which is less than the whole molecular length. During these studies, they were retracting the molecule from the surface and, before the cleavage of the junction, the tensioned angle Θ, thus formed, is of 45 degrees.

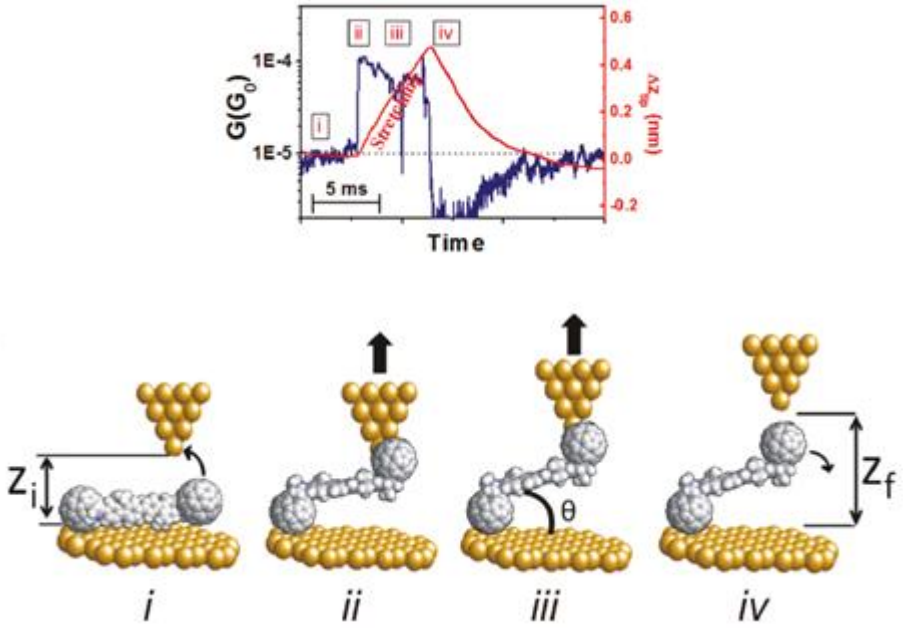

Figure 68. Stretching of molecule for testing its stability into the junction.

2.5 Fullerenes for photovoltaic devices

Nowadays, developing new methodologies to produce alternative energy represents one of the most discussed theme in the scientific community. Finding renewable energy sources to produce energy in a clean manner is essential for our life and for the future. The environmental problems are related to this new concept and a lot of European and International research projects have been created to guarantee a constant development of new technologies to improve the quality of life.

The conventional manner to create energy from petroleum has to be substituted by new ideas of making energy, first of all because the petroleum-fields are not so much and the reservoirs of petroleum are going to be over within some years. Another important theme is the air pollution which comes out from the use of energy sources not so respectable of the environment like petroleum for cars, nuclear energy centrals which produce tons of radioactive cinders and smoke. Thus, the new energy sources must be clean, economic and with long-life activity to produce, in an efficient manner, energy.

Biomass energy, windy energy, geothermic energy, hydroelectric energy and solar energy must improve the human life and work out the problems above mentioned. As reported in the histograms of the Figure 69, the projection of the renewable energy sources from 2010 to 2035 shows clearly that the solar energy is going to reach the biomass energy source. Nowadays, we are living in a middle phase of the solar energy development. Considering the global horizontal irradiation of sun light in Europe, Spain as well as Italy, are in really good positions to develop and to implant new photovoltaic panels all over the territory. The higher sunlight exposition stays in the south of Spain with more than 1950 KWh/m^2. This has to be comparable with the light exposition of Germany (around 1000 KWh/m^2) where this technology is, paradoxically, widely implemented (Figure 69).

The sunlight spectra may be divided into 5% of ultraviolet, 43% visible and 52% infrared light and we could take advantage of all these parts using photovoltaic panels based onto silicon or organic compounds. The idea to use organic compounds is strictly related with the similarity between C and Si, even though this has semi-metallic properties. Since the first photovoltaic device based on silicon was made by Chapin in 1954 with total efficacy of 6%, a great deal of materials, even organics and inorganics, have been implemented to transform solar energy in electric or chemical energy.

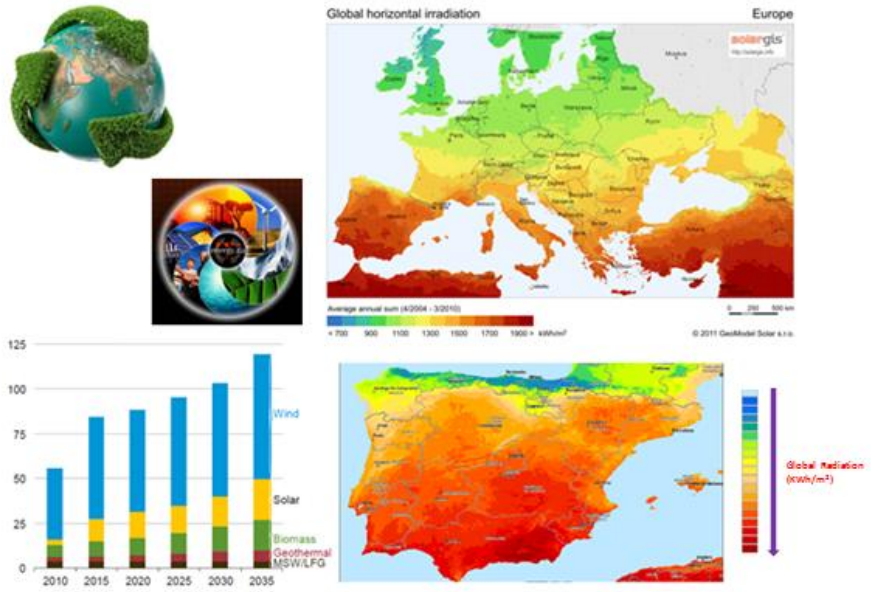

Figure 69. Renewable energy sources with particular attention to solar energy for Europe and Spain.

Even though the efficiency of silicon solar cells has not been achieved by organic solar cells, the latter seem to be a nice alternative to complement silicon panels because they can be easily prepared from solution. The resulting panels are cheaper and flexible. The flexibility is an important feature for further applications, *e.g.* panels, cars, clothes, etc, made by solar cells.
There are three main types of organic solar cells:

1. Dye-sensitized solar cells (DSSCs, or Grätzel cells) are composed of a porous layer of titanium oxide nanoparticles (semiconductor) covered by a molecular dye (generally -COOH terminated molecule) that absorbs sunlight. Once excited, it transfers the electron to the titanium oxide (anode) which is immersed into an electrolyte solution of I_3^- with a platinum bar as cathode (Figure 70).

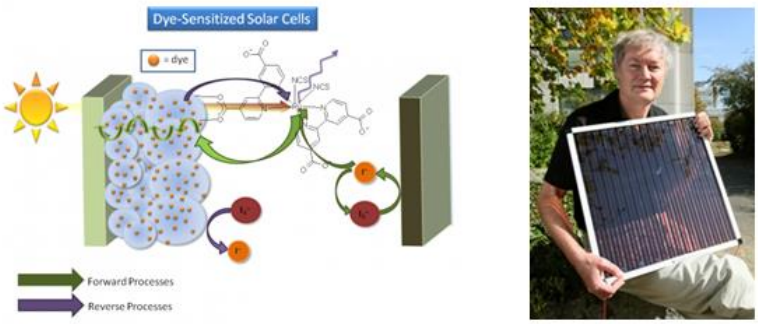

Figure 70. An example of Dye-Sensitized Solar Cell (left) and Michael Grätzel with a panel made by his own cells (right).

2. Bilayers solar cells, called also "Tang solar cells". They contain two different layers of organic photovoltaic materials correctly separated and carefully chosen to maximize the electrostatic forces created in the interface and to reduce the dispersion of energy. Both depositions must create a successful bilayer size to permit the light absorption and the charge separation of the exciton thus generated. However, a major drawback in this type of device is that only the excitons formed in the interface of the bilayer are able to produce electrons and holes. It means that all the material which lies up and down this thin area do not participate to the whole process. To avoid it, it has been thought to generate a bilayer more thin but the possibility that light can diffuse across the material, without being absorbed, must be taken into account.
3. Bulk heterojunction solar cells (BHJ) have been thought to overcome the problem presented in Tang cells. They are composed of a mixture of an acceptor molecule with a donor polymer in different ratio. It is important the grade of mixture of both entities because it enhances the interface surface in which the photoexcitation process occurs. The nano-morphology of the final cell become therefore important for its efficiency.

An example of bulk heterojunction solar cell is given in Figure 71 where the donor polymer material is *p*-type (blue material in Figure 71) and the acceptor molecule is an *n*-type material (reddish material in Figure 71).

The first represents the medium for the hole transport while the second is the medium for the electron transfer.

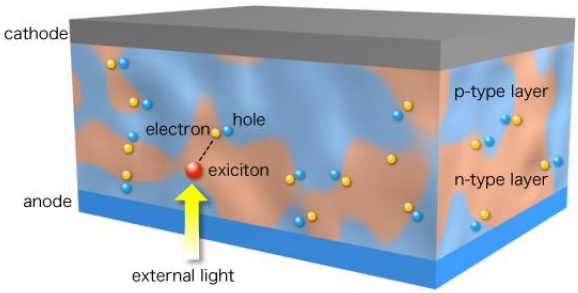

Figure 71. Typical BHJ solar cell.

The typical lifetime for the electron and hole in these materials is around 20 nm. It means that both charges can go through the material within this distance and then they have to be trapped by the electrodes to produce current. Otherwise, the whole process can be quenched by other factors, such as recombination processes occurring at the interfaces of the polymer with the acceptor domains. Thus, the nano-morphology of the device represents an important feature. For instance, the concentration of both species, their nature and properties are sometimes the responsible of the no correct nano-morphology of the device, thus producing a low efficiency of the cell. An example is shown in Figure 72, where is observed a preferential domains formation of the blend in toluene rather than in chlorobenzene, probably due to the higher solubility of the phenyl-C_{61}-butyric acid methyl ester (PCBM) molecule. This provokes changes in the efficiency of the final device.

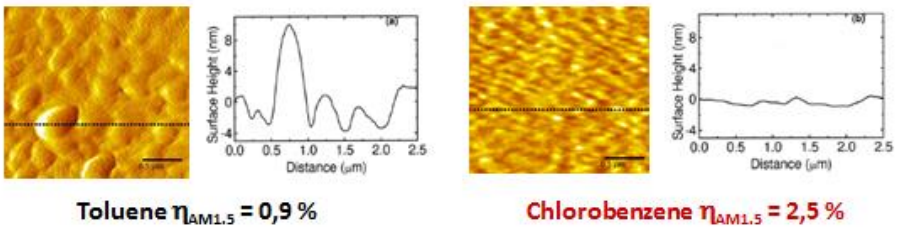

Figure 72. Nanomorphology differences seen by AFM of a BHJ blend made by PCBM/poly[2-methoxy-5-(3′,7′-dimethyloctyloxy)-1,4-phenylenevinylene](MDMO-PPV).

Furthermore, in organic semiconductor materials, if compared with inorganic ones, the moderate charge transport is caused by weak intermolecular interaction, hence resulting in electronic states localized on single molecules. To avoid such problems, scientists are studying different molecules to be mixed in BHJ with the help of useful deposition methods between the cathode and anode.

Despite the differentiation in the type of cells, currently, either the bilayer solar cells, called also planar heterojunction solar cells (PHJ) and, the bulk heterojunction solar cells are thinking to be built up following the so-called "*small molecule approach*".[164] In a few words, it consists in using one acceptor molecule as mentioned before but blended with another small molecule with donor features, thus avoiding the use of the polymer (Figure 73). They can be assembled to form a bilayer or a bulk device through two type of strategies: i) dry processing (thermal evaporation) and ii) solution processing, *e.g.* spin-coating, dip-coating, inkjet printing, spraying technique, for BHJ device fabrication. In this way, it is possible to compare the efficiency of both cells using the same materials.

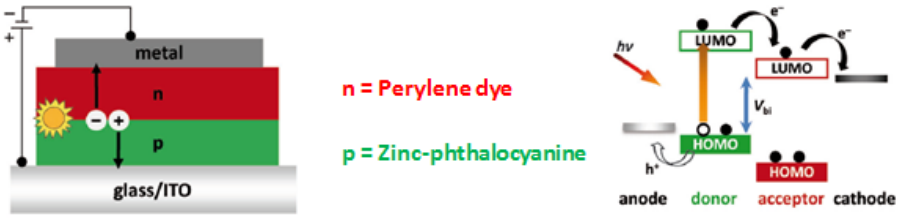

Figure 73. Example of PHJ device made by perylene dye (*n*-type material) and zinc-phthalocyanine (*p*-type material) with electron transfer mechanism.

The transformation of sunlight into current could be explained with four key points of the whole process:[165]

- **Light absorption**: the material must be photoactive. It has to absorb in the visible and IR regions in order to take advantage of the most part of the solar spectrum (95%). For this aim, it is important to have a polymer with adequate HOMO-LUMO gap to enable the photon absorption and the following excited state.

[164] A. Mishra, P. Bäuerle, *Angew. Chem. Int. Ed.* **2012**, *51*, 2020.
[165] a) G. Yu, J. Gao, J. C. Hummelen, F. Wudl, A. J. Heeger, *Science*, **1995**, *270*, 1789; b) S. Gunes, H. Neugebauer, S. Sariciftci Niyazi, *Chem. Rev.* **2007**, *107*, 1324.

- **Exciton formation**: the material uses the photon energy to form an excited state through the electron promotion to an orbital of higher energy.
- **Electron Transfer**: the exciton requires the correct lifetime to reach for the interface and generate the hole and electron which run to the electrode cells thanks to the different properties of both polymers, donor and acceptor.
- **Charge Transport**: the holes are transported through the *p*-type polymer while the electrons are transported through the *n*-type polymer. In this way they are separated and move towards the respective electrodes, giving rise to a potential difference.

At this point, it is noteworthy to establish some parameters useful for the comparison of the efficiency of solar cells. Among them, we can mention the size of the device, the nano-morphology of materials employed as already described, the type of cell and an important solar parameter: the AM1.5 as acronym of "air mass 1.5". It is based on polychromatic light and it is directly correlated with the solar spectrum. The air mass represents the reduction of power light as it passes through the atmosphere caused by the absorption and scattering of atmospheric agents, such as oxygen and carbon dioxide and other nanoparticles (Figure 74).

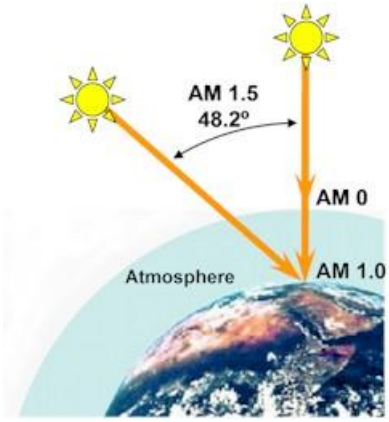

Figure 74. Solar irradiation passing the Earth's atmosphere.

One air mass, or AM1 is the thickness of the Earth's atmosphere. Air mass 0 (AM0) describes solar irradiance in space, unaffected by the atmosphere. The amount of solar radiation (insolation) over a given surface area of the earth may be reduced up to 45% by our atmosphere, primarily due to reflection and absorption. The AM1.5 spectra may be defined as solar spectra in a full sunny day with the sun disposed at 48.2° with respect the sun vertical to the Earth, as shown in Figure 74. The standard radiation intensity for AM1.5 is around 80-100 mW/cm^2 at 25°C.

A significant percentage of the total losses in a photovoltaic cell (more than 50%) are associated with the inability of the semiconductor material band-gap to absorb energy across the full solar spectrum (Figure 75).

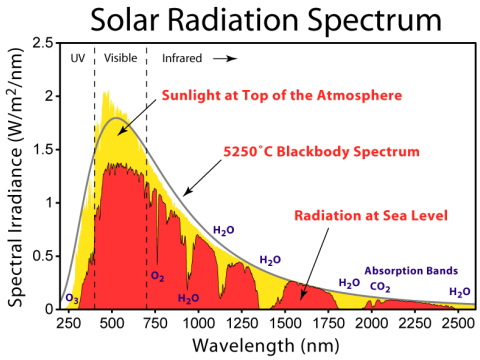

Figure 75. Solar radiation spectrum at different heights.

About half of the insolation reaching the earth's surface is in the visible portion of the electromagnetic spectrum. The amount that the direct irradiation is reduced is inversely proportional to the cosine of the incidence angle. As a consequence, the efficiency of many photovoltaic panels is reduced significantly as the incidence angle is increased.

Looking into the real function of solar cells, we have to evoke Figure 76. As it is shown, the first step is to connect the solar cell to the electrodes and measure its potential in the absence of light (dark curve in Figure 76). For little variation of applied potential, at certain point the current will increase due to the electrons streaming in the circuitry. In this case, no phenomena related to the material are under investigation because the cell is in the dark. The current in dark environment is simply obtained varying the potential without illumination. If the curve does not present that typical shape, something is getting wrong in the experiment (the shape of the cell, not well-positioned electrode contacts, etc.). After this step that we can consider as blank, the cell is exposed to the sunlight and a new J-V curve is registered. By this new curve, the solar cell's energy conversion efficiency (η) is obtained.

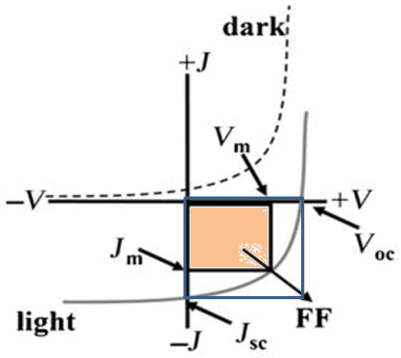

Figure 76. Current-Voltage measurement for a solar cell.

At the beginning of the process, the "short circuit current" J_{SC} is obtained when the external applied voltage is peer to zero and the electrodes are connected externally; all the current is created by the excitation of active material. It is the maximum photocurrent value. It depends by the number of the absorbed photons and, therefore, it is related to some characteristic of the device, for instance the surface area, the device thickness, etc. The "open voltage circuit" V_{OC} is the voltage when the current intensity is zero, or in other terms, when the photocurrent equalizes the external applied current or better, the maximum photo-voltage measured in the cell. It is strictly dependent by the energy levels of the HOMO of donor and the LUMO of acceptor molecule. If we consider the power of the cell as P = J × V (in Watt), at both points, it results peer to zero. The maximum value of potency (P_{MAX}) is given by the calculation of the area defined by current and voltage in which their product is maximum and, it may be calculated by the "fill factor" (*FF*) given by the following equation (Equation 4):

$$FF = \frac{P_{MAX}}{V_{OC} \times J_{SC}}$$

Equation 4. Fill Factor equation.

Fill factor is a ratio between the P_{MAX} and the theoretical potency (P_T) reachable at J_{SC} and V_{OC} value. As a consequence, this ratio gives a number always below the unity.

Eventually, the efficiency of the solar cell (η) is given by the ratio between the electrical power in output (P_{MAX}) compared with the solar power in input (P_{in}). A correction factor *m* for the spectral aberration of solar simulator is to be considered (Equation 5).

$$\eta = \frac{V_{OC} \times J_{SC}}{P_{in}} \times FF \times m = \frac{P_{MAX}}{P_{in}} \times m$$

Equation 5. Efficiency of a solar cell

where rendering explicit the fill factor, the total efficiency is giving by the ratio between the P_{MAX} and P_{in}, multiplied for the corrector parameter *m*.
Further two important parameters for the solar cells are the EQE (external quantum efficiency) and the IQE (internal quantum efficiency). The first is the number of charge collected per incident photon (expressed in %). The second is the number of charges collected per absorbed photons (also expressed in %).

2.5.1 Photovoltaic cells based onto C_{60} derivatives

Today, it results extremely important to solve the so called "problem of silicon". Once understood what progresses have to be done in this direction, we can move towards new materials which have to substitute or complement the silicon in the fabrication of the devices. In the field of solar cells, new panels or cells made by organic materials could pave the way to new possibilities thanks to their photochemical and photophysical properties.

C_{60} showed hopeful features to be used in photovoltaic devices. The first organic photovoltaic cell formed by C_{60} was made by Haddon in 1991.[166] Thanks to the already famous properties of fullerene to be a good electron acceptor, C_{60} may be used in polymer solar cells of different types together with the donor polymer, separated by the same into two layers (PHJ) or well in mixing with it into a typical bulk heterojunction (BHJ) device. This idea emerged by Alan Heeger and Fred Wudl[167]. They observed an electronic transfer from a polymer made by poly-*p*-phenylenvinylene (PPV) to C_{60}.

The first result of this kind of device showed low efficiency of the cell peer to 0.2 %.[168] To improve this value, Heeger and Yu decided to mix a donor polymer with fullerene in only one layer where, in theory, the surface contact between the polymer and fullerene might be higher.

[166] B. Miller, J. M. Rosamilia, G. Dabbagh, R. Tycko, R. C. Haddon, A. J. Muller, Herbard, *J. Am. Chem. Soc.* **1991,** *113*, 6291.
[167] N. S. Sariciftci, L. Smilowitz, A. J. Heeger, F. Wudl, *Science,* **1992**, *258*, 1474.
[168] N. S. Sariciftci, D. Braun, C. Zhang, V. I. Srdanov, A. J. Heeger, G. Stucky, F. Wudl, *Appl. Phys. Lett.* **1993**, *62*, 585.

The problem in this case was the scarce solubility of fullerene in the polymeric matrix, generating therefore acceptor islands or domains in the bulk; they generate a phase separation with the loss of total efficiency. To overcome this phenomenon, four years later, in 1995, different C_{60} derivatives were synthesized with the correct modification for this goal. An incredible example is the PCBM,[169] which matches really well with other polymers in the fabrication process of the solar cells. In 2001, Shaheen *et al.* obtained a 2.5 %[170] of efficiency simply solubilizing in chlorobenzene instead of toluene a derivative of poly-*p*-phenylenvinylene with PCBM in a ratio of 1:4 (Figure 72). The increase of efficiency has been attributed to the changes in nanomorphology of both materials in the bulk heterojunction solar cell. Changing now the donor polymer and using poly-(3-hexylthiophene), P3HT, extraordinary results have been obtained with EQE peer to 75% and η peer to more than a 5 %.[171]

Diphenylmethanofullerene (DPM is the acronym usually followed by a number indicating the length of the alkyl substituents of the phenyl ring) is another important family of fullerene acceptors that gave rise polymeric solar cells. with higher values of V_{oc}. On the other hand, the lack of crystallinity of DPM based blends is the cause of the decreased of the current and therefore of the overall efficiency.[172]

[169] J. C. Hummelen, B. W. Knight, F. LePeq, F. Wudl, J. Yao, C. L. Wilkins, *J. Org. Chem.* **1995**, *60*, 532.
[170] S. E. Shaheen, C. J. Brabec, N. S. Sariciftci, F. Padinger, T. Fromherz, J. C. Hummelen, *Appl. Phys. Lett.* **2001**, *78*, 841.
[171] a) F. Padinger, R. S. Rittberger, N. S. Sariciftci, *Adv. Funct. Mater.* **2003**, *13*, 85. b) P. Schilinsky, C. Waldauf, C. J. Brabec, *Appl. Phys. Lett.* **2002**, *81*, 3885.
[172] a) I. Riedel, E. von Hauff, J. Parisi, N. Martín, F. Giacalone, V. Diakonov, *Adv. Funct. Mater*. **2005**, *15*, 1979; b) A. Sánchez-Diaz, M. Izquierdo, S. Filippone, N. Martín, E. Palomares, *Adv. Funct. Mater.* **2010**, *20*, 2695; c) F. Piersimoni, S. Chambon, K. Vandewal, R. Mens, T. Boonen, A. Gadisa, M. Izquierdo, S. Filippone, B. Ruttens, J. D'Haen, N. Martín, L. Lutsen, D. Vanderzande, P. Adriaensens, J. V. Manca, *J. Phys. Chem. C* **2011**, *115*, 10873.

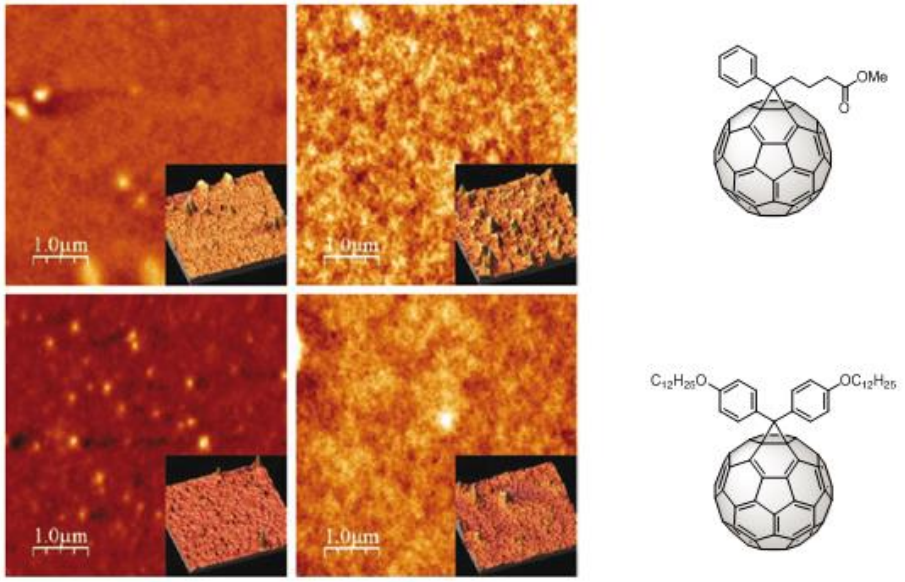

Figure 77. AFM images of two P3HT blends made by PCBM (up) and DPM-12 (down). The left surface is imaged at room temperature while the right surface after an annealing at 150°C for 20 minutes. Different roughness is visible for the blends.

Brabec *et al.* showed that exists a strict relation between the LUMO energy value of C_{60} derivative and the V_{OC} value.[173] This concept can be translated in a direct relation between the first reduction potential of the acceptor moiety and the open circuit voltage as shown in Figure 78.

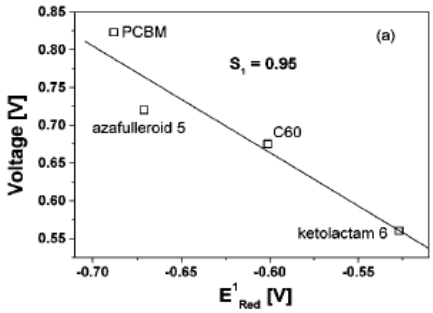

Figure 78. Relationship between LUMO of fullerene derivatives and V_{OC} through voltammetry studies.

As lower the acceptor character of the molecule (reduction potential towards higher voltage values) as higher is the V_{OC}. To study this phenomenon together

[173] C. J. Brabec, A. Cravino, D. Meissner, N. S. Sariciftci, T. Fromherz, M. T. Rispens, L. Sánchez, J. C. Hummelen, *Adv. Funct. Mater.* **2001**, *11*, 374.

with the nano-morphology of the solar cell, several C_{60} derivatives have been synthesized.

These derivatives have been covalently linked to different chemical compounds with different nature, *e.g.* acceptor,[174] donor,[175,43a] π – conjugated oligomers,[155b,176] dendrimers,[177] etc. After 20 years of research in this field, scientists have developed some helpful properties to get the best polymeric material for solar cells:[178]

1. The HOMO-LUMO band gap in a *p*-type material has to be relatively small (1.2-1.9 eV) in order to absorb the most part of photons deriving from the sunlight irradiation in the visible region. In terms of numbers, an energy gap of 1.1 eV is able to absorb 77% of irradiation. However, most of semiconductor polymers have a band gap of about 2.0 eV, which limits the total absorption to 30%. The increment of 0.9 eV in the band gap of *p*-type polymer provokes a loss of total absorption of 47%.
2. The difference in energy between the HOMO of the donor polymer (*p*-type) and the LUMO of the acceptor polymer (pristine fullerene or

[174] G. Zerza, M. C. Scharber, C. J. Brabec, N. S. Saricftci, R. Gómez, J. L. Segura, N. Martín, V. I. Srdanov, *J. Phys. Chem. A* **2000**, *104*. 8315.
[175] C. Waldauf, W. Graupner, S. Tasch, G. Leising, A. Gügel, U. Scherf, A. Kraus, M. Walter, K. Müllen, *Opt. Mater*. **1998**, *9*, 449.
[176] a) J. F. Nierengarten, J. F. Eckert, J. F. Nicoud, L. Ouali, V. Krasniko, G. Hadziioannou, *Chem. Comm*. **1999**, 617; b) D. M. Guldi, C. Luo, A. Swartz, R. Gómez, J. L. Segura, N. Martín, C. Brabec, N. S. Saricftci, *J. Org. Chem*. **2002**, *67*, 1141; c) C. Atienza, G. Fernández, L. Sánchez, N. Martín, I. S. Dantas, M. M. Wienk, R. A. J. Janssen, G. M. A. Rahman, D. M. Guldi, *Chem. Commun.* **2006**, 514; d) G. Fernández, L. Sánchez, D. Veldman, M. M. Wienk, C. Atienza, D. M. Guldi, R. A. J. Janssen, N. Martín, *J. Org. Chem*. **2008**, *73*, 3189; e) T. Gu, D. Tsamouras, C. Melzer, V. Krasnikov, J. P. Gisselbrecht, M. Gross, G. Hadziioannou, J. F. Nierengarten, *Chem. Phys. Chem.* **2002**, *3*, 124; f) N. Armaroli, G. Accorsi, J.-P. Gisselbrecht, M. Gross, V. Krasnikov, D. Tsamouras, G. Hadziioannou, M. J. Gómez-Escalonilla, F. Langa, J.-F. Eckert, J. F. Nierengarten, *J. Mater. Chem*. **2002**, *12*, 2077; g) J. F. Nierengarten, T. Gu, T. Aernouts, W. Geens, J. Poortmans, G. Hadziioannou, D. Tsamouras, *Appl. Phys. A: Mater. Sci. Process*. **2004**, *79*, 47.
[177] a) K. Felddrap, W. Brütting, M. Schoerer, M. Brettreich, A. Hirsch, *Synth. Met*. **1999**, *101*, 156; b) K. Hosomizu, H. Imahori, U. Hahn, J. F. Nierengarten, A. Listorti, N. Armaroli, T. Nemoto, S. Isoda, *J. Phys. Chem. C* **2007**, *111*, 2777.
[178] a) T. Y. Chu, J. Lu, S. Beaupré, Y. Zhang, J. R. M. Pouliot, S. Wakim, J. Zhou, M. Leclerc, Z. Li, J. Ding, Y. Tao, *J. Am. Chem. Soc.* **2011**, *133*, 4250; b) J. L. Delgado, P. A. Bouit, S. Filippone, M. A. Herranz, N. Martín, *Chem. Commun.* **2010**, *46*, 4853; c) G. Dennler, M. C. Scharber, C. J. Brabec, *Adv. Mater*. **2009**, *21*, 1323; d) B. Kippelen, J.-J. Brédas, *Energy Environ. Sci*. **2009**, *2*, 251; e) B. C. Thompson, J. M. J. Fréchet, *Angew. Chem., Int. Ed*. **2008**, *47*, 58.

fullerene derivatives, *n*-type) influences the V_{OC} parameter (Equation 6). It has been seen that fullerenes with high value of reduction potentials give rise to a high value of V_{OC} and, thereby, an increasing in the efficiency of the device.[173] For instance, the bisadducts of fullerene, deriving from its double functionalization, display this feature. However, it does not form a good mixture with the polymer in the BHJ, because of the trend to form fullerene domains.

$$V_{OC} \propto E_{LUMO\ A} - E_{HOMO\ D}$$

Equation 6. V_{OC} value depending on the difference of the acceptor LUMO and the donor HOMO energies.

3. The LUMOs levels of both species (donor and acceptor) must be separated at least 0.3 eV in order to produce an efficient charge separation without losing too much photon energy. Koster in 2006 demonstrated that the efficiency increases in a proportional way to the approach of the LUMOs levels of acceptor and donor components (Figure 79).[179]

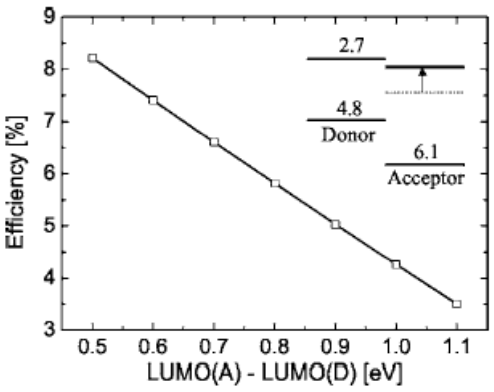

Figure 79. Efficiency dependent of difference between LUMO donor and LUMO acceptor.

4. Both materials have to guarantee good mobility for the transport of holes and electrons.

Eventually, the solubility of the molecule is important for the device making.

[179] L. J. A. Koster, V. D. Mihailetchi, P. W. M. Blom, *Appl. Phys. Lett.* **2006**, *88*, 052104.

OBJECTIVES

3. OBJECTIVES.

The present work is focused on the synthesis and chemical and/or physical characterization of new C_{60} dimers, known as "dumbbells" due to their molecular shape. The interest of this class of molecules is based on their study as molecular wires. More in detail, C_{60} will be evaluated as anchor group taking advantage of its size, shape, electronic properties and the ease to be seen onto the surface. Furthermore, we want to investigate the role of the "linker" (**X** in the figure below) between C_{60} and the molecular electro-active bridge in order to achieve a better electronic communication. Figure 80 represents our general concept for molecular wires.

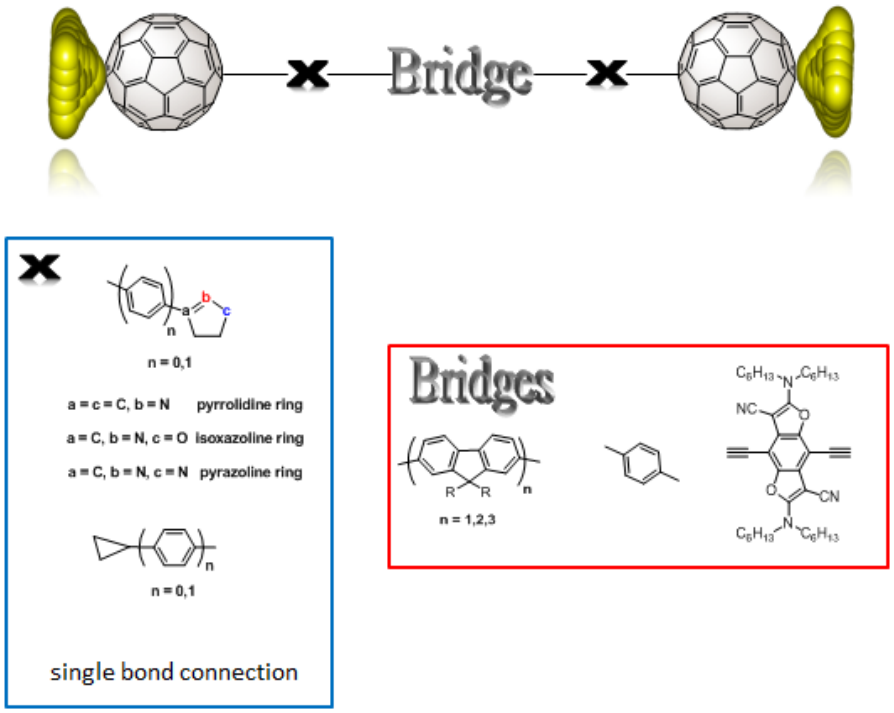

Figure 80. Design of dumbbell molecule based onto C_{60}, electro-active bridges and linkers **X**.

The following dumbbell-type molecules have been designed for this purpose and represent some goals of the present study:

1. **Synthesis of monofluorene dumbbells: linker evaluation.**
   - Five member heterocycle linker: the functionalization of C_{60} with five members heterocycle linkers such as pyrrolidine, isoxazoline and pyrazoline have been proposed for preparing dumbbell molecules. In contrast to the pyrrolidine ring, isoxazoline and pyrazoline rings present a double bond and a second heteroatom which should impact the conductance properties of the final molecular wire. However, all of them have in common that no conjugation between the bridge and the fullerene sphere is possible.

   Furthermore, the following two pyrrolidino[60]fullerenes have been synthesized to determine the contribution of only one fullerene to the conductance. Indeed, such derivatives, known as "tadpole" molecules (due to the intrinsic shape of the molecule) will be compared with analogue dumbbells in STM or MCBJ measurements.

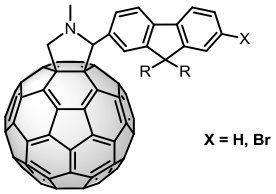

Figure 81. Tadpole molecules for the comparative study using MCBJ or STM techniques.

   - We will also carried out the synthesis of a dumbbell molecule containing two cyclopropane rings as linker. The chemical nature of cyclopropane resembles, in terms of reactivity and electronic behaviour, to that of an olefin; it should lead to a new compound with better conductance value when compared with the related pyrrolidine monofluorene dumbbell.

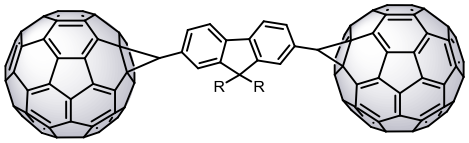

Figure 82. Cyclopropane dumbbell based on one fluorene unit. Alkyl chains are indicated with R for clarity.

- A step-forward for the linker evaluation is represented by the following molecules where the fluorene unit is directly connected to C_{60} cages. In this way, we would reduce to only one the Csp^3 atom (it belongs to the fullerene backbone and is not outside the cage). With the same strategy, the tadpole monofullerene derivative will be synthesized for comparison purposes.

Figure 83. Direct dumbbell molecule (left) and tadpole molecule (right).

2. **The development of a dumbbell series with direct linkage to C_{60}.** According to physicists, having such connection between fullerene and fluorenes together with the possibility to enhance the length of the wire, makes the whole series really prominent for the study of the attenuation factor (β) via STM conductance measurements, following the nanoscopic approach instead of the classical photoinduced electron transfer.

3. **Synthesis of dumbbell molecule based on different cores.** The versatility of fullerene chemistry and our ability to build up molecules are the key to introduce in the dumbbell molecular structures different cores with their intrinsic characteristics. In such a way, aryl and benzodifuran (BDF) cores will be inserted in the final molecule. Benzodifurans (BDFs) are *p*-type semiconductor materials and they have been proven to be excellent when applied in organic light-emitting diodes (OLEDs) or in organic field effect transistors (OFETs). Unfortunately, the difficulties in the synthetic preparation of such compounds deflates its application. In this work, we want to study BDF as π-system for the electron transfer and the photophysical characteristic of the dumbbell containing this π-extended and planar core.

4. **Synthesis of DPM-6 and its application in photovoltaic devices.** The effect of alkyl chains over the morphology of the final blend is envisaged along with its final performance when used as *n*-type material in the photovoltaic device. A further comparison will be carried out with the well-known fullerene derivative (PCBM), in the preparation of a BHJ device.

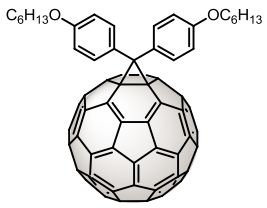

Figure 84. Diphenylmethano[60]fullerene with six member alkyl chains (DPM-6) on the benzene rings.

RESULTS AND DISCUSSIONS

4. RESULTS AND DISCUSSIONS

In this section, we propose the synthesis of dumbbell molecules to be used in STM and MCBJ experiments. In particular, the effect of the linker between the C_{60} and the bridge may play a relevant role in the transmission of electrons rendering the wire more or less conjugated, rigid, symmetric and linear. In this regard, we have synthesized dumbbell molecules with five member rings, three member rings as cyclopropane and, direct bond linker to study their effects either in typical chemical characterizations or in conductance measurements.

4.1 Dumbbells with five-members heterocycle linker

4.1.1 Synthesis of 2,7-diformylfluorene derivatives as scaffolds

2,7-diformyl-9,9'-dihexylfluorene, the common starting material for all the dumbbells with five members heterocycle rings as linker, has been synthesized following the Scheme 3:

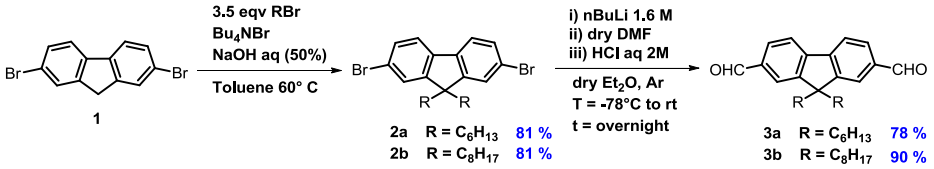

Scheme 3. Dialkylation reaction followed by diformylation reaction of dibromofluorene derivatives.

Commercially available 2,7-dibromofluorene **1** was submitted to alkylation reaction using toluene as solvent, aqueous NaOH as strong base to remove the acidic protons in 9 position of fluorene, *n*-tetrabutylammonium bromide as phase transfer agent and a slight excess of *n*-hexylbromide in order to obtain the dialkylated compounds **2a** and **2b**.[180] This step is easy to control due to the formation of the anion in position 9 which generates cyclopentyl anion conferring aromaticity and planarity to the fluorene molecule and an often orange colour to the solution (or red when DMSO is used as solvent). The direct di-alkylation occurs with good yield. Sometimes, DMSO could be employed instead of toluene at lower temperature (35 °C).

[180] a) R. Grisorio, G. Allegretta, P. Mastrorilli, G. P. Suranna, *Macromolecules* **2011**, *44*, 7977; b) P. Anuragudom, S. S. Newaz, S. Phanichphant, T. R. Lee, *Macromolecules* **2006**, *39*, 3494.

The so obtained product has been used for the formation of diformylfluorene molecules **3a** and **3b** (our scaffolds for the synthesis of the dumbbell-type molecules).[181,180b] The lithiation reaction in position 2 and 7 is quite tricky because a dianion on the fluorene must be generated. After several experiments in which the reaction conditions varied, we found the correct procedure which consists in pouring the solution of dibromide derivate in dry Et_2O into a solution of *n*-butyllithium (*n*BuLi) in dry diethylether at -78 °C (bath of acetone/CO_2) under argon atmosphere. Afterwards, dry dimethylformamide (DMF) was added to the solution and warmed at room temperature overnight. Aqueous HCl was used for its quenching and the reaction yields are reported in the scheme above.

Moreover, the enhancement of the molecular wire length has been designed using a suitably functionalised fluorene as starting scaffold. It has been symmetrically elongated with two aryl moieties through a single bond connection obtained by Suzuki coupling reaction between 2,7-diboronic-9,9'-dihexylfluorene acid and *p*-bromobenzaldehyde.[182] In such a way, we generated a new bridge which may be seen as an alternation of free biaryls/constrained biaryls/free biaryls π-system (Figure 85).

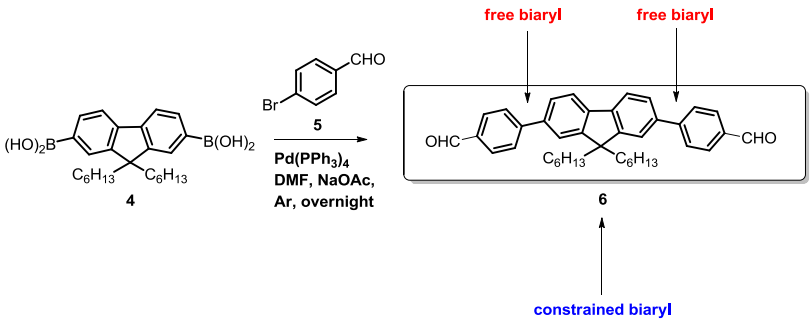

Figure 85. Suzuki coupling to synthesize the elongated diformylfluorene **6**.

[181] a) Y. Jin, J. Ju, J. Kim, S. Lee, J. Y. Kim, S. H. Park, S.-M. Son, S.-H. Jin, K. Lee, H. Suh, *Macromolecules* **2003**, *36*, 6970.
[182] Y. Long, H. Chen, Y. Yang, H. Wang, Y. Yang, N. Li, K. Li, J. Pei, F. Liu, *Macromolecules* **2009**, *42*, 6501.

Although the electronic communication between the aryl and the fluorene is not strong due to the lack of planarity of the system, we may expect a behaviour during the conductance measurements really close to that seen for one fluorene core dumbbell molecules. This scaffold will represent the starting material for the preparation of new dumbbell molecules series.

As in the case of dialdehyde scaffold, monoaldehydes **9a** and **9b** have been synthesized (Scheme 4) as precursors for the synthesis of the reference molecules where the fluorene moiety is connected with only one C_{60} in a "tadpole" shape.

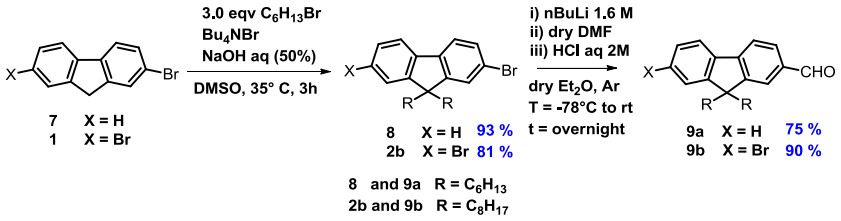

Scheme 4. Synthetic route for molecules **9a** and **9b**.

Thus, analogously to the scheme 3, the di-alkylation reaction has been carried out in almost quantitative yields and in agreement with the procedure reported in literature.[183] As concern the formylation reaction, the lithiation procedure[184] affords the synthesis of the desired compounds which were correctly characterized. **9a** and **9b** represent, therefore, another two valuable scaffolds for our molecular puzzle.

[183] M. Sonntag, K. Kreger, D. Hanft, P. Strohriegl, S. Setayesh, D. de Leeuw, *Chem. Mater.* **2005**, *17*, 3031.
[184] M. Y. Yuen, S. C. F. Kui, K. H. Low, C. C. Kwok, S. S. Y. Chui, C. W. Ma, N. Zhu, C. M. Che, *Chem. Eur. J.* **2010**, *16*, 14131.

4.1.2 Synthesis of dumbbells with five-members heterocycle linker

Dumbbell-type molecule **10** has been synthesized by treatment of 2,7-diformyl-9,9'-dihexylfluorene with N-methylglycine (sarcosine) and excess of C_{60} in a two-fold Prato reaction (Scheme 5). A large excess of pristine C_{60} has been used to push the reaction towards the formation of the dumbbell molecule in a statistic way.

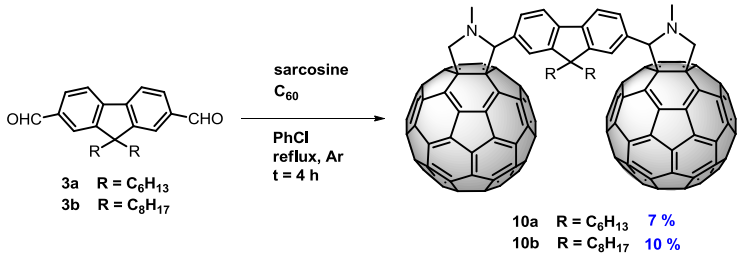

Scheme 5. Pyrrolidine fluorene dumbbells.

The solvent employed vary from toluene to chlorobenzene or 1,2-dichlorobenzene (*o*-DCB) with two important considerations: i) the solubility of C_{60} increases from toluene to *o*-DCB,[185] ii) the reflux temperatures are different for each solvent. The second one must be taken into account in the moment in which we plan the reaction in order to avoid the retrocycloaddition reaction for the final product in the same bulk. Perhaps, *o*-DCB instead of chlorobenzene may improve the yield of the reaction with the same reaction time. Pyrrolidine dumbbell molecules (**10a** and **10b**) have been isolated after purification with silica gel chromatography. Once isolated, ^{1}H-NMR spectra showed three broad peaks in the aromatic region which are referred to the protons of the fluorene. To be sure, they have been also correctly assigned thanks an HSQC analysis (Figure 86) in which the bidimensional spectrum shows, clearly and unambiguously, the correlation with the direct carbon atoms of fluorene.

[185] Y. Marcus, A. L. Smith, M. V. Korobov, A. L. Mirakyan, N. V. Avramenko, E. B. Stukalin, *J. Phys. Chem. B* **2001**, *105*, 2499.

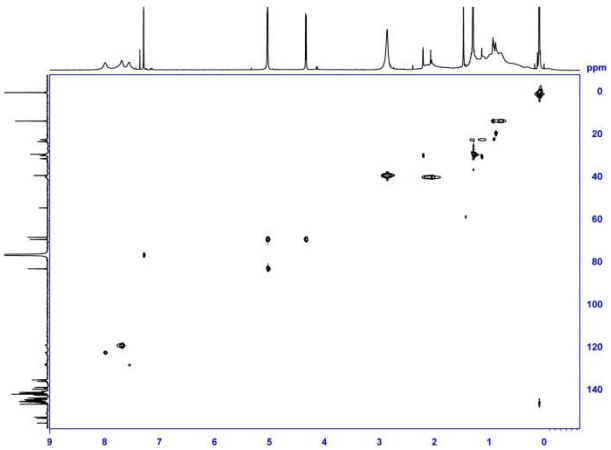

Figure 86. HSQC of compound **10a**.

The broad proton signals may be attributed to a relatively high rotational barrier around the fluorene-pyrrolidine bond and, maybe, to the presence of four stereoisomers, as results of the two chiral centres generated during the reaction. It is also easy to evidence that the two protons belonging to the methylene in the pyrrolidine ring are diastereotopic because they appear at different δ values.

Isoxazoline dumbbell-type molecule derivative **12** has been synthesized after the formation and characterization of the new compound, 2,7-bis(hydroxyimino)-9,9'-dihexylfluorene, as shown in the Scheme 6:

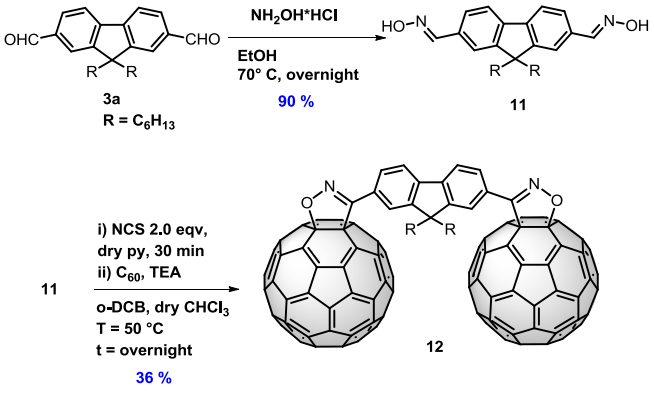

Scheme 6. Synthetic route to obtain dumbbell **12** from 2,7-diformylfluorene scaffold.

The formation of dioxime **11** has been carried out using a large excess of hydroxylamine hydrochloride in order to push the reaction towards the formation of the dioxime. It has been employed as starting material for the formation of isoxazole linker over C_{60} following the procedure which foresees a one pot reaction[186] where the chlorinated agent (N-Chlorosuccinimide, NCS) eliminates HCl by means of a base (typically triethylamine, TEA) with the subsequent formation of nitrile oxide. The 1,3 dipole, thus formed, represents the active species for the cycloaddition reaction over C_{60}. The purification of the final product has been performed using neat carbon disulphide (CS_2) to remove the unreacted C_{60}; an eluent gradient of CS_2 and DCM until pure DCM has been employed for the isolation of dumbbell molecule and monofullerene as byproduct. The desired product **12** has been characterized by NMR (^1H, ^{13}C) and exact mass using MALDI-ToF analysis.

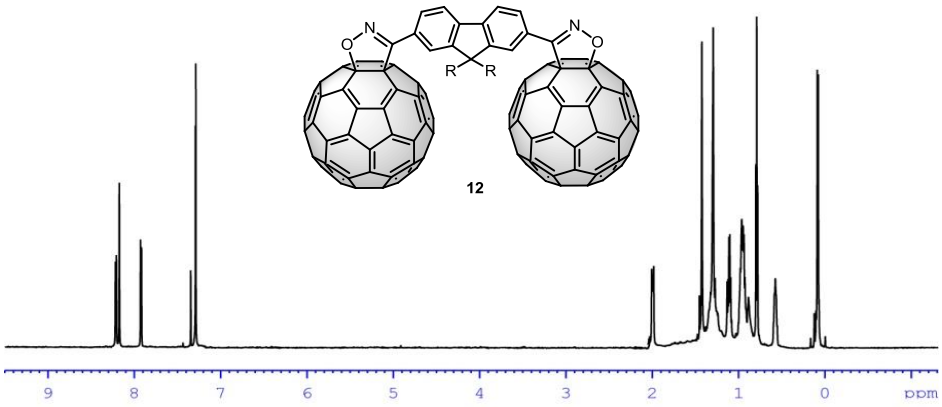

Figure 87. ^1H-NMR (CS_2/$CDCl_3$ 1:1, 700 MHz, 25 °C) of compound **12**.

The lack of stereoisomers, due to the sp^2 hybridization of the C-3 in the isoxazoline ring, renders the spectroscopic characterization easier. As shown in Figure 87, the aromatic region is now well-defined and also the aliphatic region appears better resolved. The singlet signal very close to chloroform is due to benzene trace in the carbon disulphide solvent used for the characterization.

Pyrazoline dumbbell-type molecule derivative **15** has been synthesized after the formation and characterization of dihydrazone **14** coming out by the imination reaction of dialdehyde **3a** with 4-nitrophenylhydrazine (Scheme 7).

[186] B. M. Illescas, N. Martín, *J. Org. Chem.*, **2000**, *65*, 5994.

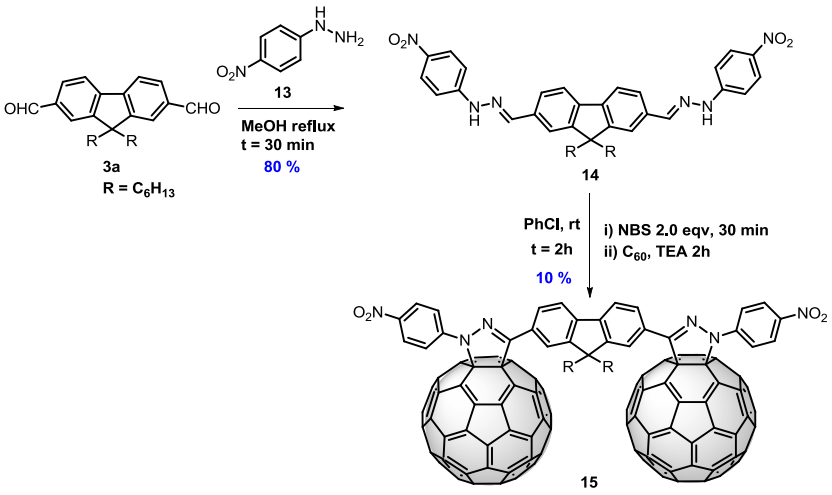

Scheme 7. Reaction scheme for the synthesis of dumbbell molecule **15**.

The reaction has been performed in MeOH at reflux temperature for 30 minutes. The product precipitates once the solution was warmed at room temperature. It has been characterized by NMR. The protons belonging to the nitrophenyl ring are splitted into two different regions of the spectra. The protons at low field (8.19 ppm) correspond to those closer to the nitro groups, while the others appear at 7.34 ppm. Compound **14** has been used in the formation of the dumbbell molecule as it is shown in the scheme above. This 1,3 dipolar cycloaddition reaction[187] has the same mechanism of that used for synthesis of the isoxazole dumbbell. In this case, N-Bromosuccinimide (NBS) is the halogenating agent. Dry conditions are still mandatory otherwise monofullerene product with hydrolysed imine could be isolated during the purification processes.

[187] F. Langa, M. J. Gomez-Escalonilla, J.-M. Rueff, T. M. Figueira Duarte, J.-F. Nierengarten, V. Palermo, P. Samorì, Y. Rio, G. Accorsi, N. Armaroli, *Chem. Eur. J.* **2005**, *11*, 4405.

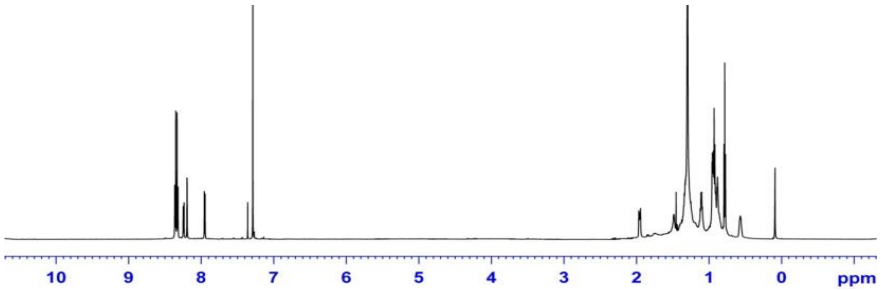

Figure 88. ^{1}H -NMR (CS_2/$CDCl_3$, 700 MHz, 25 °C) of compound **15**.

^{1}H-NMR clearly shows the typical signal related to the compound. An interesting observation comes out concerning the four protons of the *p*-nitrophenyl moiety: they are shifted to lower field (higher value of ppm) compared with the precursor **14** due to an electronic effect of C_{60} cages.

4.1.3 Cyclic voltammetry of dumbbells with five-members heterocycle linker

The electrochemical behaviour of dumbbell-type molecules described above has been studied by cyclic voltammetry in a mixture of solvents (*o*-DCB/MeCN 4:1 v/v) using Ag/Ag^{+} as reference electrode at room temperature.

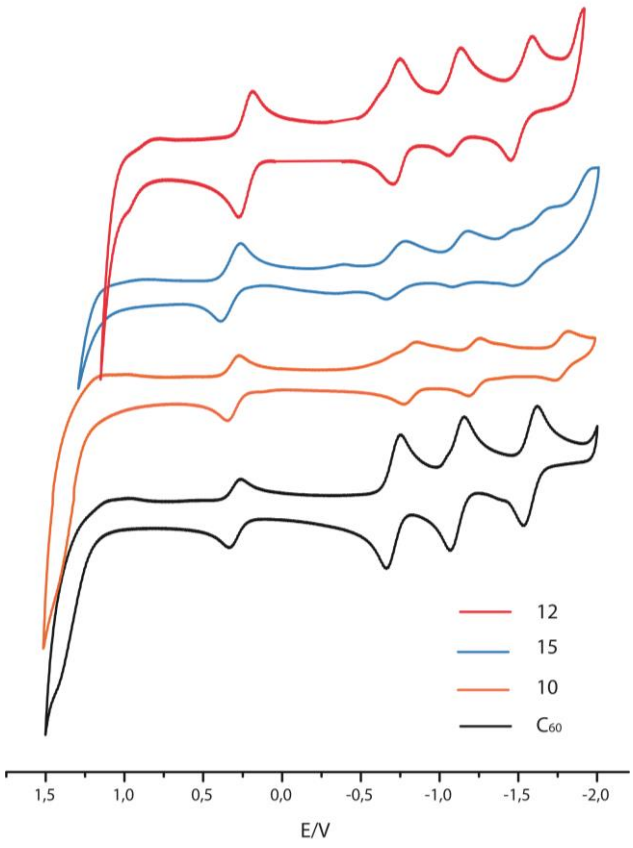

Figure 89. Cyclic Voltammetry of five member heterolinker dumbbell molecules (**10**, **12**, **15**) compared with pristine $\mathbf{C_{60}}$.

All the compounds present three reversible reduction waves corresponding to the simultaneously reduction of both C_{60} buckyballs. Interestingly, the pyrazoline dumbbell **15** shows, between the second and the third reduction waves ascribed to C_{60} cages, the reversible reduction waves of the nitro groups in agreement with the literature.[188] The oxidation part of the analysis does not show any waves under these work conditions except for molecule **12** with no difference in the electrochemical shift for this peak, when compared with 2,7-dibromofluorene. This irreversible oxidation is ascribed to the fluorene moiety.[157]

Compounds	E^1_{red}	E^2_{red}	E^3_{red}	E^4_{red}	E^5_{red}	E^1_{ox}	E^2_{ox}
C_{60}	-1.00	-1.41	-1.87				
10	-1.12	-1.53	-2.08			—	—
12	-1.03	-1.43	-1.88			0.79	—
15	-1.06	1.45	-1.79[a]	-1.91	-2.28[a]	—	—

Table 1. Cyclic voltammetry [V *vs* Fc/Fc^+] of **C_{60}** and molecules **10**, **12**, **15**. Working electrode: GCE; reference electrode: Ag/Ag^+; counter electrode: Pt; supporting electrolyte: 0.1M Bu_4NClO_4; scan rate: 100 mVs^{-1}; solvent: o-DCB/MeCN (4 : 1 v/v).
[a] Irreversible waves for the two steps reduction of nitrobenzene moiety.

The function of degree, pattern and nature of the C_{60} functionalizations has already been investigated[189] and herein, we want to focus our attention over the linker effect on cyclic voltammetry data.

The data obtained in the cyclic voltammetry experiments reveal that the saturation of one double bond of C_{60} results in a cathodic shift of 120 mV for the pyrrolidine dumbbell with respect to pristine C_{60}. In the case of pyrazoline and isoxazoline linkers, the presence of the heteroatom as well as the double bond affect the LUMO values which are anodically shifted towards values that are typical for pristine C_{60}. LUMOs are not degenerated and, they have a slight energy level differences. The possible effect of second heteroatom in the five member linker has previously been envisaged for isoxazolino[60]fullerene

[188] M. A. Herranz, M. W. J. Beulen, J. A. Rivera, L. Echegoyen, M. C. Diaz, B. M. Illescas, N. Martin, *J. Mater. Chem.* **2002**, *12*, 2048.
[189] F. Cardullo, P. Seiler, L. Isaacs, J.-F. Nierengarten, R. F. Haldimann, F. Diederich, T. Mordasini-Denti, W. Thiel, C. Boudon, J.-P. Gisselhrccht, M. Gross, *Helv. Chim. Acta* **1997**, *80*, 343.

derivatives.[190] Only in the case of the isoxazoline dumbbell, an irreversible oxidation wave has been recorded and attributed to the fluorene core, where the HOMO is localized with slight delocalization over the double bond of the isoxazoline ring (PM3 calculation).

The LUMO energy level, as well as the HOMO level, may be directly obtained from the cyclic voltammetry experiments.[191] The calculated values are -3.98 eV (pyrrolidine dumbbell), -4.04 eV (pyrazoline dumbbell), -4.07 eV (isoxazoline dumbbell). The calculated HOMO value for isoxazoline dumbbell from the oxidation potential of fluorene has been found to be -5.89 eV. All the above calculated values are consistent with the discussions arose from the cyclic voltammetry analysis.

As shown in Figure 90, the isosurface representation of HOMO level for the three molecules reveal the better π-orbital overlapping in systems containing unsaturated heterorings as linkers, with slight participation of the lone pair of the second heteroatom.

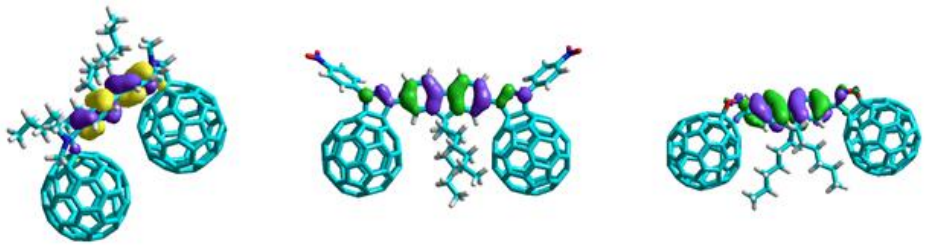

Figure 90. Geometrical optimization and isosurface representations of HOMOs (PM3 method) for pyrrolidine dumbbell (left), pyrazoline dumbbell (center), isoxazoline dumbbell (right).

[190] P. de la Cruz, E. Espíldora, J. García, A. de la Hoz, F. Langa, N. Martín, L. Sánchez, *Tetrahedron Lett.* **1999**, *40*, 4889.
[191] C. M. Cardona, W. Li, A. E. Kaifer, D. Stockdale, G. C. Bazan, *Adv. Mater.* **2011**, *23*, 2367.

4.1.4 Synthesis of dumbbells with five-members heterocycle linker and extended bridge

Dumbbell-type molecule **16** has been synthesized using a Prato reaction with N-methylglicine (sarcosine) along with compound **6** and pristine C_{60} in chlorobenzene at reflux temperature for four hours. The pyrrolidine dumbbell molecule is isolated in 99% yield, after silica gel chromatography purification, eluting with carbon disulphide (CS_2) to remove the C_{60} unreacted and then with a gradient of CS_2:DCM to pure DCM.

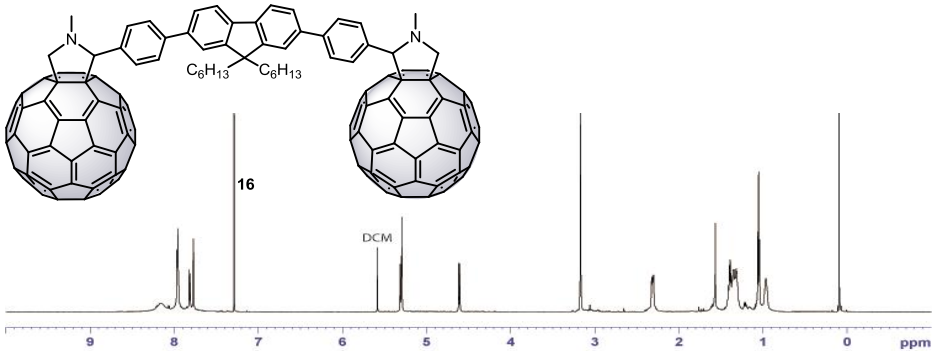

Figure 91. ^{1}H-NMR (CS_2/$CDCl_3$, 700 MHz, 25 °C) of compound **16**.

Once isolated, ^{1}H-NMR spectrum (Figure 91) showed the correct signals corresponding to the fulleropyrrolidine. The two methylene protons of pyrrolidine ring are diastereotopic and fall at 4.61 and 5.30 ppm as a doublet signal. Their differentiation is due to a well-known effect of C_{60}: one proton is shifted to low field (higher ppm) if it spatially stays over a cyclopentane ring. A carbon/proton hetero-correlated analysis (HSQC) confirms this behaviour for such functionalization: only one carbon atom correlates with the two diastereotopic protons. The proton belonging to the chiral carbon falls really close to one of the other two protons of pyrrolidine ring at 5.29 ppm as a singlet signal. Mass spectrum has been recorded in negative voltage polarity in "reflector" as acquisition operation mode using a MALDI-ToF instrument. It shows the m/z value of the desired product with its isotopic configuration.

Dumbbell-type molecule functionalized with isoxazoline heteroatom ring **18** has been obtained using the same strategy reported previously. Herein, we reported the scheme of reaction with the relative yields:

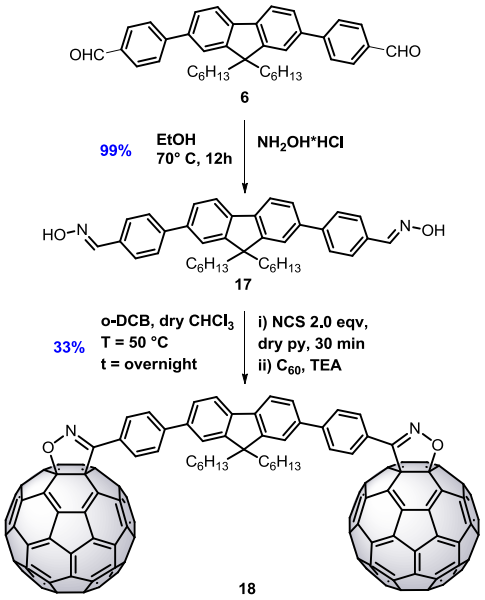

Scheme 8. Reaction scheme for the synthesis of isoxazoline dumbbell molecule **18** with the extended bridge.

The dialdehyde **6** has been treated with a large excess of hydroxylamine hydrochloride in ethanol at reflux temperature overnight. The reaction works with quantitative yield and the product precipitates from the same bulk, once cooled. The so formed product **17** has been well dried and characterized by NMR (^{1}H,^{13}C) and mass spectrometry using MALDI-ToF experiments. Dioxime **17** has been used for the next step which is exactly the same for that of dumbbell type **12**. Even in this case, dry conditions are mandatory for obtaining good yield of reaction. The recorded yield is 33%, which is reasonably better than those found for the other dumbbell molecules. The product **18** has been characterized by NMR (^{1}H, ^{13}C) and exact mass.

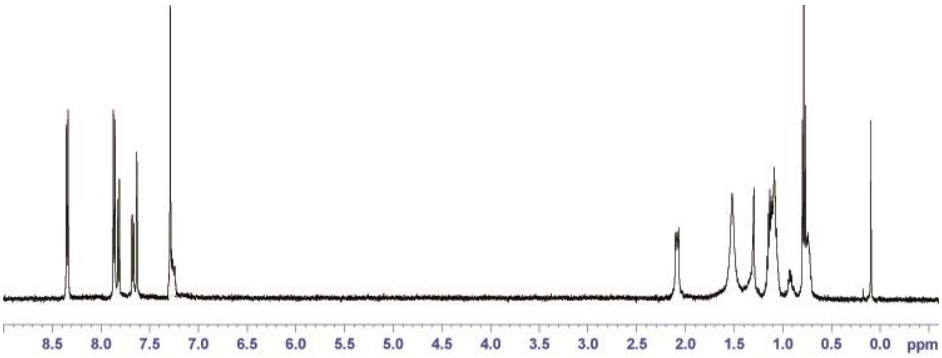

Figure 92. ^{1}H-NMR ($CDCl_3$, 500 MHz, 25 °C) of compound **18**.

The pattern of fluorene protons is well recognized from that of the *para* substituted aryls which are more intense. Alkyl chains show the same pattern already registered for other similar molecules.

Dumbbell-type molecule **20** has been synthetized by following the Scheme 9:

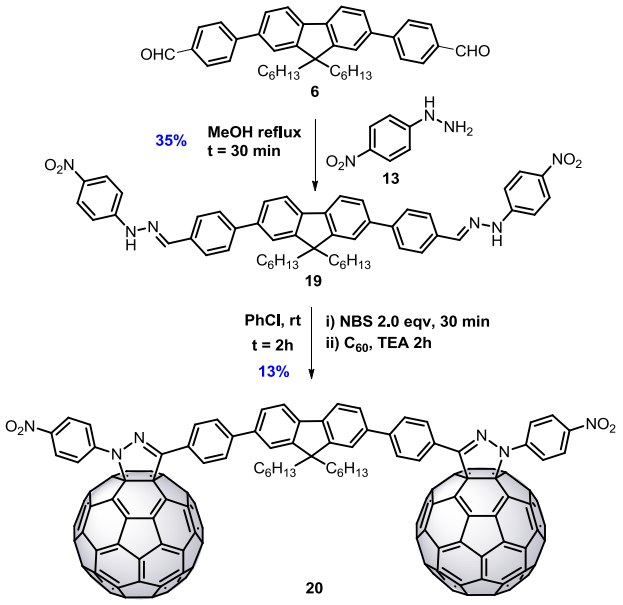

Scheme 9. Reaction scheme for the synthesis of pyrazoline dumbbell **20** with extended bridge.

Symmetric hydrazone **19** has been obtained using the same procedure reported above. The synthesis of dumbbell-type molecule **20** has been carried out with appreciable yield starting from the compound **19**. The reaction is exactly the same already described for another derivative. In this case, the product, after the first purification made by silica gel chromatography and eluting with, first, CS_2 to remove the unreacted C_{60} and then, with a gradient of CS_2 and DCM until pure DCM, needed a further purification by semipreparative HPLC eluting with pure toluene with a flow rate of 5.6 ml/min. The chromatogram shows clearly the presence of two different products: one at a retention time of 7.04 minutes, presumably assigned to the monoadduct derivative, and the second one at 25.08 minutes referred to the dumbbell molecule (Figure 93).

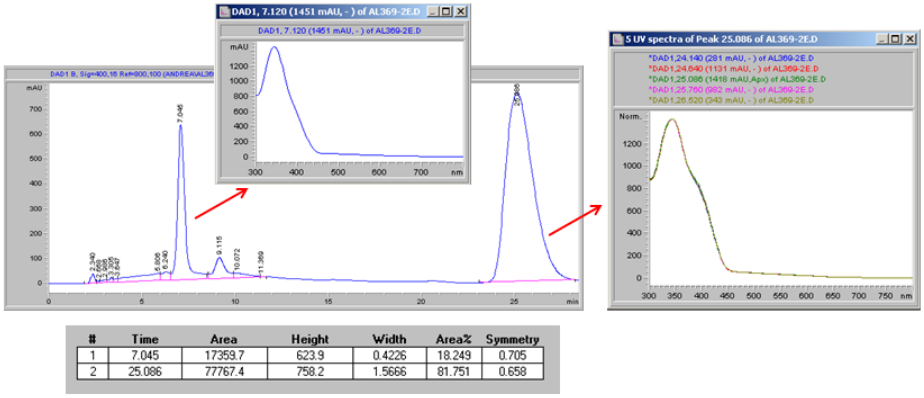

#	Time	Area	Height	Width	Area%	Symmetry
1	7.045	17359.7	623.9	0.4226	18.249	0.705
2	25.086	77767.4	758.2	1.5666	81.751	0.658

Figure 93. Chromatogram showing the of the two products derived from compound **19**. The peak at 7.04 minutes is referred to the monoadduct of C_{60} while the peak at 25.08 minutes is referred to the dumbbell molecule **20**. The corresponding UV-vis spectra are shown in the inset of the figure.

The UV-vis spectra for fullerene compounds are considered as the fingerprints for each kind of compound. For instance, in this case the UV-vis spectra show a completely saturation of the typical peak for the C_{60} derivative at about 425-430 nm due to the most active chromophore present in the molecule: the *p*-nitrophenyl substituent. This shoulder at about 400 nm is typical for this derivatives. The intense band at around 300 nm is referred to the bridge absorption. Furthermore, to be sure that under the peak at 25.08 minutes there is no more than one absorbing species, a multi-diode has been applied as tools during the analysis (show the UV-vis spectra of the Figure 93).

The ^{1}H-NMR of the isolated product (Figure 94) shows the following features:

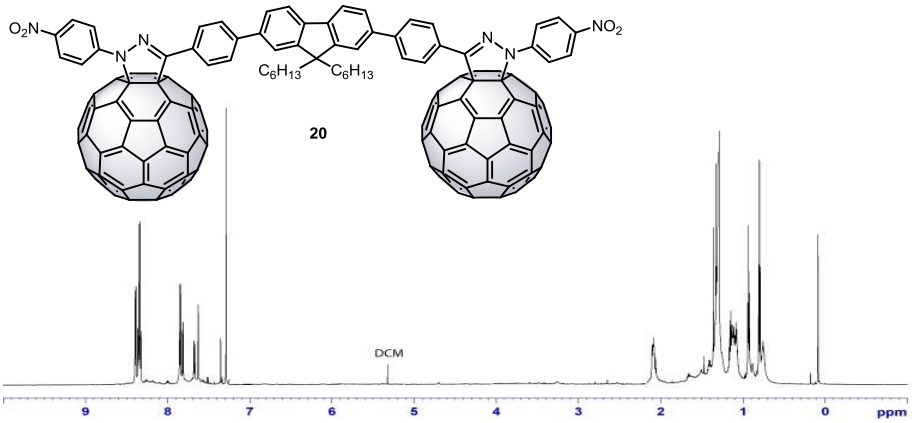

Figure 94. ^{1}H-NMR ($CS_2/CDCl_3$, 700 MHz, 25 °C) of compound **20**.

4.1.5 Cyclic voltammetry of dumbbells with five-members heterocycle linker and extended bridge

The electrochemical properties for these molecules are essentially identical to that already analysed for the molecules with one fluorene core. Indeed, the conclusions are the same except for the lack of an oxidation peak corresponding to the fluorene in all the compounds electrochemically studied. This could be explained by the presence of the aryl moieties which change the HOMO energy level of the bridge, making it more difficult to be oxidized, at least under the experimental conditions we have used.

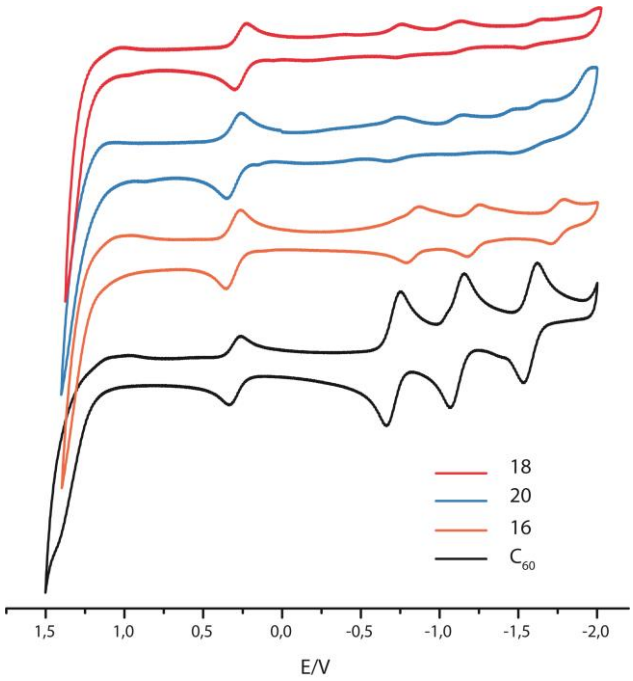

Figure 95. Cyclic voltammetry of compounds **16**, **18**, **20**. The comparison with pristine $\mathbf{C_{60}}$ is also shown in the figure.

Compounds	E^1_{red}	E^2_{red}	E^3_{red}	E^4_{red}	E^5_{red}	E^1_{ox}	E^2_{ox}
C_{60}	-1.00	-1.41	-1.87				
16	-1.13	-1.52	-2.05			—	—
18	-1.00	-1.35	-1.85			—	—
20	-1.02	-1.43	-1.77[a]	-1.88	-2.23[a]	—	—

Table 2. Cyclic voltammetry [V *vs* Fc/Fc^+] of $\mathbf{C_{60}}$ and molecules **16**, **18**, **20**. Working electrode: GCE; reference electrode: Ag/Ag^+; counter electrode: Pt; supporting electrolyte: 0.1M Bu_4NClO_4; scan rate: 100 mVs^{-1}; solvent: o-DCB/MeCN (4 : 1 v/v). [a] Irreversible waves for the two steps reduction of nitrobenzene moiety.

As depicted in Table 2, the functionalization of C_{60} with a saturated heterocycle linker like pyrrolidine produces an enhancement of about 130 mV for the first reduction potential with respect to pristine C_{60}. When the functionalization is with unsaturated heterocycles (isoxazoline and pyrazoline), the effect over the first reduction potential is remarkable and very similar to that of pristine C_{60}. This has been ascribed to the presence of double bond and also to the electronegative character of nitrogen of the heterocycle ring.

The LUMO energy levels have been calculated according to experimental CV data and they are -3.97 eV (pyrrolidine dumbbell), -4.08 eV (pyrazoline dumbbell) and -4.10 eV (isoxazoline dumbbell). The last two values are consistent with that found for pristine C_{60}. In this case, no oxidation wave has been observed during the experimental studies. Nevertheless, we claim that there is a better communication between central core and the linker for the dumbbell with unsaturated heteroring as shown in the figure below.

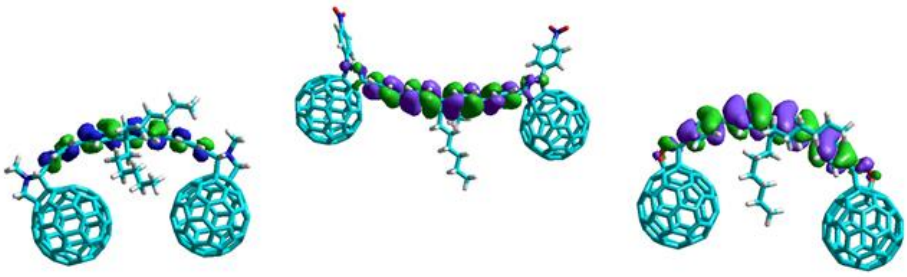

Figure 96. Geometrical optimization and isosurface representations of HOMOs (PM3 method) for pyrrolidine dumbbell (left), pyrazoline dumbbell (middle), isoxazoline dumbbell (right). A certain flexibility of the bridge arises by these calculations due to the presence of aryl moieties which better separates the C_{60} cages in the dumbbell shape.

4.1.6 Synthesis of monofullerene derivatives: "tadpole" shape

For a better understanding of the role of the C_{60} units in the aforementioned dumbbells in the mechanism of electron transport along the dumbbell-type molecular wire in STM or MCBJ experiments, the synthesis of compounds **21a** and **21b** has been carried out.

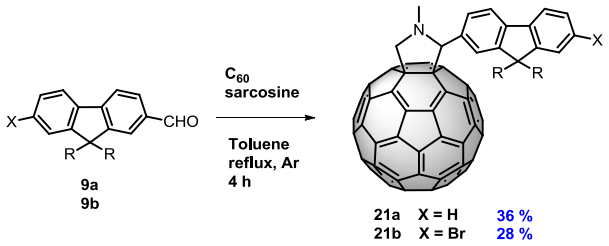

Scheme 10. Scheme of Prato reaction for two different scaffolds.

In particular, molecule **21a** can shed light onto the effect of only one C_{60} over conductance traces in STM or MCBJ experiments. In this way, we can use molecule **21a** as "molecular mean" to distinguish it by the conductance trace of analogue dumbbell molecule or by the electron transport along the fluorene moiety as shown in the figure beneath.

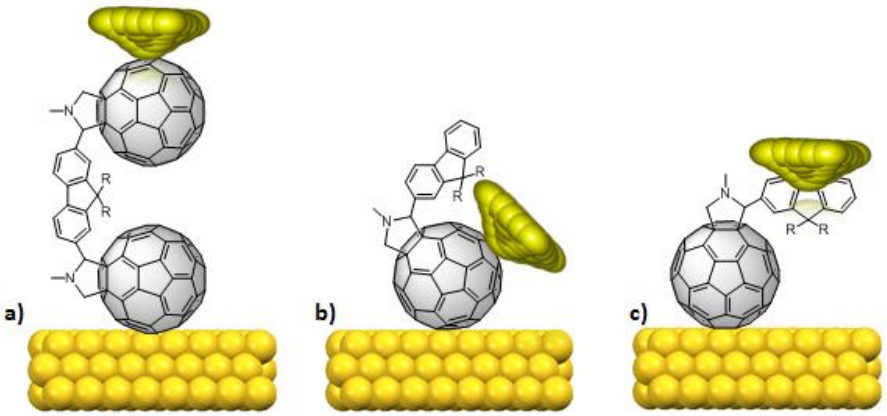

Figure 97. a) Vertical molecular configuration (STM) of dumbbell molecule when occupying the nanogap; b) STM configuration for the tadpole molecule with the only C_{60} contribution to the conductance and c) STM configuration for tadpole molecule with the fluorene contribution in the conductance values.

The ^{1}H-NMR spectrum of molecule **21a** (Figure 98) shows a complex aromatic region due to the asymmetry of the molecule. The same phenomena appears for the aliphatic region where the signals are broad with no defined shape. The clearest region is represented by pyrrolidine signals with the -NMe at 2.88 ppm as an intense singlet, the three diasterotopic protons of methylene groups of the pyrrolidine at 4.32 and 5.04 ppm as two doublets and the last proton, which belong to the chiral centre of pyrrolidine, at 5.04 ppm as a singlet.

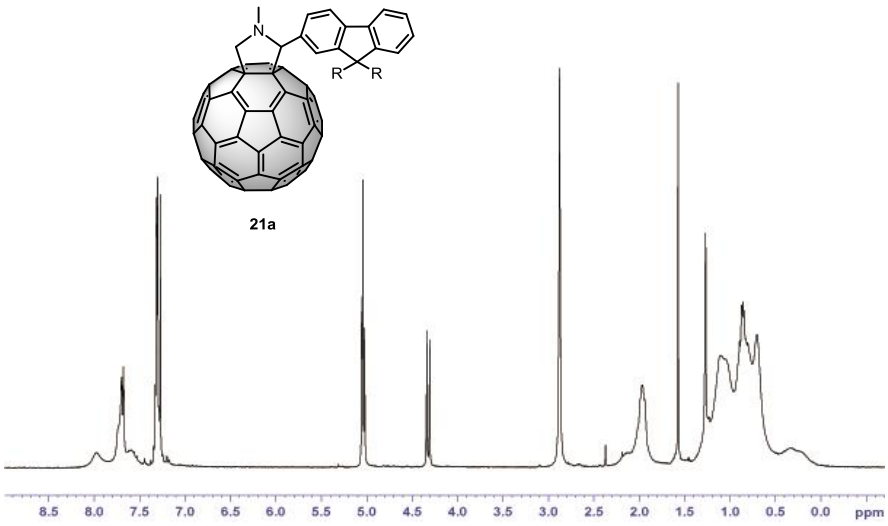

Figure 98. ^{1}H-NMR ($CDCl_3$, 300 MHz, 25 °C) of compound **21a**.

Molecule **21b** has been synthesized for further experiments over gold surface. One of them is represented by the on-surface dimerization process at high temperature through an homo-coupling reaction, as reported in literature for other related building-block molecules.[192]

[192] a) L. Lafferentz, F. Ample, H. Yu, S. Hecht, C. Joachim, L. Grill, *Science* **2009**, *323*, 1193; b) L. Grill, M. Dyer, L. Laffarentz, M. Persson, M. V. Peters, S. Hecht, *Nature Nanotech.* **2007**, *2*, 687.

4.2 Cyclopropane dumbbell molecule

The original idea to design the cyclopropane dumbbell molecule is to have a more rigid, symmetric and linear molecular wire compared with the dumbbells containing pyrrolidine as linker. The higher stiffness of these molecules is reached thanks to the cyclopropane ring and by the removal of chiral C-2 carbon atom of pyrrolidine, although we do not change the number of sp^3 carbon atoms between the C_{60} and the fluorene. The new linker constrains the C_{60} backbones to stay tilted with a certain angle from the fluorene plan, at least in the *cis* configuration, where the two C_{60} moieties are situated at the same side. The symmetry of the molecule is given by the equal substitution on both ends.

Thus, cyclopropane ring can be chemically considered in some aspects as a double bond. Wudl and co-workers determined by electrochemical analysis that the so-called "periconjugation" exists between a π-system addend and the C_{60} cage, due to the orbital overlap of p_z lobes of the addend with the perpendicularly-oriented p_z lobes of C_{60} double bond.[193] At first glance, we can figure out that this molecule will show better conductance behaviour in comparison with pyrrolidine dumbbell, thanks to this "double bond" character. Anyway, it has been demonstrated that such functionalization improves the communication between the C_{60} and various addends[193a,194] and it could also be seen as two possible pathways for the electron migration from one metal to the other.[195,148]

[193] a) M. Eiermann, R. C. Haddon, B. Knight, Q. Chan Li, M. Maggini, N. Martín, T. Ohno, M. Prato, T. Suzuki, F. Wudl, *Angew. Chem., Int. Ed.* **1995**, *34*, 1591; b) T. Ohno, N. Martín, B. Knight, F. Wudl, T. Suzuki, H. Yu, *J. Org. Chem.* **1996**, *61*, 1306.
[194] F. B. Kooistra, T. M. Leuning, E. Maroto Martinez, J. C. Hummelen, *Chem. Commun.* **2010**, *46*, 2097.
[195] M. C. Díaz, M. A. Herranz, B. M. Illescas, N. Martín, N. Godbert, M. R. Bryce, *J. Org. Chem.* **2003**, *68*, 7711.

4.2.1 Synthesis of cyclopropane dumbbell molecule

The diformyl fluorene molecules **3a** and **3b** , properly modified in position 9 for the solubility of the final product, have been used as scaffolds for the synthesis of dumbbell molecules **23a,b** according to the Scheme 11.

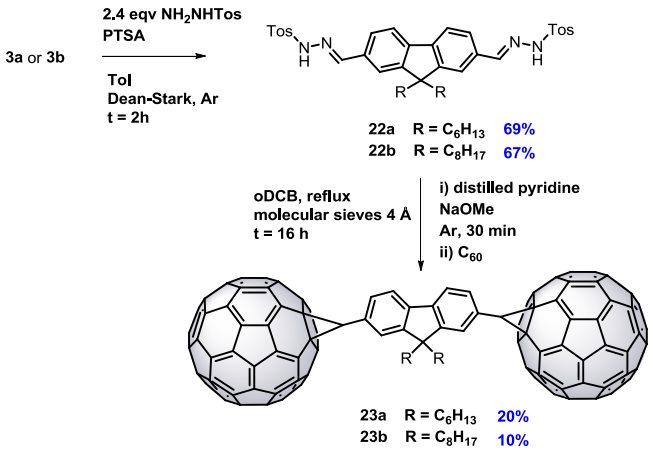

Scheme 11. Synthetic reaction strategy for molecules **23a** and **23b**.

The ditosylhydrazones of fluorene **22a** and **22b** have been obtained through an imination reaction with Dean-Stark, toluene and *p*-tosylhydrazine. The products, obtained with reasonable yields, have been correctly characterized by NMR (^{1}H,^{13}C).

Sometimes, it has been possible to differentiate the imine protons due to the two isomers, *E* and *Z*. ESI mass analysis shows the molecular peak with the addition of sodium to demonstrate the existence of the product (see experimental part).

The last step is represented by the Bamford-Stevens reaction. The yields of such reaction are consistent with the synthesis of other dumbbell molecules and are extremely sensitive to the dry conditions of equipment and reagents/reactants employed. ^{1}H-NMR spectrum of compound **23b** (Figure 99) shows the aliphatic region of the alkyl chains, the aromatic region with the perfect symmetry of the molecule where each signal integrates for two protons with their respective coupling constant value according to the *ortho*, *meta* and *para* substitution pattern.

The -CH signal of cyclopropane is perfectly visible at 5.11 ppm as a singlet which integrates for two protons.

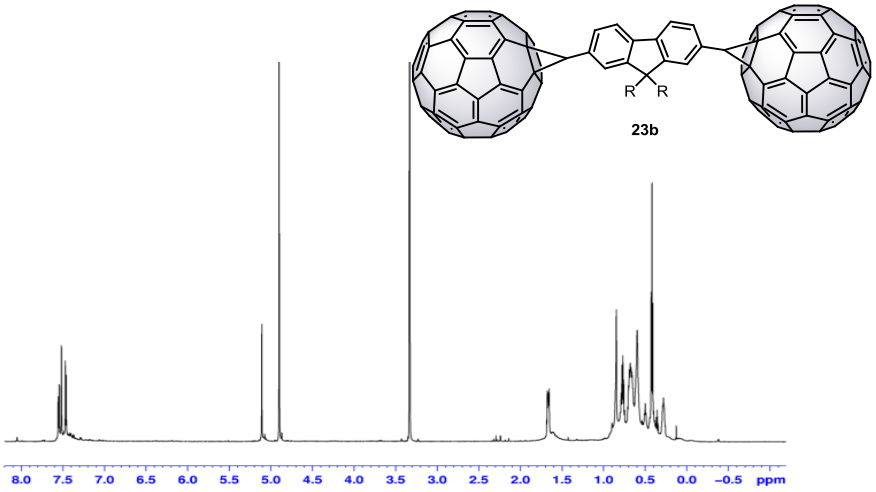

Figure 99. ^{1}H-NMR (CS_2 with internal reference CD_3OD, 700 MHz, 25 °C) of compound **23b**.

4.2.2 UV-vis and cyclic voltammetry study

To underline the effect of the new linker between fluorene and C_{60}, the pyrrolidine dumbbell **10b** and the cyclopropane dumbbell **23b** have been compared by UV-vis analysis as well as by CV experiments. The comparative study lets us to conclude whether the presence of the cyclopropane ring has a relevant effect on the electronic communication between the two electroactive species, the C_{60} and the fluorene. To support our idea, DFT calculations and STM measurements of single molecules have been reported in the next sections. Figure 100 shows the UV-vis spectra for both compounds.

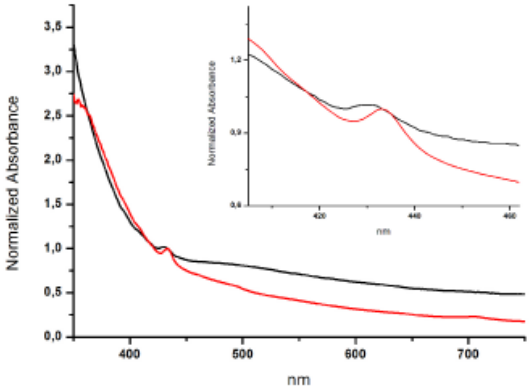

Figure 100. UV-vis spectra for **10b** (red line) and **23b** (black line) in toluene (conc. 1×10^{-4} M), normalized at 430 nm. The slight shift is seen in the inset.

The functionalization of C_{60} is marked by the sharp peak at about 430 nm as slight red shift from the typical peak of pristine C_{60} at 408-410 nm. Interestingly, molecule **23b** shows that this peak is slightly shifted towards lower value of wavelength (see the inset) compared with molecule **10b**. We claim that this finding may be ascribed to the trend for these molecules to get near the pristine C_{60} behaviour. This trend will be also observed in the cyclic voltammetry experiments, as argued thereafter. Furthermore, although it is not conclusive, the dumbbell molecule with cyclopropane presents a large and broad band at about 500 nm that is not evident in pyrrolidine dumbbell. This could be explained as a better conjugation between the C_{60} and the fluorene units. However, the lack of a clear band in the visible region of the spectrum afford us to claim that no electron transfer processes occur in the ground state.

The redox properties of both molecules have been studied by cyclic voltammetry at room temperature in comparison with that of pristine C_{60}.

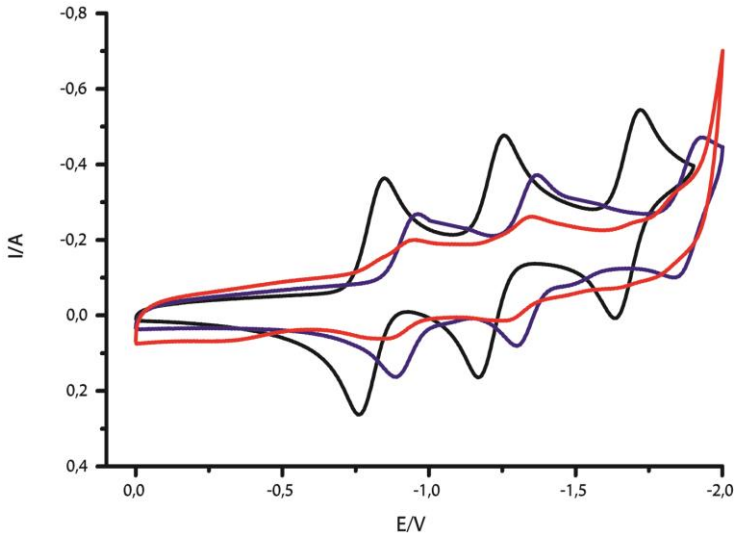

Figure 101. Comparison of reduction potentials for pristine C_{60} (black line), dumbbell type molecular wires **10b** (blue line) and **23b** (red line).

Compounds	E^1_{red}	E^2_{red}	E^3_{red}
C_{60}	-0.802	-1.209	-1.676
10b	-0.921	-1.331	-1.883
23b	-0.899	-1.309	-1.841

Table 3. Cyclic voltammetry [V *vs* Fc/Fc^+] of **C_{60}** and molecules **10b**, **23b**. Working electrode: GCE; reference electrode: Ag/Ag^+; counter electrode: Pt; supporting electrolyte: 0.1M Bu_4NClO_4; scan rate: 100 mVs^{-1}; solvent: o-DCB/MeCN (4 : 1 v/v).

The first three reduction waves of dumbbell-type molecules and pristine C_{60} are compared under the same experimental conditions and, as expected, a cathodic shift has been observed for the dumbbell molecules in comparison to the parent C_{60} as a consequence of a destabilization of LUMO level which stems from the saturation of a C_{60} double bond. Comparing the reversible reduction waves, the cyclopropane seems to mark the difference with respect to the pyrrolidine molecule. Indeed, it shows a slightly lower but consistent value in the first three reduction potentials in between 20-40 mV. We claim that this shift is due to a better electronic communication between the π-fluorene core and the π-cloud of C_{60} thanks to the "double bond" behaviour of the cyclopropane unit.

4.3 Single bond linker in dumbbell-type molecules

4.3.1 Effect of only one Csp^3

In a dumbbell-type molecule, the direct functionalization through a single bond could result important for conductance studies because, in this case, the resulting molecule is more linear and rigid, maintaining its symmetry despite the free rotation capability along the single bond. For this purpose, we use the commercially available 2,7-diboronic-9,9'-dihexylfluorene acid and Rh(I) cyclooctadiene (cod) species with BF_4 anion as counter ion.

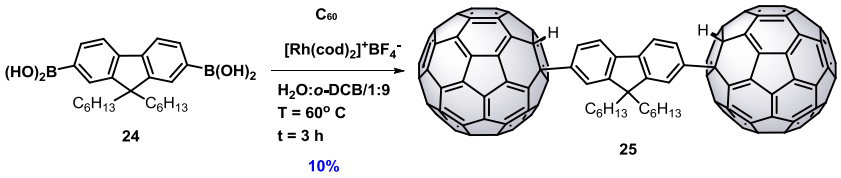

Scheme 12. Nucleophilic aryl addition over C_{60} backbone catalysed by Rh(I).

Compound **24** is dissolved with pristine C_{60} in a solution of H_2O/*o*-DCB:1/9. The solution is degased with argon stream for 30 minutes to remove the oxygen dissolved in water. Catalyst was thus added and the resulting solution is heated at 60 °C. To protect the bulk reaction from other side reactions, the bottom flask, previously flamed and put under cycles of argon and vacuum, is wrapped with aluminium foils. Light can be a further reactant for these catalysed reactions. The dumbbell-type molecule **25** is thus obtained in reasonable yields. HPLC (Figure 102) has been used for the isolation of the final compound with retention time of 8.09 minutes. The chromatogram is referred to a mixture of dumbbell molecule at 8.09 minutes and monoadduct product at 4.18 minutes with a ratio of 95:5 in favour of the dumbbell molecule (the most retained by stationary phase). Pure toluene as eluent and flow rate of 5 ml/min were the experimental conditions for the separation.

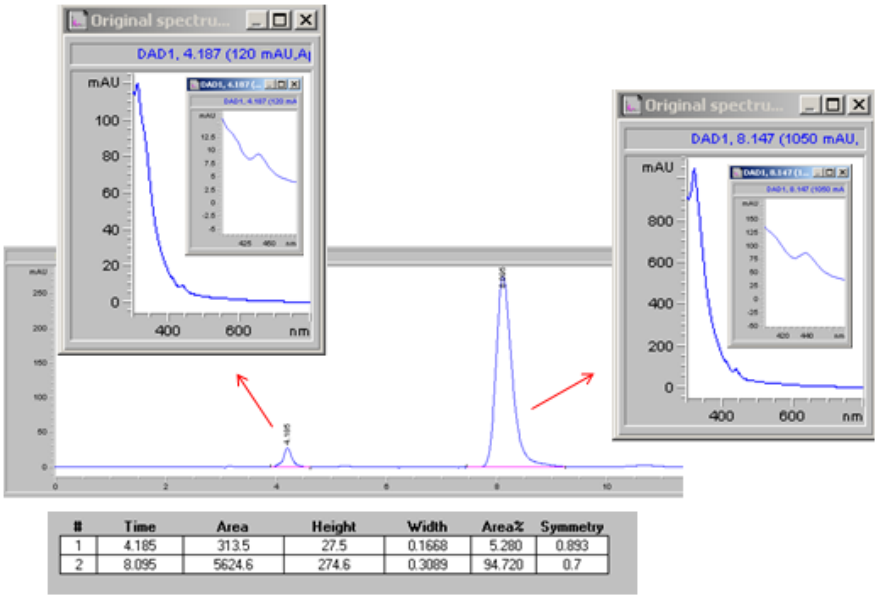

#	Time	Area	Height	Width	Area%	Symmetry
1	4.185	313.5	27.5	0.1668	5.280	0.893
2	8.095	5624.6	274.6	0.3089	94.720	0.7

Figure 102. Chromatogram of one sample after the first treatment with silica gel chromatography and a second treatment with bio-beads S-X8. The fraction collected contains either the monoadduct (4.185 minutes) and the dumbbell (8.095 minutes). Separation conditions: Buckyprep type Waters 10x250 mm, pure toluene as solvent, flow rate 5 ml/min. It is shown the relative area in % of each peaks and the typical UV-vis spectra of such products with a zoom in the inset graphic.

The ^{1}H-NMR spectrum of compound **25** is shown in Figure 103.

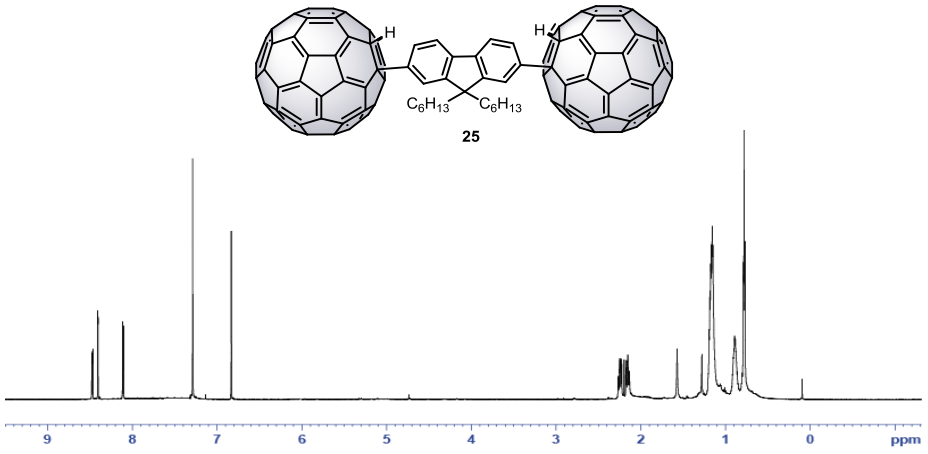

Figure 103. ^{1}H-NMR (CS_2:$CDCl_3$/2:1, 700 MHz, 25 °C) of compound **25**.

The ^{1}H-NMR spectrum has been recorded in CS_2:$CDCl_3$/2:1 due to the low solubility of this molecule in chloroform. The aromatic region shows clearly the signals of fluorene at 8.57 ppm (dd, J = 7.69 Hz and J = 1.89 Hz), 8.50 ppm (d, J = 1.77 Hz), and 8.25 ppm (d, J = 7.64 Hz). Most relevant is the presence of hydrogen linked directly to C_{60} as an intense singlet at 6.87 ppm. The high value for a -CH proton means that it is acid and, for this reason, the molecule could be unstable. This has been demonstrated solubilizing it in chlorobenzene and leaving it under light, at room temperature, without inert atmosphere. After two days, the retro-addition reaction occurs, as observed by HPLC analysis and, therefore, the product must be handled with care in the moment of the conductance measurements. ROE (stands for Rotating-Frame Overhauser Enhancement) analysis has been carried out to see how the proton belonging to C_{60} can affect the protons of the bridge. The free rotation along the single bond makes the two protons in *ortho* at this functionalization easy to spatially interact with the proton of C_{60} and, therefore, they are liable to ROE effect as shown in Figure 104:

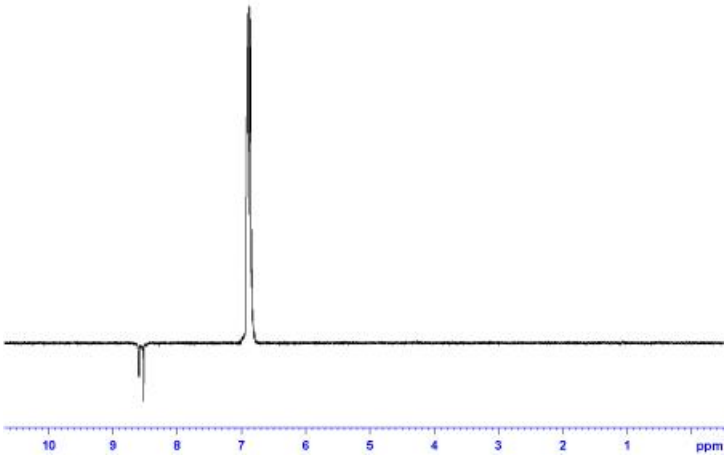

Figure 104. ROE spectrum of compound **25**.

The mass analysis made by MALDI-ToF shows the presence of a molecular peak with its typical fragmentation for such a kind of compounds. During the detailed study over the reactivity of aryl boronic acids/esters with C_{60}, we have also synthesized the monofullerene molecule in order to use it as a reference in STM or MCBJ experiments.

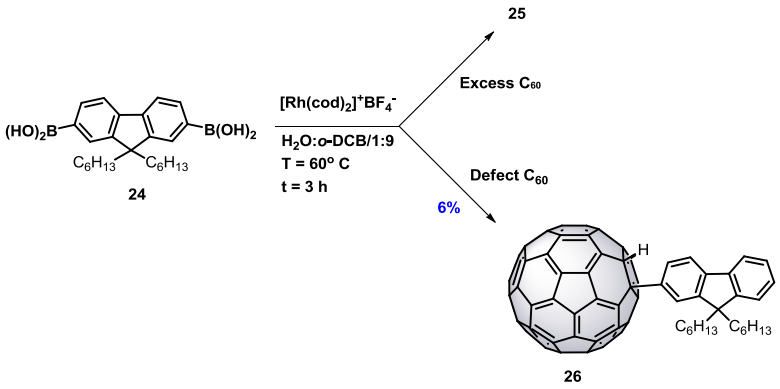

Scheme 13. Effect of the amount of pristine C_{60} used in the catalytic reaction via Rh(I) compound over 2,7-diboronic-9,9'-dihexylfluorene acid (**24**).

4.3.2 Monofluorene dumbbells (10a, 23a, 25): a linker comparison through cyclic voltammetry study

The typical experimental conditions of cyclic voltammetry have also been used for the electrochemical characterization of compounds **10a**, **23a** and **25**. The reduction waves clearly show the cathodically shift at higher potential value for the systems under study, which are consistent with the saturation of a C_{60} double bond. Moreover, the pyrrolidine dumbbell displays a different behaviour (of some mV) which makes it the most difficult to be reduced when compared with the other two molecules. This is ascribed to a certain interaction of the nitrogen lone pair over the C_{60} cage which slightly increases the energy value of the LUMO of the whole molecule. In particular, when the nitrogen atom is protected as an amide, this effect is not evident due to the delocalization of the lone pair over the carbonyl group. Figure 105 represents the reduction potential of the three molecules.

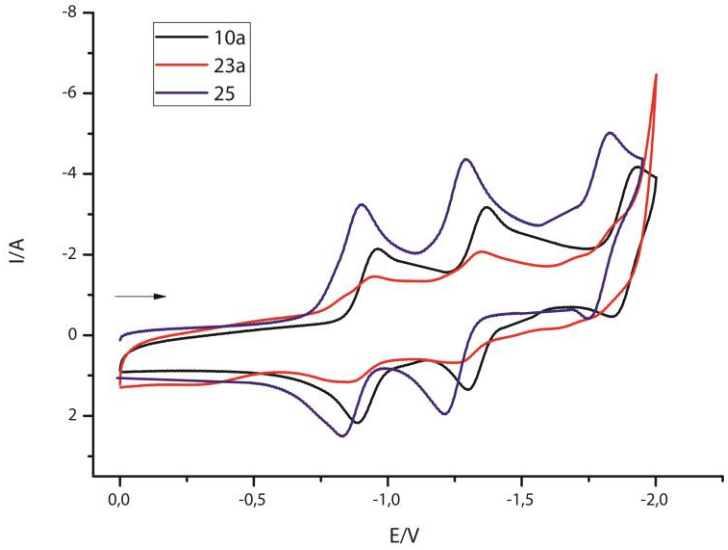

Figure 105. Cyclic voltammetry of compounds **10a**, **23a**, **25**. An electrochemical comparison is displayed for the different chemical connectivity between C_{60} and one fluorene unit.

Just comparing the cyclopropane dumbbell (in red) with the single bond dumbbell (in blue), it is possible to underline a slight anodically shift of the single bond dumbbell which demonstrates its slightly better capacity to be reduced with respect to the cyclopropane dumbbell and, of course to pyrrolidine dumbbell. These results are in agreement with our expectation to improve the electronic communication by reducing the number of carbon sp^3.

Compounds	E^1_{red}	E^2_{red}	E^3_{red}
10a	-0.921	-1.331	-1.883
23a	-0.899	-1.309	-1.841
25	-0.871	-1.259	-1.797

Table 4. Cyclic voltammetry [V *vs* Fc/Fc^+] of molecules **10a**, **23a** and **25**. Working electrode: GCE; reference electrode: Ag/Ag^+; counter electrode: Pt; supporting electrolyte: 0.1M Bu_4NClO_4; scan rate: 100 mVs^{-1}; solvent: o-DCB/MeCN (4 : 1 v/v).

4.4 Single bond dumbbell series with different length

In the previous paragraphs, we have shown that Rh(I) is an efficient catalyst which paves the way towards the single bond functionalization of fullerene's family. In collaboration with Prof. Wandlowski at University of Bern (Switzerland), we proposed the synthesis of a new series of dumbbell molecules formed by 1, 2 and 3 fluorene units. This leads to the study of β value for such series using STM or MCBJ experiments. Moreover, the comparative study between dumbbell molecules and the last step materials, boronic acids or esters, could envisage the real function of C_{60} as anchor group. Although the final products seem to be quite stable, the bottleneck is represented by the acid protons situated on C_{60} surface. The resulting stability of such molecules is extremely subjected to the light exposure and atmospheric oxygen and, as precaution, the storage in solution is not recommended.

4.4.1 Synthesis of the precursors for C_{60}-$(Fl)_n$-C_{60} (n = 2,3)

The synthetic route for the preparation of dumbbell-type molecular wire with two units of fluorene has been designed starting from the functionalization and derivatization of the fluorene unit. The scheme below resumes all the sequential steps carried out.

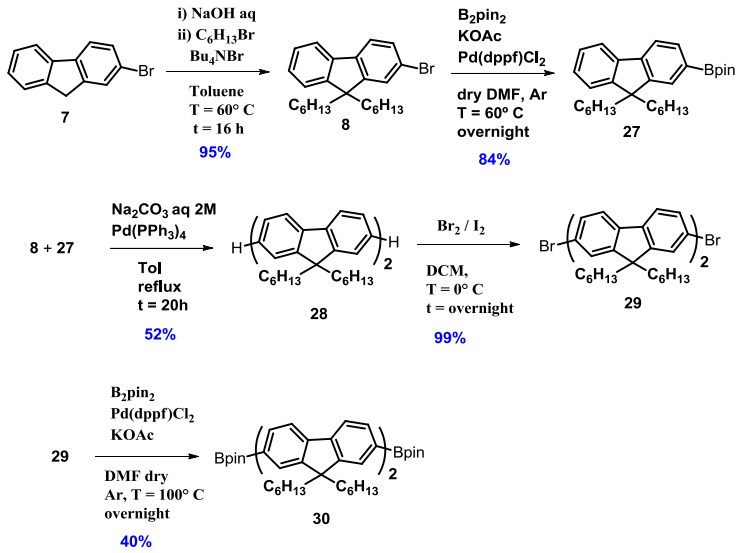

Scheme 14. Synthetic steps for molecule **30**.

- The first step is an alkylation reaction at position 9 of fluorene: a better solubility in common organic solvents of the final product is thus achieved.
- The second step is a Miyaura reaction. Thus, the bromide derivative **8** undergoes borylation in a process mediated by Pd(0) tetrakis. The following reaction scheme helps to clarify this mechanism.

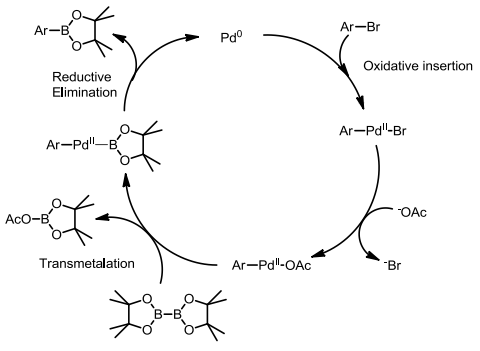

Scheme 15. Catalytic scheme of Miyaura reaction.

The resulting exchange of bromine with boropinacolate moiety using this strategy affords in good yields the 2-(9,9'-dihexylfluoren-2-yl)-4,4',5,5'-tetramethyl[1,3,2]dioxaborolane **27**.[196] An alternative to Miyaura reaction is the treatment of compound **8** with *n*-BuLi, followed by the use of 2-isopropoxy-4,4',5,5'-tetramethyl-1,3,2-dioxoborolane.

- The third synthetic step is a Suzuki coupling between **8** and **27** to obtain 2,2'-bis(9,9'-bishexylfluorene) **28**.[197] It has been performed using Pd(0) tetrakis as catalyst, aqueous solution of sodium carbonate and toluene as solvent.
- The fourth step consists in a electrophile addition of molecular bromine to the core of the difluorene, catalysed by iodine, to form compound **29**.[198] This reaction is sensitive to the dilution conditions of bromine and to the temperature: at 25 °C the reaction shows some byproducts which could be referred to multi-addition of bromine over fluorenes as well as when the solution of bromine to be added is concentrated.
- The fifth and last step consists in the substitution of bromine with boropinacolate following the Miyaura reaction, with the formation of **30**.[199]

The trifluorene dumbbell molecule is the longest molecule of the series with a direct connection between the C_{60} units and the bridge. Since the reported procedure gives rise to a lower yield,[200] we designed a slightly different synthetic route for this molecular wire based on C_{60}, shown in the Scheme 16.

[196] W. Y. Lai, R. Xia, D. D. C. Bradley, W. Huang, *Chem. Eur. J.* **2010**, *16*, 8471.
[197] N. Fomina, S. E. Bradforth, T. E. Hogen-Esch, *Macromolecules* **2009**, *42*, 6440.
[198] V. Promarak, A. Punkvuang, T. Sudyoadsuk, S. Jungsuttiwong, S. Saengsuwan, T. Keawin, K. Sirithip, *Tetrahedron* **2007**, *63*, 8881.
[199] P. H. Auberta, L. Beoucha, F. Tran-Vana, O. Stephanb, C. Chevrot, *Synt. Metals* **2006**, *156*, 898.
[200] J. Jo, C. Chi, S. Hager, G. Wegner and D. Y. Yoon, *Chem. Eur. J.* **2004**, *10*, 2681.

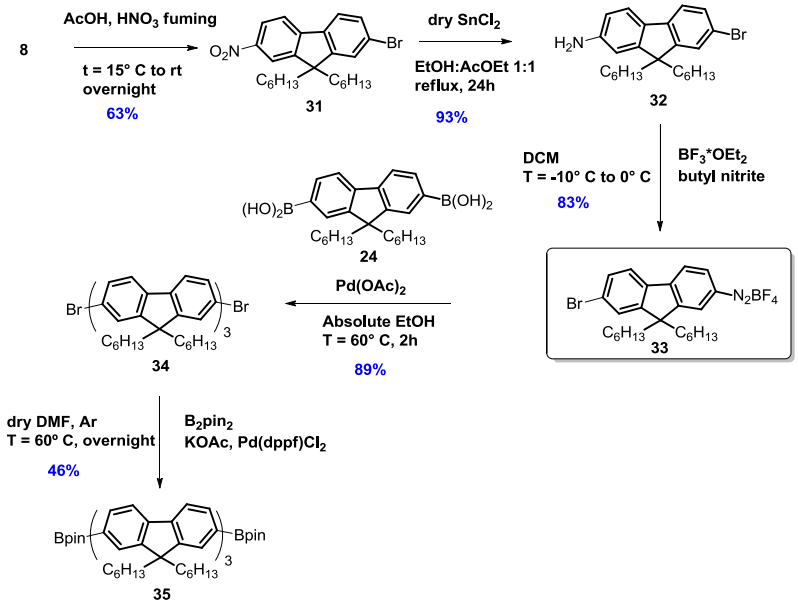

Scheme 16. Reaction scheme for the synthesis of compound **35**.

- The nitration reaction of 2-bromo-9,9'-dihexylfluorene **8** in position 7 has been performed using fuming nitric acid in acetic acid as solvent.[201] Owing to the strong nitration conditions, several byproducts have emerged. The most polar product has been attributed to the desired product **31**, after its isolation and characterization.
- The reduction of the nitro group to amine **32** has been performed in a mixture of polar solvents with ratio 1:1 using dry tin(II) chloride as reagent.[202] It affords the product in almost quantitative yield (93%) after the elimination of tin(II) chloride in excess with the use of NaOH, forming tin hydroxide that precipitates in the bulk of reaction. The acidic reduction of nitro aryl is an alternative to the reduction with Fe catalysed by inorganic acids and also to the hydrogenation mediated by metal catalysts as Pt. As concerns the hydrogenation, also C_{60} has been

[201] S. P. Dudek, M. Pouderoijen, R. Abbel, A. P. H. J. Schenning, E. W. Meijer, *J. Am. Chem. Soc.* **2005**, *127*, 11763.
[202] B. Balan, C. Vijayakumar, S. Ogi, M. Takeuchi, *J. Mater. Chem.* **2012**, *22*, 11224.

used as active molecule in a nitrobenzene reduction mediated by light.[203]

- Fluorene diazonium salt of tetrafluoroborate **33** represents an interesting intermediate in this synthetic route. Herein, we used it in a Suzuki coupling with a commercial boronic acid **24**. However, we can also employ such derivatives in azocoupling reactions[204] or in the formation of direct single bond with carbon nanoforms such as nanotubes[205] and graphenes.[206] Its synthesis has been developed in good yield starting from compound **32** under the activation of the amine group with an adduct of tetrafluoroborate Lewis acid-diethyl ether, followed by the addition of butyl nitrite at -10 °C. The product has been precipitated from the bulk using *n*-pentane to obtain a greenish solid which has been further characterized.

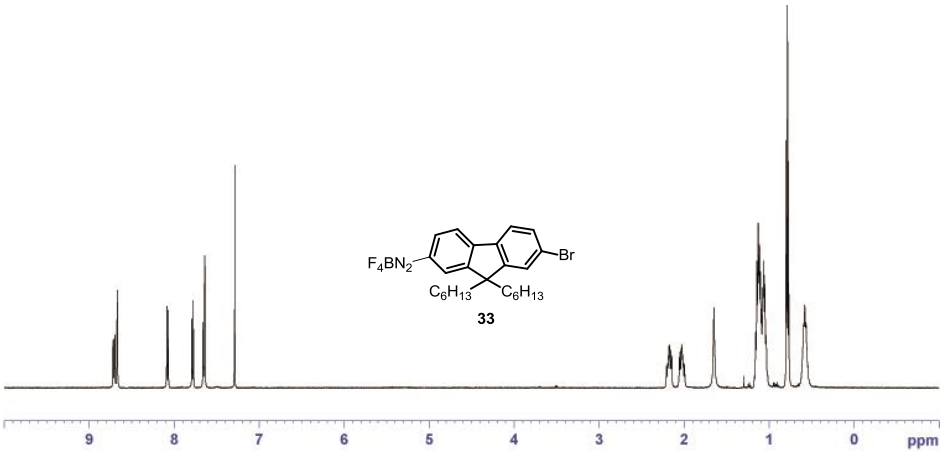

Figure 106. ^{1}H-NMR ($CDCl_3$, 500 MHz, 25 °C) of compound **33**.

Surprisingly, ^{1}H-NMR spectrum of tetrafluoroborate diazonium salt of fluorene **33** in $CDCl_3$ at 25 °C shows interesting results. If we divide the spectra in aromatic region and aliphatic region, we can discuss about the following

[203] B. Li, Z. Xu, *J. Am. Chem. Soc.* **2009**, *131*, 16380.
[204] M. E. Garst, D. Lukton, *Synth. Comm.*, **1980**, *10*, 155.
[205] a) J. L. Bahr, J. Yang, D. V. Kosynkin, M. J. Bronikowski, R. E. Smalley, J. M. Tour, *J. Am. Chem. Soc.* **2001**, *123*, 6536; b) H. Leinonen, M. Lajunen, *J. Nanopart. Res.* **2012**, *14*, 1064.
[206] a) J. R. Lomeda, C. D. Doyle, D. V. Kosynkin, W.-F. Hwang, J. M. Tour, *J. Am. Chem. Soc.* **2008**, *130*, 16201; b) Z. Jin, J. R. Lomeda, B. K. Price, W. Lu, Y. Zhu, J. M. Tour, *Chem. Mater.* **2009**, *21*, 3045.

conclusions. As concern the aromatic region, the protons of the fluorene core are different because the molecule is not symmetric. Furthermore, the presence of the diazonium salt allows a better separation of the protons of its aryl moiety where the α effect of heteroatom is more evident with respect of that of the nitro group owing to the positive charge of nitrogen. In the case of aryl substituted with bromine atom, the effect of unshielded is less evident even if the proton in β to the bromine suffers the β effect of halogen atom with a little unshield compared with that in α which are not well separated. Another aspect, which comes out in the aliphatic region, is the difference in the methylenes at about 2.0 ppm. This is the first recorded example where we are able to distinguish that those protons belong to the carbons of the alkyl chains directly linked to the C9 of fluorene (pro-chiral carbon and spiro-carbon). Cosy spectrum (Figure 107) shows the correlations of these protons with that at around 0.5 ppm which belong to the adjacent carbon atoms. Owing to the presence of one triplet of -CH_3, we suspected that the methylenes at 2.0 ppm do not correlate with them otherwise we had to obtain two signals of triplet instead of one. Indeed, the triplet signal correlates, as shown in cosy analysis, with methylene groups situated at 1.0 ppm under the broad multiplet.

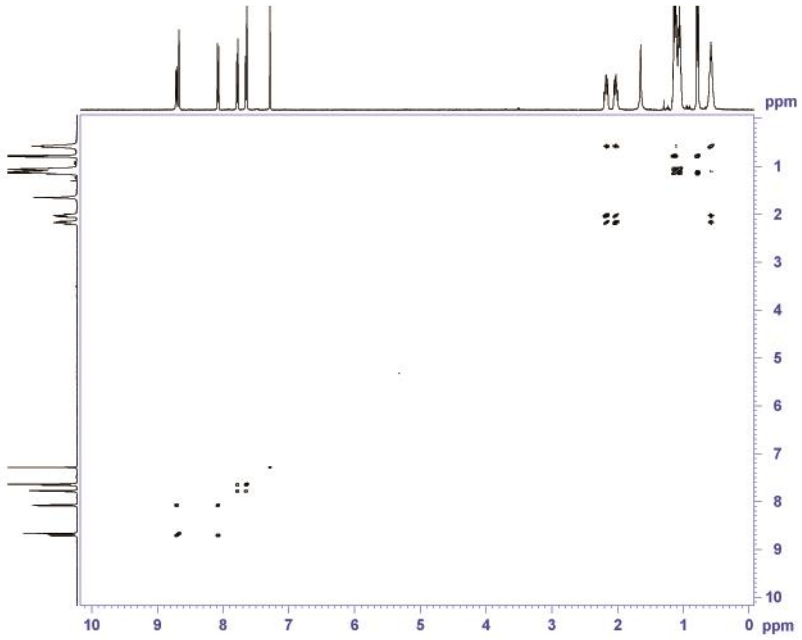

Figure 107. Cosy of compound **33**.

The ITMS (Ionic Trap Mass Spectrometry) of compound **33** does not show neither the peak of tetrafluoborate salt (527.24 uma) or the peak of the diazonium molecule (440.43 uma) but it shows a base peak at 442.9 m/z. It results from the sum of MeOH (used in the analysis) to the 2-bromofluorene cation (molecular weight is 411.9) generated by the loss of tetrafluoroborate followed by the loss of N_2 molecule. The presence of Br is demonstrated by its typical isotopic effect. Peak at 428.9 shows the same pattern of that at 442.9 with the loss of 14 uma. This peak may be attributed to a weight molecular loss of the molecular peak, demonstrated also by the presence of bromine (isotopic effect) or, perhaps, it derives from the loss of only one nitrogen atom of the diazonium salt cation (440.43 uma) with the addition of two protons to form the amine group.

- Suzuki coupling between the diazonium salt **33** and 2,7-diboronic-9,9'-dihexylfluorene acid **24**, affords the formation of **34** in acceptable yield, using polar solvent and a Pd(II) species as shown in the scheme above. NMR (^{1}H, ^{13}C) and MALDI-ToF mass analysis showed the presence of the desired product.
- The formation of diboropinacolate derivative **35** has been obtained following the same procedure seen for the formation of the analogue derivative in the case of two fluorenes.

4.4.2 Synthesis of the dumbbells C_{60}-$(Fl)_n$-C_{60} (n = 2,3)

The synthesis of dumbbell-type molecules has been performed using the same strategy described for compound **25**. The Scheme 17 resumes the reaction conditions employed with boronic acid or esters.

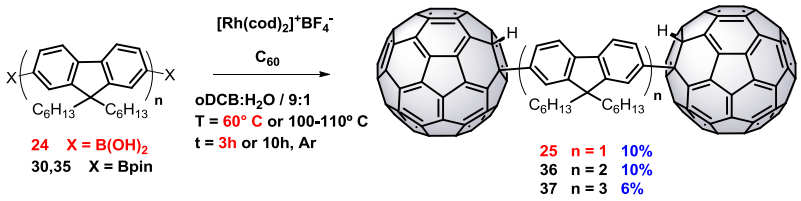

Scheme 17. General scheme of the hydroarylation reaction over C_{60} catalysed by Rh(I) complex.

The presence of boronic esters as functional group needs an increment of reaction temperature until 100-110 °C instead of 60 °C used for the hydroarylation of C_{60} with boronic acid. The product **36** has been obtained as brown solid and the ^{1}H-NMR is shown in Figure 108.

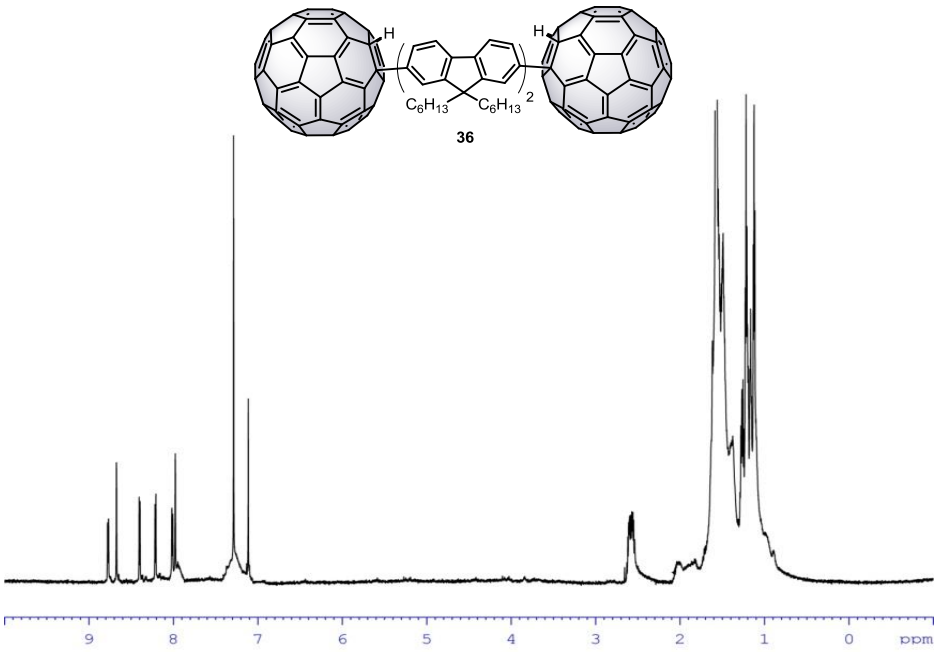

Figure 108. ^{1}H-NMR (CS_2:$CDCl_3$/2:1, 700 MHz, 25 °C) of compound **36**.

The aromatic region shows a neat pattern of protons belonging to each fluorene, also confirmed by HSQC analysis. At 7.11 ppm, appears the typical intense singlet of the two acidic protons directly linked to C_{60} which correlates with the carbon at about 65 ppm. All the precursors of such product are extremely fluorescent but when C_{60} is covalently attached, this fluorescence is quenched probably by some electronic or energetic processes.

Dumbbell-type molecular wire **37** has been obtained in low yield as brown solid but with the suitable amount in order to perform physical experiments. The product has been isolated by further semipreparative HPLC using Buckyprep type Waters column (Figure 109). An analytic confirmation with a flow rate of 1 ml/min in pure toluene shows that the compound is pure enough to be submitted for conductance measurements. The UV-vis spectrum identifies the correct functionalization over the C_{60} sphere.

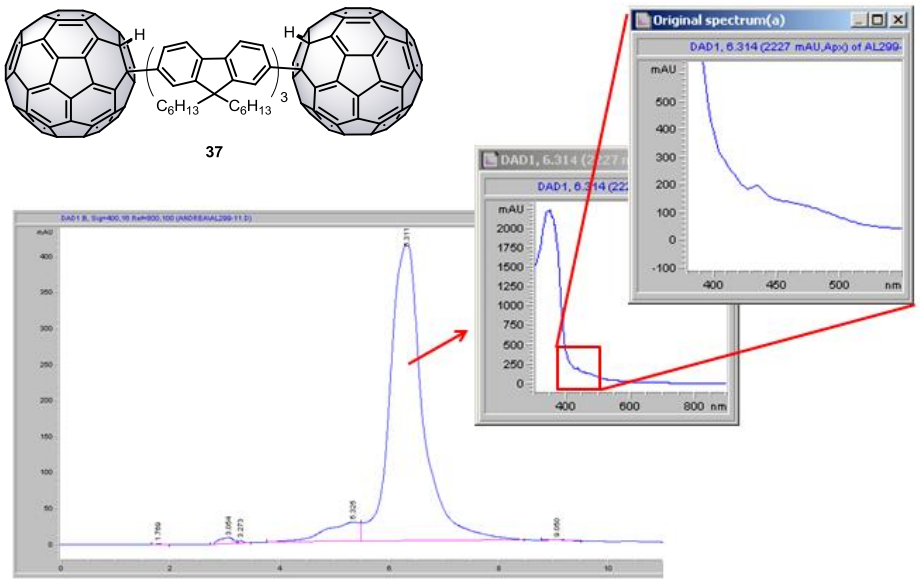

Figure 109. HPLC for the isolated product and its UV-vis spectrum with typical peak of functionalized C_{60} that, for this series, has an absorbance peak at about 440 nm.

The product thus isolated has been characterized by NMR (^{1}H, ^{13}C, dept, HSQC, HMBC, ROE) and MALDI-ToF analysis. The proton spectrum clearly

shows the functionalization of C_{60} with protons derived from the bulk of reaction (Figure 110). They appear at 6.86 ppm as an intense singlet signal which correlates with the -CH at 64 ppm. The range between 8.51-7.70 ppm represents the region in which the fluorene protons appear with different coupling constants and slightly difference in the chemical shift is observed when passing from the fluorene situated in the middle of the bridge to those situated close to C_{60} stoppers. The alkyl region appears disturbed because of the presence of six alkyl chains. Only the multiplet signal at 2.31 ppm appears clear and integrates for 12 protons, as expected.

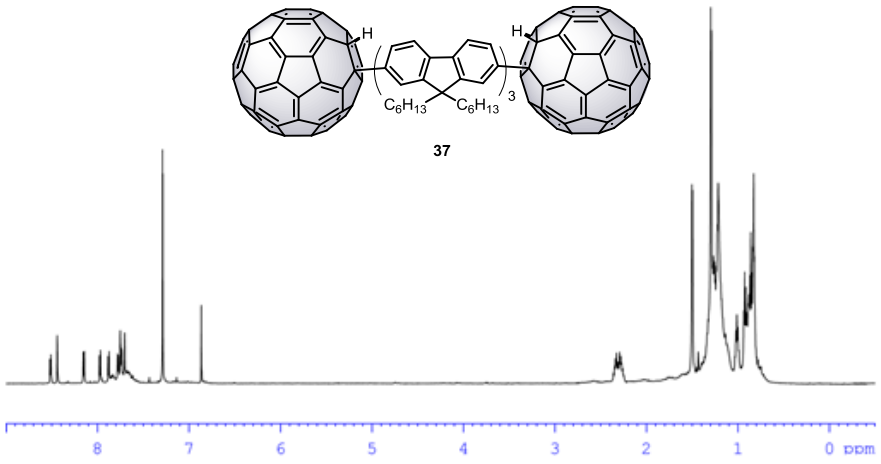

Figure 110. ^{1}H-NMR (CS_2:$CDCl_3$ / 1:1, 700 MHz, 25 °C) of compound **37**.

ROE analysis allows us to unequivocally assign what signals correspond to the protons in ortho position at the C_{60} functionalization simply irradiating the signal at 6.86 ppm. Such protons fall at 8.51 ppm as a doublet with an ortho coupling constant and at 8.43 ppm as a singlet. Evidently, these protons are related to the aryls which belong to those fluorenes more exposed to the C_{60} cages.

4.4.3 Cyclic voltammetry of single bond dumbbell-type molecules

The electrochemical features of three single bond dumbbell molecules **25**, **36**, **37**, does not show relevant differences despite the enhancement of the bridge's length of the wire. The reduction waves are consistent with the electrochemical shift observed for any C_{60} derivative reported in this Memory and, as expected, no oxidation peak is observed for such compounds.

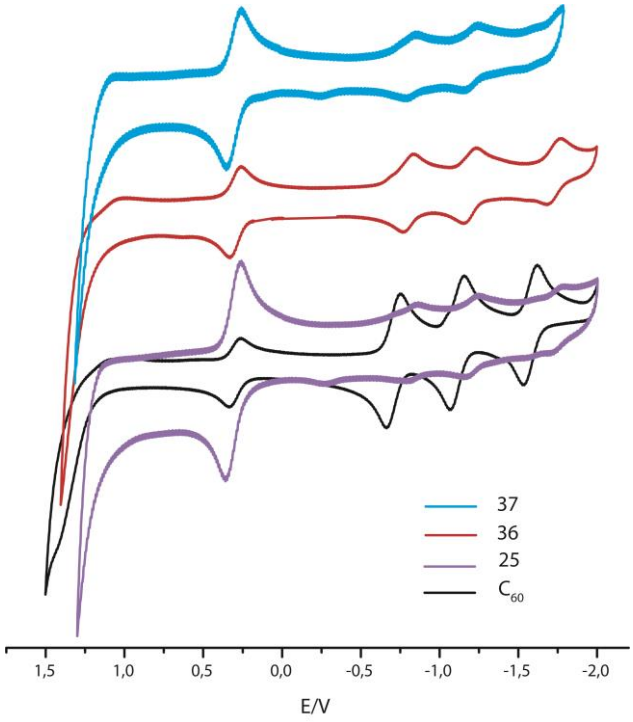

Figure 111. Cyclic voltammetry of pristine $\mathbf{C_{60}}$ and compounds **25**, **36**, **37**.

In the table below, the reduction potential values are listed. The difference of 130 mV between pristine C_{60} and the other compounds is in agreement with the saturation of a double bond of the C_{60} sphere, as previously discussed.

Compounds	E^1_{red}	E^2_{red}	E^3_{red}
C_{60}	-1.00	-1.41	-1.87
25	-1.13	-1.50	-2.05
36	-1.13	-1.53	-2.04
37	-1.13	-1.52	NR

Table 5. Cyclic voltammetry [V *vs* Fc/Fc^+] of $\mathbf{C_{60}}$ and molecules **25**, **38**, **39**. Working electrode: GCE; reference electrode: Ag/Ag^+; counter electrode: Pt; supporting electrolyte: 0.1M Bu_4NClO_4; scan rate: 100 mVs^{-1}; solvent: o-DCB/MeCN (4 : 1 v/v). NR = not recorded.

4.5 Dumbbell-type molecular wires based on different cores

Aryl and benzodifuran (BDF) cores have also been sandwiched in between two C_{60} units, thus forming the dumbbell-type molecular wires. The use of one benzene (as bridge) has been thought to create the shortest dumbbell molecule. In such a way, it is possible to compare it in conductance experiments with the molecule hanging the fluorene moiety and the same C_{60} functionalization. In contrast, the most extensive core (BDF) has been anchored to the C_{60} sphere with two different linkers. The choice of BDF core has been done in collaboration with Prof. Silvio Decurtins group of University of Bern to study the final behaviour of these molecules in PET analysis and onto surface, using STM, in typical conductance experiment which will be performed by Agraït group at Universidad Autonoma of Madrid. BDF has also been chosen thanks to its wide application in the field of molecular organic electronics.

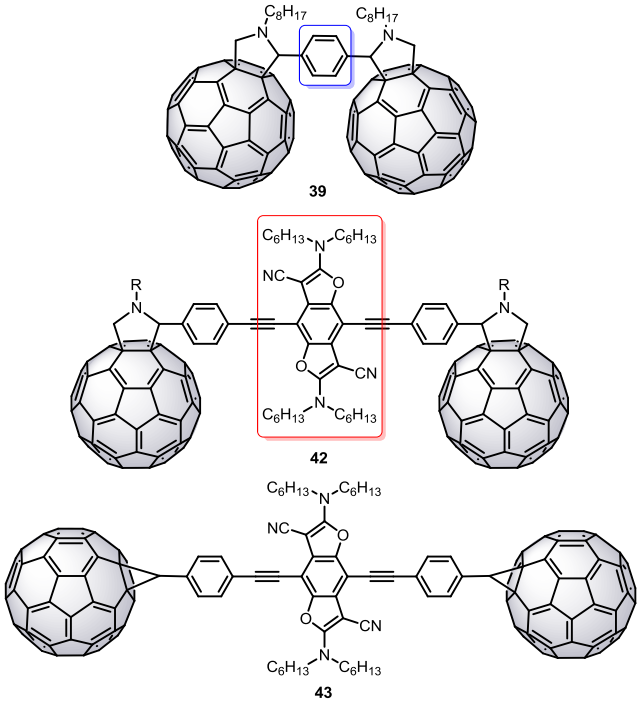

Figure 112. Two new cores (aryl squared in blue and BDF squared in red) for dumbbell systems.

The linkers employed are the pyrrolidine and the cyclopropane rings for reduced synthetic efforts. Aryl dumbbell molecule has been used for further studies of conductance whilst the BDF dumbbells have been used either for this aim or for photophysical study.

4.5.1 Dumbbell-type molecular wires with aryl core

Pyrrolidine dumbbell **39** was synthesized by employing a Prato reaction over the commercially available terephthaldehyde **38**, using N-octylglycine, previously synthesized, to form the ylide *in situ*, which is further reacted with the double bond of C_{60}.

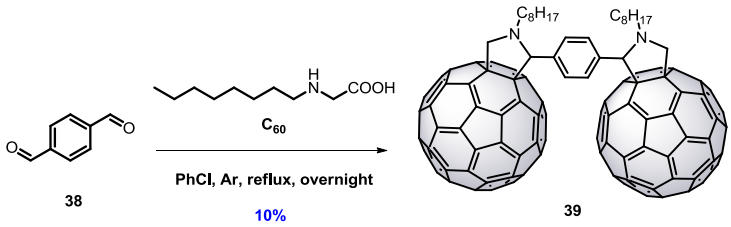

Scheme 18. One-pot Prato reaction for the synthesis of pyrrolidine dumbbell **39**.

The product has been characterized by ^{1}H-NMR. Mass spectrum, registered by MALDI-ToF setup, shows clearly the evidence of molecular peak (even though it is not so intense). The ^{1}H-NMR shows two broad peaks in the aromatic region due to the high rotational barrier around the aryl-pyrrolidine bond and, perhaps, to the presence of the four stereoisomers, as results of the two chiral centres formed during the reaction. They are attributed to the protons of the benzene core. More clearly, the pattern of the pyrrolidine system is observed.

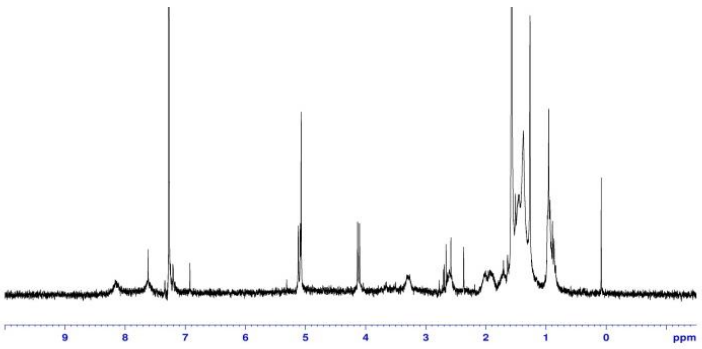

Figure 113. ^{1}H-NMR (CS_2 with internal reference $CDCl_3$, 300MHz, 25 °C) of compound **39**.

4.5.2 Dumbbell-type molecular wires with BDF core

Thanks to a collaboration with Prof. Decurtins of the University of Bern (Switzerland), BDF core has been covalently linked to two C_{60} in a dumbbell shape molecules (Scheme 19).[207]

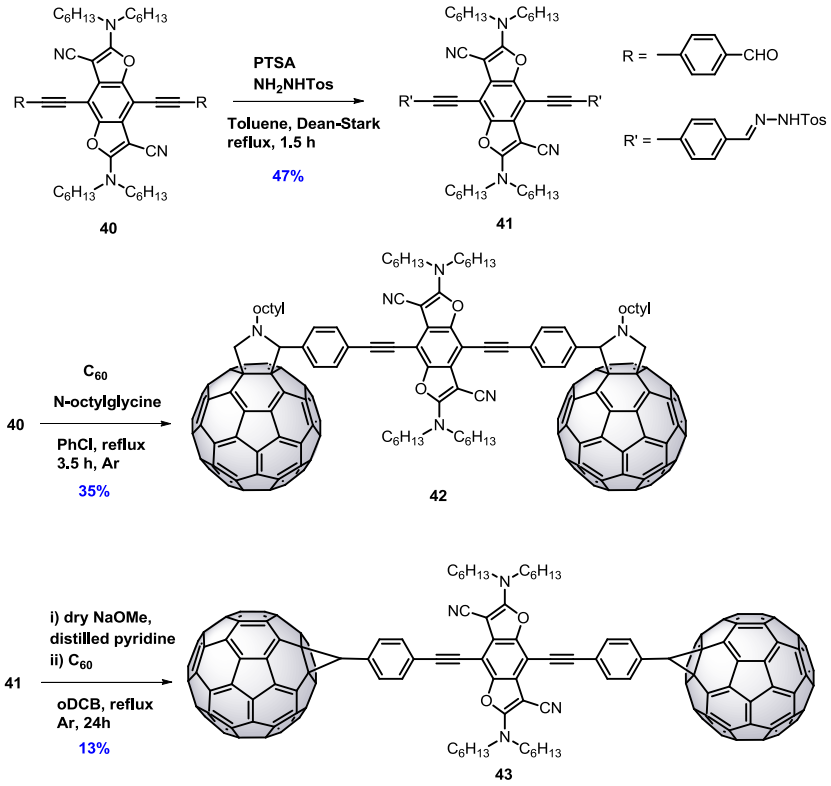

Scheme 19. Reaction scheme of the synthesis of two dumbbells (**42** and **43**) based on BDF core.

The dialdehyde **40** has been synthesized following the Sonogashira coupling reaction between diiodobenzodifuran and 4-ethynylbenzaldehyde. This scaffold has been employed as starting material for the synthesis of dumbbell-type molecular wires **42**, **43**. Compound **42** has been obtained in really good yield within the range of C_{60} dumbbell-type molecules after its separation from not reacted pristine C_{60}. Prato reaction occurs between the dialdehyde and the

[207] PhD thesis of Hui Li: "Benzodifuran derivatives for organic and molecular electronics", University of Bern (Switzerland), **2013**.

N-octylglycine under the typical conditions. The ^{1}H-NMR of **42** (Figure 114) shows two signals in the aromatic region corresponding to the eight protons of the aryl moieties. They are divided into two peaks: one broad singlet which is referred to the four protons closest to the C_{60} and another intense doublet with typical value of *ortho* coupling constant (8.15 Hz) which is referred to the internal protons of the aryls. The signals of pyrrolidine functionalization are well defined in the region between 5.09 and 4.13 with the typical pattern (doublet, singlet, doublet more shielded). At 3.58 ppm the eight protons of the four methylene groups linked to the nitrogen atom appear as a triplet.

The aliphatic region results complex due to the presence of four hydrocarbon alkyl chains in the BDF core and the eight carbon alkyl chains in the pyrrolidine rings. The correct attribution of each signal has been done thanks to hetero-correlation technique.

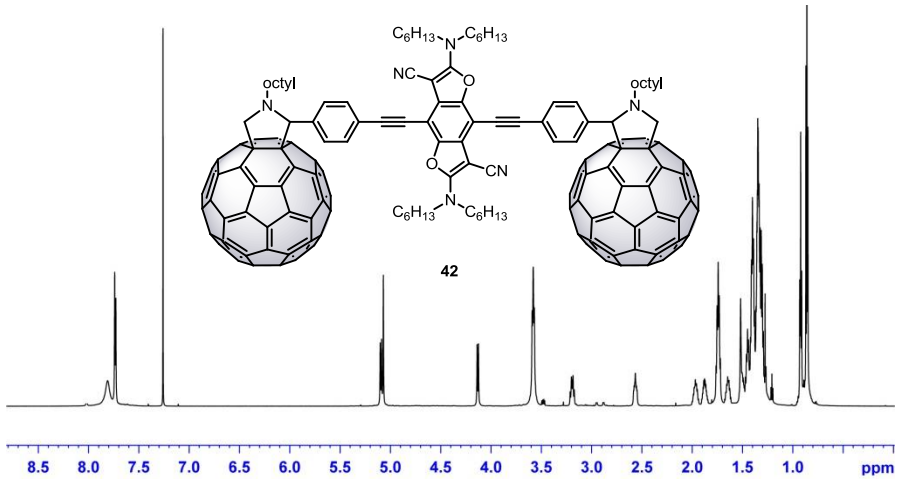

Figure 114. ^{1}H-NMR ($CDCl_3$, 700 MHz, 25 °C) of compound **42**.

As concerns as the cyclopropane formation over the C_{60} sphere, the Bamford-Stevens reaction has been used to attach the BDF core in order to form a more rigid, symmetric and linear molecular wire with the removal of the chiral centre. Thus, molecule **40** has been properly modified to form the corresponding dihydrazone **41**. The mixture of E/Z isomers has been used for the cycloaddition reaction over C_{60} following the same conditions previously reported as it is shown in the scheme. Dumbbell-type molecular wire **43** has been obtained as a stable brown solid in relatively low yield.

The ^{1}H-NMR spectrum (Figure 115) shows a perfect symmetric molecule with a characteristic singlet of -CH of cyclopropane moiety at 5.72 ppm. The other parts of the spectrum reveal that only one signal is observed for the equivalent protons, both in the aromatic and aliphatic regions.

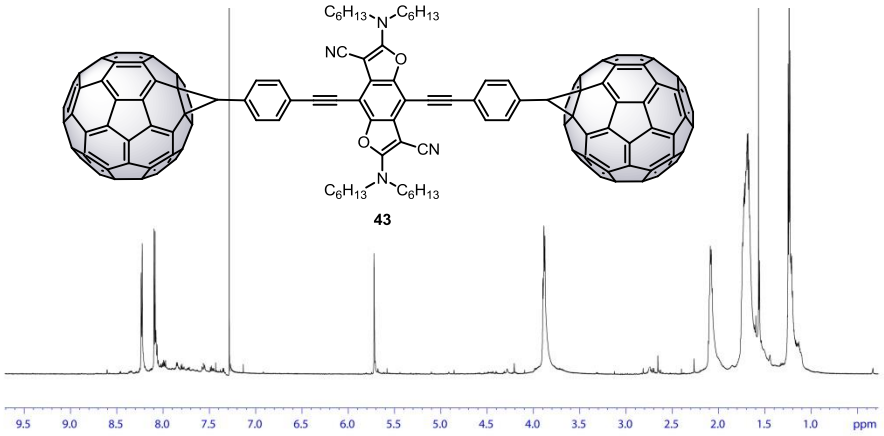

Figure 115. ^{1}H-NMR ($CDCl_3$, 700 MHz, 25 °C) of compound **43**.

Maldi-Tof analysis shows the expected molecular peak (2240,278 uma) without any kind of decomposition, by loss of C_{60}. This means that this molecule is stable under these conditions of ionization.

4.5.3 Optical properties of benzodifuran dumbbell-type molecules

The optical properties of dumbbell molecules **42** and **43** have been deeply analysed. First of all, the absorption spectrum has been registered and compared with the following molecules prepared previously as a new dumbbell (the case of **46**) or as reference molecules (**44** and **45**).

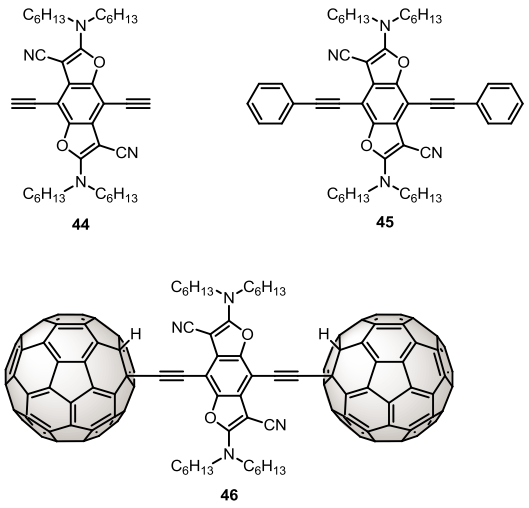

Figure 116. Individual molecular cores **44** and **45**. Triple bond directly linked to $\mathbf{C_{60}}$ in dumbbell-type molecular wire **46**.

At first glance, the absorption of dumbbell molecules results in the sum of the absorption spectra of individual BDF and pristine C_{60} (Figure 117). The most important BDF feature influence is seen in the dumbbell **46** where its molar extinction coefficient is peer to 1.5×10^4 M^{-1} cm^{-1} at around 433 nm, wavelength in which is maximized the absorption of BDF core. For the dumbbells **42** and **43**, this BDF broad absorption band is shifted at around 467 nm and another intense band at 385 nm. The presence of C_{60} is envisaged by the peak at 335 nm.

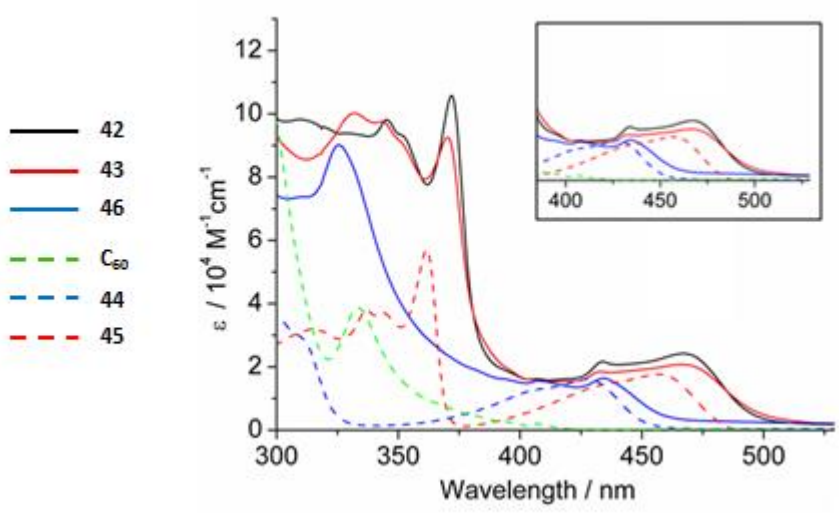

Figure 117. UV-vis spectra. Molecule **42** in black, molecule **43** in red, molecule **46** in blue. Dashed lines are referred to pristine C_{60} (green), molecule **44** (blue), molecule **45** (red). The inset shows a zoom of the region where the electronic communication has been observed.

It has been recorded a bathochromically shift of BDF and C_{60} in molecules **42** and **43** of about 10 nm which could indicate a slight electronic communication between the two electroactive species in the ground state. Comparing the bold blue line of molecule **46** with the dashed blue line of molecule **44**, only a slight red shift is observed for the BDF absorption band due to the presence of C_{60} spheres.

Time dependent DFT (TD-DFT) calculations have been used for a better understanding over the excited states of the molecules. In such a way, we demonstrate an electron transfer from the BDF core to the C_{60} cages. The intense band at about 370-385 nm is referred to the excitation of BDF core while that of C_{60} is around 320-350 nm, according to the theoretical studies. Interestingly, molecule **46** does not have the band of BDF excitation but another at about 325 nm. It may be explained by the presence of the triple bond which takes part into the HOMO of the molecule. In this way, it allows a better electronic communication between C_{60} and BDF, at least in the CT process at the excited states. For a better understanding of the CT process in excited states, experimental analysis by steady-state fluorescence spectra has been

recorded at room temperature for the tree dumbbell molecules. They show a red shift of fluorescence with respect to the simple bridge.

Neat BDF cores have a fluorescence quantum yield close to unity and fluorescence lifetime between 6 and 7 ns; when they are bridging to two C_{60} molecules (*i.e.*, molecule **42** reported in the figure below), the fluorescence is almost completely quenched by the CT process occurring in the excited state (wavelength of excitation is that of BDF core, 430 nm). It is already known that C_{60} has a fluorescence peak at about 700 nm with a fluorescence quantum yield of 6×10^{-4} (Φ_F) which can change depending by the addend system.[208] The dumbbell molecules also present this emission peak but with fluorescence quantum yields of 2×10^{-4} (molecules **42** and **43**) and 4.7×10^{-5} (molecule **46**).

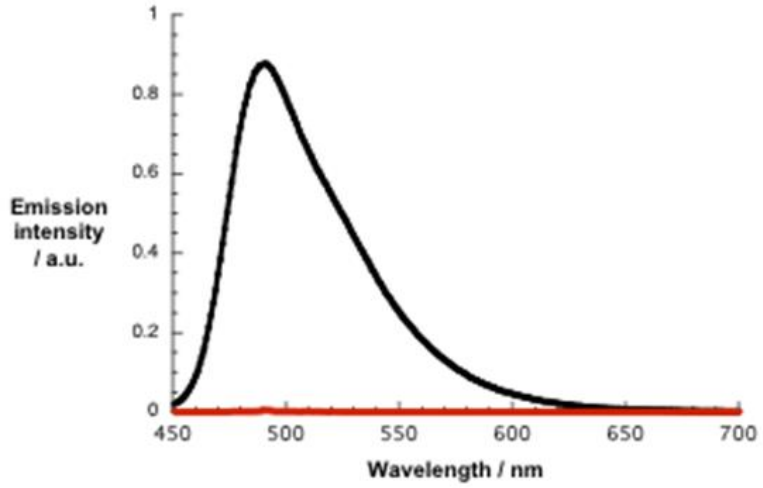

Figure 118. Steady-state fluorescence spectra, recorded in THF upon excitation at 430 nm of **45** (black) and **42** (red) with matching absorption at the excitation wavelength at room temperature.

[208] M. J. Brites, C. Santos, S. Nascimento, B. Gigante, H. Luftmann, A. Fedorovc and M. N. Berberan-Santos, *New J. Chem.*, **2006**, *30*, 1036.

4.5.4 Cyclic voltammetry of benzodifuran dumbbell-type molecules

Cyclic voltammetry experiments have been carried out under the same experimental conditions already described. The comparison between pristine C_{60}, pristine core and dumbbell molecules is mandatory to understand whether exist some electronic communication between the two electroactive species through the linker employed.

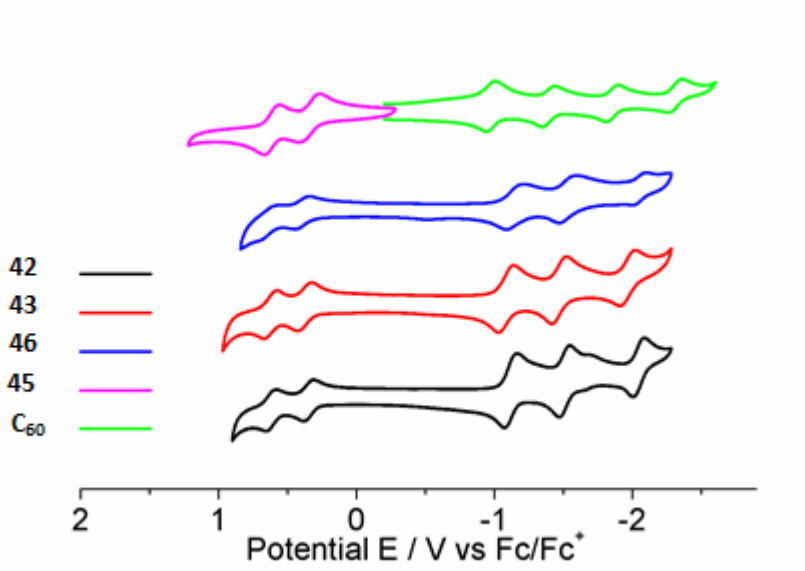

Figure 119. Cyclic voltammetry of compounds **42**, **43**, **46** (dumbbells) compared with **45** (core) and pristine **C_{60}**.

Compounds	E^1_{red}	E^2_{red}	E^3_{red}	E^1_{OX}	E^2_{OX}
C_{60}	-1.06	-1.47	-1.94		
42	-1.11	-1.51	-2.04		
43	-1.09	-1.47	-1.96		
46	-1.15	-1.53	-2.05		
45	—	—	—	0.34	0.61

Table 6. Cyclic voltammetry [V *vs* Fc/Fc^+] of **C_{60}** and molecules **42**, **43**, **46**. Working electrode: GCE; reference electrode: Ag/Ag^+; counter electrode: Pt; supporting electrolyte: 0.1M Bu_4NClO_4; scan rate: 100 mVs^{-1}; solvent: o-DCB/MeCN (4 : 1 v/v).

Analysing the voltammograms and the reduction potential values obtained, it is possible to reach the following conclusions:

1. The reversible oxidation waves of BDF core are consistent with the pristine core analysed with same method. The formation of radical cation and dication is emphasized and no relevant cathodically shift has been recorded, which evidences no electronic communication in the ground state.
2. The reversible reduction waves of C_{60} are cathodically shifted more than 100 mV compared with pristine C_{60}, as expected.
3. Both C_{60} units of dumbbell molecules are reduced at the same time and at the same potential value. This arises from the presence of only one reduction wave for each two electrons acquired.
4. A slight cathodically shift (20 mV in the first reduction potential) is observed when compared molecules **42** with the cyclic voltammetry of molecule **43** bearing the cyclopropane ring. This again remarks the function of the cyclopropane ring as "double bond", enlarging therefore the electronic communication between C_{60} and BDF.
5. Molecule **46** seems to be the most difficult to be reduced as is also observed when comparing the values of the first reduction potential for the three dumbbells under study.

4.6 STM measurements in ambient conditions of cyclopropane dumbbell

This study has been carried out in the group of Prof. Agraït from IMDEA-Nanoscience within the framework of an EU project (FunMols, Ref. FP7-People-ITN-2008). The conductance measurements of cyclopropane dumbbell molecule **23b** have been performed with an STM setup modified to be used in ambient conditions.[209]

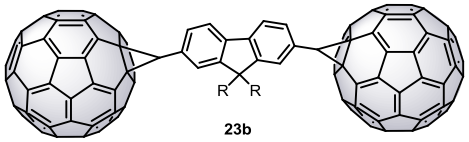

Figure 120. Molecular representation of cyclopropane dumbbell.

The direct observation of the molecule onto gold surface has been demonstrated using this technique where spherical C_{60} cages act as two beacons. This is very important during the measurements because we are certain to measure unambiguously one molecule. The concepts of rigidness, symmetry and linearity have to be kept into account together, above all when the molecule is expected to occupy the nanogap between the two metal electron reservoirs, either in STM or MCBJ experiments. This methodology differs from the main STM based techniques in which the STM tip is blindly fishing molecules over metal surface. Hence, unambiguously analysing one molecule removes uncertainty from the overall measurements about the conductance spread of individual molecule. Drop casting technique has been used to prepare the sample, depositing the molecules from a dilute solution in 1,2,4-trichlorobenzene (TCB) on the surface of the gold (previously annealed with gas flame). The concentration of the solutions used was 10^{-10} M. Such condition is used in order to i) avoid the formation of molecular clusters onto gold surface and ii) to identify only one molecule for the unimolecular conductance measurements. The sample is then mounted in the STM-microscope. After approaching the tip (increasing the bias voltage between the tip and the surface), we begin imaging the surface. Once the images are of high quality (*i.e.* recognizable features such as steps, herringbone reconstruction and molecules can be easily distinguished) and the drift experiments of the tip are

[209] K. Gillemot, C. Evangeli, E. Leary, A. La Rosa, M. T. González, S. Filippone, I. Grace, G. Rubio-Bollinger, J. Ferrer, N. Martín, C. J. Lambert, N. Agraït, *Small* **2013**, DOI:10.1002/smll.201300310.

well set, we proceed with the measurements. For instance, the drift of the tip shows a high stability with only 0.4 $Ås^{-1}$ of drift along the surface as it is possible to see in Figure 121.

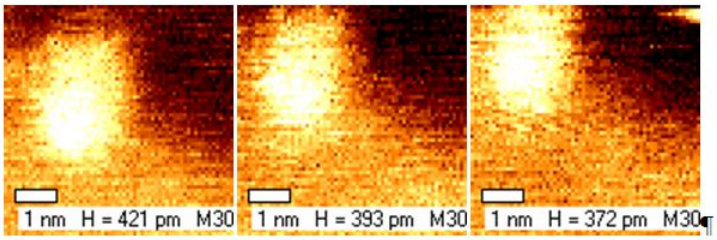

Figure 121. Sequence of images recorded over a period of 22 s before lifting the molecule. The time of each image is 3.7 s. Using the position of the centre of the circular feature we obtain a rate of drift of 0.4 $Ås^{-1}$.

Thanks to the easy visualization of C_{60} onto the surface, molecules could be found at step and terrace sites (preferred site), but those located at steps were generally found to be more stable under scanning. The molecule studied here was close to a step, but appeared not to be sitting directly in the step. The presence of co-adsorbed molecules, such as the TCB solvent and atmospheric particles, may aid the low diffusion of the molecules across the surface. It has been demonstrated that the dumbbell molecule deposited over gold surface is stable during the approaching and retracting movement of the tip. Figure 122 shows an STM image of diluted solution of compound **23b**.

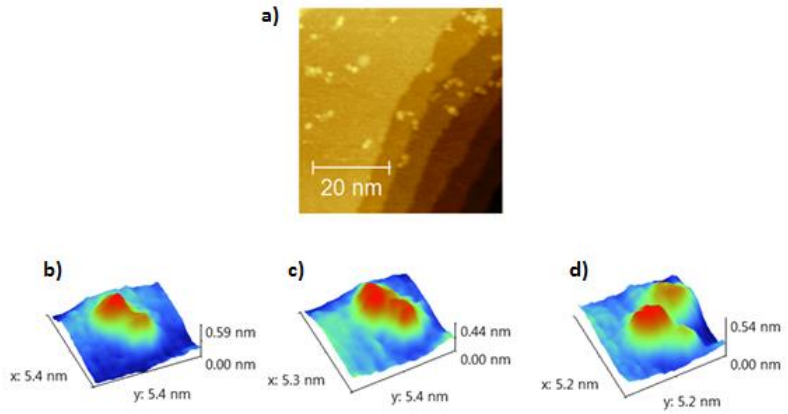

Figure 122. a) An image of a typical area after exposure to a 10^{-10} M 1,2,4-trichlorobenzene solution for 2 minutes; b) and c) Images taken between approach/retraction cycles to wire the molecule; between b) and c) the molecule maintains its position, whilst in d) it has been rotated slightly.

fits with the centre-to-centre distances found imaging the molecule, despite the impossibility to distinguish between molecular different conformations. Before wiring the molecule, the cleanliness of the tip has been checked in a molecule-free area of the sample by gently approaching the tip until slight contact with the surface was made. No evidence of conductance plateau implies that the molecule is not wired. Once observed that the tip and gold surface are clean, we proceed with the conductance experiments. They clearly show two different plateaus of conductance along with the presence of some atmospheric particles or solvent, called "adsorbates", which may affect the conductance value of dumbbell molecular junction. To elucidate these phenomena, we distinguish two types of experiments: i) the molecule is layered onto the surface and the gold tip is approaching and retracting continuously; ii) the molecule is hanged to the tip and it is approaching and retracting towards and from the flat gold surface.

The conductance traces, shown in Figure 123, resume the experiments performed. To well understand these experiments, such data are divided in different regions of conductance. Starting from the low conductance value, it has suddenly been observed a tunnelling regime between 10^{-5} G_0 and 10^{-3} G_0 which represents the movement of the tip, getting closer or farer to the C_{60} molecule, without touching the molecule.

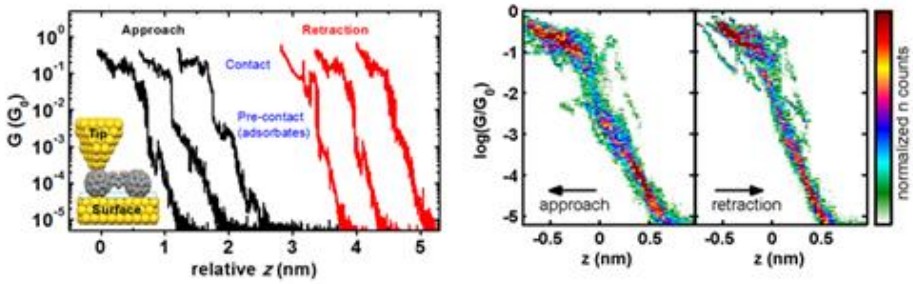

Figure 123. Individual (on the left) and 2D conductance traces (on the right) for the approach and retraction tip movement onto one C_{60} of compound **23b** with the presence of adsorbates (in blue) and the normalized counts on the right side.

The slope of such tunnelling regime differs from the typical barrier measured over C_{60} in vacuum (about 4 eV) and it is identical to the barrier found in the absence of molecule (about 1 eV). This is the first data which suggests the presence of the adsorbates.

Getting closer the tip to the C_{60}, between 10^{-3} G_0 and 10^{-2} G_0, the traces begin to fluctuate and the slope to reduce. This behaviour is again in contrast with the analysis over pristine C_{60}. This is a further demonstration of the presence of the adsorbates situated onto the tip (in Figure 123, the adsorbates onto the tip have been omitted in order to show the tip contact with C_{60}). Pressing more the tip onto the molecule, the adsorbates on the tip are displaced and, finally, the Au/C_{60}/Au junction is achieved with the consequent jump in conductance. This conductance value is attributed to the electron transport along one C_{60} molecule and the increment of such plateau is related to the area of contact between gold electrode and C_{60}.[210] This aspect, combined with the lack of a plateau below 10^{-1} G_0 in the retraction traces, indicates that the molecule probably does not lift into the vertically-wired configuration during these types of experiments. Second type of experiment (illustrated in Figure 124) consists in hanging the molecule to the tip and gently approached it to the surface.

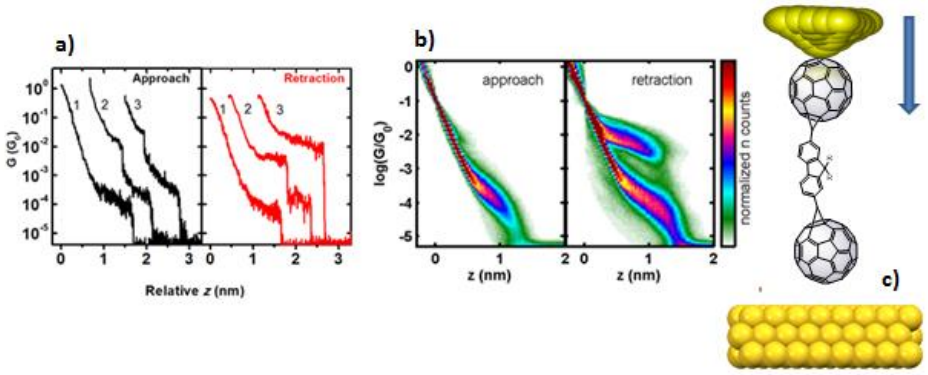

Figure 124. Individual a) and 2D conductance traces b) for the approach and retraction dumbbell-tip system, forming and breaking the molecular junction for 3700 counts; c) schematic picture of the approaching tip-molecule system.

[210] G. Schull, T. Frederiksen, A. Arnau, D. Sanchez-Portal, R. Berndt, *Nat. Nanotechnol.* **2011**, *6*, 23.

Figure 124 represents the individual and the 2D conductance traces as an attempt to the statistical formation of molecular junction. For a better comprehension of this experiment, the tip, hanging the dumbbell molecule, is only approached to the surface: a signal at 10^{-4} G_0 is recorded and it is ascribed to the molecular junction formation (low conductance state which happens in 95 % of the approach traces). The slope of such plateau rises slowly reaching, in some traces, values close to 10^{-3} G_0. For 81 % of the total approaches a tunnelling process is observed after this value of conductance (trace 1 in Figure 124 approaching mode), even if for other traces another plateau is observed at about 10^{-2} G_0, defined as high conductance state of dumbbell molecule (curve 2 and 3 in Figure 124 during the approaching experiments and happens in only 14% of the approaching traces). Whenever the high-conductance state was present in the approach, the same plateau is observed in the retraction experiment. At the end of these plateaus, the conductance drops sharply, either directly to the noise (curve 3 in Figure 124 in a retraction approach), or, as in the majority of cases, to a lower region of conductance similar to that observed on initial contact in the approach (curve 2, Figure 124 in the retraction approach). To summarize, in 2D approaching traces the high conductance value is not so evident as in the case of retraction 2D traces. Usually, the conductance trace shows some conductance fluctuations. They can be ascribed to different phenomena, *i.e.* mechanical fluctuations of the tip, atomic rearrangements in the contact, small rearrangements of the C_{60} already described in the case of pristine C_{60},[211] or configuration changes of the molecule within the junction (*e.g.*, from *cis* to *trans* configuration).

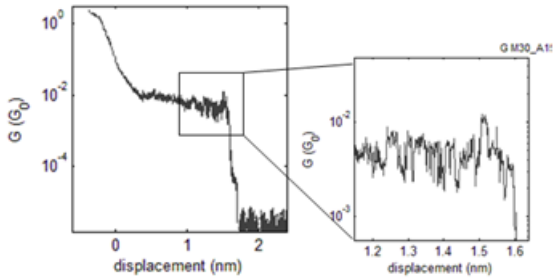

Figure 125. Conductance fluctuations of the observed plateau.

[211] N. Neel, J. Kroeger, R. Berndt, *Nano Lett.* **2011**, *11*, 3593; b) A. V. Danilov, P. Hedegard, D. S. Golubev, T. Bjornholm, S. E. Kubatkin, *Nano Lett.* **2008**, *8*, 2393.

4.6.1 STM single molecule comparison between molecules 10b and 23b

As mentioned in a previous chapter and, to corroborate the conclusions discussed for the UV-vis and CV analysis over the influence of the linker in the whole molecule, the comparison of conductance experiments has been carried out using STM technique for molecules **10b** and **23b**. At the beginning, the general method for lifting one molecule using the static tip approach has been used. Once a particular molecule has been isolated and pictured, smaller images are taken to increase the precision of positioning the tip (a.b and e in Figure 126). Once the molecule occupies the most part of the selected surface area, the tip is placed above one C_{60} molecule at a distance of approximately 0.6-0.8 nm.

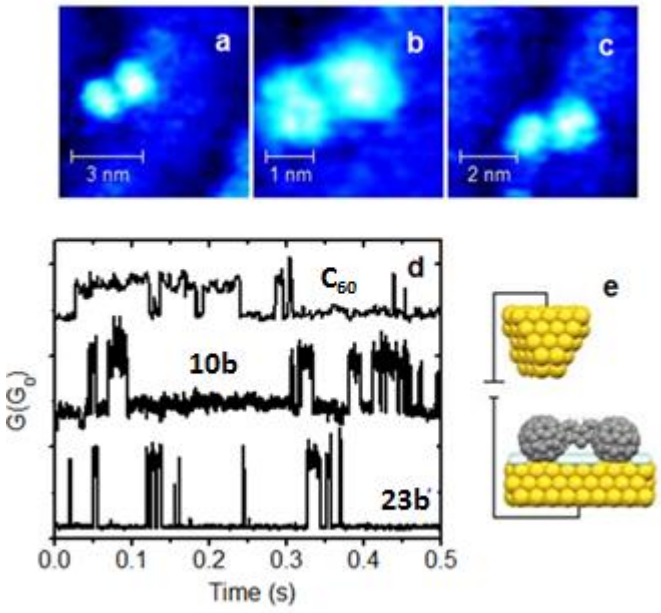

Figure 126. a) Image of **10b** located on step edge; b) a zoom-in over the same molecule; c) another image of the same molecule after one experiment; d) examples of conductance traces for **C_{60}**, **10b** and **23b**; e) schematic representation of the tip positioned over one C_{60} beacon without touching it; the adsorbates are shown as blue over the surface but not over the tip for clarity.

At this point the conductance *versus* time has been recorded for both molecules in separated experiments. Figure 126 shows the conductance traces comparison between **C_{60}**, **10b** and **23b**. There is no significant difference in the dumbbells behaviour as molecular wire in clear contrast with C_{60}, where the differences are well distinguishable. The lack of the difference in conductance traces lead us to use another approach. The next approach is to put in direct contact the tip with one C_{60} beacon, creating the contact. Both molecules have been investigated under these conditions. Molecule **10b** has been snapped before and after the experiments.

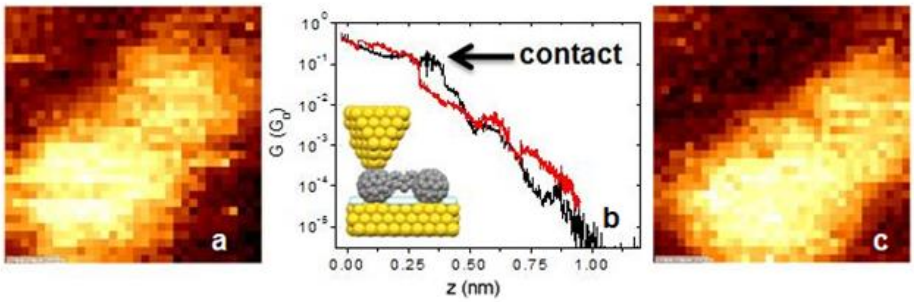

Figure 127. a) Image of molecule **10b** before the experiment; b) approaching (red line) and retracting (black line) methods; c) picture of the molecule after the measurement.

The approach trace displays an exponential increase in conductance until approximately 10^{-2} G_0 with a slope next to 1 eV. Slightly above this conductance value, there is a jump followed by a change of slope, which is indicative of the contact formation with the molecule. Upon retraction, the trace is very similar to the approach in the region above 10^{-2} G_0, indicating the stability of the molecule (in particular for C_{60}) due to tip contact formation. Below this region the conductance decays exponentially in a similar manner to the approach method (see Figure 127). The surface imaging re-examination reveals the stability of the molecule.

Molecule **23b** has been treated in the same manner and a similar behaviour has been recorded (Figure 128).

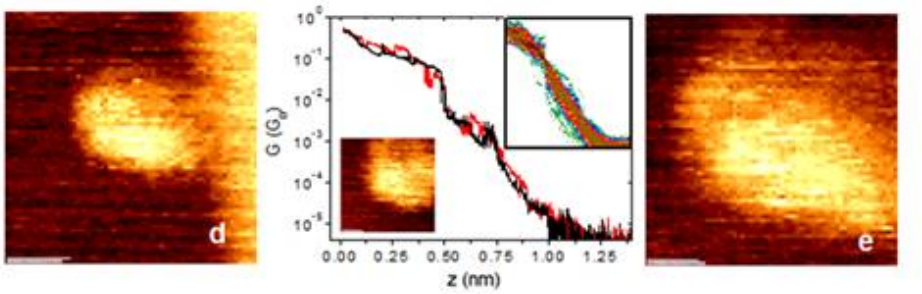

Figure 128. d) Image of an isolated molecule **23b**, showing its adsorption at a step edge; e) zoomed image directly before tip contact. The figure in the middle shows the conductance trace for molecule **23b**. The upper inset shows the 2D histogram constructed from all 134 traces recorded. The lower inset shows the image of the molecule after the experiments.

Even though the conductance behaviour is very similar for both molecule, it is reasonable to affirm that the conductance trace for molecule **23b** is more homogenous during the approaching/retraction cycle, when compared with that of **10b**. Although a value of 5×10^{-2} G_0 has been achieved for this molecule, no definitive conclusions about the linker activity on the improvement of the electrical conductivity can be figured out by this experiments. Despite this, some deductions have also been carried out. A first chance is that the molecules remain on the surface during all the cycles, without lifting them. The second possibility is that they are lifted, but the current flowing through the molecules is below the noise level. The last possibility is that the molecules are lifted, but the molecular junction breaks too soon and, no evidence of clear conductance value has been achieved. Moreover, a direct correlation between the calculated C_{60}-C_{60} distance and the found experimental distance are consistent with the value of 1.6-1.7 nm.

4.6.2 DFT calculations over cyclopropane dumbbell molecule (23b)

For a better understanding of the mechanism for the molecular wire behaviour of cyclopropane dumbbell molecule, DFT calculations have been performed and the data compared with the experimental results. In particular, DFT calculations can explain, at first glance, what is the molecular dynamics during the experiments in approaching and retracting modes. A theoretic calculation has been realized imaging the molecule hanged to the tip. The figure below clarifies what conductance trace corresponds to the molecular wire configuration.

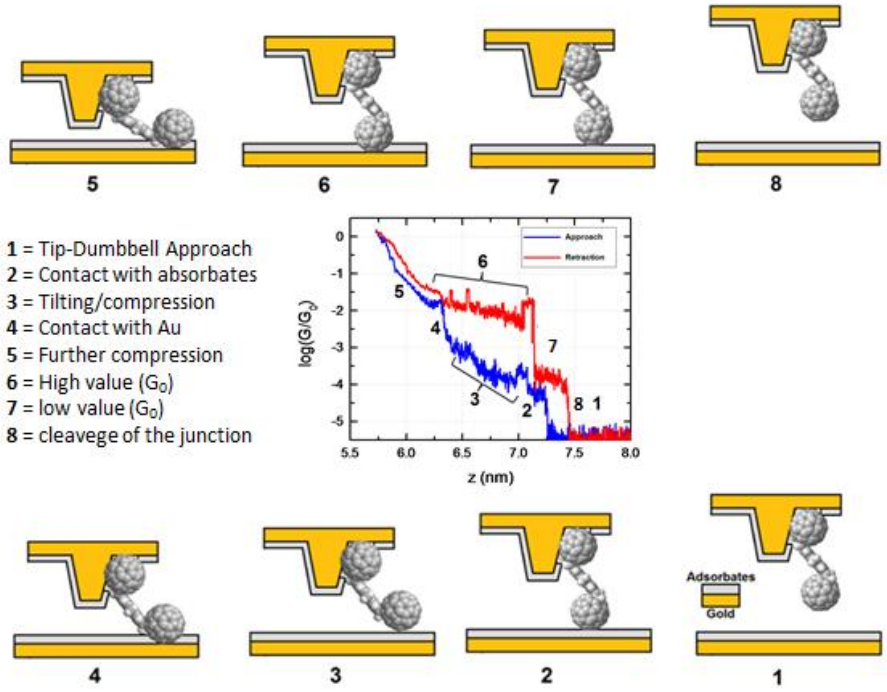

Figure 129. DFT explanation of conductance traces. Each trace and each plateau is referred to the possible molecular configuration within the junction. In blue the approach method; in red the retraction method.

The nature of the higher and the lower conductance value has been explained thanks to DFT calculations. To do that, theoreticians analysed the case in which the molecule is layered onto gold surface with the fluorene plane parallel

to the gold flat surface. With this configuration of molecule bridging the metal leads, at 0 degree of tilted angle (molecule parallel to the surface), the conductance value is similar to that found experimentally for only one C_{60}. The value of 10^{-2} G_0 is still not demonstrated and the experimental value between 10^{-3} and 10^{-4} G_0 is not supported by the theoretical data which give a constant value of 10^{-5} G_0. This could be consistent with the fact that DFT does not always predict correctly the HOMO-LUMO molecular level[212] with mismatches between experimental an theoretical point of view.

A plausible explanation of the experimental peak at 10^{-2} G_0 is given by a molecular configuration in which the tip is touching the fluorene core. In this way, the electron transfer occurs through one C_{60} and fluorene. The molecular junction model has been created with the tip attached to the fluorene under a tilt angle of 30 degrees with respect to the surface. A theoretic value of 10^{-2} G_0 has been found and it corresponds to this geometry with gold-gold separation of 2.2 nm.

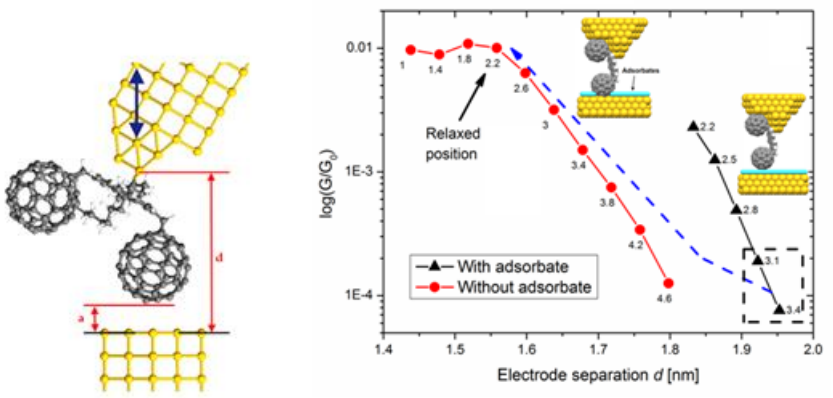

Figure 130. Molecular wire representation with the tip over fluorene and a tilt angle of 30 degrees from gold surface. The conductance traces have been calculated towards the electrode separation distance with or without the adsorbates. The blue arrow indicates in nm the pathway for the removal of adsorbates while approaching the molecule to the surface. The number close to the curves are related to the distance (a in the left figure) between the lower C_{60} to the Au surface or adsorbates.

[212] C. Toher, A. Filippetti, S. Sanvito, K. Burke, *Phys. Rev. Lett.* **2005**, *95*, 146402.

All the calculations have been done over the *cis* configuration of cyclopropane dumbbell molecule. By DFT calculation, 8 eV (184 Kcal mol^{-1}) of barrier energy between *cis* and *trans* configuration demonstrated the no spontaneous switching between them when wiring the junction. Moreover, no relevant changes have been observed in the transmission curves which theoretically indicates the HOMO-LUMO molecular level in the junction compared with the E_F of gold (dashed line in the figure below). Despite this, a slight difference in LUMO energy value is envisaged in the *cis* configuration with respect to *trans* configuration (see the red curve and green curve at E_F in the figure below). This results in a better stabilization of the LUMO for the *cis* configuration which may give rise to a better electronic communication between the two electroactive components of the dumbbell molecular wire.

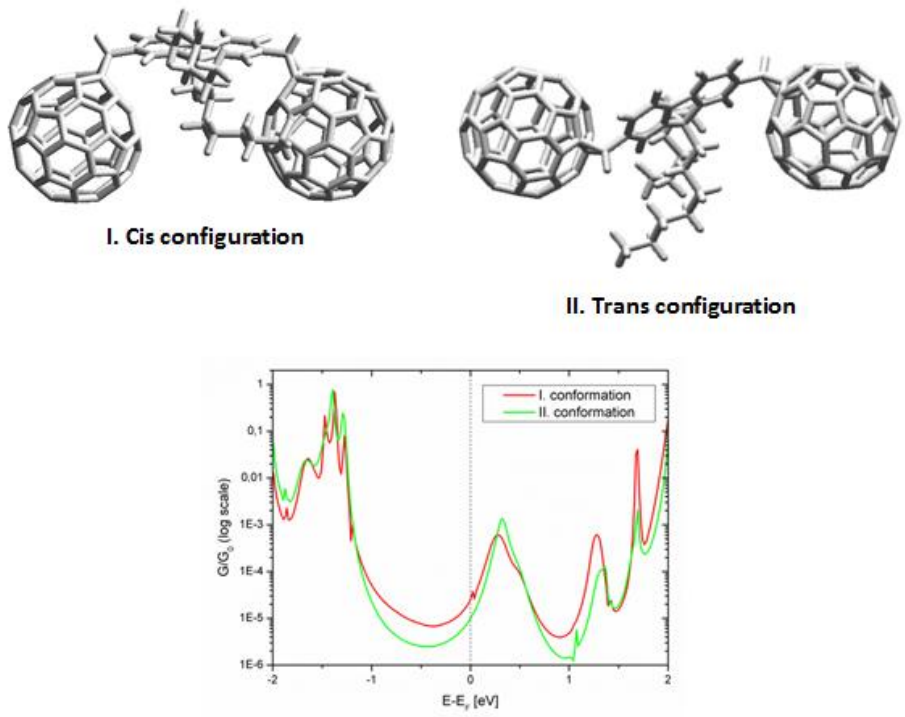

Figure 131. Transmission curves of cyclopropane dumbbell **23b** (*cis* and *trans* configurations) where HOMO and LUMO energy levels are referred to the E_F level for both configurations.

4.6.3 DFT calculations for molecules 10b and 23b

To gain more insight into the electronic structure of compounds **10b** and **23b**, large-scale density functional theory calculations combined with Green's function based transport calculations have been performed by Colin Lambert at Lancaster University. In this model, the molecules have been fitted between (111) oriented flat gold electrodes and the electronic transport properties of the system has been obtained by SMEAGOL code (*ab-initio* electronic transport code) where the current has been extracted by the Landauer formula reported thereafter in a simplified manner.

$$G = (2\,e^2/h)T(E_F)$$

Equation 7. Simplified Landauer Formula for the calculation of conductance value G.

For both compounds two isomers (*cis* and *trans*) have been considered. The figure below shows the transmission coefficient T(E) for electron energy E for both molecules in the two configurations and for pristine C_{60}.

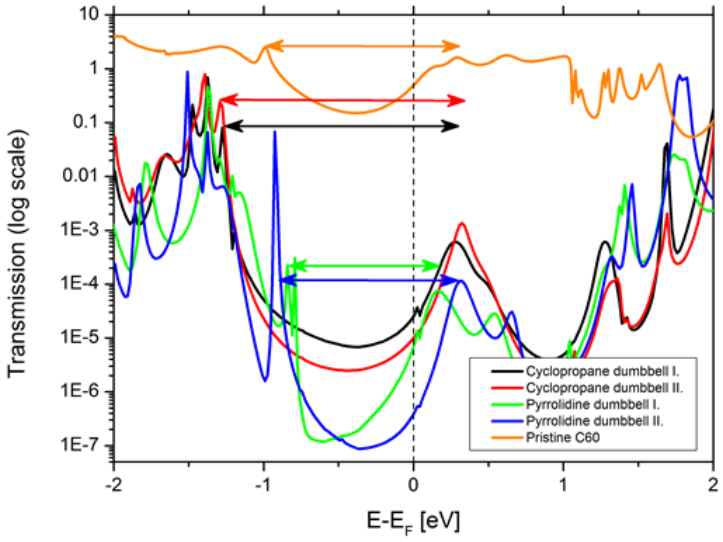

Figure 132. Transmission *vs* energy for both isomers of dumbbell molecules and for pristine C_{60}. The balck dashed line indicates the Fermi energy level.

In agreement with the notation made before, configuration I is referred to the *cis*-isomer of the molecules while configuration II is referred to the *trans*-isomer. Both molecules conduct through their LUMO level, but it is predicted that the conductance behaviour should satisfy the order C_{60} >> cyclopropane

dumbbell > pyrrolidine dumbbell, agreeing with the predicted enhanced electronic communication shown by cyclic voltammetry experiments (see chapter 4.2.2). Unfortunately, the DFT calculations usually underpredicts the gap, so it is safe to assume, that either the difference between the conductance of compound **10b** and **23b** is around 0.5 G_0 or larger. It is noteworthy as at Fermi energy level the best dumbbell in terms of conductance is the cyclopropane in *cis* configuration while its *trans* configuration is equal to the *cis* configuration of pyrrolidine dumbbell. The *trans* pyrrolidine dumbbell isomer seems to be the worst.

The LUMO peak orbital does not show a large different if we switch from one isomer to the other (during the experiment we can assume that an average of two isomers is present), however there are large difference near the HOMO. The difference in LUMO energy is observed when passing from one dumbbell to the other maintaining the same configuration at least in the *cis* configuration while the *trans* does not show remarkable differences. In a certain way, we can compare the CV data with theoretical LUMO energies of the molecule inside the junction taking into account only the charge transfer from the metal lead to onto the molecule. Although the electrodes change from theory to CV experiments (Au *vs* Ag), we expect that such difference only results in different amount of charge transferred for the two metals and not for the molecules sandwiched between them.

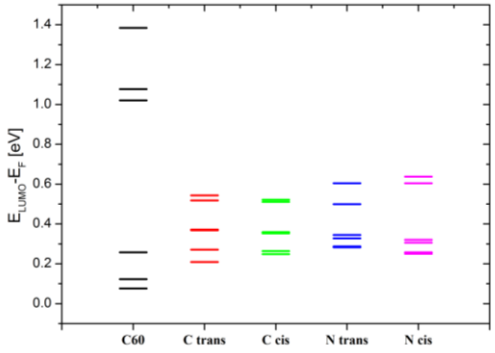

Figure 133. The first six levels for all molecules. "**C**" stands for cyclopropane dumbbell and "**N**" stands for pyrrolidine dumbbell.

Comparing the calculated energy differences between the Fermi and LUMO levels with CV measurements, we can observe the same trend between pristine C_{60} and the dumbbells. The ordering of the LUMO levels between the two isomers of dumbbells also follows that of the CV measurements above all for the *trans* configuration, while the difference is less dominant for the *cis* case. As conclusion we can affirm with certain confidence that the reduction potentials found in CV experiments follow the predicted electron affinities for these molecules. These combined results clearly indicate that electronic conductivity is more efficient in the cyclopropane molecule than in pyrrolidine dumbbell.

4.7 STM and MCBJ experiments of pyrrolidine dumbbell

STM and MCBJ are suitable setups for the conductance experiments and their comparisons. Herein, the behaviour of a fluorene-containing dumbbell-type molecular wire, in which each C_{60} cage is covalently connected to the central fluorene unit through a sp^3 carbon atom of the fused pyrrolidine ring, is studied. This connection has been already studied in terms of STM experiments for the dumbbell-type molecular wire with two fluorene units under ambient conditions.

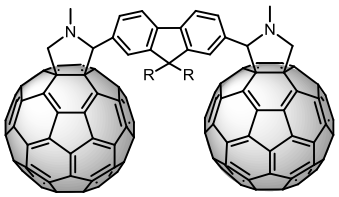

10a $R = C_6H_{13}$

Figure 134. Pyrrolidine dumbbell molecule under studying via STM and MCBJ techniques.

Herein the experiments are shown through, first STM and, then MCBJ. During my secondment in the University of Bern under the supervision of Prof. Thomas Wandlowski, we carried out several experiments at the same time which were directed to the imagining of molecule onto gold surface through STM and to the conductance experiments through MCBJ. Before doing conductance experiments with STM setup, we needed to find the exact work conditions for the characterization of the molecule onto surface. To achieve it, we performed several experiments where the work conditions were continuously changed. For giving some examples, we changed the deposition techniques of the solution, its concentration, the solvent used for solubilizing the molecule, the gold crystal employed, the metal tip (tungsten is better of gold for the imaging but not for the conductance experiments because it is mechanically stable and chemically inert in acid solution which is electrochemically used for the formation of the tip), the sharpness of the tip (better resolution are obtained with sharpest tips). The sharpness of the tip is given by the exfoliation of metal atom layers through electrochemistry: a solution of concentrated HCl in ethanol (50:50 in v/v) is employed in an electrochemical cell equipped with a anode (+) made by graphite and cathode (-) represented by the metal tip (Au, W, or Pt/Ir:70/30). When the bias is

applied, the electrochemical current slope down. This phenomenon is due to the exfoliation process of tip metal surface. Indeed, the current is proportional to the surface. The shape of the tip experimentally formed is checked under an optical microscope. Once formed the tip, we proceeded to the cleanliness of the drop crystal (shown in the figure below) and its immersion into a 1 nM solution of our molecule in mesitylene (1,3,5-trimethylbenzene).

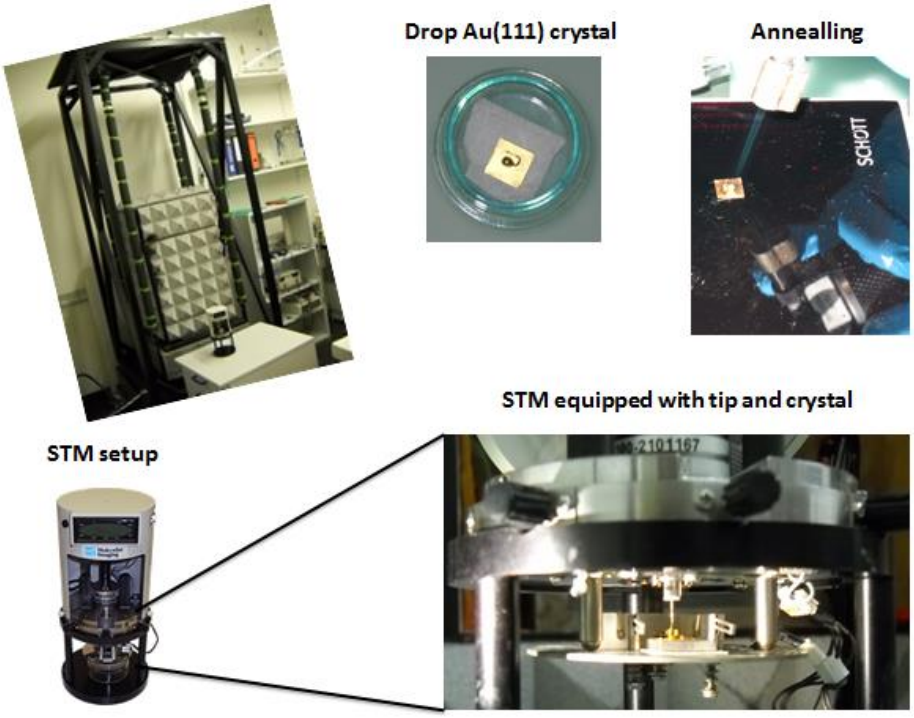

Figure 135. The top-right part of the figure shows the drop gold crystal used in our experiments and the annealing process. The top-left part of the figure shows the anti-vibrational cage for the STM setup which is visible to the bottom of the figure. The zoom shows the metallic plate in which we put the drop crystal. The gold tip is shown in the middle of the figure just above the drop gold crystal.

Several imaging experiments have been recorded in order to keep conclusions over the stability of dumbbell molecule onto surface and its organization on it. Interesting conclusions about the stability of such dumbbell are figured out. For instance, the molecule results stable even after drift experiments which demonstrate the strong interaction between the C_{60} and the gold surface. Furthermore, at this value of concentration (1nM) a cluster of three molecules has been observed. The C_{60} cages appear clearly once we got closer the cluster and the relative distance from one C_{60} to the other is more or less consistent with the calculated distance from centre to centre of each C_{60} buckyball.

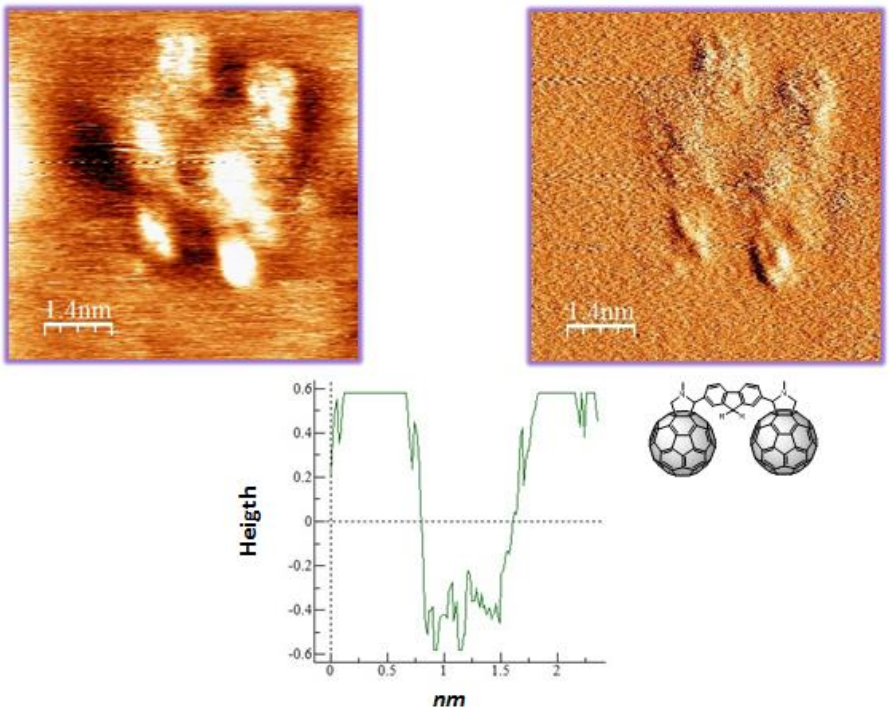

Figure 136. STM images in current view (on the left) and topography view (on the right) of the cluster formed by three molecules of C_{60} dumbbell **10a**. The height profile shows the relative height of the two C_{60} separated by the fluorene moiety. It seems that fluorene is also layered over gold surface.

The preliminary conductance experiments of molecule **10a** have been carried out with MCBJ measurements. The original idea is to find differences in terms of G_0 between our system and a similar molecule, already published, in which the fluorene moiety is connected to the C_{60} spheres through the N atoms of the fused pyrrolidine.[213]

We dropcasted, for five times (50 μL per time), 0.1 mM solution of **10a** dissolved in toluene over a metallic plate equipped with gold wire fixed over it with epoxy glue. The wire was previously cut manually using an optical microscope to reduce the wire diameter from 100 nm to about 10 nm. The plate was heated at 60 °C for 10 minutes. 150 μL of solution was poured at room temperature on it and 50 μL of *n*-decane has been added to protect the system by the adsorbates. The MCBJ cell was thus mounted over the MCBJ setup and argon flow was passed on it to protect the whole system.

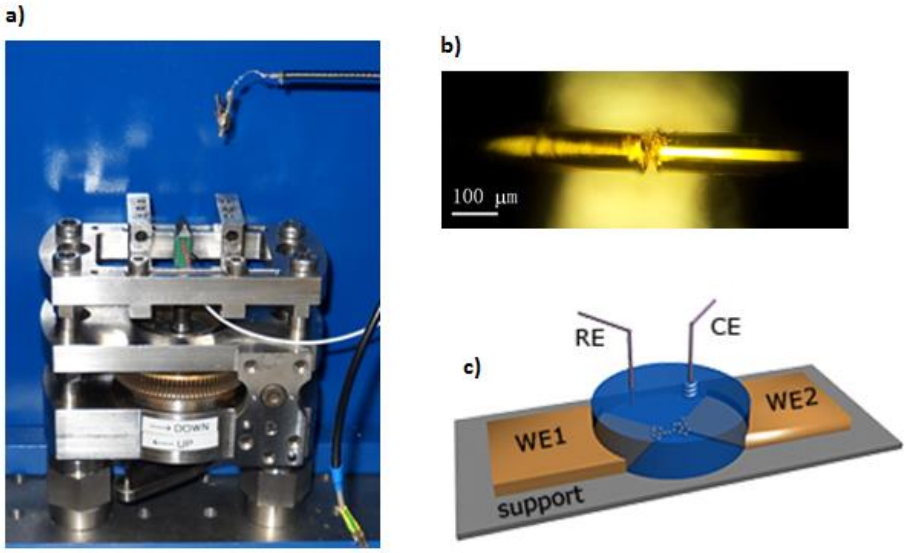

Figure 137. a) MCBJ setup used in our experiments; b) gold wire notched to reduce the diameter of metallic junction and c) image of typical liquid MCBJ cell with molecular junction formation.

[213] J. Fock, J. K. Sorensen, E. Lortscher, T. Vosch, C. A. Martin, H. Riel, K. Kilsa, T. Bjørnholm and H. van der Zant, *Phys. Chem. Chem. Phys.*, **2011**, *13*, 14325.

As first step, neat solvent has been analysed as first example and no evidence of any molecular junction formation has been observed (Figure 138). When the solution was used for the experiment, we recorded 10700 traces (opening and closing the metal contacts) and no evidence of clear conductance plateau has

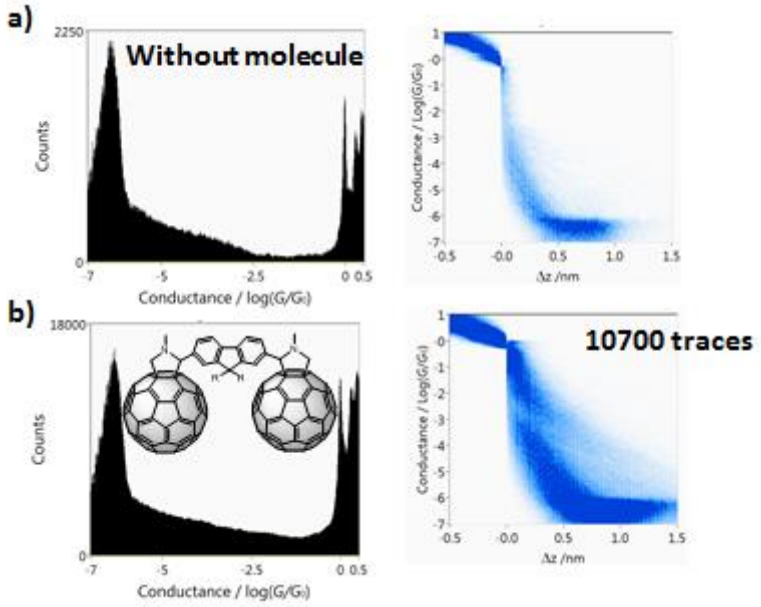

Figure 138. a) neat solvent MCBJ traces, only the gold-gold junction is observed; b) 10700 conductance traces of our molecule solution which does not show any significant plateau.

been envisaged. However, using the same experiment, we removed from the traces those related to the tunnelling processes. Doing that, we obtained preliminary results about the behaviour of this dumbbell molecule within the junction which are shown in Figure 139. The experiments clearly show two conductance peaks at -2.5 and -5 (log G/G_0) after the removal of tunnelling traces in a set of 10700 experiments in which we are continuously forming and breaking the metal junction. The duration of the experiment is around 20 minutes.

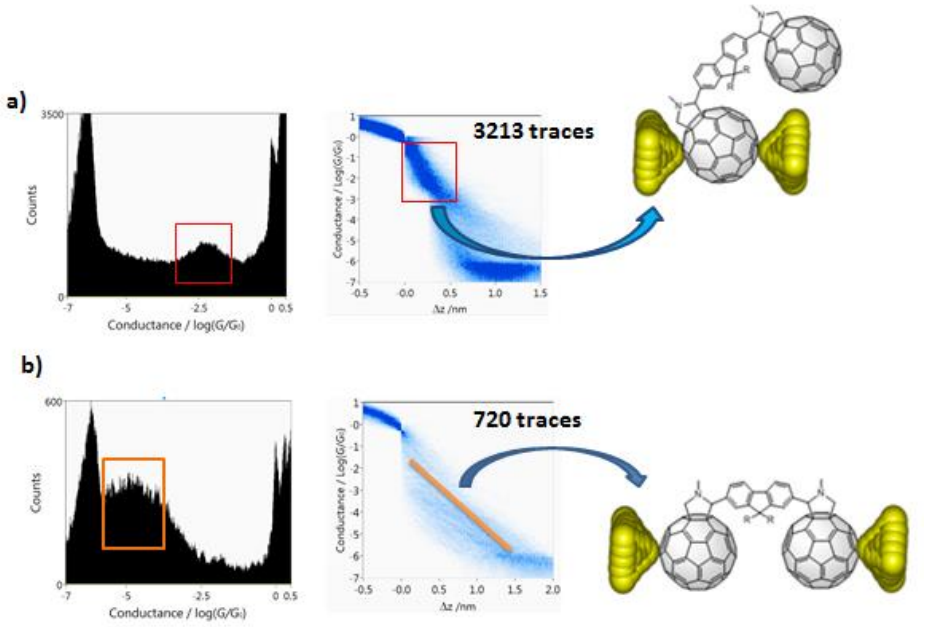

Figure 139. a) 3213 traces showing the higher conductance peak at -2.5 G_0 (squared in red) with its feasible configuration within the junction; b) 720 conductance traces showing the lower value at which, we ascribed the molecular configuration shown on the right. The length of such plateau is similar to the molecular length.

In only 3213 conductance traces, we can denote a peak at -2.5 G_0 ($logG/G_0$) which, as first hypothesis, could be represented by the spatial configuration in which the metal leads are exclusively touching one C_{60} moiety of the dumbbell. Less than the case of before and, to be precise in only 720 conductance traces, we observed a broad and more intense peak at -5 G_0 ($logG/G_0$) which could be ascribed to the situation in which dumbbell molecule is wiring the source-drain contacts. Probably, the broadness of this peak is caused by the molecular rearrangements of the molecule within the junction, the free motion of the molecule along the contact surface at room temperature or by the multiple molecular contacts due to the high concentrated solution (0.1 mM) which is, on the other hand, typical for MCBJ experiments. For sure, it is not due to the adsorbates.

Another study, we started with the same molecule at a higher concentration in STM setup, is referred to the capability of this molecule to be packed in perfect supramolecular organizations.

Its self-assembly capability has been envisaged in STM experiments. Preliminary STM images show the formation of well-organized layers in which the contact between the C_{60} units is evident.

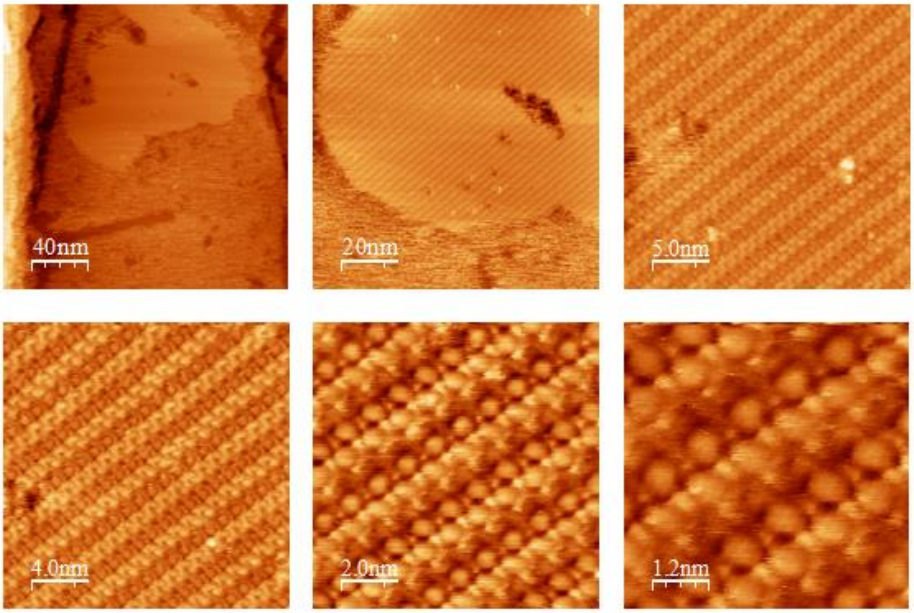

Figure 140. STM images of concentrated solution of **10a** in toluene. The zooming over the island shows a certain surface organization to be studied more deeply.

The experiment has been carried out with a solution of compound **10a** toluene and dropcasted in a STM cell equipped with crystal (111) gold drop. To prevent the formation of the adsorbates, the whole system has been protected by *n*-decane (solvent in which the molecule is not soluble). The gold drop has been previously washed, annealed and passed under argon flow for 5 minutes. The horizontal movement of the tip allows us to find a flat crystal region which will be the good substrate to be analysed. Getting closer (vertically) with the tip, it has been possible to see how the molecule is going to organize over gold surface in an ordered manner. The distance between two buckyballs are consistent with the calculated molecular length of about 1.7 Å. At first glance, it seems that one C_{60} of one dumbbell interacts, in a supramolecular manner, with other two C_{60} of another dumbbell molecules, situating itself in the middle of them. Another hypothesis could be done if we consider an effect of the alkyl chains which, in some way, organize the supramolecular architecture. This can be seen in the last figure of STM images where the scale range is 1.2 nm.

As already written, these are preliminary results and more efforts must to be done in this regard.

4.8 Imaging another dumbbell molecule in liquid-STM setup

Molecule **16** has been kept as model for further liquid-STM analysis regarding not only the imaging onto gold surface with its stability but, also its motion property and, far away, its conductance property, using MCBJ too. This preliminary work has been started during my secondment in IBM Laboratories of Zurich, where we decided to use the extended bridge dumbbell molecule with pyrrolidine as linker, for better affordable synthetic reasons. The molecule has been deposited by dropcasting and protected by a layer of *n*-decane to avoid any kind of adsorbates adsorption except the solvent employed to do the solution (toluene). Again, thanks to the easy visualization of the C_{60}, the formation of cluster has been envisaged (in the middle of STM image) but also the identification of single molecule has been captured.

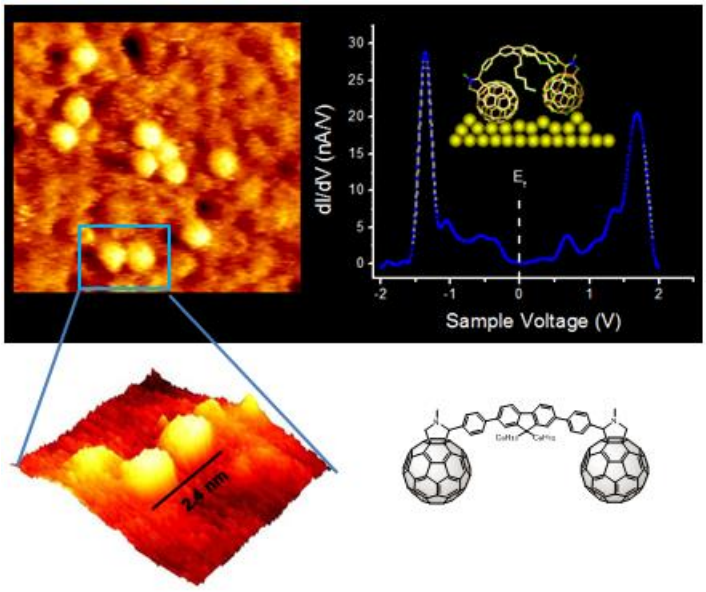

Figure 141. Image of molecule **16** with liquid-STM setup. The orbital levels, found experimentally, are shown in the right-up part of the figure and are compared to the E_F.

The experimental length between two C_{60} hills is comparable to that calculated for this molecule. Thanks to the presence of an elongated bridge, the C_{60} are spatially well separated and their final image results more defined. The graph to the right represents the experimental value of LUMO and HOMO with respect to the Fermi energy level, when the molecule is layered over gold surface through C_{60} as anchor groups. These are preliminary results and more efforts have to be done in this regard.

4.9 Photoinduced electron transfer for BDF dumbbell molecules

Photoinduced electron transfer experiments have been carried out to study the properties of the excited states over BDF cores under oxidative conditions mediated by peroxide and on N-methylfulleropyrrolidine as reference. Moreover, the dumbbell molecules have been analysed using the femtosecond transient absorption spectroscopy for a comparison with the pristine core and the C_{60} derivative. After the excitation of molecules **44** and **45** at 387 nm with a laser pulse of 150 femtoseconds, the singlet excited state feature appears immediately. The singlet excited state thus formed, decays to the triplet excited state with different lifetime depending on the nature of the BDF core but in strict agreement with the fluorescence lifetime (6.1 ns for **44** and 7.2 ns for **45**). N-methylfulleropyrrolidine has also been excited at 387 nm with the same exposure time. It generates the singlet excited state (~ 900 nm), which passes to triplet excited state (~ 700 nm) after an intersystem crossing process. The lifetime of the excited state of such C_{60} derivative is of 1.4 ns. Keeping in mind the excited features of both electroactive molecular components, the dumbbell molecules have been thus treated in the same manner with two excitation wavelengths, namely to 387 and 470 nm. At first glance, there is a difference in the deactivation of singlet excited states; for molecules **44**, **45** and C_{60} derivative, it occurs via intersystem crossing to generate triplet excited state (T_3). As concern the dumbbell molecules **42**, **43** and **46**, the deactivation of singlet excited state occurs through a charge transfer (CT) process from the donor to the acceptor units, thus forming the radical cation over the BDF core and the radical anion over C_{60} moieties (two new absorption bands at 500 nm and 1000 nm, respectively).

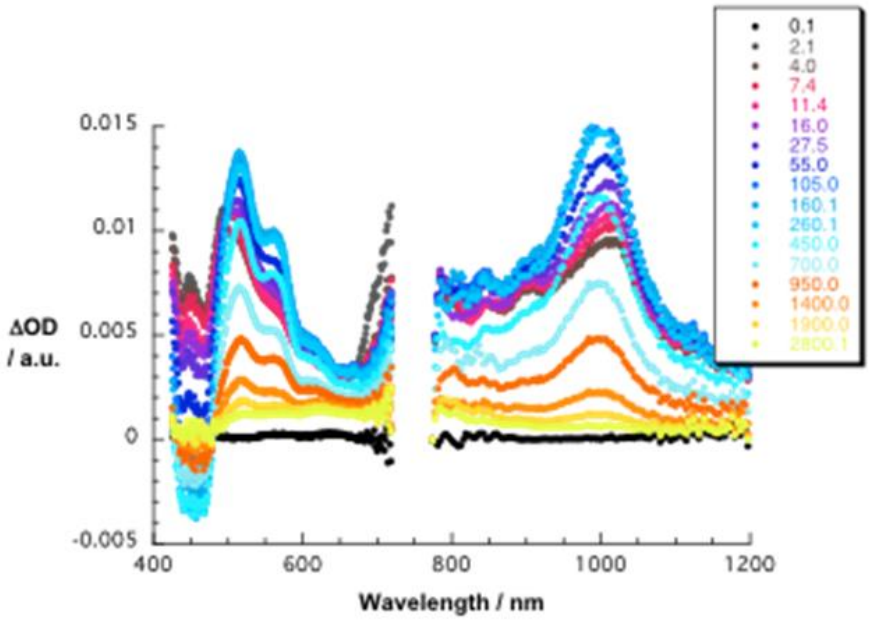

Figure 142. Differential absorption spectra obtained upon femtosecond flash photolysis of molecule **42** in *o*-DCB under argon and at room temperature. The inset shows the time delays from 0 to 2800 ps.

The charge separated state, experimentally formed, is metastable and dies in a recovery of the ground state or the triplet excited state of C_{60}, depending upon the solvent employed. Studies of charge separation and charge recombination processes have been done onto these systems and a strictly dependence of the solvent polarity has been envisaged. In particular, the enhancement of solvent polarity is reflected in an acceleration of both processes. Indeed, the lifetimes of the three dumbbells **42**, **43** and **46** in solution of anisole are in the order of ps (618, 356 and 170, respectively). These data are consistent with the charge separation process constants calculated in the same solvent (49.7, 25.3 and 6.9 ps, respectively). The same trend has been observed for the charge recombination process (CR). As described above, is going to a more polar solvent like *o*-DCB, the lifetime and the charge separation constant values descrease significantly: *i.e.*, for the dumbbell **42**, the lifetime is 414 ps and the k_{CS} is 30.5 ps. In contrast, in a less polar solvent like toluene, the lifetime and the charge separation process become slower (1539 ps for the molecule **42**).

4.10 DFT transmission theoretical calculation for molecules 10b, 23b, 25

Preliminary hypothesis over the role of the linker in dumbbell molecules bridging two metal electrodes allows us to understand which is the correct functionalization to be used between C_{60} and the π-conjugated bridge in order to have better values of conductance. Nevertheless, no many steps have been done in this regard, herein we want to suggest the conclusion we carried out over our systems based essentially over two C_{60} spheres, the same fluorene bridge but a different linker. For this reason, molecules **10b, 23b, 25**, having different sp^3 carbon atoms between the C_{60} and the unit core, have been theoretically compared. First, pyrrolidine linker has been replaced by cyclopropane ring and, then, by a single bond where the only carbon sp^3 belongs to the C_{60} cage.

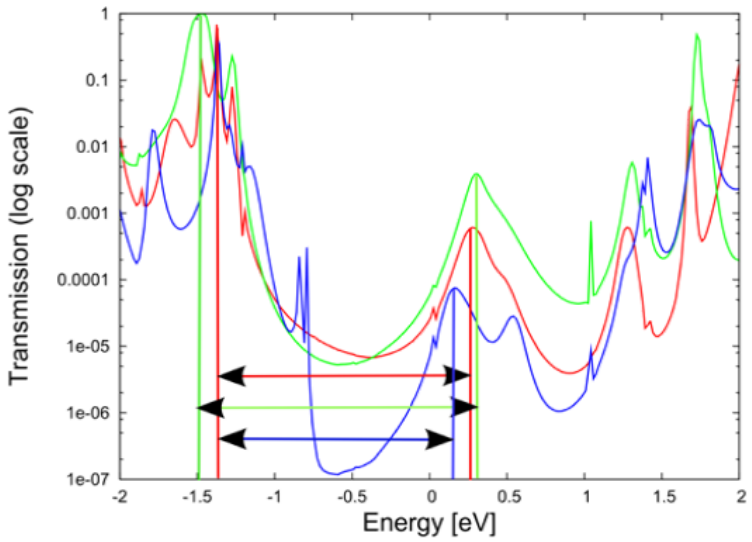

Figure 143. Transmission curves calculated for the single bond dumbbell (green), the cyclopropane dumbbell (red) and pyrrolidine dumbbell (blue).

The transmission curves have been calculated over a model based on Au/molecule/Au junction configuration. By the figure above, we can extrapolate the following conclusion:

- At Fermi energy level (0 eV), but also at every value of energy, the best dumbbell in terms of theoretical conductance is the single bond dumbbell **25** with a value of 5.3×10^{-5} G_0. The other values are 2.3×10^{-5} G_0 and 0.5×10^{-5} G_0 for cyclopropane and pyrrolidine dumbbells, respectively. This is consistent with our synthetic strategy for the improvement of electron transfer reducing the number of sp^3 carbon. Therefore, single bond is better than cyclopropane which, in turn, is better than pyrrolidine dumbbell in terms of electron transmission.
- The HOMO levels (at negative value of energy) are more or less at the same energy. It is consistent with the fact that we are not modifying the central core in which the HOMO level is localized.
- The LUMO energy values are positive and show some differences in the three systems. First of all, in pyrrolidine dumbbell its value is at lower energy but in the case of cyclopropane and direct bond dumbbell, it has more or less the same value. Secondly, the LUMO+1 level is evident for the pyrrolidine dumbbell but not for the other two molecules.

4.11 DPM-6 for photovoltaic devices

Diphenylmethano[60]fullerene (DPM) molecules have been synthesized in our group as a possible alternative to the well-known PCBM for photovoltaic applications. The synthesis of this C_{60} derivative has been performed in a straightforward manner by following the scheme below:

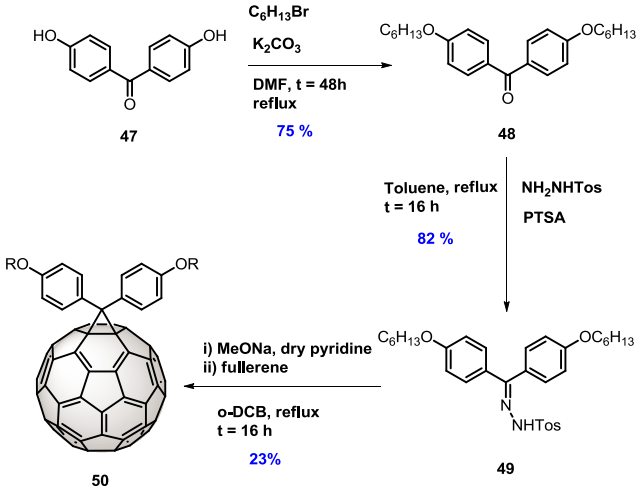

Scheme 20. Synthesis of DPM-6.

The DPM, in this case DPM-6 because of the substitution with hexyl chains, has in common with the PCBM the cyclopropane functionalization together with one aryl moiety that, in the case of PCBM, is simply a benzene ring. The influence of the alkyl chain length is reflected in the morphology of the DPM molecule when employed in the blend of bulk heterojunction solar cells. Important conclusions have been carried out comparing, for instance, PCBM with DPM-6 which will be widely argued afterwards. In our group, DPM molecules have also been functionalized with dodecyl chains and *n*-butyl chains and different behaviour are obtained from the construction of the BHJ solar cells.

Molecule **48** has been obtained with good yield after a double alkylation reaction of 4,4'-dihydroxybenzophenone to form the corresponding ether derivative which is isolated as a white solid after recrystallization with hexane. The obtained molecule has been reacted, using a Dean-Stark, with PTSA and

tosylhydrazine to form the corresponding hydrazone **49** as an E/Z mixture as a yellow solid. Such mixture of isomers has been used in the following step as well. Bamford-Stevens reaction affords thus the desired product **50** in good yield considering the feasible formation of C_{60} bis-adducts too. We have already described this reaction for the synthesis of a cyclopropane dumbbell. The NMR spectrum shows the typical signal referred to the *para* substituted aryls and hexyl chains in the aliphatic region of the spectrum, with the only exception for the methylene linked to the oxygen. Mass spectrum confirms the desired product. To confirm the similar LUMO value for DPM-6 and PCBM, cyclic voltammetry experiments have been carried out at room temperature. The reduction potentials of DPM-6 are similar to that of PCBM, which is consistent with the saturation of one double bond of C_{60}. In terms of potentials, the saturation has to shift the reduction potential waves of about 80-100 mV towards more negative values. It means that the derived compounds are more difficult to be reduced compared with pristine C_{60}. As shown in the figure below, the reduction potential values for DPM-6 are -1.084 V, -1.481 V, -1.996 V which are similar to those of PCBM (-1.077 V, -1.469 V, -1.980 V).

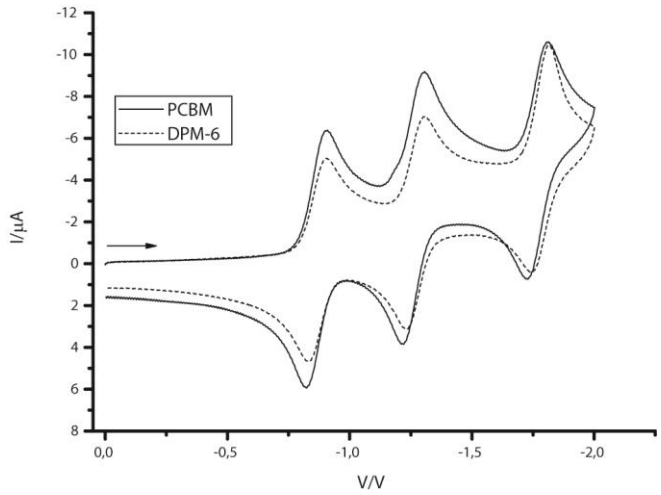

Figure 144. Cyclic voltammetry [V *vs* $Ag/AgNO_3$] of **DPM-6** and **PCBM**. Working electrode: GCE; reference electrode: Ag/Ag^+; counter electrode: Pt; supporting electrolyte: $0.1MBu_4NClO_4$; scan rate: 100 mV $\mathbf{s}^{-1}$; solvent: o-DCB/MeCN (4 : 1 v/v).

Both of them show a reversible behaviour given by a difference between reduction wave and oxidation wave of around 0.59 V for monoelectron transfer process (from Nernst Equation).

4.11.1 DPM-6 application in BHJ solar cells

Diphenylmethano[60]fullerene, functionalized with two hydrophobic alkyl chains of six carbon atoms, has been studied by blending with P3HT in a ratio 1:1 (donor:acceptor). This mixture has been found to be the optimal conditions for this system, in comparison with PCBM but not with DPM-12 where a ratio of 1:2 was better. In our study, P3HT:DPM-6 1:1 and P3HT:PCBM 1:1 solar cells have been investigated.[214]

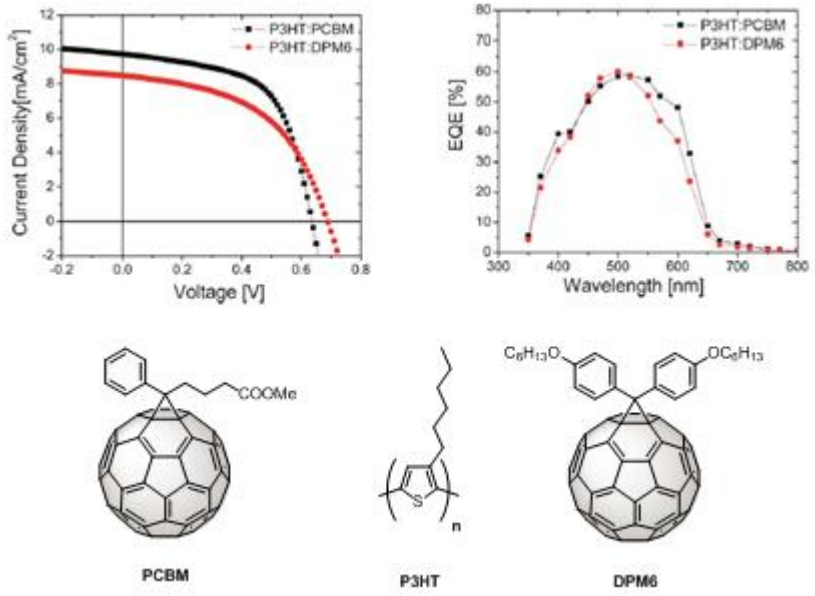

Figure 145. Current density and EQE of P3HT:PCBM and P3HT:DPM-6 blends.

[214] a) H. J. Bolink, E. Coronado, A. Forment-Aliaga, M. Lenes, A. La Rosa, S. Filippone and N. Martín, *J. Mater. Chem.*, **2011**, *21*, 1382; b) G. Garcia-Belmonte, P. P. Boix, J. Bisquert, M. Lenes, H. J. Bolink, A. La Rosa, S. Filippone and N. Martín, *J. Phys. Chem. Lett.* **2010**, *1*, 2566.

The efficiencies obtained with DPM-6 (2.6%) are superior to the previous results of DPM-12 (2.3%)[178e] in the same blend, mainly due to the higher short circuit current (J_{SC}). This higher short circuit current can be directly related to the lower optimal weight ratio of DPM-6 in the blend compared to DPM-12. Indeed, passing by P3HT:DPM-6 1:2 to a mixture of 1:1, the V_{OC} remains the same but the J_{SC} changes considerably, getting closer to the PCBM value in the same ratio blend. To understand this behaviour, mobility studies have been required.

Blend	Weight Ratio	V_{oc}/V	J_{sc}/mA cm^{-2}	FF(%)	Max EQE (%)	Intensity	PCE (%)
P3HT:PCBM	1:1	0.64	9.72	59	59	1200	3.1
P3HT:DPM-6	1:1	0.69	8.47	50	60	1200	2.6

Table 7. The solar cell characteristic of two blends with the same ratio between polymer and acceptor. The intensity is expressed in W per m^2.

DPM-12, for instance, has 40-folded reduced mobility compared with PCBM. In the case of DPM-6, an electronic mobility of 6×10^{-8} m^2 V^{-1} s^{-1} has been found, which is from three to four times than that obtained for PCBM. Despite the increased performance of DPM-6 over DPM-12, PCBM is still the superior acceptor when combined with P3HT. The lower power conversion efficiency of DPM-6 is mainly caused by a lower short circuit current (9.72 *vs* 8.47, respectively). From the EQE measurements, shown above, it is observed that the maximum quantum efficiency for both acceptors is identical, yet PCBM cells show a more pronounced shoulder at higher wavelengths which is ascribable to the increase of polymer crystallinity after thermal or solvent annealing, typical procedures to form such device. To understand this phenomenon, atomic force microscopy has been used for the pure PCBM and pure DPM-6. It is known that PCBM forms needle-like structure after thermal annealing, which indicates partial crystallization of the material.

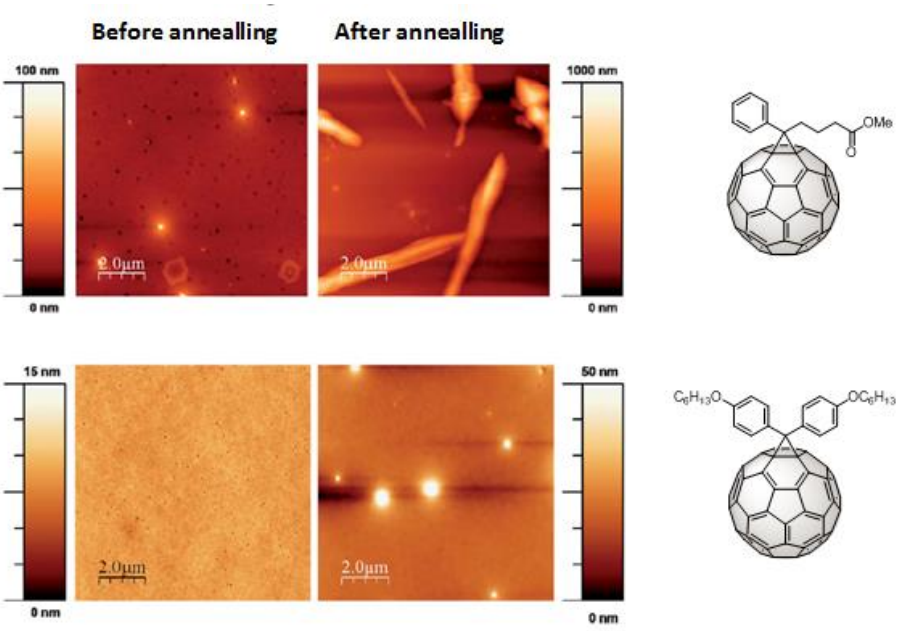

Figure 146. AFM images of two shown compounds before and after annealing up to 150 °C. Difference in morphology.

For DPM-6 however, no significant change in the surface morphology has been found when annealing up to 150 °C. We can thus affirm that in the case of DPM-6, less amount of material is required due to the high electron mobility compared with that of DPM-12, resulting in an higher J_{SC} and device performance. The lower performance *vs* PCBM could be explained by the different crystallinity degree. There is a dependence between the lower performance found for DPM-6 versus PCBM blend due to the analysis of their LDOS (density of state) in BHJ solar cells.[214b] It was found that the electronic states of the C_{60} display broad energy dispersion which can be seen as Gaussian shape. The impedance measurement of both devices stressed a shift in the V_{OC} value of about 125 mV for the DPM-6 compared with the PCBM blend device using the same polymer. The shift is ascribed to a full occupation of electronic band in the material for the DPM-6 while it is reduced in the PCBM device. Indeed, the Gaussian DOS shape is broader for PCBM molecule than for DPM-6 and it depends by the different grade of crystallinity of the material in the blend. A well-organized material, gaining grade of crystallinity, results in a stabilization of LDOS level. DPM-6 does not show this stabilization due to the lack of crystallinity.

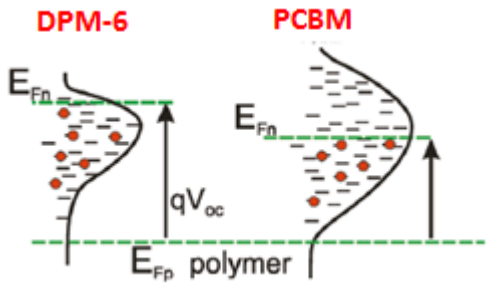

Figure 147. LDOS representation as Gaussian for the DPM-6 and PCBM in the blend, using P3HT as the polymer. The energy Fermi level for the *n*-type and *p*-type materials are shown as dashed green lines. DPM-6 presents an high value of V_{OC}.

LDOS, represented by Gaussian curve owing to the chemical or structural defects, gives us an idea about the charge mechanism occurring in the cell, above all as concern the recombination rate of the charges in the material (electron/hole). It is a localized phenomenon which occurs at the interface between polymer and acceptor molecule. A material with well surface melting distribution of polymer with the acceptor will guarantee the better charge separation, avoiding therefore the recombination process.

EXPERIMENTAL PART

5. EXPERIMENTAL PART

General employed techniques.

-***Solvents***: they have been purified and dried according the normal methods described for each case.[215]

-***Reagents****:* they have been bought by different commercial partners.

-***Thin Layer Chromatography****:* Merck (DC-Alufolien, kieselgel 60 F_{254}) of 0.2mm of thickness. To analyse the spots, ultraviolet light has been employed at two different wavelengths (254 or 366 nm), depending by the properties of each molecule.

-***Reaction mixture purification****:* it has been done through silica gel chromatography (Merck, kiesegel 60, 230-240 mesh o Scharlau 60, 230-240 mesh) without pressure or with middle pressure technique.

-***Size limit chromatography***: the isolation of dumbbell molecules has been carried out (when indicated) using a resin of styrene divinylbenzene beads (Bio-Beads S-X8), 8% crosslinkage, 40-80 μm beads size, ~1000 MW limit.

-***High Performance (Pressure) Liquid Chromatography***: Agilent 1110 Serie has been used either with analytical Buckyprep type Waters column (4.6x250 mm) or in semipreparative method (Buckyprep type Waters column 10x250 mm) for the isolation of final compounds. HPLC grade solvent have been used.

-***Melting Point****:* it has been determined (when not published) in a capillary using Gallenkamp equipment.

-***Nuclear Magnetic Spectroscopy***: the ^{1}H and ^{13}C NMR spectra have been recorded with Bruker Avance-300, Bruker AMX-500 o Bruker AMX-700 at different temperatures using commercially available typical deuterated solvents as reference. The coupling constant (*J*) are expressed in the following manner: s = singlet, bs = broad singlet, d = doublet, bd = broad doublet, t = triplet, m = multiplet, dd = double doublet.

-***Mass Spectrometry***: the mass spectra have been realized in the CAI (Centros de Asistencia a la Investigación) service of University Complutense of Madrid through i) electrospray ionization technique (ESI) using a Mass Spectrometer

[215] D. D Perrin, I. F. Amariego, D. R. Perrin, Purification of laboratory Chemicals, Pergamon Press, Oxford, **1980**.

with Ion Trap, model Bruker Esquire-LC coupled with HPLC (mass range 50-6000 uma) and MALDI-ToF/ToF (spectrometer BRUKER-ULTRAFLEX) with a N_2 laser, using in all cases as matrix (1,8,9-Antracenetriol prepared at a concentration of 10mg/mL in dichlorometane). Mass spectra were recorded using an acceleration voltage of 25kV with delayed extraction mode (delay time 130ns) in the reflector configuration and in positive or negative detection mode. The mass spectra was calibrated by a mixture of peptides recorded under similar conditions using alfa-ciano-4-hidroxycinnamic acid as a matrix, in the analysis of exact mass.

-***Cyclic Voltammetry****:* the compounds have been electrochemically characterized using a potentiostat-galvanostat Autolab PGSTAT30, equipped with a software of electrochemical analysis GPES for Windows 4.8. The measurements have been performed in a cell Metrohm EA 876-20. The working electrode (WE) is a typical glassic carbon electrode (GCE) (Metrohm 6.0804.010), Pt tip has been used as counter-electrode (CE) and, Ag/Ag^+ as reference electrode (RE). All the measurements have been done using ferrocene (Fc/Fc^+) as internal reference and the electrochemical values are referred to ferrocene potential. An argon stream has been purged in the solution for 15 minutes. During the measurements, the solution has been maintained under inert conditions. After each electrochemically measurement of one molecule, the working electrode has been cleaned up with alumina of 0.3 μ. Bu_4NClO_4 (0.1 M) has been employed as support electrolyte.

-***UV-vis****:* spectrophotometer Varian Cary 50 has been used for the UV-vis properties of desired compounds using properly solvents

-***Scanning tunnelling microscopy***: i) home built STM setup has been employed for the conductance study at molecular scale under ambient conditions (University Autonoma of Madrid); ii) liquid STM-BJ measurements at room temperature have been carried out (University of Bern, Switzerland) with a Molecular Imaging PicoSPM housed in an all-glass argon-filled chamber and equipped with a dual pre-amplifier capable of recording currents in a wide range of 1 pA to 150 mA with high resolution. The current−distance measurements were performed with a separate, lab-built analog ramp unit. The sample electrodes were Au(111) disks, 2 mm height and 10 mm in diameter, or gold single-crystal bead electrodes. The Au(111) substrates were flame-annealed prior to use. The STM tips were uncoated, electrochemically etched

gold wires (Goodfellow, 99.999%, 0.25 mm diameter), capable of imaging with atomic resolution.

-***Mechanically controllable break junction***: MCBJ setup (University of Bern, Switzerland) is based on the combination of a stepper motor (Accu-coder 95511 from Encoder Production) with a piezo stack on top. The moving distance is 17 mm for a voltage range of 110 V. Typically, a voltage between 0 to 50 V is applied. The mechanical part of the MCBJ is positioned on a vibration isolation breadboard (Newport RG Breadboard). The MCBJ experiments are based on the formation and breaking of molecular junctions between a notched, freely suspended gold wire (0.1 mm diameter, 99.999%, Goodfellow), supported on spring steel sheets (10 mm × 30 mm, thickness 0.25 mm) and fixed with a two component epoxy glue (Stycast 2850 FT with catalyst 9). The sample sheets were positioned between two holders. A Kel-F liquid cell was mounted onto the sample sheet with a Kalrez O-ring. The sample sheet was bent with a pushing rod controlled by the combination of a stepper motor and a piezo stack. The bending was initialized by the stepper motor.

-***Photophysics Experiments****:* only the BDF dumbbell-type molecules have been measured in the University of Erlangen (Germany) by Prof. D. M. Guldi. Pulsed laser Nd:YAG have been used for the photolysis study in picoseconds order (laser width: 18 ps, 2-3 mJ/pulse), model YG-501DP by Quantel. The photolysis studies in nanoseconds order have been done using a laser Nd:YAG (532 nm, pulse width 6 ns, 5-10 mJ/pulse) by Quanta-Ray CDR or a Molectron UV-400 (337.1 nm, pulse width 8 ns, 1 mJ/pulse). The output data have been digitalized through Tektronix 7912 AD. The pulse radiolysis experiments have been carried out through the electronic linear accelerator, TB-8/16-1S model. The electronic absorption spectra have been recorded with a spectrophotometer Milton Roy Spectronic Array. The emission spectra have been realized with spectrofluorimeter SLM 8100.

General procedure for the synthesis of molecules 2a,b[180]

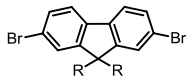

2a R = C_6H_{13}
2b R = C_8H_{17}

2,7-Dibromofluorene **1** (1.0 eq) is dissolved in 100 mL of toluene with Bu_4NBr (0.05 eqs). $NaOH_{aq}$ (50%, 40 mL) is added dropwise at the the solution. Alkylating agent (hexylbromide and octylbromide) (3.5 eqs), is added to the bulk solution and, after the addition, the temperature is arose up to 60 ºC for one night. It is cooled down to room temperature and then extracted with Et_2O. Organic layers are collected, dried on $MgSO_4$, filtered and concentrated to dryness. Crude material is purified by silica gel chromatography eluting with pure hexane.

Compounds **2a** and **2b** are obtained as white solids in 81% yield using the general procedure, above described.

General procedure for the synthesis of molecules 3a,b[180b,181]

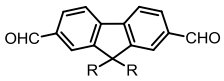

3a R = C_6H_{13}
3b R = C_8H_{17}

In a perfect dry equipment, previously heated by dryer gun under argon stream, 40 mL of dry Et_2O is poured and *n*BuLi (3.0 eqs) is added at -78 ºC. At this solution, the corresponding dialkylated dibromofluorene (1.0 eq) dissolved in 40 mL of dry Et_2O is added dropwise during 15 minutes. After the addition, the milky solution is warmed at room temperature and left for 1 h. It is again cooled at -78 ºC and dry DMF (3.0 eqs) is added dropwise. The resulting solution is warmed at room temperature for one night. The reaction is quenched with a solution of HCl 2 M. Aqueous phase is extracted with Et_2O. Organic layer is washed with water and brine, dried over $MgSO_4$, filtered and concentrated to dryness. The resulting crude material is purified by silica gel chromatography eluting with a gradient from pure hexane to hexane:DCM/1:1.

Compounds **3a** and **3b** are obtained as yellow oils in 78% and 90% yield, using the general procedure, above described.

Compound 6[182]

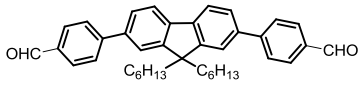

6

9,9'-dihexylfluorene-2,7-diboronic acid **4** (0.5 eqs, 1.0 g, 2.368 mmol), 4-bromo-benzaldehyde **5** (1.0 eq, 877 mg, 4.737 mmol) and AcONa (20 eqs, 6.44 g, 47,4 mmol) were dissolved in 150 mL of dry DMF and purged with argon for 1h. After this period, $Pd(PPh_3)_4$ (10% mol, 0.274 g, 0.2369 mmol) was rapidly added to the solution and the solution was still purged for further 30 minutes with argon flow before heating it at 100 ºC for 15 h. The solution was cooled at room temperature and eluted with ice/water. It was extracted with 3x100 mL of DCM and organic layers were collected, dried on $MgSO_4$, filtered and concentrated to dryness to obtain a crude material as dense oil. It was passed by silica gel chromatography eluting with a gradient from pure Cy to AcOEt. (850 mg, 1.566 mmol) of desired product was obtained as yellow dense oil in 66% yield.

2-Bromo-9,9'-dihexylfluorene (8)[183]

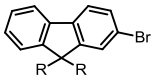

8

R = C_6H_{13}

2-Bromofluorene **7** (1.0 eq, 5.0 g, 2.0391×10^{-2} mol) was dissolved in 200 mL of DMSO with Bu_4NBr (0.05 eqs, 0.33 g, 1.019×10^{-3} mol). NaOH aq (50%, 40 mL) was added dropwise to the solution. Alkylating agent, hexylbromide (3.0 eqs, 10.10 g, 6.120×10^{-2} mol), was added and, after the addition, the solution was brought at 35 ºC for 3 h. It was, thus, cooled at room temperature and then extracted with Et_2O. Organic layers were collected, dried on $MgSO_4$, filtered and concentrated to dryness. Crude material was purified by silica gel chromatography eluting with pure cyclohexane. A dense oil was obtained (9.05 g, 2.192×10^{-2} mol) in 93% yield.

9,9'-Dihexylfluorene-2-carbaldehyde (9a)[184]

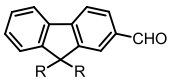

9a

In a perfect dry equipment heated by dryer gun under argon stream, 10 mL of dry Et_2O was poured and *n*BuLi (1.2 eqs, 0.91 mL, 1.455 mmol) was added at -78 ºC. At this solution, the corresponding 2-Bromo-9,9'-dihexylfluorene **8** (1.0 eq, 0.5 g, 1.213 mmol) dissolved in 20 mL of dry Et_2O was added dropwise during 15 minutes. After the addition, the milky solution was warmed at room temperature and left for 1 h. It was again cooled at -78 ºC and dry DMF (1.2 eqs, 0.11 mL, 1.455 mmol) was added dropwise. The resulting solution was warmed at room temperature and kept under the same conditions for one night. The reaction was thus quenched with a solution of HCl 2 M. Aqueous phase was extracted with Et_2O. Organic layer was washed with water and brine, dried over $MgSO_4$, filtered and concentrated to dryness. The resulting crude material is purified by silica gel chromatography eluting with pure cyclohexane. The desired product was isolated as colourless oil in 75% yield.

General Prato reaction procedure for the synthesis of dumbbell molecules 10a,b

In a round bottom flask, the corresponding aryl dialdehyde (1.0 eq) and sarcosine (8.0 eqs) are dissolved in 40 mL of chlorobenzene. C_{60} (8.0 eqs) is dissolved in further 40 mL of chlorobenzene and sonicated for 15 minutes. This solution is poured in the previous one and heated at reflux temperature for 4 h. After cooling the solution at room temperature, it is washed with 2x150 mL of H_2O and, then, with 2x50 mL of brine solution. Organic layer is collected, dried over $MgSO_4$, filtered and concentrated to dryness. Crude material is purified by silica gel chromatography eluting with pure carbon disulphide (CS_2) to remove the unreacted C_{60}, followed by a mixture of CS_2:DCM/8:2.

Dumbbell molecules **10a** and **10b** are obtained as brown solids in a 7 % and 10 % yield, respectively.

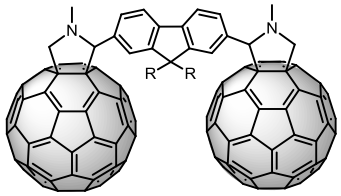

10a $R = C_6H_{13}$
10b $R = C_8H_{17}$

Characterization of compound 10a

Mp: > 300 °C

^{1}H-NMR (*CS_2:$CDCl_3$/1:1, 700 MHz, 25 °C*): δ = 7.99 (bs, **2H**), 7.69 (bs, **2H**), 7.55 (bs, **2H**), 5.04 (s, **4H$_{pyrrolidine}$**), 4.33 (d, *J = 9.32 Hz*, **2H$_{pyrrolidine}$**), 2.85 (s, **6H**), 1.30 (m, **16H**), 0.89 (m, **6H**), 0.79 (bs, **4H**) ppm.

^{13}C-NMR (*CS_2:$CDCl_3$/1:1, 175 MHz, 25 °C*): δ = 156.25, 153.97, 153.42, 147.33, 146.71, 146.47, 146.36, 146.28, 146.22, 146.17, 145.98, 145.75, 145.68, 145.60, 145.54, 145.47, 145.36, 145.20, 144.76, 144.45, 144.40, 143.18, 143.08, 142.77, 142.66, 142.30, 142.23, 142.11, 141.90, 141.76, 140.30, 140.24, 129.05, 123.14, 119.63, 83.90, 70.10, 69.10, 55.30, 40.00, 32.29, 32.01, 30.15, 23.36, 14.52 ppm.

m/z (MALDI-ToF): Calculated Mass for $C_{151}H_{44}N_2$: 1884,350 [M]; Experimental Mass: 1885,353 $[M+1]^+$

Characterization of compound 10b

Mp = > 300 °C

^{1}H-NMR (*CS_2 with internal reference $CDCl_3$, 300 MHz, 25 °C*): δ = 8.5-7.5 (bm, **6H**), 5.27 (s, **2H**), 5.27 (d, *J = 8.75 Hz*, **2H**), 4.58 (d, *J = 8.75 Hz*, **2H**), 3.10 (s, **6H**), 2.21 (bs, **4H**), 1.7-1.0 (m, **30H**) ppm.

^{13}C-NMR (*CS_2 with internal reference $CDCl_3$, 175 MHz, 25 °C*): δ = 156.47, 154.14, 153.72, 147.88, 147.40, 147.16, 147.03, 146.95, 146.91, 146.85, 146.66, 146.38, 146.28, 146.21, 146.14, 146.02, 145.98, 145.87, 145.44,

145.14, 143.86, 143.78, 143.46, 143.34, 143.00, 142.92, 142.84, 142.78, 142.56, 142.43, 141.96, 140.11, 128.05, 123.76, 118.15, 84.43, 78.05, 70.78, 69.62, 55.77, 40.73, 33.12, 31.42, 30.78, 30.38, 30.56, 24.15, 23.07, 15.52 ppm.

m/z (exact mass MALDI-ToF): Calculated mass for $C_{155}H_{52}N_2$: 1942.084 [M]; Experimental mass: 1942.404 $[M]^+$

Compound 11

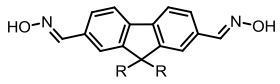

11

9,9'-Dihexyl-2,7-dicarbaldehydefluorene **3a** (1.0 eq, 0.24 g, 6.149×10^{-4} mol) was dissolved into 60 mL of ethanol and put under stirring at 70 ºC. A solution of hydroxylamine hydrochloride (28 eqs, 1.20 g, 1.722×10^{-2} mol) dissolved in 20 mL of H_2O is added dropwise. It was left under same conditions for one night. Ethanol is removed by vacuo and aqueous phase was extracted with 3x50 mL of DCM. Organic layer was collected, dried over $MgSO_4$, filtered and concentrated to dryness. Compound **11** (0.28 g, 6.832×10^{-4} mol) was obtained as white powder in 90% yield.

Mp = 73-74 °C

^{1}H-NMR (*$CDCl_3$, 300 MHz, 25 °C*): δ = 8.17 (s, **2H**), 7.64 (d, *J = 7.71 Hz* ,**2H**), 7.51 (s, **2H**), 7.47 (dd, *J = 7.81 Hz* and *J =1.33 Hz*, **2H**), 1.92 (m, **4H**), 0.96 (m, **12H**), 0.67 (t, *J = 7.24 Hz*, **6H**), 0.52 (bs, **4H**) ppm.

^{13}C-NMR (*$CDCl_3$, 75 MHz, 25 °C*): δ = 152.17, 151.18, 142.68, 131.68, 126.93, 121.48, 120.73, 55.59, 40.68, 31.83, 30.04, 24.19, 22.91, 14.41 ppm.

m/z (ESI, negative ion polarity): Calculated Mass for $C_{27}H_{36}N_2O_2$: 420.20 [M]; Experimental Mass: 419.10 $[M-1]^-$

Compound 12

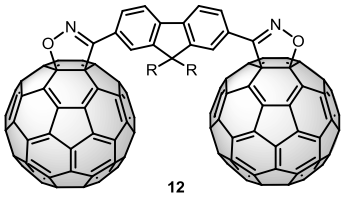

12

According to the reported procedure,[187] molecule **12** was synthesized as follows.

To a solution of N-chlorosuccinimide (NCS, 2.0 eqs, 31 mg, 0.236 mmol) and dry pyridine (0.1 mL) into 3 mL of dry $CHCl_3$, compound **11** (1.0 eq, 50 mg, 0.118 mmol), dissolved into 2 mL of dry $CHCl_3$, was added dropwise at room temperature. The reaction was left under same conditions for 30 minutes. A solution of pristine C_{60} (4.0 eqs, 340 mg, 0.472 mmol) into 30 mL of *o*-DCB, previously sonicated, was added, and the temperature raised up to 50 ºC. Triethylamine (TEA, 1 mL), dissolved into 3 mL of dry $CHCl_3$, was thus added dropwise and the reaction was left overnight under same conditions. The solvent was removed under vacuum and crude material was purified by silica gel chromatography eluting with pure CS_2 to remove the unreacted C_{60} and, then, using a gradient from CS_2 to pure DCM. By this purification, compound **12** (78.7 mg, 0.042 mmol) was isolated as brown powder in 36% yield.

Mp = > 300 °C

^{1}H-NMR (*CS_2/$CDCl_3$ 1:1, 700 MHz, 25 °C*): δ = 8.21 (d, *J = 7.69 Hz*, **2H**), 8.17 (s, **2H**), 7.92 (d, *J = 8.12 Hz*, **2H**), 1.99 (m, **4H**), 0.95 (m, **12H**), 0.79 (t, *J = 7.26 Hz*, **6H**), 0.57 (bs, **4H**) ppm.

^{13}C-NMR (*CS_2/$CDCl_3$ 1:1, 175 MHz, 25 °C*): δ = 153.51, 151.80, 147.80, 147.35, 146.52, 146.36, 146.09, 146.03, 145.80, 145.67, 145.32, 145.24, 144.86, 144.82, 144.61, 144.53, 144.12, 143.12, 142.97, 142.62, 142.60, 142.43, 142.32, 142.21, 141.72, 140.44, 140.26, 137.15, 136.76, 128.59, 123.16, 121.11, 79.50, 55.78, 40.84, 32.07, 30.10, 24.49, 23.23, 14.54 ppm.

m/z (exact mass, MALDI-ToF, negative ion polarity): Calculated Mass for $C_{147}H_{32}N_2O_2$: 1856.2426 [M]; Experimental Mass: 1855.2464 $[M-1]^-$

Compound 14

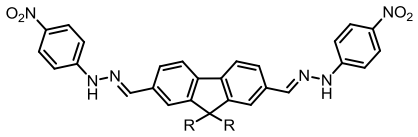

14

9,9'-Dihexyl-2,7-dicarbaldehydefluorene **3a** (1.0 eq, 0.20 g, 0,521 mmol) was dissolved into 30 mL of MeOH. At this solution, 4-nitrophenylhydrazine (2.2 eqs, 0.17 g, 1.127 mmol) was added dropwise under stirring. It was thus heated at reflux temperature for 30 minutes and then cooled at room temperature. An orange precipitate was isolated for filtration and washed with cold MeOH. The precipitate (0.43 g, 0.652 mmol) was isolated as yellow solid. The reaction yield was 80%.

Mp = 108-110 °C

^{1}H-NMR (*CD_3OD, 500 MHz, 40 °C*): δ = 8.19 (d, *J = 8.46 Hz*, **4H**), 8.17 (s, **2H**), 7.93 (s, **$2H_{fluorene}$**), 7.90 (d, *J = 7.68 Hz*, **$2H_{fluorene}$**), 7.78 (d, *J = 7.78 Hz*, **$2H_{fluorene}$**), 7.34 (d, *J = 8.46 Hz*, **4H**), 2.17 (m, **4H**), 1.11 (m, **12H**), 0.75 (t, *J = 7.05 Hz*, **6H**), 0.68 (bs, **4H**) ppm.

^{13}C-NMR (*CD_3OD, 125 MHz, 40 °C*): δ = 152.05, 151.13, 142.68 (-CH_{imine}), 142.40, 139.99, 135.05, 126.72, 126.15, 121.11, 120.69, 111.82, 55.47, 40.31, 31.67, 29.88, 24.10, 22.73, 13.72 ppm.

m/z (MALDI-ToF): Calculated Mass for $C_{39}H_{44}N_6O_4$: 660.342 [M]; Experimental Mass: 661.200 $[M+1]^+$

Compound 15

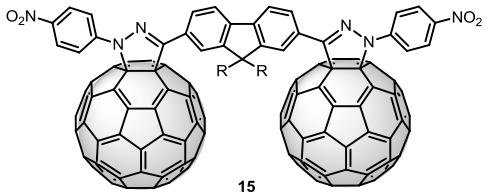

15

Compound **14** (1.0 eq, 50 mg, 0.075 mmol) was dissolved into 11 mL of PhCl (suspension) and put under stirring. N-Bromosuccinimide (NBS, 3.0 eqs, 40 mg, 0.227 mmol) was added portionwise. After 30 minutes, the starting material disappeared. It was thus poured in another solution of pristine C_{60} dissolved in PhCl (4.0 eqs, 0.217 mg, 0.302 mmol). TEA (1 mL) was added and, the reaction was left under stirring for 1h at room temperature. The reaction was thus quenched, concentrated to dryness and, crude material was passed by silica gel chromatography eluting with the a gradient from CS_2 to DCM. The triad **15** (19.7 mg, 9.397×10^{-3} mmol) was isolated after two purifications with silica gel as brown solid in 12% yield.

^{1}H-NMR (*CS_2/$CDCl_3$, 700 MHz, 25 °C*): δ = 8.36 (d, *J = 9.47 Hz*, **4H**), 8.32 (d, *J = 9.47 Hz*, **4H**), 8.24 (dd, *J = 7.86 Hz* and *J =1.53* Hz, $\mathbf{2H_{fluorene}}$), 8.19 (s, $\mathbf{2H_{fluorene}}$), 7.95 (d, *J = 7.86 Hz*, $\mathbf{2H_{fluorene}}$), 1.95 (m, **4H**), 0.94 (m, **12H**), 0.78 (t, *J = 7.46 Hz*, **6H**), 0.57 (bs, **4H**) ppm.

^{13}C-NMR (*CS_2/$CDCl_3$ 1:1, 175 MHz, 25 °C*): δ = 151.54, 149.60, 147.72, 147.30, 147.06, 146.61, 146.48, 146.26, 146.20, 146.05, 145.69, 145.58, 145.45, 145.40, 145.34, 144.67, 144.40, 144.24, 143.35, 143.16, 143.11, 143.07, 142.58, 142.44, 142.27, 142.24, 142.13, 142.12, 142.04, 141.95, 140.36, 136.60, 137.13, 136.27, 130.83, 129.20 (-$CH_{fluorene}$), 128.46, 125.46 (-$CH_{p\text{-nitrobenzene}}$), 123.33 (-$CH_{fluorene}$), 121.01 (-$CH_{fluorene}$), 119.39 (-$CH_{p\text{-nitrobenzene}}$), 90.40, 82.80, 55.80, 40.92, 32.27, 32.14, 30.06, 24.34, 14.5 ppm.

m/z (exact mass, MALDI-ToF): Calculated Mass for $C_{159}H_{40}N_6O_4$: 2096.3131 [M]; Experimental Mass: 2095.9680 $[M-1]^-$

Compound 16

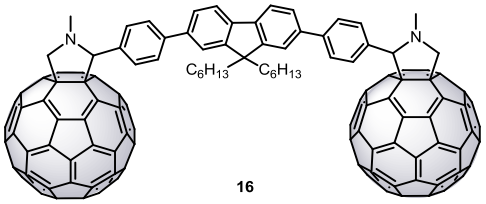

16

Compound **16** was synthesized following the general Prato reaction procedure reported above, using the aryl dialdehyde **6**. The reaction yield was 99%.

Mp = > 300 °C

^{1}H-NMR (*$CDCl_3$, 700 MHz, 25 °C*): δ = 8.16 (bs, **4H**), 7.96 (bd, **6H**), 7.81 (d, *J = 8.12 Hz*, **2H$_{fluorene}$**), 7.77 (s, **2H$_{fluorene}$**), 5.30 (d, *J = 9.44 Hz*, **2H**), 5.29 (s, **2H**), 4.61 (d, *J = 9.44 Hz*, **2H**), 3.17 (s, **6H**), 2.31 (m, **4H**), 1.35 (m, **12H**), 1.05 (t, *J = 7.48 Hz*, **6H**), 0.96 (bs, **4H**) ppm.

^{13}C-NMR (*$CDCl_3$, 175 MHz, 25 °C*): δ = 156.47, 154.20, 153.70, 153.48, 151.87, 147.60, 147.06, 146.76, 146.66, 146.60, 146.52, 146.43, 146.27, 146.09, 145.94, 145.83, 145.74, 145.60, 145.49, 145.02, 144.73, 143.50, 143.38, 143.05, 142.94, 142.60, 142.50, 142.39, 142.29, 142.05, 141.93, 140.61, 140.05, 139.81, 126.52, 121.60, 120.68, 83.72, 70.46, 69.30, 55.45, 41.24, 40.46, 32.44, 30.69, 24.71, 23.69, 15.01 ppm.

m/z (MALDI-ToF, negative): Calculated Mass for $C_{163}H_{52}N_2$: 2036.413 [M]; Experimental Mass: 2035.978 $[M-1]^-$

Compound 17

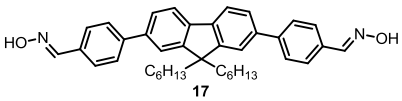

17

Compound **6** (1.0 eq, 0.129 g, 0.238 mmol) was dissolved into 60 mL of ethanol and put under stirring at 70 ºC. A solution of hydroxylamine hydrochloride (28 eqs, 0.463 g, 6.660 mmol) dissolved in 20 mL of H_2O was added dropwise. It is left under same conditions one night. Ethanol is removed by vacuo and aqueous phase was thus extracted with 3x50 mL of DCM.

Organic layer was collected, dried over $MgSO_4$, filtered and concentrated to dryness. Compound **17** (0.150 g, 0.262 mmol) was obtained as white powder with quantitative yield.

Mp = 112-114 °C

^{1}H-NMR (*$CDCl_3$, 300 MHz, 25 °C*): δ = 8.21 (s, **2H**), 7.80 (d, *J = 8.10 Hz*, **$2H_{fluorene}$**), 7.70 (s, **8H**), 7.62 (dd, *J = 8.01 Hz* and *J = 1.65 Hz*, **$2H_{fluorene}$**), 7.58 (s, **$2H_{fluorene}$**), 2.06 (m, **4H**), 1.07 (m, **12H**), 0.76 (t, *J = 7.27 Hz*, **6H**), 0.71 (bs, **4H**) ppm.

^{13}C-NMR (*$CDCl_3$, 75 MHz, 25 °C*): δ = 149.20, 148.32, 143.17, 141.15, 139.95, 131.18, 130.50, 129.74, 128.92, 128.00, 124.72, 43.93, 31.85, 29.97, 24.46, 22.72, 14.14 ppm.

m/z (MALDI-ToF): Calculated Mass for $C_{39}H_{44}N_2O_2$: 572.340 [M]; Experimental Mass: 572.212 $[M]^+$

Compound 18

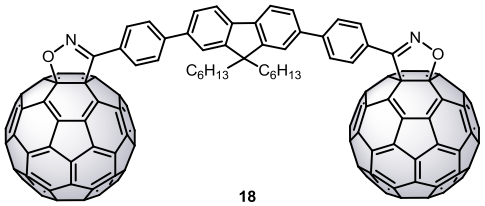

18

To a solution of NCS (2.2 eqs, 39 mg, 0.288 mmol) and dry pyridine (0.1 mL) into 3 mL of dry $CHCl_3$, compound **17** (1.0 eq, 75 mg, 0.131 mmol), dissolved into 3 mL of dry $CHCl_3$, was added dropwise at room temperature. The reaction was left under same conditions for 30 minutes. A solution of pristine C_{60} (4.0 eqs, 377 mg, 0.524 mmol) into 30 mL of *o*-DCB, previously sonicated, was added, and the temperature raised up to 50 ºC. TEA (1 mL), dissolved into 3 mL of dry $CHCl_3$, was thus added dropwise and the reaction was left overnight under same conditions. The solvent was removed under vacuum, after cooling it at room temperature. Crude material was purified by silica gel chromatography eluting with pure CS_2 to remove the unreacted C_{60} and then,

using a gradient from CS_2 to pure DCM to obtain compound **21** (86.5 mg, 0.043 mmol) as brown powder in 33% yield.

Mp = > 300 °C

^{1}H-NMR (*CS_2/$CDCl_3$ 1:1, 700 MHz, 25 °C*): δ = 8.33 (d, *J = 8.55 Hz*, **4H**), 7.89 (d, *J = 8.46 Hz*, **4H**), 7.80 (d, *J = 7.89 Hz*, $\mathbf{2H_{fluorene}}$), 7.65 (dd, *J = 7.93 Hz and J = 1.75*, $\mathbf{2H_{fluorene}}$), 7.61 (s, $\mathbf{2H_{fluorene}}$), 2.09 (m, **4H**), 1.12 (m, **12H**), 0.79 (t, *J = 7.26 Hz*, **6H**), 0.74 (bm, **4H**) ppm.

^{13}C-NMR (*CS_2/$CDCl_3$ 1:1, 175 MHz, 25 °C*): δ = 152.98, 151.92, 147.83, 147.36, 146.52, 146.37, 146.07, 146.03, 146.00, 145.75, 145.51, 145.33, 145.24, 144.88, 144.86, 144.65, 144.53, 144.18, 143.77, 143.11, 142.98, 142.60, 142.59, 142.56, 142.38, 142.19, 141.83, 140.66, 140.43, 139.12, 137.65, 137.19, 136.77, 130.60, 129.77, 129.54, 128.45, 127.80, 121.55, 120.59, 104.37, 79.19, 55.34, 40.83, 30.23, 29.56, 24.30, 23.17, 14.49 ppm.

m/z (exact mass, MALDI-ToF): Calculated Mass for $C_{159}H_{40}N_2O_2$: 2008.3090 [M]; Experimental Mass: 2008.3093 $[M]^+$

Compound 19

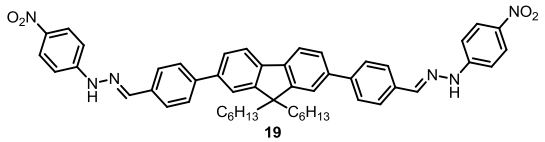

19

Compound **6** (1.0 eq, 0.300 g, 0,524 mmol) was dissolved into 90 mL of MeOH. At this solution, 4-nitrophenylhydrazine (2.2 eqs, 0.176 g, 1.153 mmol) was added dropwise under stirring. It was thus heated at reflux temperature for 1 h and then cooled at room temperature. Crude material was passed on silica gel chromatography eluting with DCM:hexane/9:1 and a pale yellow solid was obtained (0.267 g, 0.329 mmol). The reaction yield was 35%.

Mp = 115-117 °C

^{1}H-NMR (*$CDCl_3$, 500 MHz, 40 °C*): δ = 8.14 (d, *J = 9.14 Hz*, $\mathbf{4H_{p\text{-}nitrobenzene}}$), 8.00 (s, **2H**), 7.87 (s, $\mathbf{2H_{fluorene}}$), 7.76 (d, *J = 8.23 Hz*, **4H**), 7.68 (d, *J = 8.23 Hz*, **4H**), 7.59 (d, *J = 7.76 Hz* and *J = 1.59 Hz*, $\mathbf{2H_{fluorene}}$), 7.57 (2, $\mathbf{2H_{fluorene}}$),

7.12 (d, *J = 9.14 Hz*, **4H**$_{\textbf{p-nitrobenzene}}$), 2.09 (m, **4H**), 1.11 (m, **12H**), 0.79 (t, *J = 7.07 Hz*, **6H**), 0.76 (bs, **4H**) ppm.

^{13}C-NMR (*$CDCl_3$, 125 MHz, 40 °C*): δ = 152.31, 149.81, 143.26, 141.53, 141.05, 140.82, 139.72, 133.42, 130.67, 127.89, 127.65, 126.53, 121.69, 120.55, 112.26, 55.79, 40.75, 31.83, 30.04, 24.24, 22.88, 14.29 ppm.

m/z (MALDI-ToF, negative): Calculated Mass for $C_{51}H_{52}N_6O_4$: 812.996 [M]; Experimental Mass: 811.735 $[M-1]^-$

Compound 20

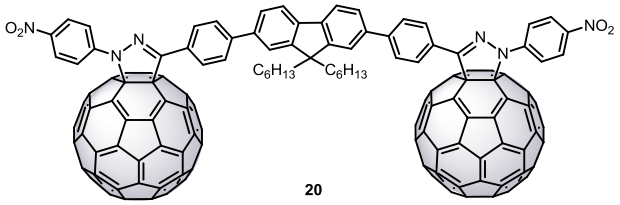

20

Dumbbell-type molecular wire **20** has been synthesized following the reported procedure for OPPV dumbbell molecules.[188]

Compound **19** (1.0 eq, 25 mg, 0.031 mmol) was dissolved into 11 mL of PhCl (suspension) and put under stirring. NBS (3.0 eqs, 16 mg, 0.092 mmol) was added portionwise. After 30 minutes, the starting material disappeared. This solution was poured in another PhCl solution containing pristine C_{60} (4.0 eqs, 89 mg, 0.124 mmol). TEA (1 mL) was added and left under stirring for 1h at room temperature. The solvent of reaction was evaporated and, crude material was passed on silica gel chromatography eluting with the a gradient from CS_2 to DCM. Compound **20** (536 mg, 0.238 mmol) was isolated as brown solid in 13% yield.

Mp = > 300 °C

^{1}H-NMR (*$CDCl_3$, 700 MHz, 25 °C*): δ = 8.39 (d, *J = 8.38 Hz* ,**4H**$_{\textbf{p-nitrobenzene}}$), 8.34 (m, **8H**), 7.85 (d, *J = 8.38 Hz*, **4H**$_{\textbf{p-nitrobenzene}}$), 7.81 (d, *J = 7.88 Hz*, **2H**$_{\textbf{fluorene}}$), 7.67 (d, *J = 7.87 Hz*, **2H**$_{\textbf{fluorene}}$), 7.62 (s, **2H**), 2.09 (m, **4H**), 1.11 (m, **12H**), 0.80 (t, *J = 7.56 Hz* , **6H**), 0.76 (bs, **4H**) ppm.

^{13}C-NMR (*$CDCl_3$ 1:1, 175 MHz, 25 °C*): δ = 151.91, 149.54, 147.72, 147.27, 146.57, 146.49, 146.30, 146.25, 146.19, 146.07, 145.80, 145.74, 145.53, 145.39, 145.35, 144.69, 144.46, 144.26, 143.35, 143.15, 143.08, 142.57, 140.58, 139.56, 139.12, 139.05, 137.14, 136.33, 130.36, 129.77, 127.67, 126.37, 125.44, 121.49, 120.59, 119.34, 90.69, 82.53, 55.39, 40.83, 31.93, 30.13, 24.22, 23.07, 14.38 ppm.

m/z (exact mass MALDI-ToF): Calculated Mass for $C_{172}H_{52}N_6O_4$: 2248.3737 [M]; Experimental Mass: 2249.3760 $[M+1]^+$

Compounds 21a,b

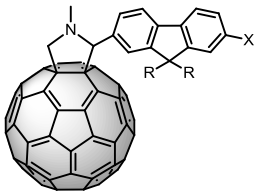

21a X = H
21b X = Br

The corresponding aldehyde **9a** and **9b** (1.0 eq) together with sarcosine (1.2 eqs) were dissolved in 10 mL of toluene. C_{60} (1.0 eq) was dissolved in 20 mL of toluene and previously sonicated for 15 minutes. The latter was poured in the first solution and the resulting mixture was heated at reflux temperature for 4 h under argon stream. After cooling it at room temperature, the reaction bulk was washed with 2x50 mL of H_2O and, then, with 2x50 mL of brine. Organic layer was collected, dried over $MgSO_4$, filtered and concentrated to dryness. Crude material was purified by silica gel chromatography eluting with pure CS_2 to remove the unreacted C_{60}, followed by a mixture of CS_2:DCM/8:2. Compounds **21a** and **21b**, as "tadpole" shape molecules, were isolated as brown solids in 36% and 28% yield, respectively.

Characterization of compound 21a

Mp = > 300 °C

^{1}H-NMR (*$CDCl_3$, 300 MHz, 25 °C*); δ = 7.98 (bs, **1H**), 7.70 (m, **2H**), 7.58 (bs, **1H**), 7.31 (m, **3H**), 5.04 (d, *J = 9.37 Hz*, **1H**), 5.04 (s, **1H**), 4.32 (d, *J = 9.37 Hz*, **1H**), 2.88 (s, **3H**), 1.96 (bs, **4H**), 1.09 (m, **12H**), 0.86 (m, **6H**), 0.32 (bs, **4H**) ppm.

^{13}C-NMR (*$CDCl_3$, 75 MHz, 25 °C*); δ = 156.59, 154.47, 154.09, 153.95, 151.31, 147.70, 147.22, 146.93, 146.72, 146.64, 146.34, 146.15, 145.91, 145.77, 145.63, 145.56, 145.10, 144.79, 143.52, 143.40, 143.10, 142.97, 142.67, 142.58, 142.49, 142.31, 142.11, 141.08, 140.60, 140.55, 139.81, 137.02, 136.29, 127.66, 127.17, 123.21, 120.21, 84.22, 70.50, 69.48, 55.57, 41.01, 40.46, 32.15, 32.01, 30.17, 29.86, 24.20, 24.06, 23.27, 23.03, 14.54, 14.46 ppm

m/z (exact mass MALDI-ToF): Calculated Mass for $C_{88}H_{39}N$: 1109.3093 [M]; Experimental mass: 1110.3162 $[M+1]^+$

Characterization of compound 21b

Mp = > 300 °C

^{1}H-NMR (*$CDCl_3$, 300 MHz, 25 °C*) δ = 7.99 (bs, **1H**), 7.70 (bs, **1H**), 7.55 (d, *J = 8.47 Hz*, **2H**), 7.45 (m, **2H**), 5.05 (d, *J = 9.44 Hz*, **1H**), 5.05 (s, **1H**), 4.34 (d, *J = 9.44 Hz*, **1H**), 2.87 (s, **3H**), 1.96 (bs, **4H**), 1.13 (m, **20H**), 0.83 (m, **10H**) ppm.

^{13}C-NMR (*$CDCl_3$, 75 MHz, 25 °C*); δ = 156.55, 154.40, 153.90, 153.85, 147.72, 147.15, 146.89, 146.73, 146.64, 146.54, 146.36, 146.15, 145.98, 145.90, 145.86, 145.76, 145.70, 145.58, 145.11, 144.80, 143.53, 143.42, 143.12, 142.97, 142.58, 142.46, 142.31, 142.12, 140.62, 140.16, 139.80, 136.96, 136.30, 130.35, 126.50, 121.58, 84.58, 70.47, 69.45, 55.92, 40.42, 32.21, 24.25, 23.58, 14.52 ppm

m/z (MALDI-ToF): Calculated Mass for $C_{92}H_{46}BrN$: 1243.281 [M]; Experimental mass: 1244.260 $[M+1]^+$

General procedure for the synthesis of compounds 22a,b

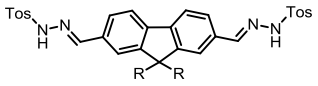

22a R = C_6H_{13}
22b R = C_8H_{17}

The corresponding dialdehyde **3a** and **3b** (1.0 eq) are put in a round bottom flask with *p*-toluensulfonic acid (PTSA, catalytic amount) and tosylhydrazine (2.4 eq). They are dissolved into 90 mL of toluene and equipped with a Dean-Stark. The resulting solution is refluxed for 2 h. The reaction is brought at room temperature and the solvent removed under vacuum. Crude material is purified by silica gel chromatography eluting with DCM:AcOEt/9:1. By purification, the products **22a** and **22b** are recovered as yellow solids in 65-70% yields.

Characterization of compound 22a

Mp = 150-153 °C

^{1}H-NMR (*$CDCl_3$, 300 MHz, 25 °C*): δ = 7.85 (d, *J = 7.36 Hz*, **4H**), 7.80 (s, **2H$_{amine}$**), 7.74 (s, **2H$_{imine}$**), 7.59 (d, *J = 7.87 Hz*, **2H$_{fluorene}$**), 7.45 (bd, **4H**), 7.22 (d, *J = 7.36 Hz*, **4H$_{fluorene}$**), 2.32 (s, **6H**), 1.91 (m, **4H**), 1.01 (m, **12H**), 0.72 (t, *J = 7.10 Hz*, **6H**), 0.46 (bs, **4H**) ppm.

^{13}C-NMR (*$CDCl_3$, 75 MHz, 25 °C*): δ = 151.79, 148.51, 144.38, 142.60, 135.45, 132.65, 129.67, 128.11, 126.97, 121.64, 120.33, 55.22, 40.21, 31.79, 29.20, 23.74, 22.62, 21.49, 14.07 ppm.

m/z (ESI): Calculated Mass for $C_{41}H_{50}N_4O_4S_2$: 726.2 [M]; Experimental Mass: 749.2 $[M+Na]^+$

Characterization of compound 22b

Mp = 155-157 °C

^{1}H-NMR (*$CDCl_3$, 300 MHz, 25 °C*): δ = 7.87 (d, *J = 7.34 Hz*, **4H**), 7.83 (s, **2H$_{amine}$**), 7.75 (s, **2H$_{imine}$**), 7.58 (d, *J = 7.88 Hz*, **2H$_{fluorene}$**), 7.47 (bd, **4H**), 7.24 (d, *J = 7.34 Hz*, **4H$_{fluorene}$**), 2.33 (s, **6H**), 1.89 (m, **4H**), 1.01 (m, **20H**), 0.72 (t, *J = 7.03Hz*, **6H**), 0.44 (bs, **4H**) ppm.

^{13}C-NMR (*$CDCl_3$, 75 MHz, 25 °C*): δ = 151.81, 148.48, 144.39, 142.63, 135.43, 132.62, 129.65, 128.12, 126.96, 121.63, 120.31, 55.20, 40.20, 31.78, 30.08, 29.19, 23.72, 22.61, 21.51, 14.04 ppm.

m/z (ESI): Calculated Mass for $C_{45}H_{58}N_4O_4S_2$: 782.4 [M]; Experimental Mass: 805.4 $[M+Na]^+$

General procedure of Bamford-Stevens reaction for the synthesis of dumbbell-type molecules 23a,b

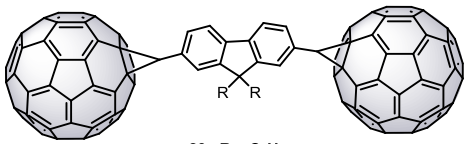

23a R = C_6H_{13}
23b R = C_8H_{17}

The normal procedure for Bamford-Stevens reaction foresees dry conditions and fresh reagents such as pyridine recently distilled and, MeONa dried in the oven. The use of molecular sieves, previously activated by microwaves, is recommended along with all the whole equipment completely dry.

The corresponding ditosylhydrazone **22a** and **22b** (1.0 eq) are dissolved in dry pyridine (3 mL for 200 mg of starting material) and MeONa (2.2 eqs) is added portionwise. The solution is left under stirring and argon atmosphere for 30 minutes. At this point, a solution of pristine C_{60} (8.0 eqs) in *o*-DCB, previously sonicated for 30 minutes, is added and the resulting mixture is heated at reflux temperature overnight. Crude material is purified by silica gel chromatography eluting with pure CS_2 to remove the unreacted C_{60}. A gradient from pure CS_2 to CS_2:DCM/1:1 is used to purify the crude material. The dumbbells **23a** and **23b** are obtained as brown solids in 20% and 10% yield respectively.

Characterization of compound 23a

Mp = > 300 °C

^{1}H-NMR (*CS_2 with internal reference CD_3OD, 700 MHz, 25 °C*): δ = 7.53 (d, *J = 8.08 Hz*, **2H**), 7.50 (s, **2H**), 7.45 (d, *J = 8.08 Hz*, **2H**), 5.10 (s, **2H**), 1.65 (m, **4H**), 0.73 (m, **12H**), 0.40 (t, *J = 7.21 Hz*, **6H**), 0.28 (bs, **4H**) ppm.

^{13}C-NMR (*CS_2 with internal reference CD_3OD, 175 MHz, 25 °C*): δ = 150.87, 149.17, 147.30, 145.18, 145.00, 144.79, 144.69, 144.60, 144.45, 144.34, 144.10, 144.00, 143.85, 143.48, 143.39, 142.70, 142.55, 142.45, 142.32, 141.78, 140.90, 140.54, 140.40, 137.87, 136.30, 131.70, 130.06 ($CH_{fluorene}$), 125.92 ($CH_{fluorene}$), 120.18 ($CH_{fluorene}$), 75.20, 54.90, 43.76, 40.65, 30.53, 29.65, 24.45, 23.03, 14.45 ppm.

m/z (MALDI-ToF): Calculated Mass $C_{148}H_{36}$: 1799.269 [M]; Experimental Mass: 1800.479 $[M+1]^+$

Characterization of compound 23b

Mp = > 300 °C

^{1}H-NMR (*CS_2 with internal reference CD_3OD, 700 MHz, 25 °C*): δ = 7.55 (d, *J = 8.03 Hz*, **2H**), 7.51 (s, **2H**), 7.47 (d, *J = 8.03 Hz*, **2H**), 5.11 (s, **2H**), 1.66 (m, **4H**), 0.84 (s, **4H**), 0.77 (m, **6H**), 0.67 (m, **10H**), 0.42 (t, *J = 7.21 Hz*, **6H**), 0.28 (bs, **4H**) ppm.

^{13}C-NMR (*CS_2 with internal reference CD_3OD, 175 MHz, 25 °C*): δ = 150.84, 149.15, 147.27, 145.16, 145.11, 144.86, 144.83, 144.78, 144.43, 144.36, 144.13, 144.10, 143.83, 143.45, 143.34, 142.72, 142.69, 142.63, 142.42, 141.77, 140.89, 140.53, 140.38, 137.86, 136.28, 131.73, 130.04 ($CH_{fluorene}$), 125.90 ($CH_{fluorene}$), 120.20 ($CH_{fluorene}$), 75.22, 54.91, 43.77, 40.67, 32.04, 30.56, 29.90, 29.68, 24.48, 23.07, 14.51 ppm.

m/z (MALDI-ToF): Calculated Mass for $C_{152}H_{44}$: 1855.332 [M]; Experimental Mass: 1856.416 $[M+1]^+$

General procedure for the direct arylation of C_{60} catalysed by Rh(I) complex

A round bottom flask containing a magnetic stirrer is flame-dried under vacuum and filled with argon after cooling to room temperature. After performing three freeze-pump-thaw cycles, the following reagents are added: C_{60} (1.0 eq) and the proper diboronic acid/ester (0.5eqs). They are dissolved in *o*-DCB:H_2O (9:1 ratio) under a stream of purging argon for 15 minutes. $[Rh(cod)_2]BF_4$ (0.1 eqs) is added to the solution and the solution is again purged with argon flow for further 15 minutes. The mixture is heated at 60 °C (for boronic acid) or 100 °C for boronic ester for several hours. The mixture is cooled to room temperature. The purification of the crude material is done using different techniques and, sometimes, a combination of them. Thus, silica gel chromatography eluting with the proper solvent, Bio-beads S-X8 resin and semipreparative HPLC analysis (Buckyprep type Waters column 10x250 mm; toluene as eluent; flow rate 5.0 mL/min; UV detection at 400 nm) are employed in different manner, according with the chemical behaviour of each molecule. The C_{60} in excess is not recovered.

Compound 25[150b]

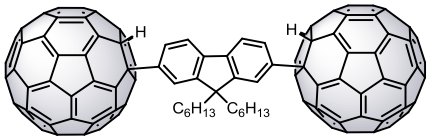

25

9,9'-dihexylfluorene-2,7-diboronic acid **24** (0.5 eqs, 7.106×10^{-5} mol, 30 mg) and C_{60} (1.421×10^{-4} mol, 102 mg) was dissolved in 20 mL of a mixture of *o*-DCB:H_2O/9:1. The catalyst (10% mol with respect to the C_{60}, 4.737×10^{-5} mol, 19.6 mg) was added and the solution purged with argon for further 15 minutes before heating it at 60 °C for 3 hours and stirring under argon stream. The reaction was cooled at room temperature and diluted with toluene. It was filtered on Celite and solvent removed under vacuum. The crude material was purified by silica gel chromatography eluting with a gradient from pure hexane to hexane:CS_2/1:1. By this purification another crude material was obtained and it was purified by HPLC using a semipreparative Buckyprep type Waters 10x250 mm (pure toluene as eluent, flow rate 5 mL/min, retention time of the

desired peak= 8.184 minutes). By such purification, the single-bond dumbbell molecule **25** was obtained as brown solid (9.4 mg, 5.298×10^{-6} mol) in 7.4 % yield. The yield was improved up to 10% in the same experiment carried out with another batch.

^{1}H-NMR (*CS_2:$CDCl_3$/2:1, 700 MHz, 25 °C*): δ = 8.57 (dd, *J = 7.69 Hz* and *J = 1.89 Hz*, **2H**), 8.50 (d, *J = 1.77 Hz*, **2H**), 8.25 (d, *J = 7.64 Hz*, **2H**), 6.87 (s, **2H C_{sp3}-$H_{fullerene}$**), 2.25 (m, **2H**), 2.15 (m, **2H**), 1.16 (m, **12H**), 0.89 (bs, **4H**), 0.78 (t, *J = 7.09 Hz*, **6H**) ppm.

^{13}C-NMR (*CS_2:$CDCl_3$/2:1, 175 MHz, 25 °C*): δ = 153.98, 153.31, 152.61, 148.10, 147.69, 147.46, 147.01, 146.62, 146.57, 146.39, 146.08, 145.99, 145.77, 145.61, 144.86, 144.74, 143.51, 143.18, 142.80, 142.48, 142.24, 142.20, 142.18, 141.89, 141.82, 140.59, 140.49, 136.56, 136.04, 122.00 ($CH_{fluorene}$), 122.10 ($CH_{fluorene}$), 121.67 ($CH_{fluorene}$), 68.39, 64.43, 56.40, 40.20, 31.40, 39.55, 23.84, 22.51, 14.09 ppm.

m/z (MALDI-ToF): Calculated Mass for $C_{145}H_{34}$: 1774.266 [M]; Experimental Mass: 1775.263 $[M+1]^+$

Compound 26

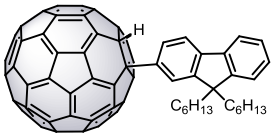

26

A 100 mL bottom flask was treated as reported in the general procedure. 9,9'-dihexylfluorene-2,7-diboronic acid **24** (1.5 eqs, 7.106×10^{-4} mol, 300 mg) and C_{60} (1.0 eq, 4.737×10^{-4} mol, 341 mg) were put together into the bottom flask and dissolved in 20 mL of a mixture of *o*-DCB:H_2O/9:1. The catalyst (10% mol referred to the C_{60} amount, 4.737×10^{-5} mol, 19.6 mg) was added and the solution purged with argon for further 15 minutes before heating it at 60 °C for 12 hours. The reaction was quenched cooling it at room temperature and diluted with toluene. It was filtered on Celite and solvent removed under vacuum. The crude material was purified by HPLC using a semipreparative Buckyprep type Waters 10x250 mm (pure toluene as eluent, flow rate 5

mL/min). The "tadpole" shape compound **26** was isolated as brown solid in 6% yield (8.3 mg, 7.873×10^{-3} mol).

^{1}H-NMR (*$CDCl_3$, 500 MHz, 25 °C*): δ = 8.47 (dd, *J = 7.82 Hz* and *J = 1.58 Hz*, **1H**), 8.41 (s, **1H**), 8.11 (d, *J = 7.85 Hz*, **1H**), 7.90 (d, *J = 7.35 Hz*, **1H**), 7.46 (m, **3H**), 6.83 (s, **1H C_{sp3}-$H_{fullerene}$**), 2.25 (m, **2H**), 2.16 (m, **2H**), 1.16 (m, **12H**), 0.78 (t, *J = 6.69 Hz*, **6H**), 0.64 (bs, **4H**) ppm.

^{13}C-NMR (*$CDCl_3$, 125 MHz, 25 °C*): δ = 154.74, 153.29, 153.22, 151.55, 148.04, 147.86, 147.82, 147.41, 146.93, 146.86, 146.73, 146.71, 146.57, 146.35, 146.00, 145.99, 145.93, 145.91, 145.18, 145.08, 143.80, 143.09, 142.82, 142.56, 142.54, 142.16, 142.12, 142.09, 141.59, 140.80, 140.72, 136.90, 136.29, 127.92, 127.43, 126.83, 123.54, 122.20, 121.34, 120.47, 68.80, 64.62, 56.12, 40.55, 31.76, 29.91, 24.22, 22.88, 14.46 ppm.

m/z (exact mass MALDI-ToF): Calculated Mass for $C_{89}H_{41}$: 1054.2661 [M]; Experimental Mass: 1055.2705 $[M+1]^+$

General procedure for the Miyaura reaction

In a perfect dry round bottom flask (made by three freeze-pump-thaw cycles) containing a magnetic stirring bar, the corresponding bromine/dibromine derivative (1.0 eq), bis(pinacolate)diboron (1.6 eqs for one bromine and 3.5 eqs for two bromines), AcOK (3.0 eqs for one bromine and 6.0 eqs for two bromines) are dissolved in dry DMF. This solution is degassed for 30 minutes with argon stream. The catalyst (5% mol referred to the bromine derivative) is poured and the solution is degased for further 15 minutes before heating it at 60 ºC overnight. It is cooled at room temperature and quenched with a mixture of H_2O/ice. The organic layers (AcOEt phase) are collected, washed with brine, dried on $MgSO_4$, filtered and the solvent removed by vacuo. Crude material is purified by silica gel chromatography.

Compound 27[196]

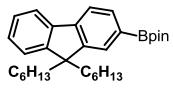

27

This compound has been obtained following the general procedure for Miyaura reaction described above, starting from compound **8**.

Silica gel chromatography eluting with pure Cy afforded 1.4 g of 2-(9,9'-dihexylfluoren-2-yl)-4,4',5,5'-tetramethyl[1,3,2]dioxaborolane (compound **27**) as dense yellow oil in 84% yield.

Compound 28[197]

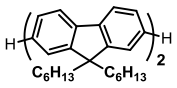

28

2-Bromo-9,9'-dihexylfluorene **8** (1.0 eq, 500 mg, 1.209 mmol) dissolved in 5 mL of toluene and compound **27** (1.0 eq, 557 mg, 1.209 mmol) dissolved in 5 mL of toluene were put under reaction. 5 mL of 2M Na_2CO_3 solution was poured and degased for 20 minutes with argon stream. $Pd(PPh_3)_4$ (0.05 eqs, 70 mg, 0.06 mmol) was poured and the resulting mixture was degassed for further 10 minutes before heating it at reflux temperature for 20 h. The reaction was quenched, after cooling it at room temperature, eluting with H_2O and extracting with Et_2O. Organic layers were collected, washed with brine, dried on $MgSO_4$, filtered and concentrated to dryness. Crude material was purified by silica gel chromatography eluting with petroleum ether. 0,420 g (compound **28**, 0.630 mmol) of 2,2'-bis(9,9'-bishexylfluorene) was obtained as white solid in 52% yield.

Compound 29[198]

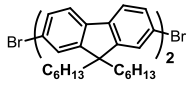

29

2,2'-Bis(9,9'-bishexylfluorene) **28** (1.0 eq, 200 mg, 0.300 mmol) was dissolved in 4 mL of DCM and iodine was added in catalytic amount. It was stirred and cooled to 0º C for 15 minutes. A solution of bromine (2.2 eqs, 105 mg, 33 μL, 0.660 mmol) in 2 mL of DCM was added dropwise into the reaction within 30 minutes. The reaction was left overnight warming at room temperature. It was quenched with few mLs of 10% solution of $NaHSO_3$. Organic phase was separated, washed with brine, dried on $MgSO_4$, filtered and the solvent was removed by vacuo. Crude material was purified by silica gel chromatography eluting with pure Cy. The 7,7'-dibromo-2,2'-bis(9,9'-bishexylfluorene) **29** was obtained as white solid in quantitative yield.

Compound 30[199]

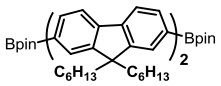

30

Analogously, compound **30** has been obtained following the general procedure of Miyaura reaction.

In dry DMF, 7,7'-dibromo-2,2'-bis(9,9'-bishexylfluorene) **29** (1.0 eq, 100 mg, 0.121 mmol) together with bis(pinacolate)diboron (3.5 eqs, 109 mg, 0.431 mmol), AcOK (6.0 eqs, 72 mg, 0.739 mmol) were dissolved and degassed for 30 minutes under argon stream. At this point, $Pd(dppf)Cl_2$ (0.06 eqs, 6 mg, 7.386×10^{-3} mmol) was rapidly added; the bulk reaction was degassed for 15 minutes and heated at 60 ºC overnight. It was cooled at room temperature and diluted with H_20 followed by the extractions with AcOEt. Organic layers were collected, dried on $MgSO_4$, filtered and crude material was purified using a gel chromatography eluting with Cy:AcOEt/9:1. 44 mg of 7,7'-di(4,4,5,5-tetramethyl-[1,3,2]dioxaborolane)-9,9,9',9'-tetrahexyl-2,2'-bifluorenyl **30** was obtained as white solid in 40% yield.

The melting point and the ^{1}H-NMR are not reported herein because they match with the literature.[199]

^{13}C-NMR and mass analysis confirm the structure of the product **30**.

^{13}C-NMR (*$CDCl_3$, 75 MHz, 25 °C*): δ = 152.09, 150.23, 143.81, 141.02, 140.20, 133.81, 128.93, 126.08, 121.60, 120.33, 119.04, 83.73, 55.25, 40.21, 31.44, 29.64, 24.97, 23.72, 22.55, 14.00 ppm.

m/z (MALDI-ToF): Calculated Mass for $C_{62}H_{88}B_2O_4$: 918.687 [M]; Experimental Mass: 918.687 [M^+]

Compound 31[201,216]

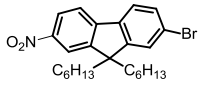

31

To form the compound **31**, we changed the reaction steps reported in literature where the spectroscopic data are also reported for compound 31.[216]

In a round bottom flask, 2-bromo-9,9'-dihexylfluorene **8** (1.0 eq, 2.0 g, 4.837 mmol) was dissolved into 24 mL of AcOH and cooled at -15 ºC. Fuming HNO_3 (27 eqs, 5.71 mL, 0.134 mol) was added dropwise to the solution and left under same conditions overnight. The reaction mixture was quenched pouring it in a bath of H_2O/ice and extracted with 3x200 mL of DCM. Organic layers were collected and the solvent was removed by vacuo. Crude material was purified by silica gel chromatography eluting with pure hexane. 2-bromo-7-nitro-9,9'-dihexylfluorene **31** was obtained as yellow dense oil in 63% yield.

[216] T.-C. Lin, C.-Y. Liu, B.-R. Huang, J.-H. Lin, Y.-K. Shen, C.-Y. Wu, *Eur. J. Org. Chem.* **2013**, *2013*, 498.

Compound 32[216]

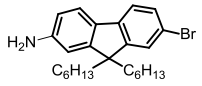

32

2-Bromo-7-nitro-9,9'-dihexylfluorene **31** (1.0 eq, 1.0 g, 2.181 mmol) was dissolved into 100 mL of a EtOH:AcOEt 1:1 mixture and purged with argon for 30 minutes. Dry $SnCl_2$ (8.75 eqs, 3.62 g, 19.08 mmol) was added portionwise. The solution was refluxed for 24 h. The reaction was quenched, cooling it at room temperature, with a solution of NaOH 1M. Tin hydroxide precipitates in the reaction medium. It was filtered and organic layers were washed twice with a solution of NaOH 1M, removing the precipitate. After this treatment, the solution was washed with H_2O and then brine, dried onto $MgSO_4$, filtered and concentrated to dryness. Crude material was passed on silica gel chromatography eluting with DCM:hex/8:2. By this purification, 2-amino-7-bromo-9,9'-dihexylfluorene **32** (0.870 g, 2.030 mmol) was obtained as dense oil in 93% yield.

Compound 33

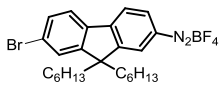

33

In a well-dried three necks round bottom flask with three freeze-pump-thaw cycles and filled by argon stream, BF_3-OEt_2 (1.6 eqs, 0.411 mL, 3.248 mmol) was poured and cooled at -10 ºC using a bath of ethylene glycol/CO_2. A solution of 2-amino-7-bromo-9,9'-dihexylfluorene **32** (1.0 eq, 870 mg, 2.030 mmol) dissolved into 10 mL of DCM was added dropwise and left under stirring and argon for 10 minutes. Butyl nitrite (1.4 eqs, 0.332 mL, 2.842 mmol) was thus added in solution of 1 mL of DCM. The evidence of the formation of diazonium salt is observed by the green colour of the solution. It was left at 0º C for 30 minutes. *n*-pentane was added to the solution and the resulting mixture was put in the freezer for one night obtaining a precipitate that was filtered and washed with cold Et_2O. The precipitate, 2-bromo-9,9'-

dihexylfluorenyl-7-diazonium tetrafluoroborate **33**, was isolated as greenish solid in 83% yield.

Mp = 133-135 °C

^{1}H-NMR ($CDCl_3$, 500 MHz, 25 °C): δ = 8.70 (dd, *J = 8.34 Hz* and *J = 1.80 Hz*, **1H**), 8.66 (s, **1H**), 8.08 (d, *J = 8.52Hz*, **1H**), 7.78 (d, *J = 7.90 Hz*, **1H**), 7.65 (d, **2H**), 2.17 (m, **2H**), 2.03 (m, **2H**), 1.09 (m, **12H**), 0.78 (t, *J = 7.21 Hz*, **6H**), 0.58 (bm, **4H**) ppm.

^{13}C-NMR ($CDCl_3$, 75 MHz, 25 °C): δ = 156.30, 154.28, 153.88, 136.45, 133.90, 132.17, 127.84, 127.49, 127.37, 124.74, 122.71, 109.48, 57.53, 39.74, 31.74, 29.67, 24.17, 22.89, 14.34 ppm

m/z (ESI-ITMS, ionic trap mass spectrometry): Calculated Mass for $C_{25}H_{32}BBrF_4N_2$: 526.1 [M]; Experimental Mass: 442.9 $[M+MeOH-N_2BF_4]^+$

Compound 34

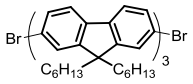

34

2-Bromo-9,9'-dihexylfluorenyl-7-diazonium tetrafluoroborate **33** (2.5 eqs, 0.600 g, 1.138 mmol) together with 9,9'-dihexylfluorene-2,7-diboronic acid **24** (1.0 eq, 0.192 g, 0.455 mmol) were dissolved into 40 mL of absolute ethanol. The solution was degassed for 15 minutes and $Pd(OAc)_2$ (0.5 eqs, 51 mg, 0.227 mmol) was poured in the reaction and degassed for further 10 minutes before heating it at 60 ºC for 2h. It was cooling at room temperature, eluting with Et_2O, washed with brine, dried onto $MgSO_4$ and filtered. The solvent was remove under vacuum and crude material was purified by silica gel chromatography eluting with pure hexane. 7,7''-dibromo-9,9,9',9',9'',9''-hexakis(hexyl)-2,2'-7',2''-terfluorene **34** was obtained as white solid (0.560 g, 0.484 mmol) in 94% yield.

The characterization of product **34** is reported in literature.[217]

Compound 35

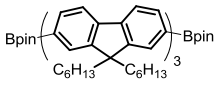

35

Miyaura reaction was used as strategy to obtain compound **35** starting from 7,7''-dibromo-9,9,9',9',9'',9''-hexakis(hexyl)-2,2'-7',2''-terfluorene **34**.

The product was isolated as dense pale oil, after silica gel chromatography eluting with hexane:AcOEt/9:1 in 46% yield.

Mp = 143-147 °C

^{1}H-NMR (*$CDCl_3$, 500 MHz, 25 °C*): δ = 7.85 (m, **8H**), 7.78 (d, *J = 7.58 Hz*, **2H**), 7.70 (d, *J = 7.38 Hz*, **4H**), 7.67 (d, **4H**), 2.10 (m, **12H**), 1.44 (s, **24H**), 1.12 (m, **36H**), 0.80 (t, *J = 7.18 Hz*, **18H**), 0.73 (bs, **12H**) ppm.

^{13}C-NMR (*$CDCl_3$, 125 MHz, 25 °C*): δ = 152.50, 152.21, 150.62, 144.23, 141.42, 140.92, 140.56, 140.44, 134.22, 129.32, 126.58, 126.45, 121.96, 121.94, 120.76, 120.37, 119.44, 84.12, 55.72, 55.66, 40.73, 40.63, 31.89, 31.84, 30.05, 25.37, 24.12, 22.97, 22.94, 14.42, 14.41 ppm.

m/z (MALDI-ToF): Calculated Mass for $C_{87}H_{120}B_2O_4$: 1250.937 [M]; Experimental Mass: 1250.812 $[M]^+$

[217] P. K. Tsolakis, J. K. Kallitsis, *Chem. Eur. J.* **2003**, *9*, 936.

Compound 36

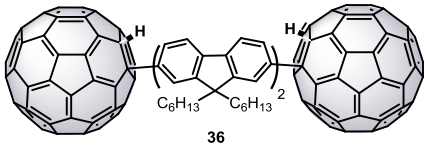

36

Single bond dumbbell molecule **36** was synthesized following the general procedure for the direct arylation of C_{60} catalysed by Rh(I) complex.

The solution was heated at 110 ºC for a period of 10 h. It was quenched bringing it at room temperature and diluting it with H_2O and toluene. Organic layer was washed with H_2O and then dried on $MgSO_4$ before filtering and concentrating to dryness. Crude material was passed on silica gel chromatography eluting with hexane:CS_2/98:2 to remove the unreacted C_{60}. The desired product was purified using hexane until hexane:DCM/3:7. 16.5 mg of compound **36** was obtained as brown solid in 10% yield.

^{1}H-NMR (*CS_2:$CDCl_3$/2:1, 700 MHz, 25 °C*): δ = 8.77 (dd, *J = 7.54 Hz and J = 1.78 Hz*, **2H**), 8.67 (s, **2H**), 8.40 (d, *J = 7.66 Hz*, **2H**), 8.21 (d, *J = 7.66 Hz*, **2H**), 8.01 (dd, *J = 7.75 Hz and J = 1.47 Hz*, **2H**), 7.97 (s, **2H**), 7.11 (s, **2H C_{sp3}-$H_{fullerene}$**), 2.58 (m, **8H**), 1.76 (m, **12H**), 1.65 (m, **10H**), 1.55 (m, **10H**), 0.92 (t, *J = 6.90 Hz*, **12H**) ppm.

^{13}C-NMR (*CS_2:$CDCl_3$/2:1, 175 MHz, 25 °C*): δ = 154.29, 153.39, 152.86, 152.13, 147.96, 147.85, 147.74, 147.29, 146.91, 146.85, 146.68, 146.36, 146.28, 146.07, 145.87, 145.14, 145.03, 143.78, 143.09, 142.76, 142.55, 142.18, 142.08, 141.42, 141.27, 140.86, 140.78, 136.86, 136.28, 127.16 ($CH_{fluorene}$), 127.13 ($CH_{fluorene}$), 122.10 ($CH_{fluorene}$), 122.01 ($CH_{fluorene}$), 121.71 ($CH_{fluorene}$), 121.06 ($CH_{fluorene}$), 68.64, 64.81, 56.14, 41.13, 30.64, 30.39, 23.94, 23.68, 15.09 ppm.

m/z (MALDI-ToF): Calculated Mass for $C_{170}H_{66}$: 2106.516 [M]; Experimental Mass: 2107.525 $[M+1]^+$

Compound 37

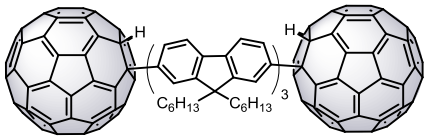

37

Single bond dumbbell molecule **37** was synthesized following the general procedure for the direct arylation of C_{60} catalysed by Rh(I) complex.

It was purified by HPLC using a semipreparative Buckyprep type Waters 10x250 mm (pure toluene as eluent, flow rate 5 mL/min). The reaction works in 6% yield.

^{1}H-NMR (CS_2:*$CDCl_3$/1:1, 700 MHz, 25 °C*): δ = 8.51 (dd, *J= 7.53 Hz* and *J = 1.79 Hz*, **2H**), 8.43 (s, **2H**), 8.15 (d, *J = 7.23 Hz*, **2H**), 7.97 (d, *J = 7.23 Hz*, **2H**), 7.87 (d, *J = 7.23 Hz*, **2H**), 7.77 (d, *J = 7.63 Hz*, **2H**), 7.74 (m, **4H**), 7.70 (s, **2H**), 6.86 (s, **2H C_{sp3}-$H_{fullerene}$**), 2.31 (m, 1**2H**), 1.22 (m, **36H**), 0.85 (t, *J = 7.21 Hz*, **18H**), 0.82 (bs, **12H**) ppm.

^{13}C-NMR (CS_2:*$CDCl_3$ /1:1, 175 MHz, 25 °C*): δ = 154.22, 153.17, 152.75, 151.90, 151.80, 147.67, 147.51, 147.43, 147.04, 146.59, 146.59, 146.53, 146.38, 146.36, 146.15, 145.98, 145.70, 145.58, 145.56, 144.84, 144.73, 143.47, 143.15, 142.75, 142.47, 142.20, 141.84, 141.76, 140.89, 140.52, 140.42, 140.21, 139.57, 136.56, 135.97, 126.72, 126.54, 126.41, 121.86, 121.72, 121.57, 121.19, 120.53, 120.28, 68.38, 64.42, 40.51, 31.78, 30.07, 29.95, 24.26, 22.98, 14.44 ppm.

m/z (MALDI-ToF): Calculated Mass for $C_{195}H_{98}$: 2440.773 [M]; Experimental Mass: 2440.559 $[M]^+$

Compound 39

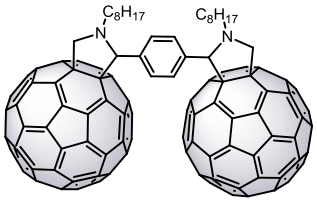

39

The reduced size dumbbell-type molecule **39** was obtained following the Prato reaction already described, using the commercially available terephthalaldheyde **38**. The purification of crude material was performed with semipreparative HPLC equipped with Byckyprep type Waters 4.6x250 mm using toluene as eluent with 5 mL/min as flow rate. The product was recovered in 10% yield.

^{1}H-NMR ($CDCl_3$, 300 MHz, 25 °C) δ = 8.16 (bs, **2H**), 7.59 (bs, **2H**), 5.10 (d, *J = 9.18 Hz*, **2H**), 5.07 (s, **2H**), 4.11 (d, *J = 9.18 Hz*, **2H**), 1.96 (bs, **4H**), 1.39 (m, **20H**), 0.93 (m, **10H**) ppm.

The ^{13}C-NMR was not well registered owing to the very low solubility of the compound **39**.

m/z (MALDI-ToF): Calculated Mass for $C_{146}H_{44}N_2$: 1825.353 [M]; Experimental Mass: 1826.381 $[M+1]^+$

Compound 41

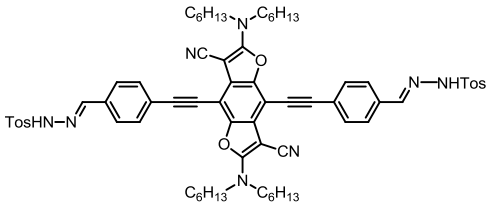

41

A mixture of compound **40** (1.0 eq, 83 mg, 0.10 mmol), *p*-toluenesulfonhydrazide (2.5 eqs, 47 mg, 0.25 mmol) and *p*-toluene sulfonic acid (PTSA) (8 mg, 0.04 mmol) was dissolved in toluene (100 mL) and refluxed for 1.5 h in a Dean-Stark equipment. After cooling down to room temperature, the resulting orange precipitate was filtered off, washed with water for several times and dried to obtain compound **41** (56 mg, 47% yield).

^{1}H-NMR (*$CDCl_3$/CD_3OD 2:1, 700 MHz, 25 °C*): δ = 7.79 (d, *J* = 7.35 Hz, **4H**), 7.71 (s, **2H**), 7.56 (d, *J* = 7.96 Hz, **4H**), 7.50 (d, *J* = 7.71 Hz, **4H**), 7.25 (d, *J* = 7.61 Hz, **4H**), 3.59 (t, *J* =7.48 Hz, **8H**), 3.32 (s, **2H**), 2.35 (s, **6H**), 1.73 (m, **8H**), 1.38 (m, **8H**), 1.29 (m, **16H**), 0.83 (t, *J* = 7.23 Hz, **12H**) ppm.

^{13}C-NMR (*$CDCl_3$/CD_3OD 2:1, 175MHz, 25 °C*): 163.20, 146.42, 145.03, 143.92, 133.77, 131.58, 129.51, 127.68, 127.00, 124.54, 123.31, 116.47, 99.64, 96.01, 81.58, 65.80, 62.29, 49.07, 31.42, 28.42, 26.13, 22.49, 21.37, 13.79 ppm.

m/z (MALDI-ToF): Calculated Mass for $C_{68}H_{78}N_8O_6S_2$: 1167.55 [M]; Experimental Mass: 1167.50 $[M]^+$.

Compound 42

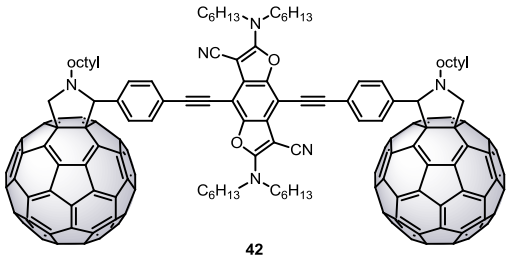

42

To a solution of dialdehyde **40** (1.0 eq, 42 mg, 0.050 mmol) and N-octylglycine (8.0 eqs, 74.8 mg, 0.40 mmol) in chlorobenzene (40 mL) was added the pristine C_{60} (8.0 eqs, 288 mg, 0.4 mmol) in chlorobenzene (40 mL, pre-sonicated for 15 min). The mixture was heated under reflux for 3.5 h. After cooling down to room temperature, the residue was washed by water (3×100 mL). The organic phase was dried by $MgSO_4$, and then filtered off. After evaporation of the solvents, the residue was purified by column chromatography on silica gel (CS_2 first to remove the unreacted C_{60} and then CS_2:CH_2Cl_2 /8:1 to afford BDF-dumbbell molecule **42** as a brown solid (45 mg, 35% yield).

Mp = > 300 °C

^{1}H-NMR (*$CDCl_3$, 700 MHz, 25 °C*): δ = 7.81 (b, **4H**), 7.74 (d, *J = 8.15 Hz*, **4H**), 5.22 (d, *J* = 9.30 Hz, **2H**)), 5.19 (s, **2H**), 4.26 (d, *J* = 9.30 Hz, **2H**), 3.58 (t, *J* = 7.63 Hz, **8H**), 3.19 (m, **2H**), 2.56 (m, **2H**), 2.10 (m, **2H**), 1.95 (m, **2H**), 1.74 (m, **8H**), 1.64 (m, **2H**), 1.45 (m, **42H**), 0.92 (t, *J* = 7.03 Hz, **6H**), 0.86 (t, *J* = 7.04 Hz, **12H**) ppm.

^{13}C-NMR (*$CDCl_3$, 175 MHz, 25 °C*): 163.40, 145.94, 145.81, 145.62, 145.58, 145.49, 145.36, 145.28, 145.23, 145.14, 144.75, 144.64, 144.40, 143.00, 142.69, 142.60, 142.22, 142.14, 142.07, 141.98, 141.92, 141.66, 141.54, 140.20, 140.16, 139.96, 139.62, 135.68, 135.59, 131.89, 129.68, 123.39, 116.41, 99.74, 96.15, 82.47, 68.61, 66.50, 62.76, 53.60, 50.03, 31.86, 31.47, 29.62, 29.57, 29.25, 28.48, 26.18, 22.55, 13.95 ppm.

m/z (MALDI-ToF): Calculated Mass for $C_{192}H_{100}N_6O_2$: 2521.79 [M], Experimental Mass: 2521.54 $[M]^+$.

Compound 43

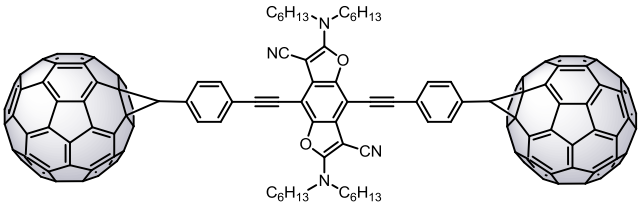

43

To a mixture of compound **41** (1.0 eq, 400 mg, 0.34 mmol) and molecular sieves (pre-activated by microwave) in dry pyridine (50 mL, freshly pre-distilled) was portionwise added MeONa (40 mg, 0.74 mmol, pre-dried in the oven) under argon atmosphere. The mixture was stirred at 25 °C for 20 min, followed by the addition of a solution of C_{60} in *o*-DCB (8.0 eqs, 300 mL, pre-sonicated for 2 h). The resulting suspension was refluxed for 24 h. After the solvent evaporation, the residue was poured into a silica gel column, eluting initially with CS_2 to remove unreacted C_{60} and then with dichloromethane to obtain triad C_{60}/BDF/C_{60} **43** as a brown solid (100 mg, 13% yield).

Mp = > 300 °C

^{1}H-NMR (*$CDCl_3$, 700 MHz, 25 °C*): δ = 8.22 (d, *J* = 7.26 Hz, **4H**), 8.09 (d, *J* = 7.87 Hz , **4H**), 5.72 (s, **2H**), 3.89 (t, *J* = 7.65 Hz, **8H**), 2.08 (m, **8H**), 1.60 (m, **24H**), 1.20 (t, *J* = 7.33 Hz, **12H**) ppm.

^{13}C-NMR (*$CDCl_3$, 175 MHz, 25 °C*): 162.87, 145.78, 145.56, 145.51, 145.46, 145.16, 145.09, 145.05, 144.90, 144.79, 144.66, 144.11, 144.06, 143.47, 143.37, 143.33, 143.04, 142.59, 142.52, 142.47, 141.53, 141.32, 138.81, 136.89, 133.50, 132.50, 131.41, 123.89, 115.58, 100.19, 96.40, 82.18, 63.95, 50.92, 43.88, 32.43, 29.41, 27.07, 23.79, 15.03 ppm.

m/z (MALDI-ToF): Calculated Mass for $C_{174}H_{62}N_4O_2$: 2239.48 [M]; Experimental Mass: 2239.28 $[M]^+$.

Compound 48[214a]

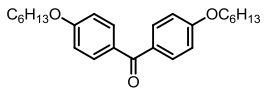

48

In a two necks round bottom flask, 4,4'-dihydroxybenzophenone **47** (1.0 eq, 1.853 g, 8.652 mmol) was dissolved in 40 mL of dry DMF and put under stirring and argon atmosphere. At room temperature, K_2CO_3 (3.0 eqs, 3.58g, 25.96 mmol) was added portionwise. After 15 minutes of stirring, 1-bromohexane (2.3 eqs, 2.79 mL, 19.90 mmol) was added dropwise in the solution and sodium iodide was added as catalyst. The mixture was heated at reflux temperature for 48 h. Thereafter, it was brought at room temperature and poured into a 1N solution of HCl. Then, it was extracted with 3x50 mL of DCM. Organic layers were collected, dried on $MgSO_4$ and filtered off. The solvent was removed under vacuum to obtained a yellow solid (6.58 g) as crude material which was recrystallized with hexane to obtain 2.482 g (6.493 mmol) of compound **48** as white solid in 75% yield.

Mp = 105-106 °C

^{1}H-NMR (*$CDCl_3$, 300 MHz, 25 °C*): δ = 7.78 (d, *J = 8.43 Hz*, **4H**), 6.96 (d, *J = 8.43 Hz*, **4H**), 4.04 (t, *J = 6.51 Hz*, **4H**), 1.82 (m, **4H**), 1.51 (m, **4H**), 1.36 (m, **8H**), 0.92 (t, *J = 6.90 Hz*, **6H**) ppm.

^{13}C-NMR (*$CDCl_3$, 300 MHz, 25 °C*): δ = 162.47, 132.22, 130.63, 129.88, 113.94, 68.28, 31.57, 29.13, 25.70, 22.60, 14.02 ppm.

m/z (ESI): Calculated Mass for $C_{25}H_{34}O_3$: 382.25 [M]; Experimental Mass: 383.25 $[M+1]^+$

Compound 49[214a]

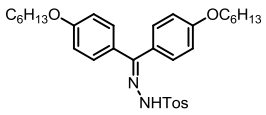

49

In a two neck round bottom flask, bis(4-hexyloxyphenyl)methanone **48** (1.0 eq, 1.0 g, 2.989 mmol) and *p*-toluenesulfonhydrazide (1.1 eqs, 0.610 g, 3.288 mmol) were dissolved in 100 mL of toluene. PTSA was added as catalyst. The solution was refluxed with a Dean-Stark equipment for 16 h. The reaction was cooled at room temperature and the solvent was removed under vacuum to obtain a yellow dense oil that was purified by silica gel chromatography eluting with a gradient from DCM:hexane 9:1 to pure DCM. By this purification, compound **49** (1.352 g , 2.460 mmol) was isolated as yellow solid in 82% yield.

Mp = 162-165 °C

^{1}H-NMR (*$CDCl_3$, 300 MHz, 25 °C*): δ = 7.69 (d, *J = 8.50 Hz*, **2H**), 7.59 (d, *J = 8.50 Hz*, **2H**), 7.26 (d, *J = 8.46 Hz*, **2H**), 7.20 (d, *J = 8.46 Hz*, **2H**), 7.00 (d, *J = 8.50 Hz*, **2H**), 6.72 (d, *J = 8.50 Hz*, **2H**), 3.98 (t, *J = 6.44 Hz*, **2H**), 3.88 (t, *J = 6.44 Hz*, **2H**), 2.30 (s, **3H**), 1.90 (m, **8H**), 1.38 (m, **8H**), 0.86 (t, *J = 7.52 Hz*, **6H**) ppm.

^{13}C-NMR (*$CDCl_3$, 75 MHz, 25 °C*): δ = 194.49, 162.48, 154.55, 143.93, 135.74, 132.22, 129.90, 129.59, 129.25, 127.94, 115.53, 114.08, 113.94, 68.25, 31.57, 29.15, 25.73, 25.70, 22.62, 22.60, 21.62, 14.03 ppm.

m/z (ESI): Calculated Mass for $C_{32}H_{42}N_2O_4S$: 550.286 [M]; Experimental Mass: 549.187 $[M-1]^-$

Compound 50 (DPM-6)[214a]

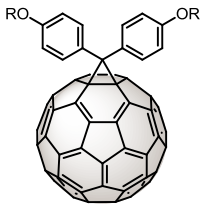

50

Bamford-Stevens reaction has been used for the synthesis of compound **50**, in agreement with the already reported reaction strategy.

Compound **49** (1.0 eq, 1.0 g, 1.817 mmol) was dissolved in 22 mL of dry pyridine and put under stirring and argon atmosphere. Sodium methoxide (1.1 eqs, 0,108 g, 1.998 mmol) was added portionwise into the solution. It was kept at same conditions for 15 minutes. A pre-sonicated solution of C_{60} (0.75 eqs, 0.981 g, 1.363 mmol) dissolved in 73 mL of *o*-DCB, was added portionwise. The resulting reaction bulk was heated at reflux temperature for 40 h. The solvent was removed under vacuum and crude material was purified by silica gel chromatography eluting with CS_2 to recover the C_{60} not reacted. Further fractions were separated with a mixture of DCM:hexane 7:3 to recover the diphenylmethano[60]fullerene **50** (monoadduct) as brown solid (450 mg, 0.414 mmol) in 23% yield. Further bisadducts have been collected as byproducts of such reaction.

Mp = > 300 °C

^{1}H-NMR (*$CDCl_3$, 300 MHz, 25 °C*): δ = 7.98 (d, *J = 8.79 Hz* , **4H**), 6.99 (d, *J = 8.79 Hz* , **4H**), 3.99 (t, *J = 6.38 Hz*, **4H**), 1.80 (m, **4H**), 1.48 (m, **4H**), 1.36 (m, **8H**), 0.92 (t, *J = 6.82 Hz*, **6H**) ppm.

^{13}C-NMR (*$CDCl_3$, 75 MHz, 25 °C*): δ = 159.11, 149.00, 145.81, 145.56, 145.47, 145.06, 144.61, 144.59, 144.24, 143.30, 142.72, 142.51, 141.19, 138.59, 132.22, 131.72, 115.02, 68.45, 57.77, 32.00, 29.68, 26.18, 23.01, 14.44 ppm.

m/z (MALDI-ToF): Calculated Mass for $C_{85}H_{34}O_2$: 1086.255 [M]; Experimental Mass:1087.249 $[M+1]^+$

CONCLUSIONS

6. CONCLUSIONS

The work presented in this Memory shows up a promising new application of C_{60} derivatives in the field of organic electronics. Thanks to its stability over different metals surfaces, in particular gold, C_{60} has been used as anchor group for dumbbell-type molecular wires in STM and MCBJ.

The conclusions of this Memory can be resumed as follows:

1. **Design, synthesis and characterization of C_{60} derivatives (dumbbells and tadpole molecules)**

C_{60} dumbbell-type molecules and tadpole shape derivatives have been synthesized with different linkers. The stiffness feature and the electronic communication of the molecules depends on the linker nature (**X**). We have employed a variety of different five member heterocycle linkers with or without aryl, cyclopropane ring and single bond. The importance of the linker has been underlined by UV-vis, cyclic voltammetry, DFT theoretical transmission curves and, in the future studies, by STM or MCBJ. The DFT calculations demonstrates a better electronic communication in the cyclopropane functionalized dumbbell, which is more efficient than the pyrrolidine containing molecule.

Figure 149. General molecular structure for dumbbell-type molecular wires based on C_{60} as anchor group.

We have also sandwiched π-system bridges such as fluorene, BDF and aryl moiety. A relevant contribution of the bridge to the higher conductance trace has been envisaged through DFT calculations in the cyclopropane dumbbell molecule. We have also designed the synthesis of a prominent new series based on fullerene directly linked to one, two and three fluorene units for the β value measurements.

2. STM measurements

The easy visualization of C_{60} over a gold surface makes the difference between typical anchor groups and C_{60}. The term "molecular beacon" has been coined for C_{60} buckyball. Snapping the molecule onto the surface paves the way to perform conductance experiments not in a blind manner as occurs for other previously reported anchor groups. Furthermore, it leads us to unambiguously wire and measure only one molecule in the junction. STM technique has been used for three main purposes: i) imaging the molecule over gold surface, either in liquid cell or in solid state, to study the molecular stability (important parameter for the reproducibility of the experiment) and/or its motion at room temperature; ii) study of ordered aggregation into SAM using a liquid cell and iii) single molecular conductance experiments in unambiguous manner, either in liquid cell or in solid state at ambient conditions, thanks to the molecular beacon.

The conductance behaviour of cyclopropane dumbbell **23b** shows two conductance traces. The higher is referred to the influence of the bridge as demonstrated by DFT calculation. Moreover, an interesting work over the influence of dumbbell configurations in the conductance traces (*cis* and *trans*) has been performed via DFT studies, otherwise unrecognizable during the measurements. The STM ambient condition measurements also shed light onto the influence of adsorbates over the mechanical and conductance properties of the dumbbell under study.

3. Preliminary mechanically controllable break junction studies

Pyrrolidine dumbbell molecule, anchored in MCBJ setup, showed two conductance plateaus. The higher value (10^{-2} G_0) has been assigned to the electron transmission only through the fullerene moiety. The lowest value (10^{-5} G_0) has been assigned to the electron transmission across the C_{60}/fluorene/C_{60} structure. In a certain way, these preliminary findings follow the same trend of the STM results for the cyclopropane molecule. More efforts have to be done in this direction.

4. Photovoltaic applications of fullerene derivatives

DPM-6 has successfully been employed in photovoltaic BHJ devices, by mixing with a donor polymer (P3HT) in a blend. The photovoltaic performances have been compared with DPM-12 and PCBM. The higher V_{OC} has been related with the nanomorphology and the DOS representation.

BIBLIOGRAPHY

7. BIBLIOGRAPHY

1. M. Reisch, *Chem. Eng. News* **2004**, *82*, 8.
2. V. Balzani, *Small* **2005**, *3*, 278.
3. S. J. Gould *Science* **1998**, *279*, 812.
4. A. Ditta, From *Advances in Natural Sciences: Nanoscience and Nanotechnology* **2012**, *3*, 033002/1.
5. S. Hatziantoniou, C. Demetzos, *Pharmakeutike* **2006**, *19*, 86.
6. P. Singh, A. Nanda, From *Toxicological & Environmental Chemistry*, Ahead of Print.
7. L. Rashidi, K. Khosravi-Darani, From *Critical Reviews in Food Science and Nutrition* **2011**, *51*, 723.
8. R. P. Feymann, *Caltech Engineering and Science*, **1960**, *23*, 22.
9. a) J. S. Miller, *Adv. Mater.* **1990**, *2*, 98; b) A. Kraft, A. C. Grimsdale, A. B. Holmes, *Angew. Chem. Int. Ed. Engl.* **1998**, *37*, 402.
10. G. E. Moore, *Electronics*, **1965**, 38.
11. a) M. R. Wasielewski, *Chem. Rev.* **1992**, *92*, 435; b) R. T. Hayes, M. R. Wasielewski, D. Gosztola, *J. Am. Chem. Soc.* **2000**, *122*, 5563; c) H. Duerr, S. Bossmann, *Acc. Chem. Res.* **2001**, *34*, 905; d) J. M. Endtner, F. Effenberger, A. Hartschuh, H. Port, *J. Am. Chem. Soc.* **2000**, *122*, 3037; e) *Acc. Chem. Res.* **1999**, *32*, 191. Special Number dedicated to *Molecular Materials in Electronics and Optoelectronic Devices.*
12. A. Aviram, M. A. Ratner, *Chem. Phys. Lett.* **1974**, *29*, 277.
13. R. F. Service, *Science* **2001**, *293*, 785.
14. a) J. C. Meyer, A. K. Geim, M. I. Katsnelson, K. S. Novoselov, T. J. Booth, S. Roth, *Nature* **2007**, *446*, 60; b) K. S. Novoselov, A. K. Geim, S. V. Morozov, D. Jiang, Y. Zhang, S. V. Dubonos, I. V. Grigorieva, A. A. Firsov, *Science* **2004**, *306*, 666.
15. E. H. L. Falcao, F. Wudl, *J. Chem. Techn. & Biotechn.* **2007**, *82*, 524.
16. a) D. M. Guldi, N. Martín Eds., *Fullerenes: From Synthesis to Optoelectronic Properties*, Kluver Academic Publishers, Dordrecht, the Netherlands, **2002**; b) F. Langa, J.-F. Nierengarten Eds., *Fullerenes. Principles and Applications*, RSC, Cambridge, United Kingdom, **2007**; c) N. Martín, F. Giacalone, Eds., *Fullerene Polymers. Synthesis, Properties and Applications*, Wiley-VCH, **2009**; d) A. Hirsch, Michael Brettreich, *Fullerenes-Chemistry and Reactions*, Wiley-VCH, **2005**.
17. R. C. Haddon, *Acc. Chem. Res.* **1992**, *25*, 127.
18. H. W. Kroto, *Nature* **1987**, *329*, 529.
19. T. G. Schmalz, W. A. Seitz, D. J. Klein, G. E. Hite, *Chem. Phys. Lett*. **1986**, *130*, 203.
20. L. W. Tutt, A. Kost, *Nature*, **1992**, *356*, 225.
21. L. Echegoyen, *Acc. Chem. Res.* **1998**, *31*, 593.

22. D. M. Guldi, M. Prato, *Acc. Chem. Res.* **2000**, *33*, 695.
23. D. M. Guldi, *Chem. Commun.* **2000**, 321.
24. R. E. Haufler, J. Conceicao, L. P. F. Chibante, Y. Chai, N. E. Byrne, S. Flanagan, M. M. Haley, S. C. O'Brien, C. Pan, *J. Phys. Chem.* **1990**, *94*, 8634.
25. Q. Xie, E. Pérez-Cordero, L. Echegoyen, *J. Am. Chem. Soc.* **1992**, *114*, 3978.
26. N. M. Alpatova, N. F. Goldshleger, E. V. Ovsyannikova, *Russian J. Electrochem.* **2008**, *44*, 79.
27. A. F. Hebard, M. J. Rosseinsky, R. C Haddon, D. W. Murphy, S. H. M. Glarum, T. T. M. Palstra, A. P. Ramirez, A. R. Kortan, *Nature* **1991**, *350*, 600.
28. a) D. M. Guldi, B. M. Illescas, C. M. Atienza, M. Wielopolski, N. Martín, *Chem. Soc. Rev.* **2009**, *38*, 1587; b) L. Ouali, V. Krasnikov, G. Hadziioannon, *J. Am.Chem. Soc.* **2000**, *122*, 7467.
29. E. Peeters, P. A. van Hal, J. Knol, C. J. Brabec, N. S. Sariciftci, J. C. Hummelen, R. A. J. Janssen, *J. Phys. Chem. B* **2000**, *104*, 10174.
30. N. J. Long, *Angew. Chem., Int. Ed.* **1995**, *34*, 21.
31. K. Kordatos, T. Da Ros, M. Prato, R. V. Bensasson, S. Leach, *Chem. Phys.* **2003**, *293*, 263.
32. E. G. Emberly, G. Kirczenow, *Phys. Rev. B* **1998**, *58*, 10911.
33. A. Nitzan, M. A. Ratner, *Science* **2003**, *300*, 1384.
34. W. B. Davis, W. A. Svec, M. A. Ratner M. R. Wasielewski, *Nature* **1998**, *396*, 60.
35. M. Mayor, H. B. Weber, *Angew. Chem. Int. Ed.* **2004**, *43*, 2882.
36. O. S. Wenger, *Chem. Soc. Rev.* **2011**, *40*, 3538.
37. a) R. A. Marcus, N. Sutin, *Biochem. Biophys. Acta*, *Rev. Bioenerg.* **1985**, *811*, 265; b) E. Emberly, G. Kirczenow, *Nanotechnology* **1999**, *10*, 285; c) J. Jortner, *J. Chem. Phys.* **1976**, *64*, 4860.
38. H. A. Kramers, *Physica* **1934**, *1*, 182.
39. P. W. Anderson, *Phys. Rev.* **1950**, *79*, 350; b) P. W. Anderson, *Phys. Rev.* **1959**, *115*, 2.
40. J. Jortner, M. Bixon, T. Langenbacher, M. E. Michel-Beyerle, *Proc. Natl. Acad. Sci. U.S.A.* **1998**, *95*, 12759.
41. M. P. Eng, B. Albinsson, *Angew. Chem. Int. Ed.* **2006**, *45*, 5626.
42. M. Wielopolski, C. Atienza, T. Clark, D. M. Guldi, N. Martín, *Chem. Eur. J.* **2008**, *14*, 6379.
43. a) N. Martín, L. Sánchez, M. A. Herranz, B. Illescas, D. M. Guldi, *Acc. Chem. Res.* **2007**, *40*, 1015; b) special number on "*Organic Photovoltaics*" (Eds.: J. L Brédas, J. R Durrant), *Acc. Chem. Res*. **2009**, *42*, 1689.
44. R. H. Goldsmith, L. E. Sinks, R. F. Kelley, L. J. Betzen, W. Liu, Emily A. Weiss, M. A. Ratner, M. R. Wasielewski, *Proc. Natl. Acad. Sci. U.S.A.,* **2005**, *102*, 3540.

45. C. Atienza-Castellanos, M. Wielopolski, D. M. Guldi, C. van der Pol, M. R. Bryce, S. Filippone, N. Martín, *Chem. Commun.* **2007**, 5164.
46. J. Loos, *Adv. Mater.* **2005**, *17*, 1821.
47. R. Landauer, *Phys. Lett. A* **1981**, *85*, 91.
48. G. Binnig, H. Rohrer, C. Gerber, E. Weibel, *Phys. Rev. Lett.* **1982**, *49*, 57.
49. a) K. S. Kwok, J. C. Ellenbogen, *Materials Today* **2002**, *5*, 28; b) K. S. Kwok, *Materials Today* **2003**, *6*, 20.
50. J. M. van Ruitenbeek, A. Alvarez, I. Pineyro, C. Grahmann, P. Joyez, M. H. Devoret, D. Esteve, C. Urbina, *Rev. Sci. Instrum.* **1996**, *67*, 108.
51. M. A. Reed, C. Zhou, C. J. Muller, T. P. Burgin, J. M. Tour, *Science* **1997**, *278*, 252.
52. C. Kergueris, J. P. Bourgoin, S. Palacin, *Phys. Rev. B* **1999**, *59*, 12505.
53. J. Reichert, R. Ochs, D. Beckmann, H. B. Weber, M. Mayor, H. von Löhneysen, *Phys. Rev. Lett.* **2002**, *88*, 176804.
54. R. H. M. Smit, Y. Noat, C. Untiedt, N. D. Lang, M. C. van Hemert, J. M. van Ruitenbeek, *Nature* **2002**, *419*, 906.
55. N. Agraït, A. L. Yeyati, J. M. van Ruitenbeek, *Phys. Rep.* **2003**, *377*, 81.
56. W. Hong, H. Valkenier, G. Mészáros, D. Zsolt Manrique, A. Mishchenko, A. Putz, P. Moreno García, C. J. Lambert, J. C. Hummelen, T. Wandlowski, *Beilstein J. Nanotechnol.* **2011,** *2*, 699.
57. a) A. I. Yanson, G. R. Bollinger, H. E. van den Brom, N. Agraït, J. M. van Ruitenbeek, *Nature* **1998**, *395*, 783; b) H. Ohnishi, Y. Kondo, K. Takayanagi, *Nature*,**1998**, *395***,** 780; c) P. Velez, S. A. Dassie, E. P. M. Leiva, *Chem. Phys. Lett.* **2008**, *460*, 261.
58. E. Lörtscher, H. B. Weber, H. Riel, *Phys. Rev. Lett.* **2007**, *98*, 176807.
59. Z. Huang, F. Chen, P. A. Bennett, N. J. Tao, *J. Am. Chem. Soc.* **2007**, *129*, 13225.
60. M. Tsutsui, K. Shoji, K. Morimoto, M. Taniguchi, T. Kawai, *Appl. Phys. Lett.* **2008**, *92*, 223110.
61. A. Ulman, *Chem. Rev.* **1996**, *96*, 1533.
62. L. Venkataraman, J. E. Klare, I. W. Tam, C. Nuckolls, M. S. Hybertsen, M. L. Steigerwald, *Nano Lett.* **2006**, *6*, 458.
63. B. Kim, J. M. Beebe, Y. Jun, X. Y. Zhu, C. D. Frisbie, *J. Am. Chem. Soc.* **2006**, *128*, 4970.
64. C.-H. Ko, M.-J. Huang, M.-D. Fu, C. H. Chen, *J. Am. Chem. Soc.* **2009**, *132*, 756.
65. S. Yasuda, S. Yoshida, J. Sasaki, Y. Okutsu, T. Nakamura, A. Taninaka, O. Takeuchi, H. Shigekawa, *J. Am. Chem. Soc.* **2006**, *128*, 7746.
66. a) B. Q. Xu, X. Y. Xiao, N. J Tao, *J. Am. Chem. Soc.* **2003**, *125*, 16164; b) M. Kamenetska, S. Y. Quek, A. C. Whalley, M. L. Steigerwald, H. J. Choi, S. G. Louie, C. Nuckolls, M. S. Hybertsen, J. B. Neaton, L. Venkataraman, *J. Am. Chem. Soc.* **2010**, *132*, 6817.

67. Y. S. Park, A. C. Whalley, M. Kamenetska, M. L. Steigerwald, M. S. Hybertsen, C. Nuckolls, L. Venkataraman, *J. Am. Chem. Soc.* **2007**, *129*, 15768.
68. a) D. M. Shewchuk, M.T. McDermott, *Langmuir* **2009**, *25*,4556; b) L. Laurentius, S. R. Stoyanov, S. Gusarov, A. Kovalenko, R. Du, G. P. Lopinski, M. T. McDermott, *ACS Nano* **2011**, *5*, 4219.
69. L. A. Zotti, T. Kirchner, J. C. Cuevas, F. Pauly, T. Huhn, E. Scheer, A. Erbe, *Small* **2010**, *6*, 1529.
70. F. Chen, X. L. Li, J. Hihath, Z. F. Huang, N. J. Tao, *J. Am. Chem. Soc.* **2006**, *128*, 15874.
71. Y. Xing, T.-H. Park, R. Venkatramani, S. Keinan, D. N. Beratan, M. J. Therien, E. Borguet, *J. Am. Chem. Soc.* **2010**, *132*, 7946.
72. M. Tachibana, K. Yoshizawa, A. Ogawa, H. Fujimoto, R. Hoffmann, *J. Phys. Chem. B* **2002**, *106*, 12727.
73. H. Basch, R. Cohen, M. A. Ratner, *Nano Lett.* **2005**, *5*, 1668.
74. C. Li, I. Pobelov, T. Wandlowski, A. Bagrets, A. Arnold, F. Evers, *J. Am. Chem. Soc.* **2008**, *130*, 318.
75. R. Huber, M. T. González, S. Wu, M. Langer, S. Grunder, V. Horhoiu, M. Mayor, M. R. Bryce, C. Wang, R. Jitchati, C. Schönenberger, M. Calame, *J. Am. Chem. Soc.***2007**, *130*, 1080.
76. W. Wang, T. Lee, M. A. Reed, *Phys. Rev. B* **2003**, *68*, 035416.
77. a) B. Xu, N. J. Tao, *Science* **2003**, *301*, 1221; b) T. Lee, W. Wang, J. F. Klemic, J. J. Zhang, J. Su, M. A. Reed, *J. Phys. Chem. B* **2004**, *108*, 8742; c) D. J. Wold, R. Haag, M. A. Rampi, C. D. Frisbie, *J. Phys. Chem. B* **2002**, *106*, 2813.
78. a) M. Taniguchi, Y. Nojima, K. Yokota, J. Terao, K. Sato, N. Kambe, T. Kawai, *J. Am. Chem. Soc.* **2006**, *128*, 15062; b) Seong Ho Choi, BongSoo Kim, C. Daniel Frisbie, *Science* **2008**, *320*, 1482; c) M. Mayor, *Angew. Chem. Int. Ed.*, **2009**, *48*, 5583.
79. M. Taniguchi, M. Tsutsui, K. Shoji, H. Fujiwara, T. Kawai, *J. Am. Chem. Soc.* **2009**, *131*, 14146.
80. F. Giacalone, M. A. Herranz, L. Grueter, M. T. Gonzalez, M. Calame, C. Shönenberger, C. R. Arroyo, G. Rubio-Bollinger, M. Velez, N. Agraït, N. Martín, *Chem. Commun.* **2007**, 4854.
81. J. S. Meisner, M. Kamenetska, M. Krikorian, M. L. Steigerwald, L. Venkataraman, C. Nuckolls, *Nano Lett.* **2011**, *11*, 1575.
82. PhD thesis of Murat Gulcur: "The Synthesis and Transport Properties of Conjugated Molecular Wires", University of Durham (England), **2012**.
83. S. Y. Quek, L. Venkataraman, H. J. Choi, S. G. Louie, M. S. Hybertsen, J. B. Neaton, *Nano Lett.* **2007**, *7*, 3477.
84. J. R. Widawsky, M. Kamenetska, J. Klare, C. Nuckolls, M. L. Steigerwald, M. S. Hybertsen, L. Venkataraman, *Nanotechnology* **2009**, *20*, 434009.
85. S. Lin, R. L. McCarley, *Langmuir* **1999**, *15*, 151.

86. J. I. Henderson, S. Feng, T. Bein, C. P. Kubiak, *Langmuir* **2000**, *16*, 6183.
87. M. Dell'Angela, G. Kladnik, A. Cossaro, A. Verdini, M. Kamenetska, I. Tamblyn, S. Y. Quek, J. B. Neaton, D. F. Cvetko, A. Morgante, L. Venkataraman, *Nano Lett.* **2010**, *10*, 2470.
88. L. Venkataraman, Y. S. Park, A. C. Whalley, C. Nuckolls, M. S. Hybertsen, M. L. Steigerwald, *Nano Lett.* **2007**, *7*, 502.
89. S. Y. Quek, M. Kamenetska, M. L. Steigerwald, H. J. Choi, S. G. Louie, M. S. Hybertsen, J. B. Neaton, L. Venkataraman, *Nat. Nanotechnol.* **2009**, *4*, 230.
90. Y. Ie, T. Hirose, H. Nakamura, M. Kiguchi, N. Takagi, M. Kawai, Y. Aso, *J. Am. Chem. Soc.* **2011**, *133*, 3014.
91. a) M. Frei, S. V. Aradhya, M. Koentopp, M. S. Hybertsen, L. Venkataraman, *Nano Lett.* **2011**, *11*, 1518; b) M. Frei, S. V. Aradhya, M. S. Hybertsen, L. Venkataraman, *J. Am. Chem. Soc.* **2012**, *134*, 4003.
92. A. Mishchenko, L. A. Zotti, D. Vonlanthen, M. Burkle, F. Pauly, J. C. Cuevas, M. Mayor, T. Wandlowski, *J. Am. Chem. Soc.* **2011**, *133*, 184.
93. M. Kiguchi, S. Miura, K. Hara, M. Sawamura, K. Murakoshi, *Appl. Phys. Lett.* **2006**, *89*, 213104.
94. R. Parameswaran, J. R. Widawsky, H. Vazquez, Y. S. Park, B. M. Boardman, C. Nuckolls, M. L. Steigerwald, M. S. Hybertsen, L. Venkataraman, *J. Phys. Chem. Lett.* **2010**, *1*, 2114.
95. W. Hong, H. Li, S.-X. Liu, Y. Fu, J. Li, V. Kaliginedi, S. Decurtins, T. Wandlowski, *J. Am. Chem. Soc.* **2012**, *134*, 19425.
96. B. K. Price, J. M. Tour, *J. Am. Chem. Soc.* **2006**, *128*, 12899.
97. M. Busson, A. Berisha, C. Combellas, F. Kanoufi, J. Pinson, *Chem. Commun.* **2011**, *47*, 12631.
98. T. Hines, I. Díez-Pérez, H. Nakamura, T. Shimazaki, Y. Asai, N. J. Tao, *J. Am. Chem. Soc.* **2013**, *135*, 3319.
99. W. Chen, J. R. Widawsky, H. Vázquez, S. T. Schneebeli, M. S. Hybertsen, R. Breslow, L. Venkataraman, *J. Am. Chem. Soc.* **2011**, *133*, 17160.
100. Z. L. Cheng, R. Skouta, H. Vazquez, J. R. Widawsky, S. Schneebeli, W. Chen, M. S. Hybertsen, R. Breslow, L. Venkataraman, *Nat. Nanotechnol.* **2011**, *6*, 353.
101. M. Guohui, S. Xin, L. Sun, R. Zhang, P. Wei, S. Sanvito, S. Hou, *Nanotechnology* **2010**, *21*, 495202.
102. L. Cui, B. Liu, D. Vonlanthen, M. Mayor, Y. Fu, J.-F. Li, T. Wandlowski, *J. Am. Chem. Soc.* **2011**, *133*, 7332.
103. V. Kaliginedi, P. Moreno-García, H. Valkenier, W. Hong, V. M. García-Suárez, P. Buiter, J. L. H. Otten, J. C. Hummelen, C. J. Lambert, T. Wandlowski, *J. Am. Chem. Soc.* **2012**, *134*, 5262.
104. T. Kirchner, B. Briechle, E. Scheer, *Acta Physica Polonica A*, **2012**, *121*, 410.
105. X. Zeng, C. Wang, A.S. Batsanov, M.R. Bryce, J. Gigon, B. Urasinska-Wojcik, G.J. Ashwell, *J. Org. Chem.* **2010**, *75*, 130.

106. X. L. Li, J. He, J. Hihath, B. Q. Xu, S. M. Lindsay, N. J. Tao, *J. Am. Chem. Soc.* **2006**, *128*, 2135.
107. a) S. Kim, J. K. Lee, S. O. Kang, J. Ko, J. H. Yum, S. Fantacci, F. De Angelis, D. Di Censo, M. K. Nazeeruddin, M. Grätzel, *J. Am. Chem. Soc.* **2006**, *128*, 16701; b) M. Grätzel, *Inorg. Chem.* **2005**, *44*, 6841; c) A. Hagfeldt, M. Grätzel, *Acc. Chem. Res.* **2000**, *33*, 269.
108. A. V. Tivanski, Y. F. He, E. Borguet, H. Y. Liu, G. C. Walker, D. H. Waldeck, *J. Phys. Chem. B* **2005**, *109*, 5398.
109. M. A. Bennett, S. K. Bhargava, D. C. R. Hockless, L. L. Welling, A. C. Willis, *J. Am. Chem. Soc.* **1996**, *118*, 10469.
110. a) H. Shiromaru, Y. Achiba, K. Kimura, Y. T. Lee, *J. Phys. Chem.* **1987**, *91*, 17; b) J. Segall, R. Lavi, Y. Wen, C. J. Wittig, *Phys. Chem.* **1989**, *93*, 7287.
111. a) K. Kamata, S. Yamaguchi, M. Kotani, K. Yamaguchi, N. Mizuno, *Angew. Chem. Int. Ed.* **2008**, *47*, 2407; b) S. Adimurthy, C. C. Malakar, U. Beifuss, *J. Org. Chem.* **2009**, *74*, 5648; c) W. Yin, C. He, M. Chen, H. Zhang, A. Lei, *Org. Lett.* **2009**, *11*, 709; d) Z. Chen, H. Jiang, A. Wang, S. Yang, *J. Org. Chem.* **2010**, *75*, 6700; e) M. Zhu, M. Ning, W. Fu, C. Xu, G. Zou, *Bull. Korean Chem. Soc.* **2012**, *33*, 1325.
112. M. Mayor, H. B. Weber, J. Reichert, M. Elbing, C. von Hänisch, D. Beckmann, M. Fischer, *Angew. Chem. Int. Ed.* **2003**, *42*, 5834.
113. S. V. Aradhya, J. S. Meisner, M. Krikorian, S. Ahn, R. Parameswaran, M. L. Steigerwald, C. Nuckolls, L. Venkataraman, *Nano Lett.* **2012**, *12*, 1643.
114. S. V. Aradhya, M. Frei, M. S. Hybertsen, L. Venkataraman, *Nature Mater.* **2012**, *11*, 872.
115. V. Mujica, A. Nitzan, Y. Mao, W. S. D. M. Kemp, A. Roitberg, M. A. Ratner *Adv. Chem. Phys.* **1999**, *107*, 403.
116. a) L. Venkataraman, J. E. Klare, C. Nuckolls, M. S. Hybertsen, M. L. Steigerwald, *Nature* **2006**, *442*, 904; b) A. Mishchenko, D. Vonlanthen, V. Meded, M. Burkle, C. Li, I. V. Pobelov, A. Bagrets, J. K. Viljas, F. Pauly, F. Evers, M. Mayor, T. Wandlowski, *Nano Lett.* **2010**, *10*, 156.
117. C. Rogero, J. I. Pascual, J. Gómez-Herrero, A. M. Baró, *J. Chem. Phys.* **2002**, *116*, 832.
118. X. Lu, M. Grobis, K. H. Khoo, S. G. Louie, M. F. Crommie, *Phys. Rev. Lett.* **2003**, *90*, 096802.
119. A. Strózecka, J. Myslivecek, B. Voigtlander, *App. Phys. A* **2007**, *87*, 475.
120. M. Kiguchi, *App. Phys. Lett.* **2009**, *95*, 073301.
121. a) T. Hashizume, K. Motai, X.D. Wang, H. Shinohara, Y. Saito, Y. Maruyama, K. Ohno, Y. Kawazoe, Y. Nishina, H.W. Pickering, Y. Kuk, T. Sakurai, *Phys. Rev. Lett.* **1993**, *71*, 2959; b) C. Silien, N.A. Pradhan, W. Ho, P.A. Thiry, *Phys. Rev. B* **2004**, *69*, 115434.
122. I. F. Torrente, K. J. Franke, J. I. Pascual, *J. Phys. Condens. Matter* **2008**, *20*, 184001.

123. X. Lu, M. Grobis, K. H. Khoo, S. G. Louie, M. F. Crommie, *Phys. Rev. B* **2004**, *70*, 115418.
124. N. Néel, J. Kroger, L. Limot, T. Frederiksen, M. Brandbyge, R. Berndt, *Phys. Rev. Lett.* **2007**, *98*, 065502.
125. S. Nakanishi, M. Tsukada, *Phys. Rev. Lett.* **2001**, *87*, 126801.
126. J. T. Lyon, L. Andrews, *Chem. Phys. Chem.* **2005**, *6*, 229.
127. M. K. Shukla, M. Dubey, J. Leszczynski, *ACS Nano*, **2008**, *2*, 227.
128. X. Zheng, Z. Dai, Z. Zeng, *J. Phys. Condens. Matter* **2009**, *21*, 145502.
129. A. J. Pérez-Jiménez, J. J. Palacios, E. Louis, E. SanFábian, J. A.Vergés, *Chem. Phys. Chem.* **2003**, *4*, 388.
130. Y. Guo, M. Kiguchi, J. Zhao, K. Murakoshi, *Chem. Phys. Lett.* **2009**, *477*, 189.
131. L. Wang, H. Cheng, *Phys. Rev. B* **2004,** *69*, 165417.
132. C. Joachim, J. K. Gimzewski, R. R. Schlittler, C. Chavy, *Phys. Rev. Lett.* **1995**, *74*, 2102.
133. R. Stadler, S. Kubatkin, T. Bjørnholm, *Nanotechnology* **2007**, *18*, 165501.
134. J. J. Palacios, A. J. Pérez-Jimenez, E. Louis, J. A. Vergés, *Phys. Rev. B* **2001**, *64*, 115411.
135. a) E. I. Altman R. J. Colton, *Phys. Rev. B* **1993**, *48*, 18244; b) A. J. Maxwell, P. A. Bruhwiler, D. Arvanitis, J. Hasselstrom, M. K. J. Johansson, N. Martensson, *Phys. Rev. B* **1998**, *57*, 7312.
136. T. Bohler, A. Edtbauer E. Scheer, *Phys. Rev. B* **2007**, *76*, 125432.
137. H. Park, J. Park, A. Lim, E. Anderson, A. Alivisatos, P. Mceuen, *Nature* **2000**, *407*, 57.
138. R. S. Ruoff, D. S. Tse, R. Malbrota, D. C. Lorents, *J. Phys. Chem.* **1993**, *97*, 3379.
139. F. D. Novaes, *Rev. Lett.* **2003**, *90*, 036101.
140. M. Kiguchi, S. Miura, K. Hara, M. Sawamura, K. Murakoshi, *App. Phys. Lett.* **2007**, *91*, 53110.
141. J. L. Segura, N. Martín, *Chem. Soc. Rev.* **2000**, *29*, 13.
142. S. Lu, T. Jin, M. Bao, Y. Yamamoto, *J. Am. Chem. Soc.* **2011**, *133*, 12842.
143. H. L. Anderson, R. Faust, Y. Rubin, F. Diederich, *Angew. Chem., Int. Ed.*, **1994**, *33*, 1366.
144. N. Dragoe, S. Tanibayashi, K. Nakahara, S. Nakao, H. Shimotani, L. Xiao, K. Kitazawa, Y. Achiba, K. Kikuchi, K. Nojima, *Chem. Commun.* **1999**, 85.
145. a) J. P. Bourgeois, F. Diederich, L. Echegoyen, J. F. Nierengarten, *Helv. Chim. Acta*, **1998**, *81*, 1835; b) S. Higashida, H. Imahori, T. Kaneda, Y. Sakata, *Chem. Lett.* **1998**, 605.
146. D. Armspach, E. C. Constable, F. Diederich, C. E. Housecroft, J. F. Nierengarten, *Chem. Eur. J.* **1998**, *4*, 723.
147. S. Ravaine, P. Delhaès, P. Leriche, M. Sallé, *Synth. Met.* **1997**, *87*, 93.

148. S. González, N. Martín, D. M. Guldi, *J. Org. Chem.* **2003**, *68*, 779.
149. a) J. L. Segura, N. Martín, *Tetrahedron Lett.* 1999, **40**, 3239; b) R. A. J. Janssen, P. A. van Hal, J. Knol, K. Hummelen, *European Conference on Organic Solar Cells (ECOS* 1998).
150. a) S. Mori, M. Nambo, L.C. Chi, J. Bouffard, K. Itami, *Org. Lett.* **2008**, *10*, 4609; b) M. Nambo, Y. Segawa, A. Wakamiya, K. Itami, *Chem. Asian J.* **2011**, *6*, 590.
151. A. I. De Lucas, N. Martín, L. Sánchez, C. Seone, *Tetrahedron Lett.*, **1996**, *52*, 9391.
152. F. Giacalone, J. L. Segura, N. Martín, *J. Org. Chem.* **2002**, *67*, 3529.
153. a) P. A. van Hal, J. Knol, B. M. W. Langeveld-Voss, S. C. J. Meskers, J. C. Hummelen, Renè A. J. Janssen, *J. Phys. Chem. A* **2000**, *104*, 5974; b) E. H. A. Beckers, P. A. van Hal, A. Dhanabalan, S. C. J. Meskers, J. Knol, J. C. Hummelen, R. A. J. Janssen, *J. Phys. Chem. A* **2003**, *107*, 6218.
154. L. Sánchez, M. A. Herranz, N. Martín, *J. Mater. Chem.* **2005**, *15*, 1409.
155. a) K. Komatsu, Y. Murata, N. Takimoto, S. Mori, N. Sugita, S. M. Wan, *J. Org. Chem.* **1994**, *59*, 6101; b) J. F. Eckert, J. F. Nicoud, J. F. Nierengarten, S. G. Liu, L. Echegoyen, N. Armaroli, F. Barigelletti, L. Ouali, V. Krasnikov, G. Hadziioannou, *J. Am. Chem. Soc.* **2000**, *122*, 7467; c) S. Fukuzumi, H. Imahori, H. Yamada, M. E. El-Khouly, M. Fujitsuka, O. Ito, D. M. Guldi, *J. Am. Chem. Soc.* **2001**, *123*, 2571; d) Y. Shirai, Y. Zhao, L. Cheng, J. M. Tour, *Org. Lett.* **2004**, *6*, 2129.
156. C. Atienza, B. Insuasty, C. Seoane, N. Martín, J. Ramey, G. M. A. Rahman, D. M. Guldi, *J. Mater. Chem.* **2005**, *15*, 124.
157. C. van der Pol, M. R. Bryce, M. Wielopolski, C. Atienza-Castellanos, D. M. Guldi, S. Filippone, N. Martín, *J. Org. Chem.* **2007**, *72*, 6662.
158. C. A. Martin, D. Ding, J. K. Sorensen, T. Bjornholm, J. M. van Ruitenbeek, H. S. J. van der Zant, *J. Am. Chem. Soc.* **2008**, *130*, 13198.
159. T. Tada, K. Yoshizawa, *Chem. Phys. Chem.* **2002**, *3*, 1035.
160. E. Leary, M. T. González, C. van der Pol, M. R. Bryce, S. Filippone, N. Martín, G. Rubio-Bollinger, N. Agraït, *Nano Lett.* **2011**, *11*, 2236.
161. X. D. Cui, A. Primak, X. Zarate, J. Tomfohr, O. F. Sankey, A. L. Moore, T. A. Moore, D. Gust, G. Harris, S. M. Lindsay, *Science* **2001**, *294*, 571.
162. G. Schull, N. Néel, M. Becker, J. Kröger, R. Berndt, *New J. Phys.* **2008**, *10*, 065012.
163. C. Evangeli, K. Gillemot, E. Leary, M. T. González, G. Rubio-Bollinger, C. J. Lambert, N. Agraït, *Nano Lett.* **2013**, *13*, 2141.
164. A. Mishra, P. Bäuerle, *Angew. Chem. Int. Ed.* **2012**, *51*, 2020.
165. a) G. Yu, J. Gao, J. C. Hummelen, F. Wudl, A. J. Heeger, *Science*, **1995**, *270*, 1789; b) S. Gunes, H. Neugebauer, S. Sariciftci Niyazi, *Chem. Rev.* **2007**, *107*, 1324.

166. B. Miller, J. M. Rosamilia, G. Dabbagh, R. Tycko, R. C. Haddon, A. J. Muller, Herbard, *J. Am. Chem. Soc.* **1991,** *113*, 6291.
167. N. S. Sariciftci, L. Smilowitz, A. J. Heeger, F. Wudl, *Science*, **1992**, *258*, 1474.
168. N. S. Sariciftci, D. Braun, C. Zhang, V. I. Srdanov, A. J. Heeger, G. Stucky, F. Wudl, *Appl. Phys. Lett.* **1993**, *62*, 585.
169. J. C. Hummelen, B. W. Knight, F. LePeq, F. Wudl, J. Yao, C. L. Wilkins, *J. Org. Chem.* **1995**, *60*, 532.
170. S. E. Shaheen, C. J. Brabec, N. S. Sariciftci, F. Padinger, T. Fromherz, J. C. Hummelen, *Appl. Phys. Lett.* **2001**, *78*, 841.
171. a) F. Padinger, R. S. Rittberger, N. S. Sariciftci, *Adv. Funct. Mater.* **2003**, *13*, 85; b) P. Schilinsky, C. Waldauf, C. J. Brabec, *Appl. Phys. Lett.* **2002**, *81*, 3885.
172. a) I. Riedel, E. von Hauff, J. Parisi, N. Martín, F. Giacalone, V. Diakonov, *Adv. Funct. Mater*. **2005**, *15*, 1979; b) A. Sánchez-Diaz, M. Izquierdo, S. Filippone, N. Martín, E. Palomares, *Adv. Funct. Mater*. **2010**, *20*, 2695; c) F. Piersimoni, S. Chambon, K. Vandewal, R. Mens, T. Boonen, A. Gadisa, M. Izquierdo, S. Filippone, B. Ruttens, J. D'Haen, N. Martín, L. Lutsen, D. Vanderzande, P. Adriaensens, J. V. Manca, *J. Phys. Chem. C* **2011**, *115*, 10873.
173. C. J. Brabec, A. Cravino, D. Meissner, N. S. Sariciftci, T. Fromherz, M. T. Rispens, L. Sánchez, J. C. Hummelen, *Adv. Funct. Mater.* **2001**, *11*, 374.
174. G. Zerza, M. C. Scharber, C. J. Brabec, N. S. Saricftci, R. Gómez, J. L. Segura, N. Martín, V. I. Srdanov, *J. Phys. Chem. A* **2000**, *104*. 8315.
175. C. Waldauf, W. Graupner, S. Tasch, G. Leising, A. Gügel, U. Scherf, A. Kraus, M. Walter, K. Müllen, *Opt. Mater*. **1998**, *9*, 449.
176. a) J. F. Nierengarten, J. F. Eckert, J. F. Nicoud, L. Ouali, V. Krasniko, G. Hadziioannou, *Chem. Comm*. **1999**, 617; b) D. M. Guldi, C. Luo, A. Swartz, R. Gómez, J. L. Segura, N. Martín, C. Brabec, N. S. Saricftci, *J. Org. Chem*. **2002**, *67*, 1141; c) C. Atienza, G. Fernández, L. Sánchez, N. Martín, I. S. Dantas, M. M. Wienk, R. A. J. Janssen, G. M. A. Rahman, D. M. Guldi, *Chem. Commun.* **2006**, 514; d) G. Fernández, L. Sánchez, D. Veldman, M. M. Wienk, C. Atienza, D. M. Guldi, R. A. J. Janssen, N. Martín, *J. Org. Chem*. **2008**, *73*, 3189; e) T. Gu, D. Tsamouras, C. Melzer, V. Krasnikov, J. P. Gisselbrecht, M. Gross, G. Hadziioannou, J. F. Nierengarten, *Chem. Phys. Chem.* **2002**, *3*, 124; f) N. Armaroli, G. Accorsi, J.-P. Gisselbrecht, M. Gross, V. Krasnikov, D. Tsamouras, G. Hadziioannou, M. J. Gómez-Escalonilla, F. Langa, J.-F. Eckert, J. F. Nierengarten, *J. Mater. Chem*. **2002**, *12*, 2077; g) J. F. Nierengarten, T. Gu, T. Aernouts, W. Geens, J. Poortmans, G. Hadziioannou, D. Tsamouras, *Appl. Phys. A: Mater. Sci. Process*. **2004**, *79*, 47.
177. a) K. Felddrap, W. Brütting, M. Schoerer, M. Brettreich, A. Hirsch, *Synth. Met*. **1999**, *101*, 156; b) K. Hosomizu, H. Imahori, U. Hahn, J. F. Nierengarten,

A. Listorti, N. Armaroli, T. Nemoto, S. Isoda, *J. Phys. Chem. C* **2007**, *111*, 2777.
178. a) T. Y. Chu, J. Lu, S. Beaupré, Y. Zhang, J. R. M. Pouliot, S. Wakim, J. Zhou, M. Leclerc, Z. Li, J. Ding, Y. Tao, *J. Am. Chem. Soc.* **2011**, *133*, 4250; b) J. L. Delgado, P. A. Bouit, S. Filippone, M. A. Herranz, N. Martín, *Chem. Commun.* **2010**, *46*, 4853; c) G. Dennler, M. C. Scharber, C. J. Brabec, *Adv. Mater*. **2009**, *21*, 1323; d) B. Kippelen, J.-J. Brédas, *Energy Environ. Sci*. **2009**, *2*, 251; e) B. C. Thompson, J. M. J. Fréchet, *Angew. Chem., Int. Ed*. **2008**, *47*, 58.
179. L. J. A. Koster, V. D. Mihailetchi, P. W. M. Blom, *Appl. Phys. Lett.* **2006**, *88*, 052104.
180. a) R. Grisorio, G. Allegretta, P. Mastrorilli, G. P. Suranna, *Macromolecules* **2011**, *44*, 7977; b) P. Anuragudom, S. S. Newaz, S. Phanichphant, T. R. Lee, *Macromolecules* **2006**, *39*, 3494.
181. a) Y. Jin, J. Ju, J. Kim, S. Lee, J. Y. Kim, S. H. Park, S.-M. Son, S.-H. Jin, K. Lee, H. Suh, *Macromolecules* **2003**, *36*, 6970.
182. Y. Long, H. Chen, Y. Yang, H. Wang, Y. Yang, N. Li, K. Li, J. Pei, F. Liu, *Macromolecules* **2009**, *42*, 6501.
183. M. Sonntag, K. Kreger, D. Hanft, P. Strohriegl, S. Setayesh, D. de Leeuw, *Chem. Mater.* **2005**, *17*, 3031.
184. M. Y. Yuen, S. C. F. Kui, K. H. Low, C. C. Kwok, S. S. Y. Chui, C. W. Ma, N. Zhu, C. M. Che, *Chem. Eur. J.* **2010**, *16*, 14131.
185. Y. Marcus, A. L. Smith, M. V. Korobov, A. L. Mirakyan, N. V. Avramenko, E. B. Stukalin, *J. Phys. Chem. B* **2001**, *105*, 2499.
186. B. M. Illescas, N. Martín, *J. Org. Chem.*, **2000**, *65*, 5994.
187. F. Langa, M. J. Gomez-Escalonilla, J.-M. Rueff, T. M. Figueira Duarte, J.-F. Nierengarten, V. Palermo, P. Samorì, Y. Rio, G. Accorsi, N. Armaroli, *Chem. Eur. J.* **2005**, *11*, 4405.
188. M. A. Herranz, M. W. J. Beulen, J. A. Rivera, L. Echegoyen, M. C. Diaz, B. M. Illescas, N. Martin, *J. Mater. Chem.* **2002**, *12*, 2048.
189. F. Cardullo, P. Seiler, L. Isaacs, J.-F. Nierengarten, R. F. Haldimann, F. Diederich, T. Mordasini-Denti, W. Thiel, C. Boudon, J.-P. Gisselhrccht, M. Gross, *Helv. Chim. Acta* **1997**, *80*, 343.
190. P. de la Cruz, E. Espíldora, J. García, A. de la Hoz, F. Langa, N. Martín, L. Sánchez, *Tetrahedron Lett.* **1999**, *40*, 4889.
191. C. M. Cardona, W. Li, A. E. Kaifer, D. Stockdale, G. C. Bazan, *Adv. Mater.* **2011**, *23*, 2367.
192.) L. Lafferentz, F. Ample, H. Yu, S. Hecht, C. Joachim, L. Grill, *Science* **2009**, *323*, 1193; b) L. Grill, M. Dyer, L. Laffarentz, M. Persson, M. V. Peters, S. Hecht, *Nature Nanotech.* **2007**, *2*, 687.
193. a) M. Eiermann, R. C. Haddon, B. Knight, Q. Chan Li, M. Maggini, N. Martín, T. Ohno, M. Prato, T. Suzuki, F. Wudl, *Angew. Chem., Int. Ed.* **1995**,

34, 1591; b) T. Ohno, N. Martín, B. Knight, F. Wudl, T. Suzuki, H. Yu, *J. Org. Chem*. **1996**, *61*, 1306.
194. F. B. Kooistra, T. M. Leuning, E. Maroto Martinez, J. C. Hummelen, *Chem. Commun.* **2010**, *46*, 2097.
195. M. C. Díaz, M. A. Herranz, B. M. Illescas, N. Martín, N. Godbert, M. R. Bryce, *J. Org. Chem*. **2003**, *68*, 7711.
196. W. Y. Lai, R. Xia, D. D. C. Bradley, W. Huang, *Chem. Eur. J.* **2010**, *16*, 8471.
197. N. Fomina, S. E. Bradforth, T. E. Hogen-Esch, *Macromolecules* **2009**, *42*, 6440.
198. V. Promarak, A. Punkvuang, T. Sudyoadsuk, S. Jungsuttiwong, S. Saengsuwan, T. Keawin, K. Sirithip, *Tetrahedron* **2007**, *63*, 8881.
199. P. H. Auberta, L. Beoucha, F. Tran-Vana, O. Stephanb, C. Chevrot, *Synt. Metals* **2006**, *156*, 898.
200. J. Jo, C. Chi, S. Hager, G. Wegner, D. Y. Yoon, *Chem. Eur. J.* **2004**, *10*, 2681.
201. S. P. Dudek, M. Pouderoijen, R. Abbel, A. P. H. J. Schenning, E. W. Meijer, *J. Am. Chem. Soc.* **2005**, *127*, 11763.
202. B. Balan, C. Vijayakumar, S. Ogi, M. Takeuchi, *J. Mater. Chem.* **2012**, *22*, 11224.
203. B. Li, Z. Xu, *J. Am. Chem. Soc.* **2009**, *131*, 16380.
204. M. E. Garst, D. Lukton, *Synth. Comm.*, **1980**, *10*, 155.
205. a) J. L. Bahr, J. Yang, D. V. Kosynkin, M. J. Bronikowski, R. E. Smalley, J. M. Tour, *J. Am. Chem. Soc.* **2001**, *123*, 6536; b) H. Leinonen, M. Lajunen, *J. Nanopart. Res.* **2012**, *14*, 1064.
206. a) J. R. Lomeda, C. D. Doyle, D. V. Kosynkin, W.-F. Hwang, J. M. Tour, *J. Am. Chem. Soc.* **2008**, *130*, 16201; b) Z. Jin, J. R. Lomeda, B. K. Price, W. Lu, Y. Zhu, J. M. Tour, *Chem. Mater.* **2009**, *21*, 3045.
207. PhD thesis of Hui Li: "Benzodifuran derivatives for organic and molecular electronics", University of Bern (Switzerland), **2013**.
208. M. J. Brites, C. Santos, S. Nascimento, B. Gigante, H. Luftmann, A. Fedorovc, M. N. Berberan-Santos, *New J. Chem.* **2006**, *30*, 1036.
209. K. Gillemot, C. Evangeli, E. Leary, A. La Rosa, M. T. González, S. Filippone, I. Grace, G. Rubio-Bollinger, J. Ferrer, N. Martín, C. J. Lambert, N. Agraït, *Small* **2013**, DOI:10.1002/smll.201300310.
210. G. Schull, T. Frederiksen, A. Arnau, D. Sanchez-Portal, R. Berndt, *Nat. Nanotechnol.* **2011**, *6*, 23.
211. N. Neel, J. Kroeger, R. Berndt, *Nano Lett.* **2011**, *11*, 3593; b) A. V. Danilov, P. Hedegard, D. S. Golubev, T. Bjornholm, S. E. Kubatkin, *Nano Lett.* **2008**, *8*, 2393.
212. C. Toher, A. Filippetti, S. Sanvito, K. Burke, *Phys. Rev. Lett.* **2005**, *95*, 146402.

213. J. Fock, J. K. Sorensen, E. Lortscher, T. Vosch, C. A. Martin, H. Riel, K. Kilsa, T. Bjørnholm, H. van der Zant, *Phys. Chem. Chem. Phys.*, **2011**, *13*, 14325.
214. a) H. J. Bolink, E. Coronado, A. Forment-Aliaga, M. Lenes, A. La Rosa, S. Filippone, N. Martín, *J. Mater. Chem.*, **2011**, *21*, 1382; b) G. Garcia-Belmonte, P. P. Boix, J. Bisquert, M. Lenes, H. J. Bolink, A. La Rosa, S. Filippone, N. Martín, *J. Phys. Chem. Lett.* **2010**, *1*, 2566.
215. D. D Perrin, I. F. Amariego, D. R. Perrin, Purification of laboratory Chemicals, Pergamon Press, Oxford, **1980**.
216. T.-C. Lin, C.-Y. Liu, B.-R. Huang, J.-H. Lin, Y.-K. Shen, C.-Y. Wu, *Eur. J. Org. Chem.* **2013**, *2013*, 498.
217. P. K. Tsolakis, J. K. Kallitsis, *Chem. Eur. J.* **2003**, *9*, 936.

ANNEX 1 - SUMMARY

SUMMARY

Introduction

Nowadays, the terms *Nanoscience* and *Nanotechnology* are taking part into our life with giant steps. The definition for both terms is in agreement with the idea that science and technology has to still make progress but in the nanoscale world,[1] where most of the employed materials in nanoscale show properties completely different from that of the macroscopic world (graphene is an example). Materials smaller than 1 micron belong to this new scientific branches. Such scientific melting-pot area needs innovative materials with optical, magnetic, electronic and optoelectronic properties; organic chemistry, in particular, represents a powerful tool for the fabrication of new materials for devices in agreement with two miniaturization processes: the "top-down" (physical concept) and the "bottom-up" (chemical concept). A strong impulse in the development of this field is given by the different probe microscopy techniques, namely STM and AFM, that paved the way to the study of materials at nanoscopic level.

Within the *Nanoscience* and *Nanotechnology* world, the field of molecular organic electronics is one of the most important with many expectations and, where "molecular wires", for instance, represent a big theme of paramount interest. A molecular wire is defined as a molecule capable to transport electrons between two electron reservoirs in an efficient manner.[2] We can study their electronic behaviour with photoinduced electron transfer processes for the donor-bridge-acceptor molecules, and with STM or MCBJ techniques for molecular wires composed of anchor group/π-conjugated bridge/anchor group. We have focused our attention in the second class of molecular wires with a deep treatment of the anchor groups for the better understanding of their chemical and physical behaviour. Therefore, all the existing anchor groups have been divided into monodentate (thiols,[3] amine,[4] cyano or isocyanate,[5] isothiocyanate,[6] selenium compounds,[7] pyridine,[8] phosphine,[9] diazonium compounds[10]), bidentate (nitro compounds,[11] carboxylic acids[12] and dithiocarboxilic acid[13]) and multidentate, such as C_{60}. The experimental data of the metal/C_{60}/metal junction formation have been stressed[14] to mark the difference with other anchor groups but, also, to promote it as new candidate for the metal contact in the conductance properties of dumbbell-type molecular

wires.[15] Thanks to the good stability of C_{60} (lower electric coupling with metal lead and appreciable lifetime when the junction is formed) over gold surface at low temperature[16] and room temperature, C_{60} can be a good candidate as anchor group. The shape of C_{60} allows us to identify the molecule over gold surface and to isolate it. In such a way, we can use STM tip to measure the conductance properties of only one molecule without working in blind regime (stressful difference among C_{60} and the other typical anchor groups). The new molecular "beacon" (C_{60}) makes easier the visualization of the molecule before and after the measurements with a consequent better reproducibility of the experiments (Figure 1).[17]

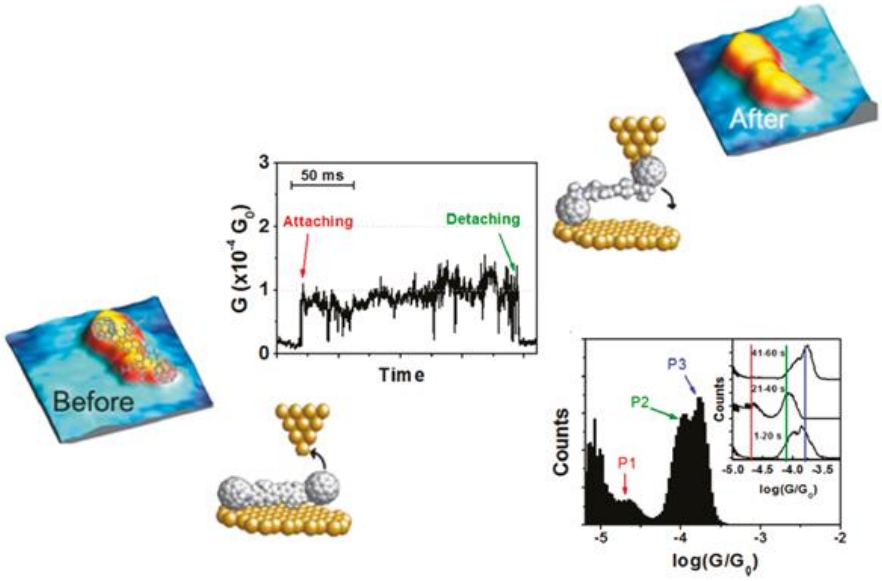

Figure 1. Evidence of molecular junction formation for dumbbell molecule and its conductance values in the histogram.

Results and Discussion

Once established the C_{60} stability over gold surface, we want to stand out its application in molecular wires with dumbbell-type shape. For this purpose, we have planned the synthesis of a collection of C_{60} dumbbell-type molecular

wires with the general structure reported in Figure 2. Moreover, we want to understand what are the mechanisms that are behind the electron transfer in such systems. To do that, we have employed different linkers (**X**) to modify the electronic communication between C_{60} and the bridge.

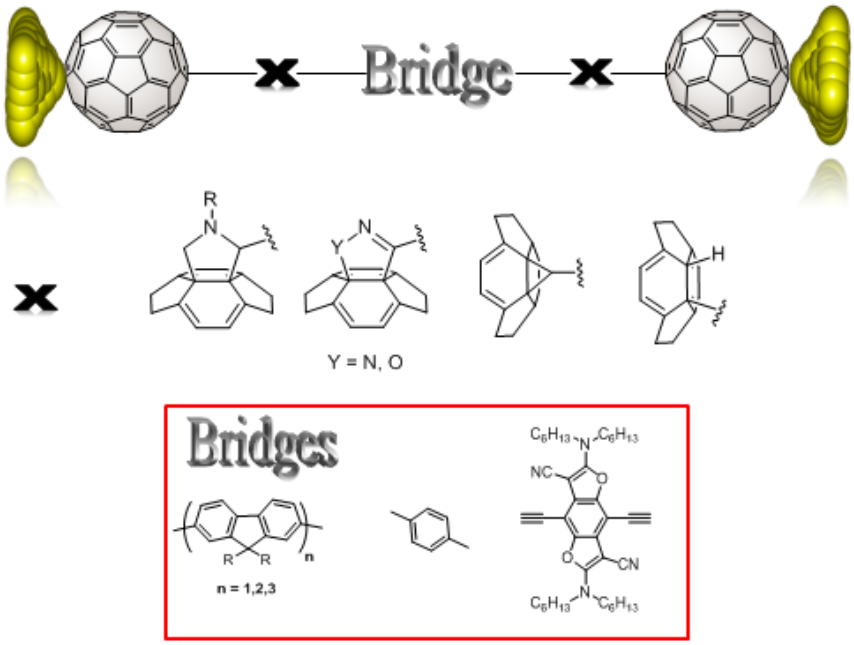

Figure 2. Design of a dumbbell molecule based onto C_{60}, electro-active bridges and linkers **X**. The used connections are also shown.

An evaluation study of different linkers has been done either with heteroatoms or with carbon atoms, using fluorene as molecular bridge. In particular, we have synthesized dumbbells with pyrrolidine, isoxazoline and pyrazoline linkers to carry out a comparison, among these five member heterocycle linkers, on the electronic effects. Using carbon atoms as linkers, we have synthesized the cyclopropane and the single bond dumbbell molecules. In such a way, the stiffness, linearity and symmetry of the molecule have been improved, which are important parameters at the moment of the conductance measurements. Moreover, the progressive reduction of carbon sp^3 as spacer

between C_{60} and fluorene units could improve the electronic communication. To clarify this point, preliminary DFT electronic transmission calculations shows that the single bond molecule seems to be the most prominent at every value of bias (potential difference, *V*) applied, followed by CV and UV-vis experiments. Such experiments demonstrate a better electronic communication for the cyclopropane linker between C_{60} and the bridge, when compared with the pyrrolidine linker. We suggested that the double bond nature of the cyclopropane ring is responsible for this behaviour. This important aspect has also been corroborated by previous works.[18] The conductance values of cylopropane dumbbell molecule[19] under ambient conditions have been measured through two different STM operational modes. The first one consists in depositing the molecule over gold surface and approaching the STM tip over one fullerene, easy to be visualized. The conductance value of 10^{-2} G_0 has been registered and it has been ascribed to the electron transfer across the half of the molecular wire considering that the tip is touching the fluorene surface. This idea has been underlined by DFT studies over the geometry of the molecular junction. Another value of 10^{-4} G_0 has been registered only once the molecule was hanged to the STM gold-tip and vertically approached to the gold crystal (surface). Such conductance value has been ascribed to the electron migration across the whole molecule when vertically covers the nanogap between the metal leads. The better plateau observed for this operational mode, in terms of length and shape, is a consequence of a sharpest shape of the STM tip, made by the anchoring of one molecule on the tip itself (better resolution in the images too).

After the deep treatment of the linker evaluation, we moved our attention over the bridge function, employing two different approaches for the synthesis of new dumbbells: i) the elongation of the fluorene bridge up to three units directly linked one to each other and, ii) the substitution of fluorene with aryl and BDF cores. Thereafter, we want to give just some comments about these choices.

The elongation of the bridge has been thought for the β value study. Such parameter is independent of the molecular wire-length and, it is correlated to the chemical nature of the bridge, *i.e.* fluorenes bridge has a β value of 0.09 $Å^{-1}$. The olygomers made by two and three fluorenes have been sandwiched

within two C_{60} stoppers, using the direct bond functionalization. It has been chosen on the better transmission property, supported by DFT calculations at least for the monofluorene dumbbell.

The second strategy employed foresaw the synthesis of aryl dumbbell molecule to mark the effect of a size-reduced bridge compared with fluorene in conductance experiments. In the case of BDF core, its insertion in dumbbell molecular structures with pyrrolidine and cyclopropane linker connection paved the way to use an interesting core (already known in organic electronics for other kinds of devices) for photoinduced electron transfer processes. It has been demonstrated to be a good core for the stabilization of the radical cation after the excitation of the molecule. The radical anion over fullerene has been also sketched as a consequence of charge separation process. Furthermore, a deep analysis over the optical properties of such derivatives have been carried out using UV-vis technique.

Currently, most of the synthesized molecules in this Memory are under studying either using STM or MCBJ techniques for the experimental characterization of their conductance values.

Photovoltaic results

Diphenylmethano[60]fullerenes (DPMs, Figure 3) are derivatives with cyclopropane functionalization hanging two aryl moieties with alkoxy chains of different length (the number 6 and 12 are referred to the number of carbon forming the alkyl chain). They are used as acceptors in polymeric solar cells.[20]

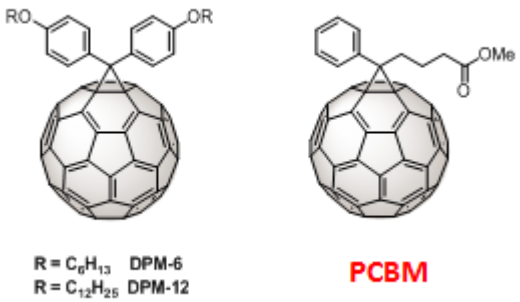

Figure 3. Diphenylmethano[60]fullerene (DPM) and PCBM molecule structures.

When compared with PCBM, DPMs showed always a higher value of V_{OC}, despite their same reduction potential values. The lower performance of DPM-6 *vs* PCBM has been accounted for by the different crystallinity degree, observed through AFM. A more deep explanation to this result has been found by considering the LDOS of the acceptor molecules in the mixture blend with the P3HT.[21]

Conclusions

Dumbbell-type molecular wires based on C_{60} stoppers as anchoring groups have been synthesized for further electron transport study through STM and MCBJ techniques. A deep analysis of the conductance properties of some dumbbells have been carried out, either experimentally or theoretically. The improvement of electronic communication between fullerene and the bridge has been realized using cyclopropane linker instead of pyrrolidine. The visualization of the dumbbell molecule over surface denotes its stability before and after the measurements with STM technique. The implementation of

further π-conjugated bridge was useful for the study of this new systems in photoinduced electron transfer processes. Moreover, a large discussion has been done regarding the application of some C_{60} derivatives in photovoltaic devices, field in which C_{60} is currently used as a fundamental and singular acceptor molecule.

Bibliography

1. V. Balzani, *Small* **2005**, *1*, 278.
2. a) E. G. Emberly, G. Kirczenow, *Phys. Rev. B* **1998**, *58*, 10911; b) A. Nitzan, M. A. Ratner, *Science* **2003**, *300*, 1384; c) W. B. Davis, W. A. Svec, M. A. Ratner, M. R. Wasielewski, *Nature* **1998**, *396*, 60.
3. A. Ulman, *Chem. Rev.* **1996**, *96*, 1533.
4. L. Venkataraman, J. E. Klare, I. W. Tam, C. Nuckolls, M. S. Hybertsen, M. L. Steigerwald, *Nano Lett.* **2006**, *6*, 458.
5. B. Kim, J. M. Beebe, Y. Jun, X. Y. Zhu, C. D. Frisbie, *J. Am. Chem. Soc.* **2006**, *128*, 4970.
6. C.-H. Ko, M.-J. Huang, M.-D. Fu, C.-h. Chen, *J. Am. Chem. Soc.* **2009**, *132*, 756.
7. S. Yasuda, S. Yoshida, J. Sasaki, Y. Okutsu, T. Nakamura, A. Taninaka, O. Takeuchi, H. Shigekawa, *J. Am. Chem. Soc.* **2006**, *128*, 7746.
8. a) B. Q. Xu, X. Y. Xiao, N. J. Tao, *J. Am. Chem. Soc.* **2003**, *125*, 16164; b) M. Kamenetska, S. Y. Quek, A. C. Whalley, M. L. Steigerwald, H. J. Choi, S. G. Louie, C. Nuckolls, M. S. Hybertsen, J. B. Neaton, L. Venkataraman, *J. Am. Chem. Soc.* **2010**, *132*, 6817.
9. Y. S. Park, A. C. Whalley, M. Kamenetska, M. L. Steigerwald, M. S. Hybertsen, C. Nuckolls, L. Venkataraman, *J. Am. Chem. Soc.* **2007**, *129*, 15768.
10. a) D. M. Shewchuk, M. T. McDermott, *Langmuir* **2009**, *25*, 4556; b) L. Laurentius, S. R. Stoyanov, S. Gusarov, A. Kovalenko, R. Du, G. P. Lopinski, M. T. McDermott, *ACS Nano* **2011**, *5*, 4219.
11. L. A. Zotti, T. Kirchner, J. C. Cuevas, F. Pauly, T. Huhn, E. Scheer, A. Erbe, *Small* **2010**, *6*, 1529.
12. F. Chen, X. L. Li, J. Hihath, Z. F. Huang, N. J. Tao, *J. Am. Chem. Soc.* **2006**, *128*, 15874.
13. Y. Xing, T.-H. Park, R. Venkatramani, S. Keinan, D. N. Beratan, M. J. Therien, E. Borguet, *J. Am. Chem. Soc.* **2010**, *132*, 7946.
14. a) Y. Guo, M. Kiguchi, J. Zhao, K. Murakoshi, *Chem. Phys. Lett.* **2009**, *477*, 189; b) C. Joachim, J. K. Gimzewski, R. R. Schlitter, C. Chavy, *Phys. Rev. Lett.* **1995**, *74*, 2102; c) T. Böhler, A. Edtbauer, E. Scheer, *Phys. Rev. B*

2007, *76*, 125432; d) H. Park, J. Park, A. Lim, E. Anderson, A. Alivisatos, P. McEuen, *Nature* **2000**, *407*, 57.
15. C. A. Martin, D. Ding, J. K. Sørensen, T. Bjørnholm, J. M. van Ruitenbeek, H. S. J. van der Zant, *J. Am. Chem. Soc.* **2008**, *130*, 13198.
16. I. F. Torrente, K. J. Franke, J. I. Pascual, *J. Phys.: Condens. Matter* **2008**, *20*, 184001.
17. E. Leary, M. T. González, C. van der Pol, M. R. Bryce, S. Filippone, N. Martín, G. Rubio-Bollinger, N. Agraït, *Nano Lett.* **2011**, *11*, 2236.
18. a) M. Eiermann, R. C. Haddon, B. Knight, Q. C. Li, M. Maggini, N. Martín, T. Ohno, M. Prato, T. Suzuki, F. Wudl, *Angew. Chem. Int. Ed.* **1995**, *34*, 1591; b) T. Ohno, N. Martín, B. Knight, F. Wudl, T. Suzuki, H. Yu, *J. Org. Chem.* **1996**, *61*, 1306; c) F. B. Kooistra, T. M. Leuning, E. Maroto Martinez, J. C. Hummelen, *Chem. Comm.* **2010**, *46*, 2097.
19. K. Gillemot, C. Evangeli, E. Leary, A. La Rosa, M. T. González, S. Filippone, I. Grace, G. Rubio-Bollinger, J. Ferrer, N. Martín, C. J. Lambert, N. Agraït, *Small* **2013**, DOI:10.1002/smll.201300310.
20. H. J. Bolink, E. Coronado, A. Forment-Aliaga, M. Lenes, A. La Rosa, S. Filippone, N. Martin, *J. Mater. Chem.* **2011**, *21*, 1382.
21. G. Garcia-Belmonte, P. P. Boix, J. Bisquert, M. Lenes, H. J. Bolink, A. La Rosa, S. Filippone, N. Martín, *J. Phys. Chem. Lett.* **2010**, *1*, 2566.

ANNEX 2-RESUMEN

NUEVAS APLICACIONES DEL [60]FULLERENO EN NANOCIENCIA

Introducción

Las palabras *Nanociencia* y *Nanotecnología* están tomando progresivamente más importancia en nuestra vida cotidiana. Si pensamos por un momento que Intel ha sacado un procesador de 32 nm, podemos entender como la tecnología se está moviendo en esta dirección. El termino *"nano"* representa algo muy pequeño que, para ser preciso, es del orden de 10^{-9} m. La *Nanociencia* es una rama de la Ciencia que tiene el objetivo de conseguir este tamaño simplemente construyendo materiales y dispositivos ultra pequeños, en torno a 1-100 nm, con la posibilidad de poder manipular moléculas o átomos. La *Nanotecnología* puede ser considerada como la aplicacción directa de la *Nanociencia*. Hasta hoy, se han dado muchos significados a estas dos palabras pero, los más precisos, segun Balzani en un trabajo publicado en 2005[1] donde se hace una clasificación de las palabras en *Nano*, *Ciencia* y *Tecnología* explicando el significado de cada una de ellas.

Las dos ramas nacen como medio de desarrollo en la vida cotidiana (los progresos de la ciencia se manifiestan en el desarrollo de la tecnología) y eso se puede comprobar en los objetos que nos rodean: ordenadores, dispositivos electrónicos para imágenes, libros electrónicos, paneles solares, sin olvidar su progreso en campos como la medicina, la agricultura, la cosmética y la industria alimentaria.

Richard Feymann propuso la existencia de un mundo aún más pequeño de lo explorado y fácil de lograr a través de procesos de miniaturizacion mediante el enfoque "top-down" y "bottom-up". Una idea de como va evolucionando la *Nanotecnología* viene dada por la ley de Moore. La misma deja claro que la evolución electrónica de circuitos basados en silicio, tienden a ser siempre más pequeños, a medida que pasan los años. Esto es posible gracias al enfoque "top-down" que, sin embargo, tiene un limite por debajo de los 100 nanometros[2] debido al limite de la longitud de onda utilizada en el proceso de litografia y técnicas similares. Por esa razón, los químicos están cambiando su idea de hacer moléculas y organizarlas en superficies para acercarse a la formación de estructuras desde abajo (enfoque "bottom-up").

A pesar de todo, la *Ciencia* y la *Tecnología* siempre han caminado juntas y lo seguirán haciendo tambien en el mundo *"nano"* donde las características de los materiales pueden cambiar sustancialmente. Un ejemplo muy reciente es el grafeno (Premio Nobel en Física en el año 2010 a sus descubridores André Geim y Kostantin Novoselov): este material es un aislante en la escala microscópica en forma de grafito y, se convierte en conductor en el mundo nanoscópico. Además, la posibilidad de poder manipular las moléculas y los átomos según lo que había previsto Richard Feyman, es ahora un hecho real gracias a dos técnicas como son el AFM (microscópia de fuerza atómica) y el STM (microscópia de efecto túnel).

Dentro de la gran esféra de conocimiento de la *Nanociencia* y *Nanotecnología*, la electrónica orgánica molecular representa un gran componente de importancia relevante. De hecho, muchos temas cientificos pertenecen a este campo. En nuestro grupo, en particular, nos hemos centrado en la síntesis y caracterización química de estructuras de tipo cable molecular basados en C_{60}. La gran ventaja de su empleo en el campo de la electrónica molecular orgánica es debido a sus propiedades opticas[3], electrónicas[4] y fotofisícas[5] que hacen de ella una molécula única. Su gran capacidad de aceptar hasta seis electrones, siendo así una molécula prometedora como material de tipo *n*, ha sido analizada mediante voltamperometría cíclica.[6] Además, su baja energía de reorganización hace del C_{60} una molécula única en procesos de transferencia electrónica fotoinducida.[7]

El término "cable molecular" ha sido empleado en la bibliografia tanto en química, como en física y ciencia de materiales. En algunos casos, se describe un sistema con un comportamiento muy específico, en otros, se refiere simplemente a la forma de la molécula. Un cable molecular es, por definición, el componente más sencillo de un circuito eléctrico, conectado entre dos depósitos de electrones como por ejemplo dos placas de metal.[8] Más a menudo, nos referimos a su comportamiento como una molécula capaz de dejar pasar corriente eléctrica entre dos electrodos de metales;[9] en otros casos, hablamos de cables moleculares como un dispositivo que es capaz de conducir en un régimen particular, donde la dependencia con la distancia de la transferencia electrónica resulta ser muy débil.[10] Más importante que la nomenclatura es la función que deben desempeñar estos cables moleculares, los cuales deben ser

sistemas robustos y capaces de transportar electrones de forma direccional a distancias nanométricas. Debido a que pueden ser modificados químicamente en etapas previas y a la gran versatilidad que presentan, ofrecen un potencial similar al de los metales y los semimetales.

En general, para estudiar el comportamiento de los cables moleculares, se utilizan dos aproximaciones diferentes. La primera es la "transferencia electrónica fotoinducida" típica de sistemas dotados de una molécula dadora, un puente y un aceptor de electrones (DBA) que actúan como cables moleculares.[11] En este caso, los depósitos de electrones se encuentran en la misma molécula. Esta primera aproximación nos da un enfoque más macrodimensional debido a que el análisis se hace en disolución. El segundo enfoque de tipo nanodimensional está basado en estudios de conductancia usando dos técnicas recientes, el STM y MCBJ. Es imprecindible discutir sobre cada una de las dos técnicas, puesto que serán ampliamente utlizadas en esta Memoria.

La tecnica de STM tiene más o menos la misma edad que el C_{60}; fue introducida hace 25 años por parte de Binnig y Rohrer[12] en los laboratorios de investigación de IBM en Zurich (Figura 1), recibiendo el Premio Nobel en el 1986 por este invento. El STM nació como un aparato para la visualización de átomos y moléculas y, en la actualidad, se ha extendido al estudio de conductancia, sea en líquido o en sólido, a través de una molécula o más moléculas organizadas sobre la superficie. El principio de funcionamiento del STM está basado en el "efecto túnel", conocido en la mecánica cuántica, donde, una partícula de pequeña dimensión puede atravesar una barrera energética más alta de su propia energía cinética (lo que supone una importante diferencia con la mecánica clásica). La probabilidad de que un electrón pase de un lado al otro de la unión genera la corriente eléctrica del circuito que está directamente relacionada con la masa del electrón, la barrera energética y la amplitud de la nano-unión.

El STM está constituido por un soporte metálico (por ejemplo oro) y una punta de distintos materiales metálicos que tiene que ser igual al metal de la superficie en el estudio de conductancia o distinto en estudios de imágenes de superficie. El STM puede ser ajustado para que trabaje de dos maneras distintas: en "modo de corriente constante" y en "modo de altura costante". Los dos dan una idea de como es el comportamiento real de la molécula sobre la superficie y de su conductividad. No obstante, aunque el STM está teniendo mucha aplicación, existe una limitación importante: es, una técnica que no da la información química de la muestra bajo análisis.

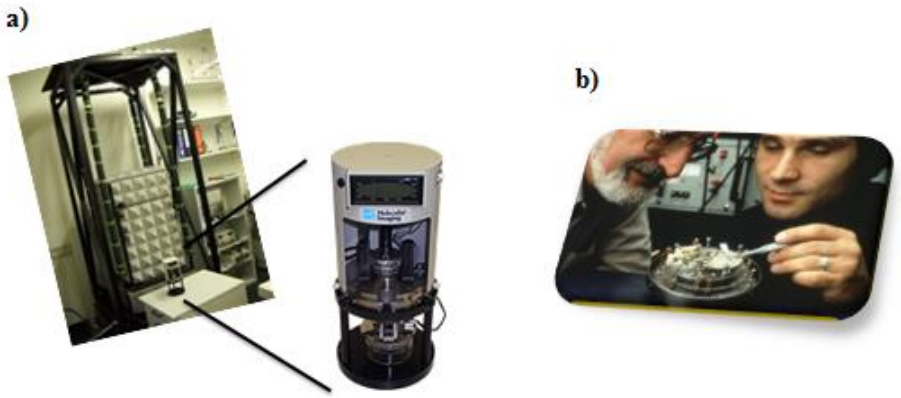

Figura 1. a) microscopio de STM con jaula antivibraciones de la Universidad de Berna; b) Binnig y Rohrer trabajando sobre el STM.

Más o menos la misma edad tiene la técnica de MCBJ. En 1985 fue introducida por parte de Moreland y Ekin usando un hilo de Nb-Sn como aleación metálica. Solamente con Muller *et al.* y Van Ruitenbeek, la MCBJ se utilizó para hacer medidas de conductancia.[13] La MCBJ es una plataforma metálica fácilmente plegable donde el hilo metálico conductor (por ejemplo oro) está fijado con una resina dejando libre pocos milimetros para que se pueda crear la unión, en primer lugar cortando el cable manualmente con un microscópio óptico y, posteriormente, creando la verdadera unión con un motor piezoelectrico propio del aparato. La MCBJ puede ser utilizada para medidas de "conductancia-distancia" o de "corriente-voltaje".

Durante las medidas de conductancia-distancia, solamente las trazas abiertas del circuito eléctrico vienen registradas, es decir, cuando el cable de oro está roto y se genera una unión molécular. Las medidas se hacen en un tiempo razonable de aproximadamente veinte minutos donde se registran miles y miles de trazas de conductancia. La Figura 2 muestra un ejemplo real de una sola medida de conductancia para una molecula lineal.

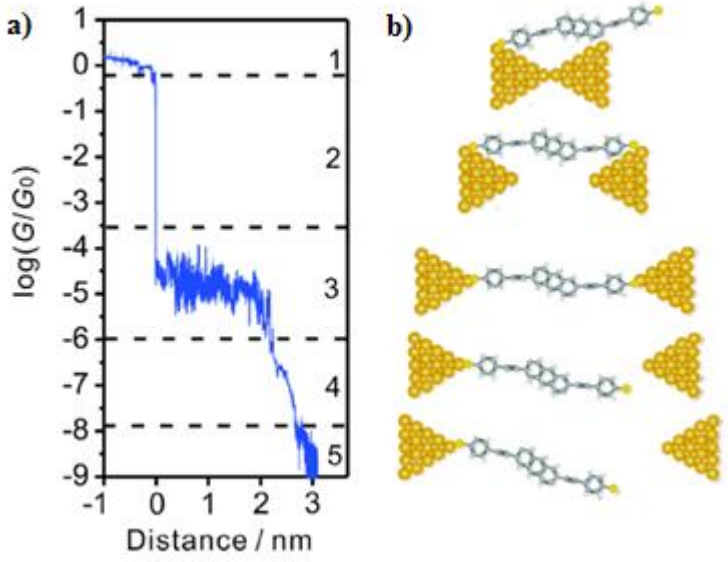

Figura 2. a) Ejemplo de gráfico de medida de conductancia obtenido con MCBJ; b) dibujo esquematico monstrando, paso a paso, la formación de la unión unimolécular entre los electrodos de oro.

La misma traza se puede dividir en distintas regiones. La region **1** se refiere al contacto oro-oro entre las dos extremidades. Típicamente, se puede notar esta unión metálica en el rango entre 0 y 1 (log G/G_0) con un ligero descenso que varía con la distancia; eso indica claramente que la unión se está reduciendo hasta un valor de 1 G_0 (*G cero*, $G_0=2e^2/h=1/12.9k\Omega$), lo que indica que la unión está hecha solo para un átomo de oro. La region **2** indica un descenso por el efecto túnel donde la molécula no está conectada todavía. En la region **3** se puede destacar la formación de la unión molecular debida a la presencia de un "plateau" de conductancia cuya longitud está en concordancia con la longitud

de la molécula. Las fluctuaciones son debidas a cambios de configuraciones de la molécula dentro la unión y también al ruido del aparato. Las regiones **4** y **5** indican la ruptura de la unión molécular y el efecto túnel es nuevamente observado con una descenso pronunciado del valor de conductancia. Dentro de las ventajas podemos destacar su uso a temperatura ambiente, la rápida respuesta de las medidas y la posibilidad de trabajar con concentraciones del orden de 10^{-3} M, seguramente muy alta para la técnica de STM. Por otro lado, las desventajas, comparándola con STM, son la imposibilidad de saber cuantas moléculas se están midiendo y la forma imperfecta del electrodo. Una vez definidas las técnicas que hemos utlizado para la caracterización fisíca de nuestras moléculas, es útil entender como las moléculas se pueden anclar a la superficie de oro de un STM o de una MCBJ. Para ello, hay que introducir un nuevo término: el "grupo de anclaje". La naturaleza química y la capacidad de los grupos de anclaje para poder anclarse a superficies metálicas deja abierto un tema importante sobre el estudio de moléculas sencillas como cables moleculares. Tanto la naturaleza de esta parte de la molécula como la del puente juegan un papel fundamental en el estudio del transporte de electrones a través la molécula (Figura 3).

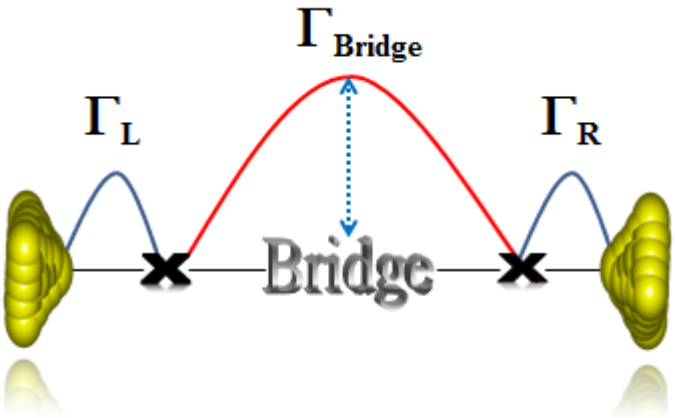

Figura 3. Representación esquematica de las barreras energéticas implicadas en un proceso de unión entre el cable molécular y los electrodos de oro. Las barreras energéticas están relacionadas tanto con la naturaleza del puente como la de los grupos de anclaje.

La correcta elección del grupo de anclaje es un desafío para los químicos orgánicos. Se trata de encontrar un grupo de anclaje que tenga una buena estabilidad y una alta transparencia de contacto con el metal, debiendo

presentar ambas propiedades. Para hacer esto, es importante decidir bien el grupo que se está utilizando en función de su "acoplamento electrónico" con el metal, definido tambien como "contacto metal-molécula" (Γ_L y Γ_R).

Este parámetro es un coeficiente que representa una barrera energética correcta, según el tipo de grupo de anclaje. Los electrones, para pasar de un metal al otro, tienen que sobrepasar esta barrera energética, asegurando así una cierta comunicación electrónica. Por ejemplo, los tioles tienen menor acoplamento electrónico que el ciano y eso da lugar a un mejor comportamiento como grupo de anclaje. La estabilidad de un grupo de anclaje puede ser vista en términos de tiempo de vida de la unión molecular (Figura 4). Eso es fácil de demostrar durante las medidas de STM: cuando un "plateau" de conductancia viene registrado, su longitud está directamente relaccionada con el tiempo de vida de la unión molecular según la fórmula que deriva de la física clásica ($L = v\Delta t$).

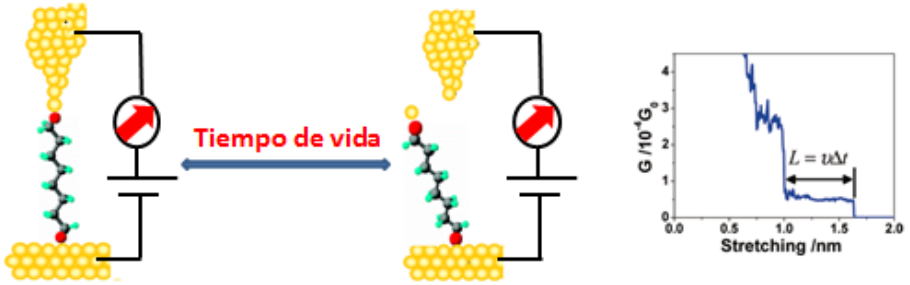

Figura 4. Proceso de formación de la unión unimolecular y su tiempo de vida. Este último está relacionado con la longitud del "plateau" de conductancia.

Es entonces necesario dar una panorámica general de todos los grupos de anclaje descritos en bibliografia para medidas de conductancia. Por esa razón, se han dividido en tres grupos:

1. Monodentados: tioles,[14] aminas,[15] ciano (isocianato),[16] isotiocianato,[17] compuestos de selenio,[18] piridina,[19] fosfina[20], sales de diazonio[21]
2. Bidentados: nitrocompuestos,[22] ácidos carboxílicos,[23] ácidos ditiocarboxílicos[24]
3. Multidentados: C_{60}

En esta Memoria se ha realizado una amplia discusión de la eficacia de cada uno de los grupos de anclaje, haciendo una comparativa entre ellos. Además, se

ha definido la naturaleza del enlace con el oro para cada uno de los casos, su estabilidad y el consecuente estudio de la fuerza de ruptura del enlace así como las medidas de conductancia realizadas, en la mayoría de los casos, usando STM. Por otro lado, se han obtenido conclusiones acerca de moléculas sencillas, como pueden ser alcanos o bifenilos.

La introducción del C_{60} en esta temática resultaría interesante dado que gracias a su geometría esférica, el C_{60} ha sido considerado como un grupo de anclaje multidentado. Este puede dar lugar a multi-interaciones con los átomos de oro. Antes de entrar en los detalles, comentaremos su estabilidad sobre superficies metalicas, en particular sobre oro.

Recientemente, la molécula de C_{60} ha demostrado una buena afinidad con superficies como Ag,[25] Cu[26] y Pt.[27] Su immovilización ha sido posible trabajando a bajas temperaturas y su visualización gracias a técnicas de STM. También con el oro (Au), el C_{60} demuestra una buena estabilidad y eso es de importancia fundamental para nuestros estudios. Por ejemplo, Pascual *et al.*,[28] han immovilizado el C_{60} en una terraza de un cristal de oro usando un STM de alta resolución, a baja temperatura y condiciones de alto vacío. (Figura 5)

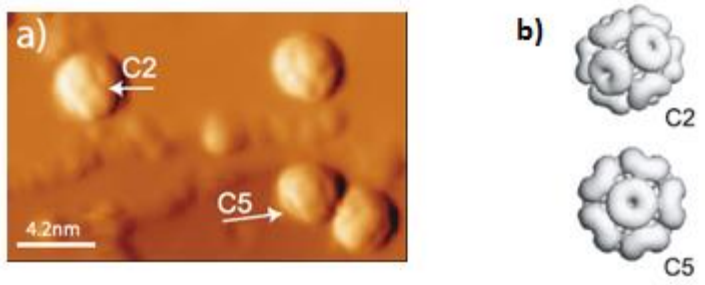

Figura 5. Imagen de unidades de C_{60} de alta resolución de STM a baja temperatura y en condiciones de alto vacío. En esta imagen se puede distinguir dos simetrías distintas de la molécula sobre la superficie.

Aunque la interacción entre el oro y el C_{60} es más débil que con otros metales, la molécula por sí misma presenta una buena energía de absorción (40-60 Kcal mol^{-1}). Los valores de conductancia de los C_{60}/Au, C_{60}/Ag, C_{60}/Pt son 0.3 ± 0.1 G_0, 0.5 ± 0.1 G_0 y 0.7 ± 0.1 G_0, respectivamente. En el caso de Cu/C_{60} este valor es 0.25 G_0.[29]

Para elucidar el modo de anclaje del C_{60} con la superficie de oro, se han realizado muchos estudios teóricos. La coordinacción del oro con la superficie del C_{60} es un fenómeno bastante complicado y basándose en resultados de IR, Lyon y Andrews han sugerido que el C_{60} se pueda anclar a través del anillo pentagonal.[30] Pero, desde el punto de vista teórico, el punto de anclaje puede ser representado por parte de distintas zonas de la jaula del C_{60}.[31] Al llevar a cabo los cálculos, no solamente el C_{60} cubre un papel importante. También la superficie de oro juega su parte en cuanto al resultado final de conduntancia.

Por esa razón parece que haya un efecto "cooperativo" de los átomos de oro en el valor de conductancia sobre el C_{60} anclado entre dos electrodos. En general, se emplean dos modelos de anclaje que se usan para entender el contacto átomico entre C_{60} y la superficie de oro. La Figura 6 muestra los dos: electrodo nanocable y electrodo atómico que dan origen a distintos valores de conductancia (2.18 G_0 frente a 0.027 G_0), evidencia del efecto cooperativo de los átomos de oro,[32] con una diferencia de unos dos órdenes de magnitud.

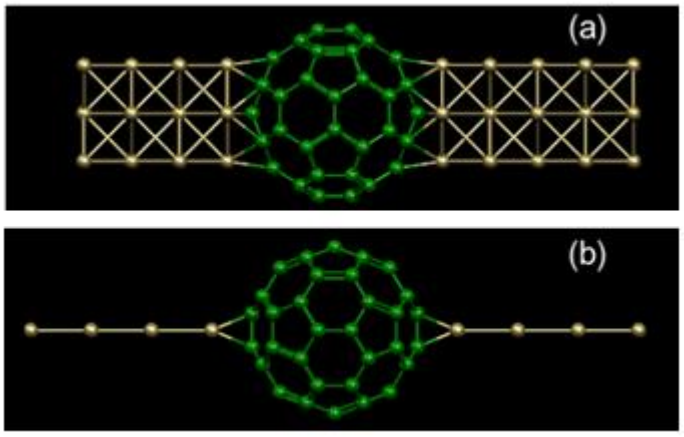

Figura 6. a) Configuración de nanocable con una unión de C_{60} y b) configuración a cadena de átomos de oro con el C_{60}.

Las conclusiones teóricas hechas para los dos modelos necesitan ser comprobadas experimentalmente. La posibilidad de que el C_{60} interaccione con uno o más átomos de oro está en la curvatura de la propia molécula. La interacción múltiple está relacionada con la capacidad de rotación del C_{60} sobre

la superficie.[33] A través de la técnica de STM, el C_{60} ha sido comprimido y descomprimido evidenciando distintos valores de conductancia debidos a cambios mecánicos de la nube electrónica fullerénica.[34] Se ha demostrado con STM que cuando el bias (diferencia de potential) aplicado es cero, el C_{60} se encuentra pegado a una protuberancia de la superfice de oro. Cuando el potential aplicado es distinto de cero (nos estamos moviendo de la condición de equilibrio) el fullereno salta sobre la punta de la protuberancia.[35] Debido a la gran variedad de métodos para depositar, analizar y medir el C_{60}, se han registrado muchos valores de conductancia para esta molecula,[36] lo que nos abre una nueva vía de interés científico para una posible futura aplicación como cable molecular donde el propio C_{60} actuaría como "grupo de anclaje". Eso se basa en sus propiedades que lo hacen único en su genero; además, la posibilidad de obtener imágenes de la molécula apoyado en la superficie como si fuese un "faro" antes y después de una medida de conductancia, nos garantiza realizar medidas de manera que no sean al azar.[37] Esto resulta en una mejoría de la reproducibilidad del experimento, como se ha demostrado recientemente en medidas de MCBJ (Figura 7).[38]

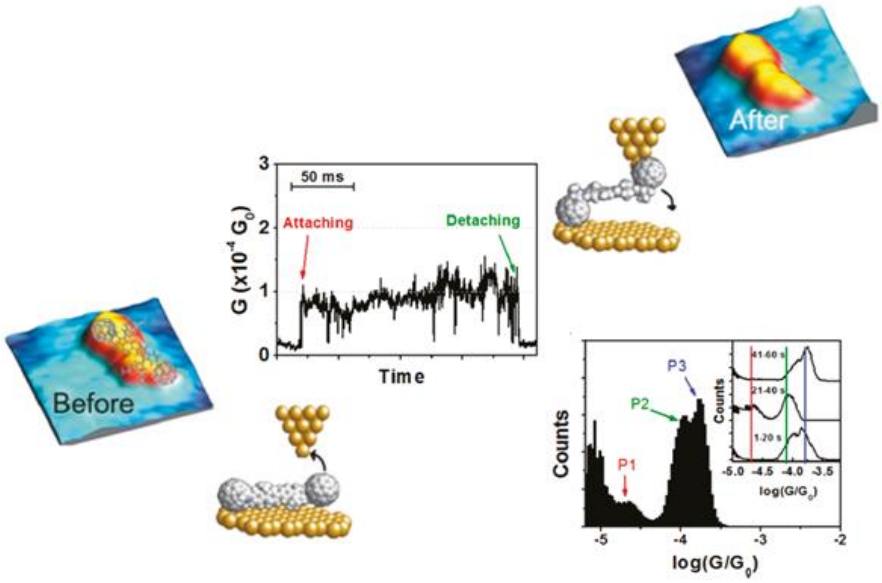

Figura 7. Formación de la unión unimolecular de un sístema tipo dumbbell mediante STM. Los picos de conductancia se muenstran en el histograma.

Entre las propiedades que hacen del C_{60} un buen grupo de anclaje, podríamos destacar las siguientes: i) la alta simetría, ii) la extensa superficie de contacto generada por varias interacciones débiles entre el orbital π del C_{60} y los átomos de oro, iii) la propiedad de ser un material de tipo *n* para el transporte de los electrones, iv) orientación molecular, relajación atómica de la molécula, buena afinidad con distintas superficies con un alto nivel de hibridación de los orbitales del fullereno sobre la superficie. Esta última propiedad genera un desplazamiento de la nube electrónica del fullereno hacia el oro y, por eso, puede ser vista como una retro-donación desde el C_{60} al electrodo, si consideramos que los electrones se mueven en sentido opuesto.

Como regla general, para obtener una alta conductancia necesitamos que se dá de manera simultanea una extensa hibridación y un extenso LDOS junto con una pequeña diferencia de energía entre la molécula y el metal. En el C_{60}, todas estas características se manifiestan.

Resultados y discusiones

Una vez establecido porqué el C_{60} es un buen candidato como grupo de anclaje, propusimos síntetizar una nueva colección de cables moleculares con forma de "dumbbell". Dado que el C_{60} se ancla bien a la superficie de oro con buena estabilidad, se pensó en entender de alguna manera cual es el mecanismo que está detrás de la transferencia electrónica en medidas tipo STM o MCBJ. Así, el C_{60} ha sido unido a diferentes puentes moleculares (bridge en la figura de abajo) a través de distintas conexiones (**X** en la Figura 8).

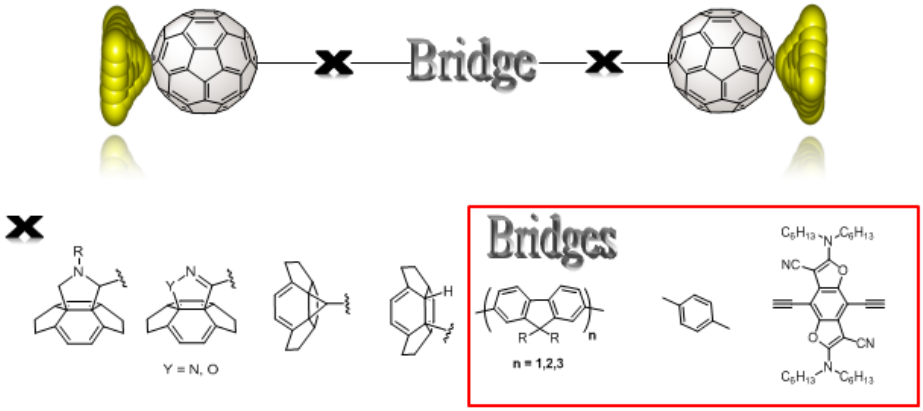

Figura 8. Representación de un cable molécular usando unidades de C_{60} como grupos de anclaje y distintos puentes. Las uniones covalentes entre los anclajes (C_{60}) y el puente se muestran como **X.**

Para empezar, nos fijamos en el empleo como puente de una molécula plana y π-conjugada como el fluoreno para favorecer el transporte de electrónes a través de su sistema π. Además, el fluoreno es una molecula muy versatil que se puede modificar químicamente y tratar en función del fin propuesto. En efecto, la funcionalización en la posición 9 permite una mejoría en la solubilidad del cable final y no va a influir el transporte de electrónes porque se encuentran dispuestas de manera perpendicular al plano π del fluoreno. Además, la funcionalización de las posiciones 2 y 7 garantiza una amplia posibilidad de productos finales gracias a las transformaciones químicas. De esta manera, un fluoreno funcionalizado de manera adecuada ha sido anclado al C_{60} mediante un anillo de pirrolidina, ciclopropano y mediante un enlace sencillo. Las dos primeras funcionalizaciones son resultados de una doble

reacción de cicloadición sobre un doble enlace del C_{60}: en el primer caso a través de la reacción de Prato[39] que da lugar a la formación de productos estables y fácilmente manejables, la segunda a través de una reacción de Bamford-Stevens donde el intermedio de reacción ha sido generado *in situ*. Esta molécula ha sido ampliamente estudiada como demuestran los resultados obtenidos. La tercera molécula tipo dumbbell ha sido sintetizada a través del uso de un metal de transición, el rodio (Rh) según un esquema síntetico propuesto por parte de Itami *et al*.[40] Basándonos en los primeros dos dumbbells, hemos demostrado a través de la voltamperometría cíclica y de la espectroscopia ultravioleta que el ciclopropano mejora la comunicación electrónica entre el C_{60} y el fluoreno. Este aspecto está de acuerdo con el hecho de que el ciclopropano pueda actuar como un doble enlace extendiendo así la conjugación al sistema C_{60}/fluoreno/C_{60}. Wudl *y col.* han descrito de una "hiperconjugacción" entre el ciclopropano y la nube π del C_{60}[41] que apoya nuestra idea. Los cálculos teóricos sobre los niveles LUMO de los dos dumbbells están de acuerdo con los datos experimentales. Así como estudios experimentales han demonstrado esta mejoría, estudios de DFT (Figura 9) sobre la transmision electrónica de los tres dumbbells obtenidos, ha dado lugar a interesantes conclusiones que apuntan hacia el mismo resultado experimental.

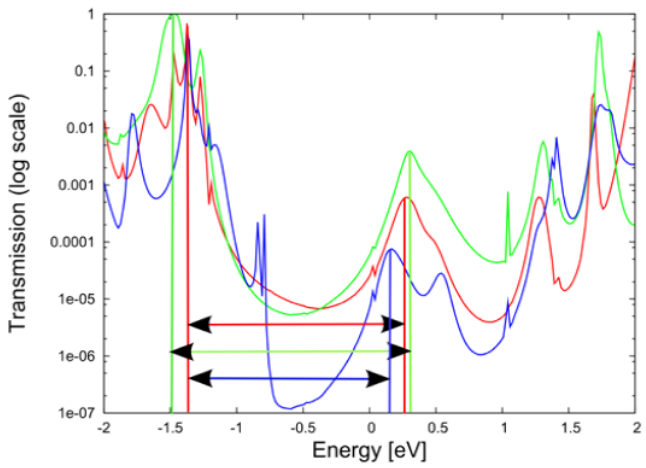

Figura 9. Curvas de transmisión calculadas para los dumbbells: pirrolidina **10b** (azul), ciclopropano **23b** (rojo) y de unión directa **25** (verde).

Según las curvas de transmisión, el dumbbell donde el fluoreno está directamente unido al C_{60} manifiesta un mejor comportamiento de cable molecular a cualquier diferencía de potencial aplicado. Dicha mejoría se nota también comparando el dumbbell con pirrolidina y con el ciclopropano.

Como se ha dicho anteriormente, el dumbbell con ciclopropano fue objeto de un profundo estudio en fase solida de conductancia mediante el uso del STM en condiciones ambientales.[42] Para la obtención de medidas de conductancia, se procede de la siguiente manera: una disolución muy diluida (10^{-10} M) de la molécula en triclorobenceno se deposita gota a gota sobre un substrato de oro. Una vez seca, se empieza a investigar la superficie en busqueda de moléculas aisladas (favorecidas por la muy baja concentración). Se ha visto que las moléculas prefieren estar en los escalones de la superficie donde la molécula se encuentra más estable por la interación química y fisíca con más átomos de oro. Está situación de estabilidad se conserva durante las medidas de conductancia como queda demostrado en la Figura 10.

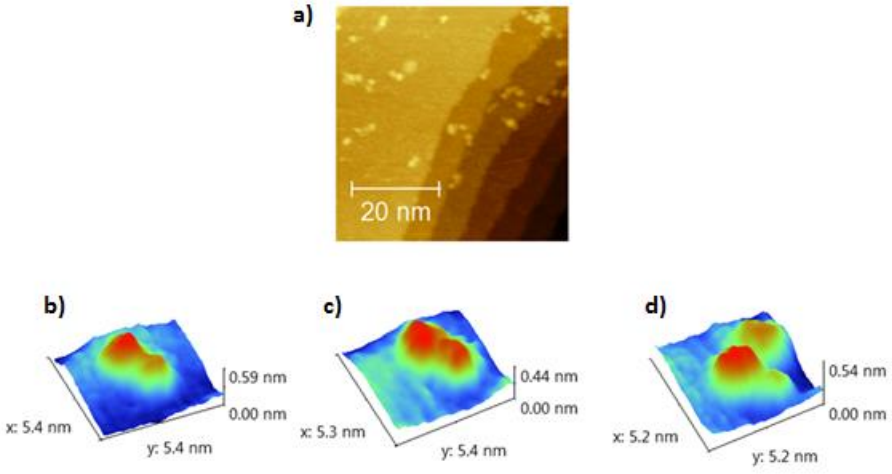

Figura 10. a) Imagen de una area expuesta durante 2 minutos obtenida de una disolución 10^{-10} M del dumbbell **23b** en 1,2,4-triclorobenceno. (b-c) Imágenes tomadas entre los ciclos de medidas. En b) y c) la molécula sigue en la misma posición, mientras que en d) se encuentra ligeramente rotada.

Las medidas de conductancia revelan dos valores a 10^{-2} G_0 y 10^{-4} G_0 que han sido obtenidos siguiendo dos procedimientos de análisis distintos. En el primer caso, después de que la molécula haya sido depositada sobre la superficie de oro, nos hemos acercado con la punta del STM sobre un C_{60}, fácilmente reconocible sobre la superficie. En este proceso, se ha registrado el primer valor que se ha imputado a la transferencía electrónica a través del propio C_{60} y del fluoreno, sin tener en cuenta la otra parte de la molécula. Estudios DFT han demostrado este detalle con un profundo análisis. El segundo valor, claramente menor, ha sido registrado después de que una sola molécula anclada a la punta se iba acercando a la superficie. Hasta que el contacto no se produce, no se observa ningún "plateau". Una vez formado el contacto, aparece un plateau bastante largo y estable debido al paso de los electrones a lo largo de todo el cable. La Figura 11 resumen estos datos.

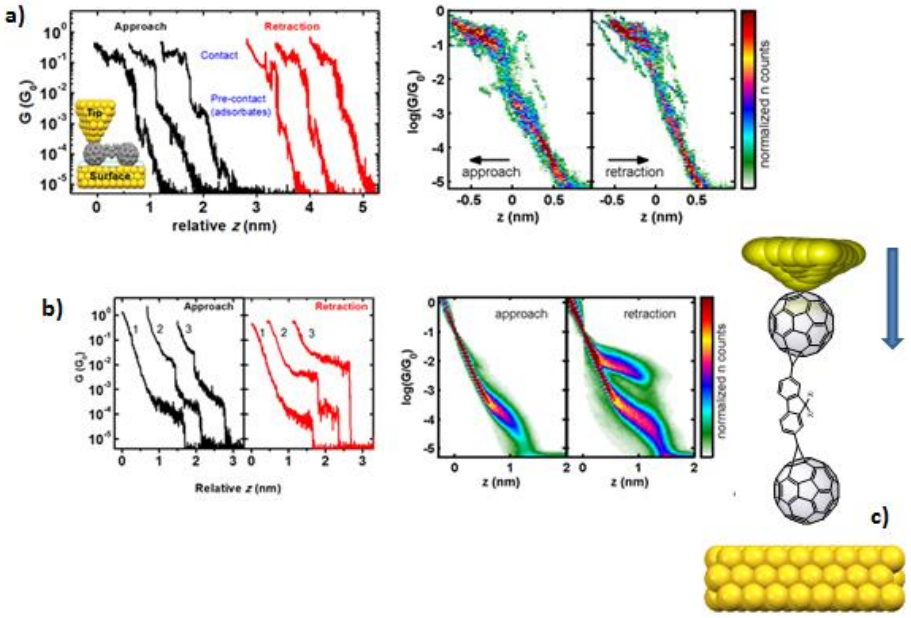

Figura 11. a) descripción del primer método: la molécula se ha depositado previamente sobre la superficie de oro y la punta del STM se va acercando para medir la conductancia; b) descripción del segundo método: la molécula ha sido anclada sobre la punta del STM y progresivamente acercada a la superficie de oro. Para ambos métodos, las medidas de conductancia están representadas mediante curvas individuales y en graficos 2D; c) representación equematica de la segunda aproximación.

Como otro planteamiento sintético, se pensó en conectar un solo fluoreno a través de anillos de cinco átomos con nitrógeno y oxígeno tales como pirrolidina, isoxazolina y pirazolina. La síntesis se ha llevado a cabo a través de unos precursores de fácil obtención donde el C_{60} se ha unido en la última etapa de la reacción, siguiendo los protocolos generales para la formación de estos anillos a través de reacciones de cicloadición. La funcionalización con isoxazolina y pirazolina nos ha permitido averiguar que existe un efecto de estabilización del LUMO de estas moléculas en comparación a la pirrolidina dumbbell, aproximandose de esta forma a los valores de LUMO del C_{60} no modificado. Este hecho parece ser debido a la presencia de un doble enlace y un heteroátomo cercano al doble enlace, en lo que es la estructura química del conector molecular (**X**).

Los mismos resultados se obtuvieron con moléculas dumbbells con el mismo conector pero espaciados mediante un puente arilo. Estas nuevas moléculas han sido diseñada para llevar a cabo, en primer lugar, estudios de movimiento sobre la superficie en colaboración con el IBM de Zurich. Los resultados se muestran en la Figura 12.

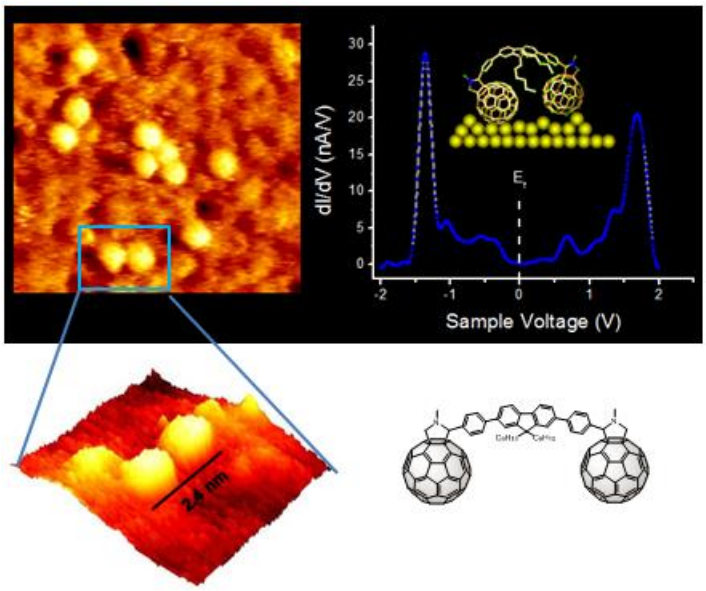

Figura 12. Imagen STM del dumbbell **16** depositado sobre oro. A la derecha, representación de la energía de los orbitales moléculares con respecto al nivel de energía de Fermi, E_F.

La presencia de un cluster de dos moléculas ha sido resaltada en esta imagen (el centro de la imagen de STM) y también una sola molécula aparece en la superficie de oro con una distancia (2.4 nm) cercana a la calculada por la molécula mostrada en la figura. La ampliación del puente por la presencia de dos arilos, deja mejor separados los fullerenos sobre la superifice para una mejor ubicación de la molécula y sus futuras medidas de conductancia. Hasta ahora, hemos mantenido siempre fijo el fluoreno como puente, cambiando la conexión entre C_{60} y fluoreno. ¿Que pasaría si nos planteamos la síntesis de dumbbells con una mayor distancia entre las dos unidades de fullereno? Y, ¿que resultados podríamos obtener de esta nueva serie de moléculas? Una respuesta a las dos preguntas ha sido la de sintetizar cables moleculares tipo dumbbell con dos oligomeros de fluoreno (respectivamente con 2 y 3 unidades directamente unidos entre ellos con un enlace sencillo). Para ello, se han utilizados distintas estrategias sintéticas. El dumbbell de difluoreno ha sido obtenido como se muestra en el Esquema 1:

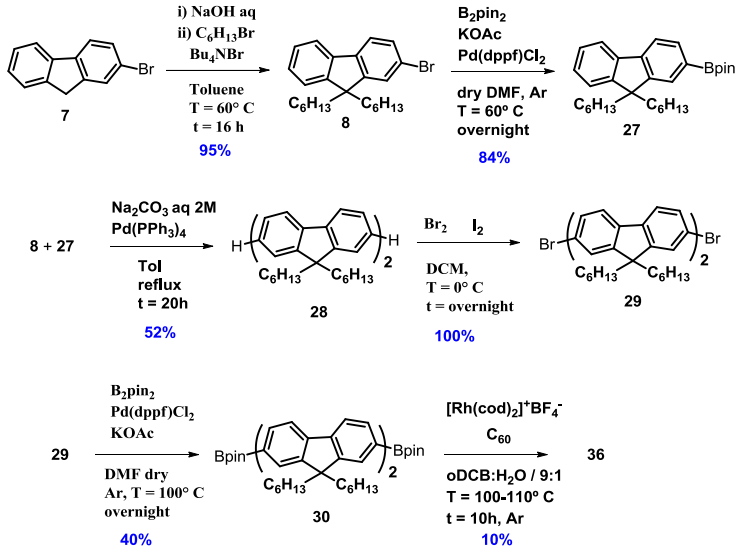

Esquema 1. Procedimiento síntetico para la obtención del dumbbell **36**.

Mientras que para la síntesis del dumbbell de trifluoreno se ha recurrido a un cambio en la estrategía síntetica que prevé la obtención del trimero del fluoreno con las posiciones 7 y 7' preparadas para una ulterior modificación química. El Esquema 2, resume todas las etapas.

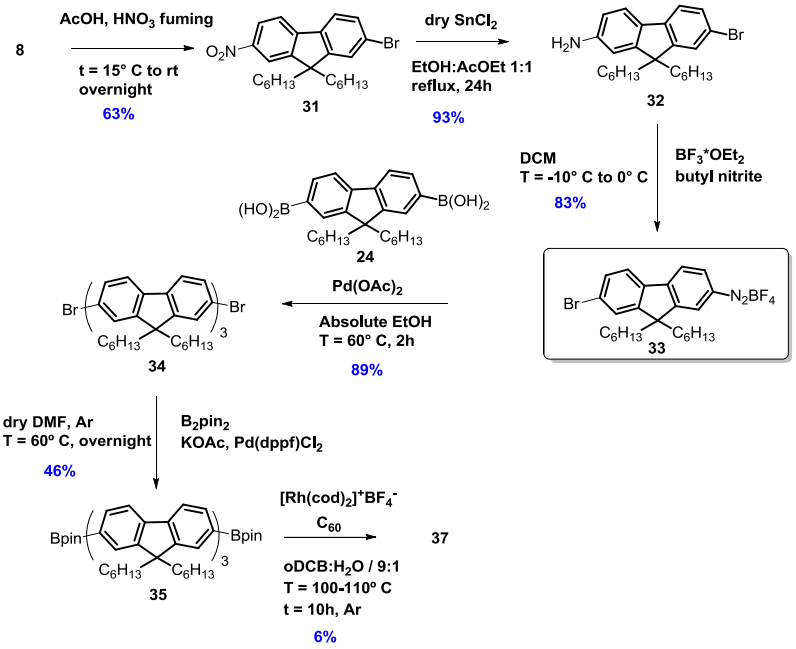

Esquema 2. Procedimiento síntetico para la obtención del dumbbell **37**.

Como se puede apreciar en los esquemas, para ambos dumbbell el precursor es un compuesto de fluoreno con boropinacolato como extremo terminal y reactivo. En efecto, esto ha sido empleado en una reacción catalizada por rodio para la obtención de dumbbells donde el C_{60} está directamente unido al fluoreno mediante un enlace sencillo que, según la teoria, representaría el mejor dispositivo para conducir electrones desde un electrodo al otro. Con esta nueva serie podriamos ser capaces de medir, también, el valor de β propio de la naturaleza del puente e independiente de la longitud, y compararlo con el ya publicado a través de cables moleculares dadores-puente-aceptores, con un valor de 0.09 $Å^{-1}$.[43]

Además de modificar los connectores, hemos sido capaces de unir dos unidades de C_{60} a otros dos tipos de puentes moleculares. Un solo arilo se ha colocado en el medio de la molécula para dar origen a un nuevo dumbbell con un puente limitado en tamaño de superficie π. En principio, esto nos sirve para compararlo con el mismo dumbbell pero dotado de fluoreno como puente.

También el benzodifurano (BDF) ha sido empleado como puente para estos sistemas electroactivos comunicando con el C_{60} a través de anillos de pirrolidina y ciclopropano. Sus propiedades electrónicas y fotofisícas han sido estudiadas a través de espectroscopia ultravioleta y de transferencia electrónica fotoinducida. Se ha podido determinar que el BDF es un buen puente en terminos de estabilidad del cation radical que se genera en el proceso así como la formación del anion radical en los análisis de PET (Transferencia de Electrones Fotoinducida) como se muestra en la Figura 13.

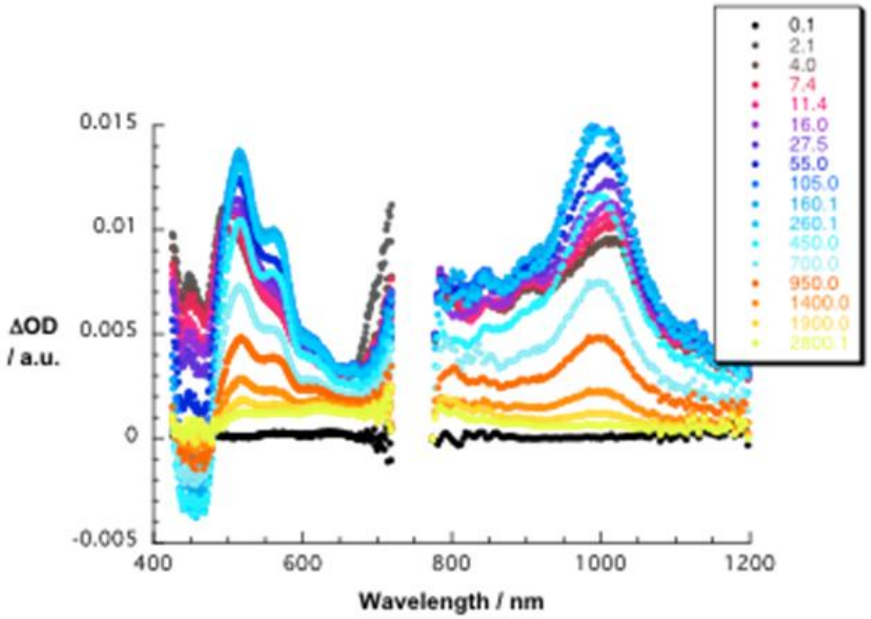

Figura 13. Experimentos de transferencia electrónica fotoinducida por la molécula **42**.

Los dumbbells representan una colección de moléculas que están sujetas a otros tipos de estudios con la técnica del STM, como por ejemplo la formación de estructuras organizadas en superficies donde también la cadena alquílica del

fluoreno podría jugar un papel fundamental. Así, para empezar esta investigación, decidimos estudiar una pirrolidina dumbbell y depositarla sobre una superficie de oro. Los primeros resultados, aún preliminares, han demostrado una cierta organización de la molécula a nivel supramolecular (Figura 14).

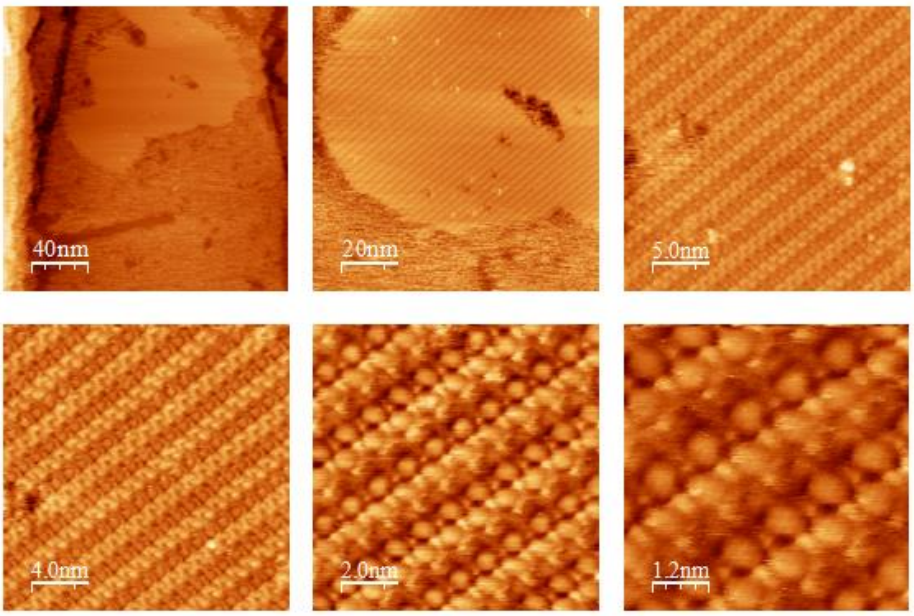

Figura 14. Imágenes de STM de una solución concentrada de la molécula **10a** en tolueno. Distintas ampliaciones de una area demuestran la formación de agregados moleculares, organizados sobre la superficie de oro.

Además, la misma molécula que ha dado estos resultados, se ha utilizado para la medida de conductancia con la MCBJ (Figura 15). Los resultados muestran lo siguiente: dos valores de conductancia se han registrado después de una aproximación donde las trazas, debida al efecto túnel, han sido eliminadas. El valor 10^{-2} G_0, más alto, está de acuerdo con la posibilidad de que la transferencia electrónica ocurra a través de un C_{60} y no de toda la molécula. El segundo valor, mucho más bajo, 10^{-5} G_0 es posible que sea debido a la transferencia electrónica a lo largo de todo el cable molecular. Probablemente, la anchura de los picos de conductancia, que denota un rango bastante amplio de valores, puede ser debido a una reorganización de la molécula bajo el estrés de la medida y de las condiciones de trabajo o, tambien puede ser debido, a una multiunión de moleculas en el contacto por la alta concetración (10^{-4} M) en la que trabajamos (parámetro que no se puede cambiar para el MCBJ).

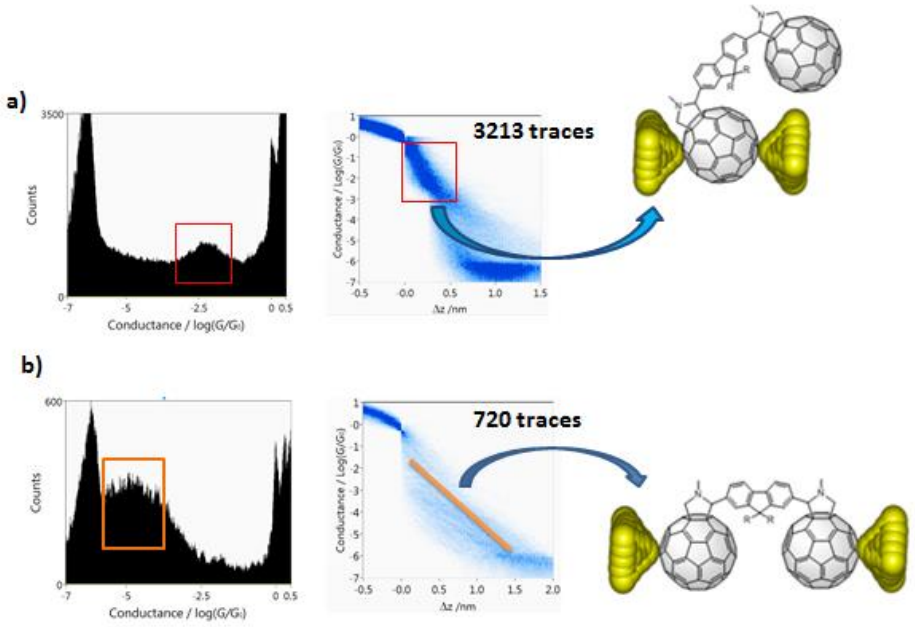

Figura 15. a) conjunto de 3213 trazas que muestran el pico de conductancia a -2.5 G_0 con su possible configuración en la unión metálica; b) conjunto de 720 trazas que muestran el pico de conductancia más bajo con su posible configuración en la unión. La longitud de el "plateau" es similar a la longitud de la molécula.

Como consecuencia de los resultados obtenidos mediante MCBJ, nos hemos propuesto investigar más en detalle, cuál es la naturaleza y la fuente del valor de conductancia de 10^{-2} G_0. Lo que proponíamos tiene que ser demostrado científicamente y eso se está haciendo en los laboratorios de la Universidad de Berna mediante una colaboración actualmente abierta. La molécula asimetrica sintetizada por nuestra parte y que tiene forma de "renacuajo" (desde ahora se hablará de "tadpole") nos permitiría saber con seguridad si aquel valor de conductacia se refiere de verdad a la transferencia de electrones a través del C_{60} o si el fluoreno juega un papel en este mecanismo (Figura 16).

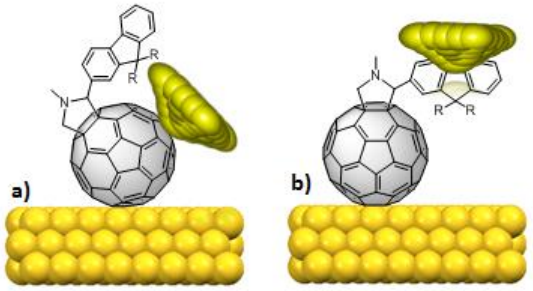

Figura 16. a) representación esquemática de la unión molécular a través de un solo C_{60}; b) posible participación del fluoreno en los picos de conductancia.

Resultados fotovoltaicos

Derivados de C_{60} se han utlizado ampliamente para dispositivos fotovoltaicos. Entre aquellos que han dado un mejor rendimiento fotovoltaico del dispositivo final, hay que nombrar el difenilmetano[60]fullereno, con el acrónimo DPM. La síntesis de uno de estos derivados ha sido llevada a cabo siguiendo el Esquema 3.

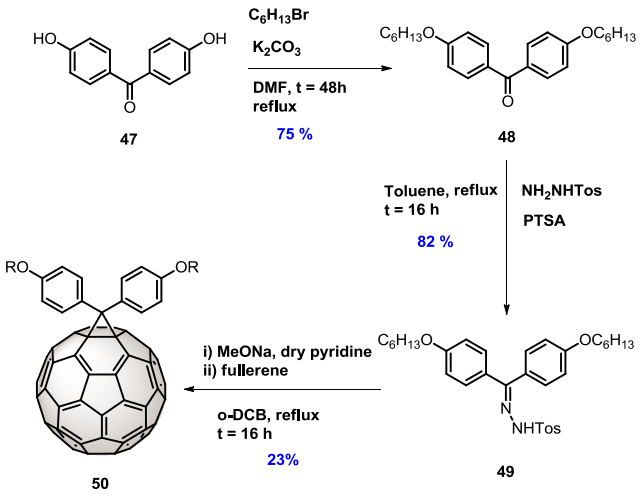

Esquema 3. Procedimiento síntetico para la obtención del DPM-6.

La funcionalización del C_{60} es practicamente idéntica a la del PCBM, la molécula de C_{60} más utilizada para la construcción de dispositivos fotovoltaicos. Estudios de voltamperometría cíclica muestran los mismos valores de potenciales de redución (para el DPM6 son -1.084, -1.481, -1.996 V mientras que para el PCBM son -1.077, -1.469, -1.980 V, respectivamente para las tres ondas de redución del fullereno). Particular importancía tendrá la cadena alquílica lateral en el momento de construir el dispositivo ya que puede influir en distintas nanomorfologías del material final con cambios consecuentes en los rendimientos de la célula fotovoltaica.

Una comparación entre el DPM-6 (cadena alquílica constituida por 6 atomos de carbono) y el PCBM (Figura 17) ha demostrado un aumento de 50 mV del parametro fotovoltaico del potencial de circuito abierto (V_{OC}) en el DPM-6 con una menor eficacia total de la celula BHJ (2.6% frente a un 3.1%).[44]

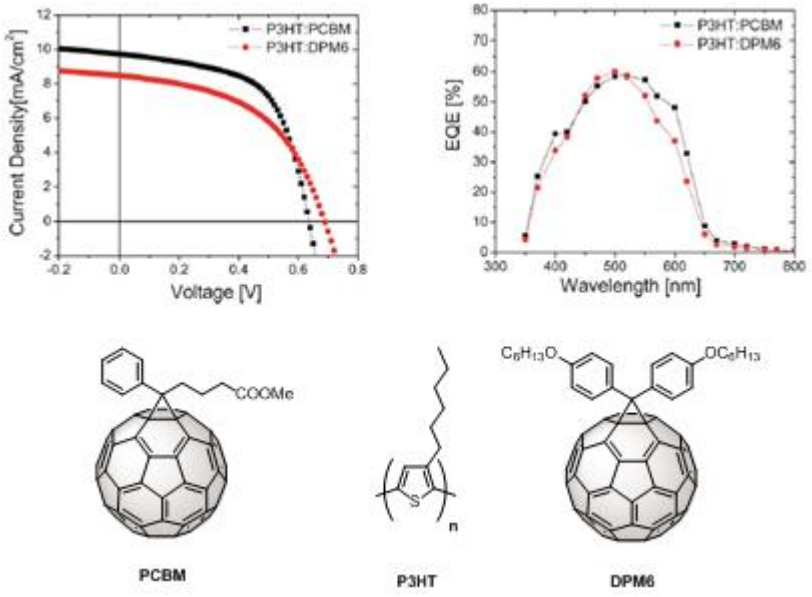

Figura 17. Curva I/V y EQE de las mezclas P3HT:PCBM y P3HT:DPM-6.

Este resultado ha sido explicado en función del aspecto nanomorfologico de la mezcla final a través de AFM donde el polímero dador (P3HT) y el aceptor se han mezclado en una proporción 1:1. La menor cristalinidad del DPM-6 es la causa de esta disminución de la eficacia fotovoltaica. Por otro lado, estudios de LDOS han justificado el valor de V_{OC} más alto en el DPM-6 (Figura 18).[45]

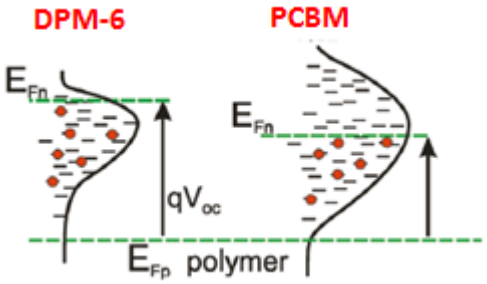

Figura 18. Representación LDOS para el DPM-6 y el PCBM en la mezcla con el P3HT. El nivel de la energía de Fermi para el polímero dador está marcado con una linea verde.

Conclusiones

Se han sintetizados nuevas moléculas electroactivas basadas en el C_{60} con forma de "dumbbell". Estudios de caracterización física y electroquímica a través de espectroscopia ultravioleta y voltamperometría cíclica han dado interesantes conclusiones sobre el verdadero papel del conector (**X**) entre el fullereno y el puente, constituido por un sistema π-conjugado (fluoreno, arilo y el BDF). Cálculos DFT han subrayado esta función del conector mediante las energías de los orbitales moléculares, en particular para el LUMO, o mediante la transferencía electrónica donde una mejor conjugación a lo largo de todo el cable molecular ha sido acentuada. Igualmente importante es, también, la función de este conector en hacer más rígida, linear y simétrica, una molécula con respecto a la otra; las tres caracteristicas son determinante a lo hora de hacer la medida de conductancia donde pueden o no jugar un papel fundamental en el funcionamento de la molécula como cable molecular. Datos experimentales de imágenes y de conductancia, obtenidos mediante STM, han demonstrado que: i) las moléculas son sistemas estables sobre superficie de oro

antes y después de las medidas, ii) es posible visualizar la molécula gracias a la forma esférica del fullereno (“faro molecular”) y hacer medidas de conductancia a través de una sola molécula, iii) el ciclopropano dumbbell ha mostrado dos valores de conductancia, iv) los dumbbells se pueden organizar en la superficie de manera supramolecular formando una monocapa.

La técnica MCBJ ha sido empleada sobre la pirrolidina dumbbell. Las conclusiones están relacionadas con su establidad en esta técnica. La aparición de dos valores de conductancia, uno similar al del ciclopropano dumbbell estudiado por STM y, el otro más bajo en valor de G_0 confirma una mejor comunicación electrónica en el ciclopropano comparando con la pirrolidina dumbbell.

Además, los resultados de los dispositivos fotovoltaicos siguen abriendo temáticas sobre como poder mejorar la eficacia de una célula utilizando materiales de naturaleza orgánica basados en C_{60} u otros fullerenos superiores.

Bibliografía

1. V. Balzani, *Small* **2005**, *1*, 278.
2. R. F. Service, *Science* **2001**, *293*, 785.
3. L. W. Tutt, A. Kost, *Nature* **1992**, *356*, 225.
4. L. Echegoyen, L. E. Echegoyen, *Acc. Chem. Res.* **1998**, *31*, 593.
5. D. M. Guldi, M. Prato, *Acc. Chem. Res.* **2000**, *33*, 695.
6. Q. Xie, E. Pérez-Cordero, L. Echegoyen, *J. Am. Chem. Soc.* **1992**, *114*, 3978.
7. D. M. Guldi, *Chem. Comm.* **2000**, 321.
8. E. G. Emberly, G. Kirczenow, *Phys. Rev. B* **1998**, *58*, 10911.
9. A. Nitzan, M. A. Ratner, *Science* **2003**, *300*, 1384.
10. W. B. Davis, W. A. Svec, M. A. Ratner, M. R. Wasielewski, *Nature* **1998**, *396*, 60.
11. D. M. Guldi, B. M. Illescas, C. M. Atienza, M. Wielopolski, N. Martín, *Chem. Soc. Rev.* **2009**, *38*, 1587.
12. G. Binnig, H. Rohrer, C. Gerber, E. Weibel, *Phys. Rev. Lett.* **1982**, *49*, 57.
13. J. M. van Ruitenbeek, A. Alvarez, I. Pineyro, C. Grahmann, P. Joyez, M. H. Devoret, D. Esteve, C. Urbina, *Rev. Sci. Instrum.* **1996**, *67*, 108.
14. A. Ulman, *Chem. Rev.* **1996**, *96*, 1533.
15. L. Venkataraman, J. E. Klare, I. W. Tam, C. Nuckolls, M. S. Hybertsen, M. L. Steigerwald, *Nano Lett.* **2006**, *6*, 458.
16. B. Kim, J. M. Beebe, Y. Jun, X. Y. Zhu, C. D. Frisbie, *J. Am. Chem. Soc.* **2006**, *128*, 4970.
17. C.-H. Ko, M.-J. Huang, M.-D. Fu, C.-h. Chen, *J. Am. Chem. Soc.* **2009**, *132*, 756.
18. S. Yasuda, S. Yoshida, J. Sasaki, Y. Okutsu, T. Nakamura, A. Taninaka, O. Takeuchi, H. Shigekawa, *J. Am. Chem. Soc.* **2006**, *128*, 7746.
19. a) B. Q. Xu, X. Y. Xiao, N. J. Tao, *J. Am. Chem. Soc.* **2003**, *125*, 16164; b) M. Kamenetska, S. Y. Quek, A. C. Whalley, M. L. Steigerwald, H. J. Choi, S. G. Louie, C. Nuckolls, M. S. Hybertsen, J. B. Neaton, L. Venkataraman, *J. Am. Chem. Soc.* **2010**, *132*, 6817.
20. Y. S. Park, A. C. Whalley, M. Kamenetska, M. L. Steigerwald, M. S. Hybertsen, C. Nuckolls, L. Venkataraman, *J. Am. Chem. Soc.* **2007**, *129*, 15768.
21. a) D. M. Shewchuk, M. T. McDermott, *Langmuir* **2009**, *25*, 4556; b) L. Laurentius, S. R. Stoyanov, S. Gusarov, A. Kovalenko, R. Du, G. P. Lopinski, M. T. McDermott, *ACS Nano* **2011**, *5*, 4219.
22. L. A. Zotti, T. Kirchner, J. C. Cuevas, F. Pauly, T. Huhn, E. Scheer, A. Erbe, *Small* **2010**, *6*, 1529.
23. F. Chen, X. L. Li, J. Hihath, Z. F. Huang, N. J. Tao, *J. Am. Chem. Soc.* **2006**, *128*, 15874.

24. Y. Xing, T.-H. Park, R. Venkatramani, S. Keinan, D. N. Beratan, M. J. Therien, E. Borguet, *J. Am. Chem. Soc.* **2010**, *132*, 7946.
25. X. Lu, M. Grobis, K. H. Khoo, S. G. Louie, M. F. Crommie, *Phys. Rev. Lett.* **2003**, *90*, 096802.
26. A. Stróżecka, J. Mysliveček, B. Voigtländer, *App. Phys. A* **2007**, *87*, 475.
27. M. Kiguchi, *Appl. Phys. Lett.* **2009**, *95*, 073301.
28. I. F. Torrente, K. J. Franke, J. I. Pascual, *J. Phys.: Condens. Matter* **2008**, *20*, 184001.
29. N. Neel, J. Kroger, L. Limot, T. Frederiksen, M. Brandbyge, R. Berndt, *Phys. Rev. Lett.* **2007**, *98*, 065502.
30. J. T. Lyon, L. Andrews, *ChemPhysChem* **2005**, *6*, 229.
31. M. K. Shukla, M. Dubey, J. Leszczynski, *ACS Nano* **2008**, *2*, 227.
32. Z. Xiaohong, D. Zhenxiang, Z. Zhi, *J. Phys.: Condens. Matter* **2009**, *21*, 145502.
33. L. Wang, H. Cheng, *Phys. Rev. B* **2004**, *69*, 165417.
34. C. Joachim, J. K. Gimzewski, R. R. Schlittler, C. Chavy, *Phys. Rev. Lett.* **1995**, *74*, 2102.
35. R. Stadler, S. Kubatkin, T. Bjørnholm, *Nanotechnology* **2007**, *18*, 165501.
36. a) T. Böhler, A. Edtbauer, E. Scheer, *Phys. Rev. B* **2007**, *76*, 125432; b) H. Park, J. Park, A. Lim, E. Anderson, A. Alivisatos, P. McEuen, *Nature* **2000**, *407*, 57; c) J. J. Palacios, A. J. Pérez-Jiménez, E. Louis, J. A. Vergés, *Phys. Rev. B* **2001**, *64*, 115411.
37. E. Leary, M. T. González, C. van der Pol, M. R. Bryce, S. Filippone, N. Martín, G. Rubio-Bollinger, N. Agraït, *Nano Lett.* **2011**, *11*, 2236.
38. C. A. Martin, D. Ding, J. K. Sørensen, T. Bjørnholm, J. M. van Ruitenbeek, H. S. J. van der Zant, *J. Am. Chem. Soc.* **2008**, *130*, 13198.
39. M. Maggini, G. Scorrano, M. Prato, *J. Am. Chem. Soc.* **1993**, *115*, 9798.
40. M. Nambo, Y. Segawa, A. Wakamiya, K. Itami, *Chem. Asian J.* **2011**, *6*, 590.
41. M. Eiermann, R. C. Haddon, B. Knight, Q. C. Li, M. Maggini, N. Martín, T. Ohno, M. Prato, T. Suzuki, F. Wudl, *Angew. Chem. Int. Ed.* **1995**, *34*, 1591.
42. K. Gillemot, C. Evangeli, E. Leary, A. La Rosa, M. T. González, S. Filippone, I. Grace, G. Rubio-Bollinger, J. Ferrer, N. Martín, C. J. Lambert, N. Agraït, *Small* **2013**, DOI:10.1002/smll.201300310.
43. C. Atienza-Castellanos, M. Wielopolski, D. M. Guldi, C. van der Pol, M. R. Bryce, S. Filippone, N. Martín, *Chem. Comm.* **2007**, 5164.
44. H. J. Bolink, E. Coronado, A. Forment-Aliaga, M. Lenes, A. La Rosa, S. Filippone, N. Martín, *J. Mater. Chem.* **2011**, *21*, 1382.
45. G. Garcia-Belmonte, P. P. Boix, J. Bisquert, M. Lenes, H. J. Bolink, A. La Rosa, S. Filippone, N. Martín, *J. Phys. Chem. Lett.* **2010**, *1*, 2566.